

# **The Effect of Climate Change on Water Resources Potential of Omo Gibe Basin, Ethiopia**

**Dissertation**

**zur Erlangung des akademischen Grades**

**Doktor-Ingenieur (Dr.-Ing.)**

Fakultät für Bauingenieurwesen und Umweltwissenschaften

Universität der Bundeswehr München

vorgelegt von

**Abdella Kemal Mohammed (M.Sc.)**

**Vorsitzender: Prof. Dr.-Ing. Wolfgang F. Günthert, Universität der Bundeswehr München**

**Erstprüfer: Prof. Dr.-Ing. Markus Disse, Technische Universität München**

**Zweitprüfer: Prof. Dr. rer. nat. Robert Jüpner, Technische Universität Kaiserslautern**

**Einreichung der Dissertation bei der Universität der Bundeswehr München: 09.10.2013**

**Tag der mündlichen Prüfung: 13.12.2013**



**München, Dezember 2013**



## Abstract

Nowadays, climate change impact imposes serious challenges on water resources potential that can be used for useful developmental projects. As a result, this study investigates the effect of climate change on water resources potential of Omo Gibe basin, Ethiopia. The study area is located south western part of the country lies between 4<sup>00</sup>'N & 9<sup>22</sup>'N latitude and 34<sup>44</sup>'E & 38<sup>24</sup>'E longitude. One of the main scientific puzzles in climate change study is getting reliable and bias free climate model outputs that can be used as an input to hydrological models. Therefore, this research addresses two different methods, cumulative distribution mapping and statistical downscaling method to downscale coarse resolution regional and global climate model outputs to point scale resolution.

The other basic result of climate change studies is daily discharge at the point of interest. Prediction of this discharge for un-gauged basin is still a big challenge especially in developing country like Ethiopia, because most of the catchments are not well organized to measure this flows. As a result this research proposes a methodology to produce daily flows data from un-gauged watersheds corresponding to reference time period.

Understanding how the influence and changes imposed by climate change on available water resource potential corresponding to future time period enhances on the capacity and ability of planners, decision makers and designers to manage, design and plan this scarce resources under climate change conditions for different projects. With regard to this, the thesis proposes modeling of daily flow at Gibe III dam site under climate change scenarios for future water use.

The proposed downscaling methodologies were employed to downscale regional and global climate model outputs in the Omo Gibe basin. Two REMO scenarios for two conditions each A1B\_911 and A1B\_912 wet and optimum B1\_921 and B1\_923 wet and dry conditions were considered. Here wet, optimum and dry conditions used for this particular study based on simulated rainfall values of the scenarios before downscaling.

The efficiency of the methodologies was validated in a number of ways by comparing with observed results, and they performed very well in producing current climate conditions that have similar statistical parameters with observed values. As a result five climate scenarios were projected corresponding to future time period 2020-2050.

Semi distributed physically based hydrological model SWIM was utilized to estimate daily flows from un-gauged part of the basin for reference time period. Initially, this model was calibrated and validated at Abelti flow measuring station with satisfactory results. The performance of the model has been evaluated by Nash–Sutcliffe efficiency and total water difference between observed and simulated flow. Reasonable assumptions have been made between Abelti and un-gauged part of the basin to utilize (transfer) all model calibrated parameters obtained from Abelti to un-gauged basin. Consequently, by considering full climatological and hydrological processes of un-gauged basin and Abelti's calibrated parameter, 29 years (1970-1998) daily flows data generated from this basin.

Observed daily flow on Gibe River at Abelti, Wabe River at Wolkite and Gojeb River at OM19 flow stations were routed to Gibe III dam site. The result of routed flow summed up with generated un-gauged flow to get total inflow at Gibe III dam site for current time. This flow was used to calibrate SWIM at Gibe III dam site to study effects of climate change on water resources potential of the basin. SWIM has been utilized at Gibe III outlet to model hydrological response of Gibe III catchment under climate change conditions. The performance of this model at this station has been evaluated through sensitivity analysis, calibration and validation. During validation the Nash–Sutcliffe efficiency has been found greater than 90% and the overall water difference was less than 2% which is the most important requirement for climate change.

Detail investigation of downscaled results from climate model scenarios were analyzed individually and spatially based on monthly seasonal and annual projected climate outputs. Areal analysis of downscaled results pointed out that the downscaling models projected increased maximum and minimum temperature throughout the basin from all scenarios as compared to current climate condition. Accordingly, areal average maximum temperature is expected to increase in the range of  $0.86^{\circ}\text{C}$  to  $1.37^{\circ}\text{C}$  and minimum temperature is expected to rise in the range of  $0.7^{\circ}\text{C}$  to  $1.9^{\circ}\text{C}$  in the upper part of the basin above Gibe III dam site. On the other hand rainfall behavior from projected scenarios show very mixed patterns of change in the upper part of the basin. The southern part of the basin characterized increased rainfall pattern from three climate stations Sawula Jinka and Morka by GCM scenario in average of 30%. However, the three RCM scenarios (REMO) do not show significant change. The average areal rainfall in the upper part of the basin projected to increase as 6.5%, 4.5% 2.4% and 1.9% by A1B\_911, GCM, A1B\_912 and B1\_921 scenarios respectively, where as one scenario (B1\_923) projected decreased rainfall by -1.4%.

The calibrated model parameters at Gibe III dam site and results from climate change scenarios downscaled from regional and global climate model for scenario period were used to model inflow at Gibe III dam site corresponding to future time frame (2020-2050). As a result, hypothetical daily flow at the aforementioned site considering climate change effects projected from five scenarios, and flow duration curves of these flows were developed. These streamflow data were applied to analyze monthly, seasonal and annual stream flow variability in relation to climate change. The projected streamflow analysis revealed that spring flows from all scenarios projected increased value due to increases precipitation at this season, to the contrary Autumn and peak flow projected decreased results from all scenarios.

Evaporation losses due to Gilgel Gibe I and Gibe III reservoirs were projected by using projected climate outputs of (2020-2050) with modified Penman and Priestly Taylor equations. Results of this loss estimated a gross mean annual loss of  $12.8\text{m}^3/\text{s}$  flow in the form of evaporation from the two reservoirs. Finally this loss was deducted from projected flows to estimate net inflows to Gibe III outlet. Eventually, one of the scenarios A1B\_911 projected 6.7% increased net mean annual flow, whereas B1\_923 projected moderately decreased flow as -17.2% in the net mean annual flow.

The developed downscaling technique, cumulative distribution mapping can be used in other basins to downscale regional or global climate model outputs especially maximum and minimum temperatures to get bias free climate scenarios. Moreover, the results of this study can be used as a quick access to water resources potential of the basin in consideration of climate change that can be used by decision makers and planners for developmental projects in the basin.

## Zusammenfassung

Der Einfluss des Klimawandels führt heutzutage zu ernstzunehmenden Herausforderungen hinsichtlich der Wasserressourcenverfügbarkeit, die für Entwicklungsprojekte genutzt werden kann. Diese Studie untersucht den Einfluss des Klimawandels auf das Wassernutzungspotential im Omo Gibe Becken, Äthiopien. Das Untersuchungsgebiet liegt im Südwesten des Landes ( $4^{\circ}00' - 9^{\circ}22'$  nördl. Breite sowie  $34^{\circ}44' - 38^{\circ}24'$  östl. Länge). Eines der Hauptziele in Klimawandelstudien ist es, verlässliche Ergebnisse aus Klimamodellen zu generieren, die ihrerseits als Eingangsdaten in hydrologischen Modellen verwendet werden können. Daher widmet sich diese Studie zweier Methoden, um die grob aufgelösten regionalen und globalen Klimamodelle auf die Punktskala herab zu skalieren bzw. zu verfeinern. Dies sind das „cumulative distribution mapping“ sowie das „statistical downscaling“.

Ein weiteres wesentliches Ergebnis von Klimawandelstudien ist der tägliche Zufluss an einem Untersuchungspunkt für einen bestimmten Bezugszeitraum. Die Vorhersage von Abflüssen in pegellosen Einzugsgebieten ist immer noch eine große Herausforderung, besonders für Entwicklungsländer wie Äthiopien, wo in vielen Einzugsgebieten keine Messstationen vorhanden sind. Daher wird in dieser Studie eine Methode entwickelt, um tägliche Abflussdaten aus pegellosen Einzugsgebieten für einen Bezugszeitraum zu generieren.

Das Verständnis über Einflüsse und Veränderungen des Klimawandels auf das zukünftige Potential von Wasserressourcen erweitert die Möglichkeiten von Planern und Entscheidungsträgern, die knappe Ressource Wasser bestmöglich zu bewirtschaften. Daher behandelt diese Arbeit die Modellierung des täglichen Zuflusses für zukünftige Wassernutzung am Gibe III Damm unter Berücksichtigung des Klimawandels.

Die hier vorgestellten Skalierungsmethoden werden benutzt, um räumlich hochaufgelöste Eingangsdaten von regionalen und globalen Klimamodellen für die hydrologische Modellierung des Einzugsgebiets des Omo Gibe zu erhalten. Es werden zwei Szenarien des Modells REMO für je zwei unterschiedliche Bedingungen verwendet. Die Szenarien A1B\_911 und A1B\_912 (feucht bzw. optimal) sowie die Szenarien B1\_921 und B1\_923 (feucht bzw. trocken). Die in dieser Studie verwendeten feuchten, mittleren sowie trockenen Bedingungen der Klimamodelle basieren auf simulierten Niederschlägen der jeweiligen Szenarien.

Eine Validierung und Beurteilung der Güte der Methoden erfolgt an beobachteten Pegeln. Durch Anwendung der Methoden können aktuelle Klimabedingungen, deren statistische Eigenschaften gut mit denen aus beobachteten Daten übereinstimmen, generiert werden. Darauf aufbauend werden fünf Klimaszenarien für die Periode von 2020-2050 erstellt.

Um den täglichen Zufluss aus dem pegellosen Teil des Einzugsgebiets für den Referenzzeitraum zu schätzen, wurde das semi-flächenverteilte, physikalisch basierte hydrologische Modell SWIM benutzt. Eine zufriedenstellende Kalibrierung / Validierung des Modells wird zunächst an der Pegelstation „Abelti“ durchgeführt. Zur Beurteilung der Modellgüte dienen die Nash-Sutcliffe Effizienz (NSE) sowie der Volumenfehler. Auf Grundlage sinnvoller Annahmen wird die Parametrisierung des kalibrierten SWIM-Modells für die Pegelstation „Albeti“ auf den pegellosen Teil des Einzugsgebiets übertragen. Darauf

aufbauend wird für dieses Einzugsgebiet eine 29-jährige tägliche Abflusszeitreihe für den Zeitraum von 1970-1998 generiert.

Die gemessenen Abflüsse des Gibe Flusses bei der Pegelstation Albeti, des Wabe River bei der Pegelstation Wolkite sowie des Gojeb Flusses bei der Pegelstation OM19 werden dem Gibe III Damm zugeführt. Zu diesem Abfluss wird der generierte Abfluss aus dem pegellosen Gebiet addiert. Die Summe aus beiden Abflusskomponenten bildet den Gesamtzufluss zum Gibe III Damm. Der Abfluss des Gibe III Damms wird anschließend zur Kalibrierung /Validierung des SWIM-Modells genutzt und die Auswirkungen des Klimawandels auf die Hydrologie untersucht. Für die Validierung ergibt sich ein NSE > 0.9 sowie ein Volumenfehler von < 2%. Gerade der Volumenfehler ist für die Betrachtung von Auswirkungen des Klimawandels von Bedeutung.

Des Weiteren erfolgt eine detaillierte Analyse der skalierten Modellergebnisse der Klimaszenarien. Die Analyse wird sowohl punktuell als auch flächig vorgenommen, jeweils für monatliche sowie jährliche Modelldaten der Klimaprojektionen. Für den flächigen Vergleich der skalierten Ergebnisse zeigt sich gegenüber dem aktuellen Klima eine Zunahme der Minima und Maxima der Lufttemperatur über das ganze Einzugsgebiet. Dieser Befund gilt für alle Szenarien. Bezüglich der durchschnittlichen Maximaltemperatur wird eine Zunahme von 0.86°K bis 1.37°K erwartet, für die durchschnittliche Minimaltemperatur eine Zunahme im Bereich von 0.7°K bis 1.9°K (jeweils für den Teil des Einzugsgebiets oberhalb des Gibe III Damms). Demgegenüber zeigt das Verhalten des projizierten Niederschlags im oberen Teil des Einzugsgebiets kein eindeutiges Muster. Szenario A1B\_911 resultiert in einer Zunahme des Niederschlags von 6.5%, für die Szenarien des GCM sowie A1B\_912 und B1\_921 ergeben sich etwas geringere Zunahmen von 4.5%, 2.4% bzw. 1.9%. Das Szenario B1\_923 ergibt eine Abnahme des Niederschlags um 1.4%. Für den südlichen Teil des Einzugsgebiets ergibt sich aus dem GCM eine signifikante Zunahme des Niederschlags an den Klimastationen Sawula, Jinka und Morka von 30%. Die Ergebnisse der RCM Szenarien (REMO) zeigten allerdings keine signifikanten Änderungen.

Das kalibrierte SWIM-Modell wird nun mit den Ergebnissen der skalierten Klimaszenarien betrieben, um den Zufluss zum Gibe III Damm für den Zeitraum von 2020-2050 zu simulieren. Daraus ergeben sich hypothetische Abflüsse und Abflussdauerlinien für jedes der fünf Klimaszenarien. Diese Abflussdaten werden genutzt, um monatliche, saisonale und jährliche Abflüsse in ihrer Variabilität hinsichtlich des Klimawandels zu analysieren. Die Analyse der projizierten Abflüsse zeigt für alle Szenarien eine Zunahme im Frühjahr. Grund hierfür ist eine Zunahme der Niederschläge. Demgegenüber prognostizieren alle Szenarien einen niedrigeren Abfluss im Herbst und darüber hinaus einen niedrigeren Spitzenabfluss.

Die Evaporation der Becken Gilgel Gibe I und Gibe III wurde anhand der Ergebnisse der Klimamodelle für den Zeitraum von 2020-2050 mittels eines modifizierten Penman Verfahrens sowie der Priestley-Taylor Methode geschätzt. Aufgrund einer steigenden Evaporation aus den Becken ergibt sich eine mittlere jährliche Verringerung des Abflusses um 12.8 m<sup>3</sup>/s. Zur Bestimmung des Nettozuflusses zu den Gibe III Becken werden die projizierten Zuflüsse um diesen Betrag verringert. Das Szenario A1B\_911 zeigt eine Zunahme des mittleren jährlichen Abflusses (netto) um 6.7%, wohingegen das Szenario B1\_923 eine moderate Abnahme des mittleren jährlichen Abflusses von 17.2% prognostiziert.

Die entwickelten Methoden zur Skalierung der Ergebnisse von regionalen und globalen Klimamodellen (downscaling) sowie das „cumulative distribution mapping“ sind räumlich übertragbar und eignen sich besonders für die Parameter maximale bzw. minimale Lufttemperatur. Darüber hinaus können die Ergebnisse dieser Studie genutzt werden, um das Wasserressourcenpotential im Einzugsgebiet vor dem Hintergrund des Klimawandels zu betrachten. Diese Informationen können von Entscheidern und Planern für Entwicklungsprojekte genutzt werden.

## **Acknowledgment**

First and above all, I thank my almighty GOD for giving me this chance. Without his help, I would never have traveled this far.

I would like to thank my beloved families; Tarikua, Wintana, Kemal, Ahmed, Geno and all my sisters. Their love, support and encouragement made the success of this effort feasible. Especially the effort and encouragement from Tarikua and my brother Ahmed made me very strong and courageous to finish my study. I'm very proud to be part of such beautiful family.

My sincere and special thanks go to my major supervisor Prof. Dr.-Ing Markus Disse, for his supervision, encouragement and all rounded support he has provided me throughout my study. Thank you for introducing me new, interesting and thoughtful ideas throughout my study. His critical and frequent advice helped me to explore many ideas and thoughts. His keen supervision and frequent advises made my study feasible. For this I very much appreciate from my heart. I also thank to Prof. Dr. Robert Jüpner from (Technical University of Kaiserslautern), for his enthusiasm and willingness to supervise my work. I also would like to thank the chairman of the examination committee, Prof. Dr.-Ing. Wolfgang Günthert (Universität der Bundeswehr München), for coordinating of the examination processes and his kind support during my stay at the University. My special thank go to my co-supervisor Dr. Semu Ayalewu from Addis Ababa University for his willingness and imputes to my work

I am thankful for Engineering Capacity Building Program (ECBP) that made this research possible through financing for my stay in Germany and during filed work in Ethiopia. Thanks to the Germany Academic Exchange Service (DAAD) for additional support during my stay in Germany and processing of my travel document whenever necessary.

My special gratitude go to Ethiopian National Meteorological Service, Ministry of Water and Energy of Ethiopia and Ethiopian Electric and Power Cooperation for providing me the necessary input data and kind collaboration during my study.

I would like to thank my colleague in Arbaminch University particularly Ato Tamirat Chane, Dr. Belete Yilma and Ato Abiyu Kerebo for their cooperation whenever I need any support from Arbaminch University.

Last but not least, I am grateful to all my colleagues at (Universität der Bundeswehr München), Institut für Wasserwesen, for your continuous support that you made during my stay in Germany. And it was a pleasure for me to work with you.



<b>Table of contents</b>	<b>Pages</b>
<b>Abstract</b> .....	i
<b>Zusammenfassung</b> .....	iii
<b>Acknowledgment</b> .....	vi
<b>Table of content</b> .....	vii
<b>List of figures</b> .....	x
<b>List of tables</b> .....	xiii
<b>List of abbreviations</b> .....	xv
<b>List of nomenclatures and symbols</b> .....	xvii
<b>CHAPTER 1 INTRODUCTION</b> .....	<b>1</b>
1.1 BACKGROUND .....	1
1.2 WHAT IS CLIMATE CHANGE?.....	2
1.3 CLIMATE CHANGE AND WATER RESOURCES MANAGEMENT .....	3
1.4 PROBLEM STATEMENT.....	3
1.5 OBJECTIVE OF THE RESEARCH.....	5
1.6 IMPORTANCE OF THE STUDY .....	6
1.7 THESIS LAYOUT .....	6
1.8 FRAME WORK OF THE STUDY .....	7
<b>CHAPTER 2 LITERATURE REVIEW ABOUT CLIMATE CHANGE</b> .....	<b>10</b>
2.1 INTRODUCTION.....	10
2.2 CLIMATE MODELS.....	11
2.2.1 (GCM) General circulation model .....	11
2.2.2 Regional climate model.....	11
2.3 DOWNSCALING TECHNIQUES .....	12
2.4 SCENARIOS AND THEIR PURPOSE.....	13
2.5 THE EXPECTED IMPACTS FROM CLIMATE CHANGE.....	16
2.5.1 Hydropower impact.....	16
2.5.2 Water supply and flood impact .....	16
2.5.3 Effects on drought .....	16
2.6 CLIMATE CHANGE STUDIES IN ETHIOPIA .....	17
2.6.1 Rainfall variability and trend .....	17
2.6.2 Temperature variability and trend .....	18
2.6.3 Case studies related to climate change in Ethiopia .....	18
2.7 CONCLUSION.....	20
<b>CHAPTER 3 HYDROLOGICAL MODELS</b> .....	<b>21</b>
3.1 INTRODUCTION AND DEFINITION .....	21
3.1.1 Hydrological modeling in the context of climate change .....	21
3.1.2 Importance of hydrological modeling.....	22
3.2 CLASSIFICATION OF HYDROLOGICAL MODELING .....	22
3.3 MODELING APPROACHES FOR CLIMATE CHANGE ASSESSMENT .....	25
3.4 SELECTION CRITERIA FOR HYDROLOGICAL MODELS .....	26

3.5 DESCRIPTION OF SELECTED MODEL .....	29
3.5.1 <i>The SWIM model</i> .....	29
3.5.2 <i>Model history</i> .....	29
3.6 HYDROLOGICAL PROCESSES IN SWIM .....	31
3.6.1 <i>Overland flow generation</i> .....	32
3.6.2 <i>Peak runoff rate</i> .....	32
3.6.3 <i>Computation of evapotranspiration</i> .....	33
3.6.4 <i>Water movement in soil</i> .....	34
3.6.4.1 Percolation .....	34
3.6.4.2 Lateral subsurface flow .....	35
3.6.4.3 Ground water Flow .....	36
3.7 CONCLUSION.....	36
<b>CHAPTER 4 DESCRIPTION OF THE STUDY AREA .....</b>	<b>37</b>
4.1 ETHIOPIA.....	37
4.2 WATER RESOURCES POTENTIAL OF THE COUNTRY .....	38
4.3 LOCATION AND DESCRIPTION OF OMO GIBE BASIN.....	40
4.3.1 <i>Climate of the study area</i> .....	41
4.3.1.1 Rainfall .....	41
4.3.1.2 Meteorological stations .....	42
4.3.1.3 Temperature .....	43
4.3.2 <i>Topography and river systems of the basin</i> .....	43
4.3.3 <i>Geology soil and land use</i> .....	44
4.3.3.1 Geology .....	44
4.3.3.2 Soil.....	44
4.3.3.3 Land use .....	46
4.4 HYDROPOWER DEVELOPMENT IN THE BASIN .....	48
4.5 DESCRIPTION OF THE THREE HYDROPOWER STATIONS .....	49
<b>CHAPTER 5 DATA, METHODOLOGY &amp; DOWNSCALING OF CLIMATE MODEL OUTPUTS .....</b>	<b>53</b>
5.1 CLIMATE DATA.....	53
5.1.1 <i>Observed climate data</i> .....	53
5.1.2 <i>REMO and GCM data</i> .....	54
5.1.3 <i>Filling of observed precipitation and temperature missed data</i> .....	54
5.1.4 <i>Hydrological data</i> .....	55
5.2 DISTRIBUTION MAPPING METHOD TO DOWNSCALE REMO OUTPUT.....	57
5.2.1 <i>Cumulative distribution mapping method (CDM) for precipitation</i> .....	57
5.2.1.1 Distribution mapping of gamma equation to Omo Gibe precipitation .....	60
5.2.1.2 Results and discussion on precipitation downscaling .....	61
5.2.2 <i>Cumulative distribution mapping (CDM) for temperature data</i> .....	65
5.2.2.1 Selection of best cumulative distribution equation .....	67
5.2.2.2 Distribution mapping from selected equations to temperature data .....	73
5.2.2.3 Results and discussion on temperature downscaling .....	74
5.3 DOWNSCALING OF GCM OUTPUT USING SDSM MODEL .....	78
5.3.1 <i>Calibration of SDSM model</i> .....	80
5.3.2 <i>Results and discussion on GCM downscaling</i> .....	81
5.4 ERROR EVALUATION OF DOWNSCALING METHODS .....	82
5.5 FUTURE CLIMATE SCENARIOS FROM REMO AND GCM.....	85
5.5.1 <i>REMO scenarios</i> .....	85
5.5.2 <i>GCM scenarios</i> .....	86

5.5.3 Climate trend analysis from downscaled scenarios.....	86
5.6 CONCLUSION.....	91
<b>CHAPTER 6 APPLICATION OF SWIM FOR ABELTI AND UN-GAUGED BASINS.....</b>	<b>93</b>
6.1 INTRODUCTION.....	93
6.2 APPLICATION OF SWIM AT ABELTI.....	93
6.2.1 Methodology.....	95
6.2.2 Preparation of Model input data.....	96
6.2.3 Preparation of additional input data by SWIM/MapWindow interface.....	98
6.3 MODEL CALIBRATION AND VALIDATION PROCEDURE AT ABELTI STATION.....	100
6.3.1 Performance evaluation of the model.....	100
6.3.2 Results and discussion on model calibration and validation.....	101
6.4 APPLICATION OF SWIM FOR UN-GAUGED BASIN.....	104
6.5 VALIDATION OF SWIM RESULT FOR UN-GAUGED BASIN.....	106
6.5.1 Estimation of mean annual flow in the study area.....	106
6.5.2 Approaches used for estimation of mean annual flow.....	107
6.5.2.1 Derivation of empirical relationship between flow and catchment size.....	107
6.5.2.2 Rational method.....	110
6.6 CONCLUSION.....	115
<b>CHAPTER 7 APPLICATION OF SWIM AT GIBE III BASIN.....</b>	<b>116</b>
7.1 INTRODUCTION.....	116
7.2 FLOW ROUTING IN OMO GIBE BASIN.....	116
7.3 SWIM SETUP AT GIBE III DAM SITE.....	121
7.3.1 Sensitivity analysis.....	122
7.3.2 Results and discussion on sensitivity analysis.....	123
7.3.3 Calibration and validation of SWIM at Gibe III basin.....	125
7.3.4 Results and discussion on calibration and validation.....	127
7.4 CONCLUSION.....	130
<b>CHAPTER 8 MODELING OF GIBE III BASIN UNDER CLIMATE CHANGE SCENARIOS.....</b>	<b>131</b>
8.1 INTRODUCTION.....	131
8.2 METHODOLOGY.....	131
8.3 RESULTS AND DISCUSSION ON CLIMATE CHANGE IMPACTS.....	132
8.3.1 Impacts on monthly, low and high flows.....	133
8.3.2 Impacts on seasonal and annual flows.....	133
8.3.3 Impacts on evaporation loss from the reservoirs.....	135
8.4 ESTIMATION OF NET INFLOWS TO GIBE III RESERVOIR FROM 2020 TO 2050.....	137
8.5 ESTIMATION OF FLOW DURATION CURVE FROM NET INFLOW AT GIBE III DAM SITE.....	138
8.6 CONCLUSION.....	139
<b>CHAPTER 9 CONCLUSIONS AND RECOMMENDATIONS.....</b>	<b>140</b>
9.1 CONCLUSIONS.....	140
9.2 RECOMMENDATIONS.....	142
REFERENCES.....	143
APPENDICES.....	154
Curriculum vitae.....	183

## List of figures

Figure 1.1 Flow chart of the methodology followed throughout of this research .....	9
Figure 2.1 The four IPCC SRES scenario storylines (after Nakicenovic et al., 2000).....	13
Figure 2.2 Structure of the storylines and scenarios in the IPCC special report on emissions scenarios .....	15
Figure 2.3 global CO <sub>2</sub> emissions related to energy and industry (IPCC 2000).....	15
Figure 2.4 Year to year variability of annual rainfall over the whole country, northern half, central and south western Ethiopia expressed in normalised deviation. ....	18
Figure 2.5 Year to year annual mean maximum and minimum temperature variability trend over Ethiopia respectively. ....	18
Figure 2.6 Climate model projections of wet season (June–August) temperature and rainfall for the 2020s, 2050s, and 2080s with 18 climate models for all Ethiopia (Conway D. et al., 2011).....	20
Figure 3.1 Hydrological models classification by Shaw (1983).....	23
Figure 3.2 Hydrological models classification by Chow et al. (1988) .....	23
Figure 3.3 Hydrological models classification by Gosain et al. (2009) .....	25
Figure 3.4 SWIM model development based on CREAMS model (Krysanova V. et al., 2005). ....	30
Figure 3.5 Flow chart of the SWIM model, integrating hydrological processes, nitrogen, phosphorus and crop/vegetation growth at the river basin scale (after Krysanova et al., 2005). ....	31
Figure 4.1 Location map of Ethiopia.....	37
Figure 4.2 Rainfall distributions in Ethiopia .....	38
Figure 4.3 Ethiopian river basin map.....	39
Figure 4.4 Location map of Omo Gibe basin .....	40
Figure 4.5 Mean annual rainfalls (isohyetal map of the basin).....	41
Figure 4.6 All and selected weather stations respectively .....	42
Figure 4.7 Mean monthly rainfall, maximum and minimum temperature for three regions.....	43
Figure 4.8 Elevation and river system of Omo Gibe as extracted from SRTM data of the basin.....	44
Figure 4.9 Soil map of Omo Gibe basin .....	46
Figure 4.10 Omo Gibe River and part of the catchment; smoke is seen as people clearing the forest for preparation of charcoal .....	46
Figure 4.11 Land use map of Omo Gibe basin.....	47
Figure 4.12 Location of main hydropower stations in omo Gibe basin .....	49
Figure 4.13 Gilgel Gibe I and II hydropower plant respectively .....	51
Figure 4.14 Bird eye view of Gibe III reservoir (EEPCo, 2009).....	52
Figure 5.1 locations of representative meteorological stations mean monthly rainfall histogram (1970-2000) from east and western part of the basin. ....	55
Figure 5.2 Flow measuring stations in the upper part of the basin and observed, REMO and GCM grind node in the entire Omo Gibe basin.....	56
Figure 5.3 Representations of Remo grind nodes and one weather observation station .....	57
Figure 5.4 Comparisons of mean annual precipitation, spatially interpolated using inverse distance weighing for observed and historical REMO simulations (1970-2000) respectively .....	58
Figure 5.5 Schematic representation bias correction methodology: (a) frequency, (b) intensity (Ines & Hansen 2006). Where $x_i$ and $x'_i$ refer to REMO and observed rainfall on day $i$ , respectively .....	60
Figure 5.6 The effect of gamma fitting on June precipitation at Limu observation station .....	61
Figure 5.7 RMSE for corrected and uncorrected REMO in historical period 1970-2000 .....	63

Figure 5.8 Comparison of monthly sum of daily precipitation (mm/month) and variance at Assendabo and Limu from 1970-2000 for observed, corrected and Remo simulation.....	63
Figure 5.9 Comparison of mean annual rainfall observed and corrected Remo (1970-2000) respectively for upper part of the basin.....	64
Figure 5.10 Cumulative distributions of observed, corrected and uncorrected Remo precipitation at Bonga and Bele weather stations for reference time period.....	64
Figure 5.11 Spatially interpolated maximum temperature for upper part of the basin observed and Remo before correction for historical time frame respectively.....	66
Figure 5.12 Illustration of the two-sample Kolmogorov-Smirnoff statistic. Red and blue lines each correspond to an empirical and teoretical distribution function, and the black arrow is the K-S statistic. ....	68
Figure 5.13 PDF of January minimum temperature at Bonga reference time.....	70
Figure 5.14 Probability-Probability plot of January minimum temperature at Bonga for Kumaraswaqmy distribution .....	70
Figure 5.15 Mean monthly observed, corrected and Remo simulated maximum and minimum temperature at Assendabo for historical period.....	75
Figure 5.16 Graphical presentation of RMSE for temperature data.....	75
Figure 5.17 Effects of CDM on the variance of maximum and minimum temperature over the entire historical time period 1970-2000.....	76
Figure 5.18 None exceedence probability of observed, corrected and Remo simulated minimum and maximum temperature at Bonga and Assendabo. ....	77
Figure 5.19 Daily maximum observed and Remo temperatures before and after correction at Assendabo. ....	77
Figure 5.20 Left panel shows spatially interpolated mean annual observed maximum temperature and right panel is spatially interpolated mean annual corrected Remo maximum temperature in the upper part of omo Gibe basin. ....	78
Figure 5.21 Comparison of mean monthly precipitation, maximum and minimum temperature after downscaling from GCM scenario, current time .....	81
Figure 5.22 Model errors (absolute value) in monthly $T_{max}$ and $T_{min}$ downscaling with SDSM and CDM at Jimma station .....	83
Figure 5.23 Model errors (absolute value) in monthly precipitation and % of wet days respectively at Jimma station .....	84
Figure 5.24 Mean dry-spell and mean wet-spell length at Jimma station respectively.....	84
Figure 5.25 Change in mean annual maximum and minimum temperature in 2020 to 2050.....	87
Figure 5.26 Spatial changes in mean annual maximum and minimum temperatures from Remo average result of all scenarios for upper part of the basin .....	88
Figure 5.27 Projected change in mean annual precipitation from all scenarios at the end of 2050 ....	89
Figure 5.28 Monthly sum of observed (1970-2000) and projected (2020-2050) areal precipitation upper part of the basin.....	91
Figure 5.29 Mean monthly observed and projected (2020-2050) areal maximum and minimum temperature for upper part of the basin. ....	91
Figure 6.1The three main flow measuring stations and their watershed area.....	94
Figure 6.2 Part of soil survey site locations during master plan study and developed soil data base respectively .....	97
Figure 6.3 Format of one climate station input data for interpolation purpose .....	98

Figure 6.4 (a) Hydrotope structures, (b) routing structures developed during preprocessing of SWIM at Abelti catchment respectively.....	99
Figure 6.5 Overplayed sub-basins, land use and soil map of Abelti catchment respectively .....	99
Figure 6.6 Graphical comparison of daily simulated and observed discharge upper panel, and monthly simulated and observed discharge lower panel during calibration period at Abelti .....	102
Figure 6.7 Yearly values of precipitation and evapotranspiration left panel and yearly hydrograph separation during calibration period at Abelti station right panel. ....	103
Figure 6.8 Graphical comparison of daily simulated and observed discharge upper panel, and monthly simulated and observed discharge lower panel during validation period at Abelti station. ....	103
Figure 6.9 Yearly values of precipitation and evapotranspiration left panel and yearly hydrograph separation during validation period at Abelti station. ....	103
Figure 6.10 Calculated sub-basin, hydrotopes and routing structures of un-gauged basin .....	105
Figure 6.11 Generated daily and mean monthly flows from 1970 to 1998 from un-gauged basin....	105
Figure 6.12 Mean annual runoff volume at Abelti and Un-gauged basin .....	106
Figure 6.13 Curve of mean annual runoff vs. drainage area for studying basin .....	109
Figure 6.14 Main catchment areas of Gibe III dam site and rainfall gauging stations .....	111
Figure 6.15 Thiessen polygons for Gibe III dam site.....	111
Figure 7.1 Flow contribution catchments to Gibe III dam site .....	117
Figure 7.2 Monthly flow contributions from four catchments to Gibe III dam site after routing .....	120
Figure 7.3 Comparisons of mean annual and percentage contributions of flows from all catchments to Gibe III dam site.....	121
Figure 7.4 Annual runoff volumes at Gibe III dam site.....	121
Figure 7.5 Sensitivity of discharge at Gibe III dam site to bff parameter.....	123
Figure 7.6 Sensitivity of discharge at Gibe III dam site to thc parameter .....	123
Figure 7.7 Sensitivity of discharge at Gibe III dam site to sccor parameter.....	124
Figure 7.8 Overplayed sub-basins, land use and soil map of Gibe III catchment respectively .....	126
Figure 7.9 Hydrotope and routing structure developed during preprocessing of SWIM at Gibe III catchment.....	126
Figure 7.10 Graphical comparisons between observed and simulated daily discharge upper panel and monthly discharge lower panel during calibration period at Gibe III outlet.....	128
Figure 7.11 Yearly values of precipitation and evapotranspiration during calibration period at Gibe III outlet .....	128
Figure 7.12 Yearly hydrograph separations during calibration period at Gibe III outlet .....	128
Figure 7.13 Graphical comparisons between observed and simulated daily discharge upper panel and monthly discharge lower panel during validation period at Gibe III outlet .....	129
Figure 7.14 Yearly values of precipitation and evapotranspiration during validation period at Gibe III outlet .....	129
Figure 7.15 Yearly hydrograph separations during validation period at Gibe III outlet.....	129
Figure 8.1 Comparisons of observed and projected monthly, seasonal and annual flows at gibe III dam site. ....	133
Figure 8.2 Impacts on mean annual runoff 2020-2050.....	134
Figure 8.3 Observed and projected flow duration curves.....	139

## List of tables

Table 3.1 Description of five screened semi distributed hydrological models .....	28
Table 4.1 Irrigation and hydropower potential of Ethiopian river basins .....	39
Table 4.2 Percentage of land use type in Gibe basin .....	48
Table 4.3 Basic features of Gilgel Gibe I hydropower plant (EEPCo, 2004). .....	49
Table 4.4 Basic features of Gibe II hydropower plant .....	50
Table 4.5 Basic features of Gibe III hydropower plant (EEPco, 2009). .....	51
Table 5.1 List of selected weather stations in Omo Gibe basin .....	53
Table 5.2 List of flow measuring stations .....	56
Table 5.3 Mean annual precipitation observed and interpolated from REMO simulations for current time period (1970-2000). .....	58
Table 5.4 Performance parameters for bias correction methodology between observed, corrected and current time Remo simulation (1970-2000).....	62
Table 5.5 Mean annual maximum and minimum surface temperature of observed and interpolated REMO simulations for current time. ....	65
Table 5.6 Different distribution equations used to fit distributions of maximum and minimum temperature in Omo Gibe basin.....	66
Table 5.7 Root mean square error for maximum and minimum temperature before and after correction .....	76
Table 5.8 Example of correlation results between GCM and observed maximum temperature at Jimma. ....	79
Table 5.9 Large-scale predictor variables selected for downscaling precipitation and temperature in Omo Gibe basin .....	80
Table 5.10 Change in maximum and minimum temperature in Omo Gibe basin 2020-2050 .....	87
Table 5.11 Change in mean annual precipitation (2020-2050) in reference to control period .....	89
Table 5.12 Comparison of areal precipitation between current and projected scenario 2020 to 2050 for upper part of the basin above Gibe III dam site in mm .....	90
Table 6.1 Available flow records and basin area.....	94
Table 6.2 Calibrated parameters and their range for Abelti flow station .....	101
Table 6.3 Calibration and verification results at Abelti flow station .....	102
Table 6.4 Mean monthly flows contributed to Gibe III dam site from un-gauged part of the basin..	105
Table 6.5 Flow measuring stations used to establish area discharge relationship .....	108
Table 6.6 Mean discharge contribution from four catchments to Gibe III dam site.....	110
Table 6.7 Mean areal rainfall rate in mm/year for catchments of hydrometric stations .....	112
Table 6.8 Runoff coefficients for hydrometric stations upstream of gibe III dam site. ....	112
Table 6.9 Calculated mean annual discharge at Gibe III dam site using rational method .....	113
Table 6.10 Runoff coefficients for Abelti, Wolkite, Un-gauged and Gibe III dam site .....	114
Table 6.11 Comparisons of mean annual flows generated from un-gauged and Gibe III dam site computed from three methods.....	114
Table 7.1 Watershed parameters of Gibe III basin.....	118
Table 7.2 Values of K for OM19, Abelti and Wabi calculated using equation 7.8 and 7.9.....	119
Table 7.3 Calculated Muskingum routing coefficients for OM19, Abelti and Wabe.....	120
Table 7.4 Mean monthly and mean annual flow at Gibe III dam site after routing.....	120
Table 7.5 Parameters and parameter ranges used in sensitivity analysis in SWIM model.....	122
Table 7.6 Sensitivity characteristics of calibration parameter towards water flow at Gibe III basin..	125

Table 7.7 Calibration and verification results at Gibe III outlet .....	127
Table 8.1 Observed and projected discharge at Gibe III dam site. Monthly, seasonal and annual values .....	132
Table 8.2 Change in seasonal discharge at Gibe III dam site for future time.....	133
Table 8.3 Percentage change in mean annual runoff at Gibe III dam site .....	134
Table 8.4 Estimated evaporation from Hosanna and jimma 2020-2050 .....	136
Table 8.5 Estimated monthly evaporation loss from Gibe III and Gilgel Gibe I reservoirs.....	137
Table 8.6 Projected mean monthly and annual net inflow to gibe III reservoir .....	138



## List of Abbreviations

ANN	Artificial neural network
ASCE	American society of civil engineers
AWC	Available water content
BCM	Billion cubic meters
°C	Degree centigrade
CDF	Cummulative distribution function
CDM	Cummulative distribution mapping
CL	Clay content
Co <sub>2</sub>	Carbon dioxide
CN	Curve number
CREAMS	Chemicals, Runoff, and Erosion from Agricultural Management Systems
CV	Coefficient of Variation
Cms	Centimeters
DEM	Digital Elevation Model
DJF	December, January and February
DS	Drain space
E	East
ECDF	Empirical distribution function
EEPCo	Ethiopian electric power corporation
EPIC	Environmental policy Impact Climate
ERG	Ethio resource groupe
FAO	Food and Agriculture Organization of the United Nations
FDC	Flow duration curve
FDRE	Federal democratic republic of Ethiopia
GCM	General circulation model
GDP	Gross domestic product
GEV	Generalized extream value
GHG	Greenhouse gas
GLEAMS	Ground water loading effects on agriculcural managment
GoE	Government of Ethiopia
GOF	Goodness of fit test
GRU	Grouped response unit
GTP-1	Growth and transformation plan-1
GTP-2	Growth and transformation plane-2
GWH/yr	Giga watt hour per year
GWH	Ground water table height
GWQ	Groundwater contribution to streamflow
Ha	Hectare
HadCM3	Hadley Centre for Climate Prediction and Research Coupled Model, UK
HBV	Hydrologisika Bayraans Vattenbalans-avediling
HEC-HMS	Hydraulic Engineering Centre- Hydrologic Modeling System
HRU	Hydrological response units
IPCC	Intergovernmental panel on climate change
IWMI	International Water Management Institute
JAS	July, August and September
Km <sup>2</sup>	Kilometer square
LAI	Leaf area index

LARS-WG	Long ashton research station weather generator
m.a.s.l	Meter above sea level
MLM	Maximum likelihood method
MoWEE	Ministry of water resources and energy of Ethiopia
MW	Mega watt
N	North
N%	Nitrogen content %
MAR	Mean annual runoff
NCEP	National Centre for Environmental Prediction
NMAE	National meteorological agency of Ethiopia
mm	Milimiter
Obs	Observed
OAGCM	Atmospher ocean general circulation model
OC%	Organic carbon content %
ODMP	Omo Gibe integrated development master plan study
OND	October, November and December
Para	Parameter
PPT	Precipitation
PDF	Probability density function
PERC	percolation
PEST	Parameter estimation
Ppm	Part per million
RCC	Roller compacted concrete
RCH	Recharge
RCM	Regional Climate Model
REA	representative element area
RMSE	Root mean square error
SC	Saturated conductivity
SCS	Soil conservation service
SDSM	Statistically downscaling model
SEEP	Seepage
SAW	Shallow aquifer storage
SMX	Retantion coefficient
SNNPR	Southern Nations, Nationalities and Peoples Region
SN	Sand content in %
SRES	Special Report on Emission Scenarios
SRTM	Shuttle Radar Topographic Mission
SWAT	Soil and Water Assessment Tool
SWIM	Soil and water integrated model
SWRRB	Simulator for Water Resources in Rural Basins
TOPMODEL	Topographic Model
UNFCCC	United Nations Framework Convention on Climate Change
UNDP	United nation development programe
WMO	World Meteorological Organization
WASIM	Water balance Simulation Model

## List of nomenclatures and symbols

A	Drainage area (km <sup>2</sup> )
abf0	Alfa factor for ground water
bff	Base flow factor
C <sub>1</sub> , C <sub>2</sub> , C <sub>3</sub>	Muskingum routing coefficients
CLR	Wave celerty
chwco	Coefficient to correct the channel width
d <sub>r</sub>	Inverse relative distance Earth-Sun
elev	Ground elevation (m)
ea	Actual daily vapor pressure (kpa)
FC <sub>i</sub>	Water content of the soil layer at field capacity (mm)
gwq0	Initial ground water contribution to stream flow in mm/day
Gsc	Solar constant (0.082 MJm <sup>-2</sup> min <sup>-1</sup> )
HC <sub>i</sub>	Saturated hydraulic conductivity for the soil layer (mm/hr)
HV	Latent heat of vaporization (MJ kg <sup>-1</sup> )
K	Routing parameter in Muskingum routing equation (days)
KD	Hydraulic conductivity of ground water (mm/day)
PET	Potential evapotranspiration (mm)
p	Precipitation (mm)
PORD	Drainable porosity of the soil (m/m)
Q	Surface runoff (mm)
Q <sub>obs</sub>	Observed discharge (m <sup>3</sup> /s)
Q <sub>sim</sub>	Simulated discharge (m <sup>3</sup> /s)
$\bar{Q}_{obs}$	Mean values of observed discharge (m <sup>3</sup> /s)
$\bar{Q}_{sim}$	Mean values of simulated discharge (m <sup>3</sup> /s)
Q <sub>peak</sub>	Peak runoff rate (m <sup>3</sup> /s)
L	River reach length (m)
Ra	Extraterrestrial radiation (MJ M <sup>-2</sup> day <sup>-1</sup> )
REVAP	Water flow from the shallow aquifer back to the soil profile (mm/day)
RI	Rainfall intensity (mm/hr)
R <sub>n</sub>	Net radiation (MJ m <sup>-2</sup> day <sup>-1</sup> )
R <sub>ns</sub>	Net incoming shortwave radiation (MJ m <sup>-2</sup> day <sup>-1</sup> )
R <sub>nl</sub>	Net outgoing longwave radiation (MJ m <sup>-2</sup> day <sup>-1</sup> )
roc2	Routing coefficient to calculate storage time constant for the reach of surface flow
Roc4	Routing coefficient to calculate storage time constant for the reach of sub surface flow
Rso	Clear sky radiation (MJ m <sup>-2</sup> day <sup>-1</sup> )
sccor	Correction factor for saturated conductivity
SL	Hill slope length (m)
SLW	Hillslope width (m)
SSF	Subsurface flow (mm/day)
stinco	Initial water content as a fraction of field capacity

SW(t)	Soil water content in the day t (mm)
SUB	Drainable volume of water stored in the saturated zone
Thc	Evaporation correction factor
$T_{max}$	Maximum temperature ( $^{\circ}\text{C}$ )
$T_{min}$	Minimum temperature ( $^{\circ}\text{C}$ )
$TT_i$	Travel time through soil layer (hr)
WIR	Rate of water input to saturated zone ( $\text{m}^2/\text{hr}$ )
V	Average stream velocity (m/s)
VEL	Velocity of flow at the outlet (mm/s)
$\delta$	The solar declination (rad)
$\gamma$	Psychrometer constant ( $\text{Kpa C}^{-1}$ )
$\alpha$	Albedo
$\sigma$	Stefan-Boltzmann constant ( $\text{MJ K}^{-4} \text{m}^{-2} \text{day}^{-1}$ )
$\omega_s$	Sunset hour angle (rad)
$\phi$	Latitude of the climate station (rad)
$\beta$	Slope of the saturation vapor pressure curve ( $\text{Kpa C}^{-1}$ )

# Chapter 1 Introduction

## 1.1 Background

Projected twenty first century changes in air temperature and precipitation patterns due to climate change may alter the availability of water leading to new challenges for water supply planning and management in many regions throughout the world (Bates et al. 2008; Hunt and Watkiss 2011). The potential impact of climate change on the ability to meet future demands for high quality drinking water and satisfy other competing goals for surface water supplies is an issue of importance in many regions (Bates et al. 2008; Brekke et al. 2009). In consideration of climate change problems the assessment of potential impacts of climate change is progressing from taxonomies and enumeration of the magnitude of potential direct effects on hydrology and ecosystems. Nowadays, there is strong scientific evidence that the average temperature of the Earth's surface is increasing due to greenhouse gas emissions. Climate change affects poor nations in particular, because of their weak adaptive capacities due to lack of finance and knowledge gap.

Climate change will reduce water availability, hydropower potential and changing seasonality of flows in many regions (IPCC, 2010). For instance, the average annual global surface air temperature have increased by about 0.6 °C while sea level has risen by 10-25 cms over the last hundred fifty years and these increases have been partially attributed to the accumulation of greenhouse gases in the atmosphere (IPCC, 2001).

What is more worrying in the future? According to the fourth assessment report (AR4) of the Intergovernmental panel on climate change (IPCC), if steps are not taken to reduce emission of greenhouse gases (i.e. business as usual scenario continues), the global surface temperatures at the end of the twenty-first century (2090–2099) are projected to increase higher than 4°C, in the range of 1.8 to 4°C relative to 1980–1999. The upper bounds of projected sea-level rise for these same emission scenarios ranged from 48 to 59cm (IPCC, 2007). Such drastic change of climate and sea level rise in a short span of time is expected to have adverse impacts on many socio-economic sectors like; low-lying areas and coastal wetlands, agricultural production, water supplies, human health and terrestrial and aquatic ecosystems will be in danger. It is also expected that changes in the earth's climate will hit developing countries like Ethiopia, because their economies are strongly dependent on crude forms of natural resources and their economic structure is less flexible to adjust to such drastic changes. It is a fact that climate change has adverse impacts on socio-economic development of all nations. But, it is expected that its impact will hit developing countries the worst. A good example for this the drought which was occurred recently (2011) in East Africa which left the loss of so many human lives.

Regions with an arid and semi-arid climate could be sensitive to even insignificant changes in climatic characteristics. Therefore, quantitative estimates of hydrologic effects of climate change are essential for understanding and solving the potential water resource management problems associated with water supply for domestic and industrial water use, power generation, and agriculture as well as for future water resource planning, reservoir design and management, and protection of the natural environment and human lives from disasters like flood and drought. It is estimated that, by 2080s, the proportion of arid and semi-arid lands in Africa is likely to increase by 5-8% (IPCC 2007). In South Africa and Ethiopia, minimum temperatures have increased slightly faster than maximum or mean temperatures (Boko M. et al, 2007). Ricardian studies in Burkina Faso, Cameroon, Egypt, Ethiopia, Ghana, Kenya, Niger, Senegal, South Africa, Zambia, & Zimbabwe indicate a potential fall in net revenues from farming in all of Africa \$23 billion with 2.5°C of temperature change (Watkiss, 2009).

For countries that are highly dependent on natural resources, these challenges may be amplified by extreme events having social and economic impacts that far outweigh their

apparent probabilities of occurrence (Thornton et al. 2009). Climate change is one of the more imperative issues that attract the attention of scientists and policy makers. Many scientists are developing necessary methodologies to better understand the impacts of climate change, and support the development of appropriate adaptation measures. Literature on the application of adaptation measures to changing climatic conditions is very limited and the need for more work is evident on the development of adaptation strategies for mitigating negative impacts of climate change in water resources management practice especially in developing country like Ethiopia.

Past studies addressing climate change impacts on water resources and hydrology in Ethiopia in general and Omo Gibe basin in particular are very limited even it is possible to say nothing has been done in Omo Gibe basin regarding to climate change. As a result the principal aim of this research is to explain the relationship between climatic conditions, hydrological conditions and surface water condition in Omo basin. Despite the fact that the impact of climate change is commonly projected at continental or global scale, the magnitude and type of impact at regional-scale catchments is not investigated in many parts of the world that also includes Ethiopia. Therefore, the other objective of this study is to assess impacts of climate changes in regional-scale.

## 1.2 What is climate change?

United Nations Framework Convention on Climate Change (UNFCCC) defines climate change as: “a change of climate which is attributed directly or indirectly to human activity that alters the composition of the global atmosphere and which is in addition to natural climate variability observed over comparable time periods”. In other words, the UNFCCC uses the term climate change to mean only those changes induced by human activities. According to Oxford dictionary it is defined as, changes in the earth's weather, including changes in temperature, wind patterns and rainfall, especially the increase in the temperature of the earth's atmosphere that is caused by the increase of particular gases, especially carbon dioxide. Earth's atmosphere comprises of "green-house gases". This allows heat to penetrate the Earth and keep us warm. Water vapor and carbon dioxide are examples of the green-house gases. Without them, the Earth would be cooler than it is now, so they are essential for survival on Earth. However, over the past few decades, more and more green-house gases are being released by the people. The burning of coal and oil results in more heat being trapped inside of the Earth by the atmosphere. Deforestation (the cutting down of trees) is also a reason for global warming because trees absorb the carbon dioxide or greenhouse gas emissions.

Heat exits the Earth system as the Earth's surface, warmed by solar energy, radiates heat away. However, greenhouse gases allow the lower atmosphere to absorb the heat radiated from the Earth's surface, trapping heat within the Earth system. Over the past century the amounts of greenhouse gases within our atmosphere have been increasing rapidly. Consequently, in the past one hundred years global temperatures have been increasing more rapidly than the historic record shows. Scientists believe this accelerated heating of the atmosphere is because increasing amounts of these greenhouse gases trap more and more heat<sup>1</sup>.

---

<sup>1</sup> [http://www.eo.ucar.edu/basics/cc\\_1.html](http://www.eo.ucar.edu/basics/cc_1.html)

### 1.3 Climate change and water resources management

Climate change affects the hydrological cycle, through changes in precipitation, maximum and minimum temperature and evapotranspiration. As it is clearly known that evapotranspiration is one of the main components of hydrological cycle, as the evaporation rate changes it has a direct impact on the hydrological regimes of a specific watershed.

The relation between water resources and evaporation can be explained as follow: water molecules are always moving. At the water surface some molecules are bumped by molecules below them and gain enough speed to break free and escape it to the air as gas (water vapour). This escape of surface molecule is called evaporation. Evaporation takes place in all times and at any temperature. The higher the temperature the higher the rate of evaporation, when the temperature of the water or the surrounding air increases the water molecule will gain more energy to escape at a faster rate. This indicates that in addition to the changing pattern of the rainfall due to climate change there will be a direct influence on evaporation and ultimately on water resources potential.

Complex impacts of climate change affect all sectors of society. This research is focused on water resources potential of Omo-Gibe basin. In many cases and in many locations, there is compelling scientific evidence that climate changes will pose serious challenges to the water systems (Biggs et al., 2012). It is very important to understand how current climate change affects the availability and variability of regional water resource as well as the frequency of extreme cases such as floods and droughts. With this regard the study of availability of water for future in the changing climate condition is unquestionable.

So far especially in Africa quantification of climate change on basin scale is not studied in detail. Meeting the new challenges on water resources management, implies the quantification of climate change impact on basin-scale hydrology (Varies et al., 2004). Certain aspects of water resources are very sensitive to both climate and to how the complex water systems are managed (Gleick and Adams, 2010), therefore, the complexity of the impacts of climate and socio-economic changes should be addressed by looking at the combined impacts of changes on hydrology and on the human and environmental use of water. It is now well accepted that modelling seems to be the only resort to address this complex problems (Xu et al., 2005). Therefore, the regional scale simulation of hydrological consequences of climate change has received increasing attention.

### 1.4 Problem statement

With respect to available water resources, any climate change may affect the hydrological cycle and its water balance terms. For instance, changes in temperature and precipitation will have direct impact on the processes of runoff production. Consequently, any change in the spatial and temporal availability of water resources affects agriculture, industry and urban development. As such climate change is expected to have adverse impacts on socio-economic development in most nations, although, the degree of the impact will differ. However, there are few countries benefited from climate change especially on those who live in the coldest climates, for instance Canada. Just a brief list of the benefits to coldest province in Canada, Manitoba, and the coldest city, Winnipeg, illustrates the positive potential of global warming; reduced heating costs, reduced fuel bills for travel, a longer growing season allowing a greater variety of crops, less frost damage and crop loss<sup>2</sup>.

IPCC findings indicate that developing countries such as Ethiopia will be more vulnerable to climate change, and climate change may have far reaching implications for Ethiopia because of its economic, climatic and geographic settings. The economy of the country mainly depends on agriculture that largely depends on available water resources while a large part of the country is arid and semi-arid that is highly prone to drought and desertification. Also

---

<sup>2</sup> <http://www.fcpp.org/publication.php/1365>



the country has a fragile highland ecosystem that is currently under stress due to still increasing population pressure. Rising temperatures and increasing climate variability is already imposing a significant challenge to Ethiopia by affecting food security, water and energy supply, poverty reduction and sustainable development efforts. It also exacerbates natural resource degradation and natural disasters (NMAE, 2007).

One of the important causes for vulnerability of Ethiopia to climate variability and change is very high dependence on rainfall patterns and rain fed farming for food production. This is very sensitive to climate variability and change. The overall performance of the economy depends on the agricultural production. It also severely impacts the water resources of the country and indirectly on the hydropower production capacity. This in turn affects the country's economy and its developmental goals and poverty reduction capacity.

The big and main water resources problem in Ethiopia is uneven distribution of the rainfall, which can be linked to impacts of climate change. Between 80-90% of Ethiopia's water resources is found in the four river basins namely; Abay (Blue Nile), Tekeze, Baro Akobo, and Omo Gibe in the west and south-western part of Ethiopia where the population is no more than 30 to 40 percent. On the other hand, the water resources available in the east and central river basins are only 10 to 20 percent whereas the population in these basins is over 60 percent (MoWE, 2001). Existing power generation in Ethiopian is highly dominated by hydropower resources; this is the source of 95% of current total electricity.

For instance in 2009 power cuts cost the Ethiopian economy 1% in GDP growth. Future power disruptions will cost more due to increased dependence of the economy on power (ERG, 2009). These are some of the problem recently existed, in addition to these problems with climate change the situation will be exacerbated and will have much impact on social, economy and the overall water resources of the country. A hydro dominated strategy makes the power system and the economy vulnerable to climatic variations.

The overall coefficient of variability in rainfall of the country ranges from 10-50%. The arid and semi-arid regions which constitute 60% of the country's surface area experience a coefficient of variation of 50% whereas the rainfall fluctuation in the South-Western regions is usually less than 20% (the coefficient of variation is simply the standard deviation divided by the average annual rainfall). Although long-term records are generally lacking, the potential evapotranspiration in the arid and semi-arid areas exceeds precipitation by a factor of more than 4 (Workineh, 1987). The high rainfall deviation together with the high evapotranspiration increases the vulnerability of these areas to drought. The recurrence of drought is a clear indication of the decreasing trend in the overall moisture availability in terms of rainfall. Areas that used to get enough rain to grow crop in the past have now become arid areas and they have been deserted. A good example for this is the Awash rift valley and Eastern part of Ethiopia.

Between July 2011 and mid of 2012, a severe drought affected the entire East Africa region. Said to be "the worst in 60 years", the drought caused a severe food crisis that threatened the livelihood of 9.5 million people across the region. Many refugees from southern Somalia fled to neighboring Kenya and Ethiopia, where crowded, unsanitary conditions together with severe malnutrition led to a large number of deaths<sup>3</sup>.

In addition to the above mentioned problems the level of awareness about the environment and climate change is still very low among most Ethiopians. Issues pertaining to climate change and the vulnerability of Ethiopia are not yet sufficiently addressed. For instance climate change is projected with in near future to reduce yields of the wheat staple crop in Ethiopia by 33% (NMAE, 2007). Therefore there is a need to carry out climate change research and studies to better understand impacts of current climate variability particularly on hydrology. It is a clear fact that in any water related engineering activities proper estimation

---

<sup>3</sup> [https://en.wikipedia.org/wiki/2011\\_East\\_Africa\\_drought](https://en.wikipedia.org/wiki/2011_East_Africa_drought) as visited on May 2013



of runoff magnitude is required. For efficient design, planning, and management of river basin projects that deals with conservation and utilization of water for various purposes, the long-term water availability and mean annual flows are of vital interest especially at present time due to the climate change effect.

In 2006/07, agricultural production in Ethiopia generated around 46 percent of Ethiopia's gross domestic product and employed 80 percent of the working population (Arndt et al, 2009). According to Deressa, 2006 Ethiopia has about 16.4 million hectares of arable land (14.6 percent of its total land area), of which about 8 million hectares are used for crop production. However, most of the agricultural sectors are dominated by mixed rain fed small-scale farming based on traditional technologies. These traditional technologies are easily susceptible to climate change factors.

## **1.5 Objective of the research**

### **I. General Objective**

The general objective of this research is to derive the amount of water resources potential available from future climate scenarios for water resources development in the basin. That would help to better understand and optimize available and limited water resources utilization strategies under the changing climate. And to develop techniques useful in assessing the sensitivity of water resources to climate change. Focus was given for downscaling of climate data output to get spatio-temporal, refined and accurate climate data scenarios for near future.

Furthermore, there are one reservoir (Gibe I) and one tunnel (Gibe II) hydropower systems which are already constructed and functional; additionally one reservoir (gibe III) hydropower plant is under construction, therefore this study will have a significant implication by modeling the basin under climate change scenarios for estimation of available water resources for power production, irrigation and other uses.

### **II. Specific objectives of the research**

The specific objectives of this research mainly focus on the following core points:

- To develop reliable methodology to downscale coarse resolutions of climate model outputs
- To provide temporal climate change scenarios of precipitation and temperature of the basin for current and hypothetical future climate conditions.
- To develop GIS-based rainfall runoff hydrologic modeling and to model the basin under climate change scenarios.
- To investigate the possible hydrological impact of climate change in Omo-Gibe river basin based on the downscaled precipitation and temperature scenarios data.
- To quantify the possible impacts of the climate change on the water resources availability of Omo-Gibe river basin for the coming 31 years (2020 to 2050); this includes assessment of inflow in to Gibe III reservoir with the changing climate condition.
- Developing of daily flow data for un-gauged part of the catchment, which is one of the flow contribution catchment to Gibe III dam site.
- Estimating of evaporation loss from Gilgel Gibe I and Gibe III reservoir for future time period
- And finally to give the necessary information and create awareness for planners, decision makers and communities for the necessary preparation related to the availability of water with the hypothetical climatic change conditions in the future.

## 1.6 Importance of the study

The significance of investigating climate change and their impacts on economy, social life, food security, hydrology and hydropower generation has been highlighted by many researchers for planning and sustainable management of natural resources in many parts of the world. Climatic variability, including changes in the frequency of extreme events (like droughts, floods and storms) have always had a large impact on humans. Particularly severe drought. Regarding with water resource use is the generation of energy by constructing renewable hydroelectricity generating dams will face problems because of the change in hydrological regimes of the basin due to climate change.

Current power generation capacity in Ethiopia is approximately 2,060 MW, of which 95 percent is generated from hydroelectric generators. Out of these power generation plants currently two of them are found in Omo-Gibe basin these are; Gibe I which has the installed capacity of 184 MW and Gibe II total installed capacity of 420 MW. This constitutes nearly 30.2%. Presently Gibe III hydropower project is on construction. At completion the project will generate 1780MW.

Ministry of water and energy in Ethiopia is a governmental organization which is responsible for the country's water and energy sector development, with the mission to play a significant goal in the socio-economic development of Ethiopia through development and management of its water and energy resources in a sustainable manner and provision of quality and equitable supplies in the entire food security and foreign currency earning (Geteneh A., 2013).

It is clear that climate change already has severed human impact today, but it is one of the neglected study areas in Ethiopia especial in Omo-Gibe basin. Because of this, there is no systematic research on techniques that deal with effects of climate change on water resources potential in Omo-Gibe basin for sustainable water resources management which have been carried out in detail before. Accordingly, an integrated climate change and hydrology simulation approach that takes in to account the availability of water under prediction of the different climatic scenarios will have a paramount importance in the development of sustainable water resources management and in fulfilling of the mission of Ministry of water and energy of Ethiopia. Understanding the types and impacts of climate change is an essential indicator for resource base analysis and development of effective and appropriate infrastructure for sustainable management of natural resources in the country in general and at the study area in particular.

Therefore, the contribution of this research is a newly developed technique with the objective of downscaling climate scenario and assessing future available water resources for different use. Moreover, it presents a method to quantify climate change and their impact on hydrological regime. This has been achieved through a method that combines climate outputs and physical-based, semi-distributed hydrological models (SWIM) to simulate the hydrological processes and geographical Information. In addition to this one of the hindrances in Omo-Gibe basin for research is, availability of flow data especially daily flow data, since the basin has poorly developed hydrometric networks because of lack of human and financial resources. With this regard also this research filled the gap in getting of flow data on the main river course for reference time period of 29 years (1970-1998).

## 1.7 Thesis layout

The thesis is organized into nine chapters; Chapter 1 highlights the research in the form of introduction by giving some background and rational of the study, also pin points the general objective and specific objectives of the study together with the significance of this study to Omo Gibe basin are discussed. Chapter 2 presents the review of previous work of various researchers about climate change in general. Moreover, assessing of climate change problems and their effects in Ethiopia has been described in detail. Chapter 3 describes

hydrological modeling in the context of climate change, selection criteria of hydrological modeling for climate change study, description of the selected hydrological model and hydrological processes in the model elaborated. Chapter 4 presents descriptions of the study area and salient features of available hydropower stations in the study area are clarified. Chapter 5 deals with description of hydrological and meteorological data used for this study, methodology that have been employed for downscaling of REMO and GCM meteorological data sets, their results and discussion elaborated in detail.

Chapter 6 encompasses application of SWIM hydrological model for Abelti and Un-gauged basin, calibration and validation of the model also described for the purpose of derivation of daily flow data from un-gauged part of the basin for reference time period. Moreover, estimation of mean annual flow at Gibe III dam site and un-gauged part of the basin using different empirical relationships for reference time period has been elaborated.

Chapter 7 focuses on setup and calibration of SWIM at Gibe III dam site, mainly for the purpose of investigating, effects of climate change on Gibe III inflows for the coming 31 years (2020-2050). Chapter 8 focuses on modeling of the basin under climate change scenarios and analysis of future time flow carried out. Chapter 9 provides conclusion and recommendation of the entire work.

## **1.8 Frame work of the study**

The method to evaluate the impacts of climate change on water resources potential of Omo Gibe basin can be achieved through integrating climate modeling like REMO and GCM outputs, GIS and hydrological model SWIM.

At the beginning of the work precipitation and temperature scenarios for the years 1970–2050 with daily temporal resolution interpolated with bilinear interpolation from the four nearest RCM (REMO) grid points to all weather observation stations. In addition to this; precipitation and temperature scenarios downscaled using SDSM model from the nearest GCM point to each weather observation station of Omo Gibe basin. Impact studies on climate change require realistic assessments of future climate change at specific regions or locations. In consideration of this, for the purpose of getting bias free climate model outputs a distribution mapping method employed for adjusting dynamically downscaled interpolated precipitation and temperature scenarios.

In order to create an initial model setup for SWIM, records of stream flow data are needed as input to the model in addition to other sources of data. Therefore, these inflows time series data should be available in both appropriate quantity and quality. Such inflow time series data is missing in some part of un-gauged Omo basin. This un-gauged basin is one which doesn't have any records for historical period of hydrological observations to enable computations of hydrological variables of interest (both model calibration and calculation of available water for future time series) at the appropriate spatial and temporal scales. This was a major difficulties encountered either for the simulation of current or future SWIM model set up. However, to fill this gap rainfall runoff modeling technique was employed to generate daily flow from this un-gauged catchment.

SWIM semi-distributed, process-based eco-hydrological model that allows several different subunits or objects to be defined within a watershed is utilized (Huang et.al, 2010). This can be parameterized using regionally available data. Simulation of the model for gauged catchment offers outputs that assist to integrate our knowledge of hydrologic systems of the gauged catchment to un-gauged catchment of the basin. Using this technique daily flow data for un-gauged catchment was developed. After wards estimation and projection of available water resources for Omo Gibe basin developed, which is particularly useful in the estimation and projection of future water requirements for hydropower generation and other uses under the changing climate condition.

This research therefore extends the integration of a hydrologic model SWIM with a newly developed climate downscaling methodology for the purpose of determining future water availability and strategies for the management of scarce water resources for production of hydropower and other uses. Details of the approaches are given in Figure 1.1.

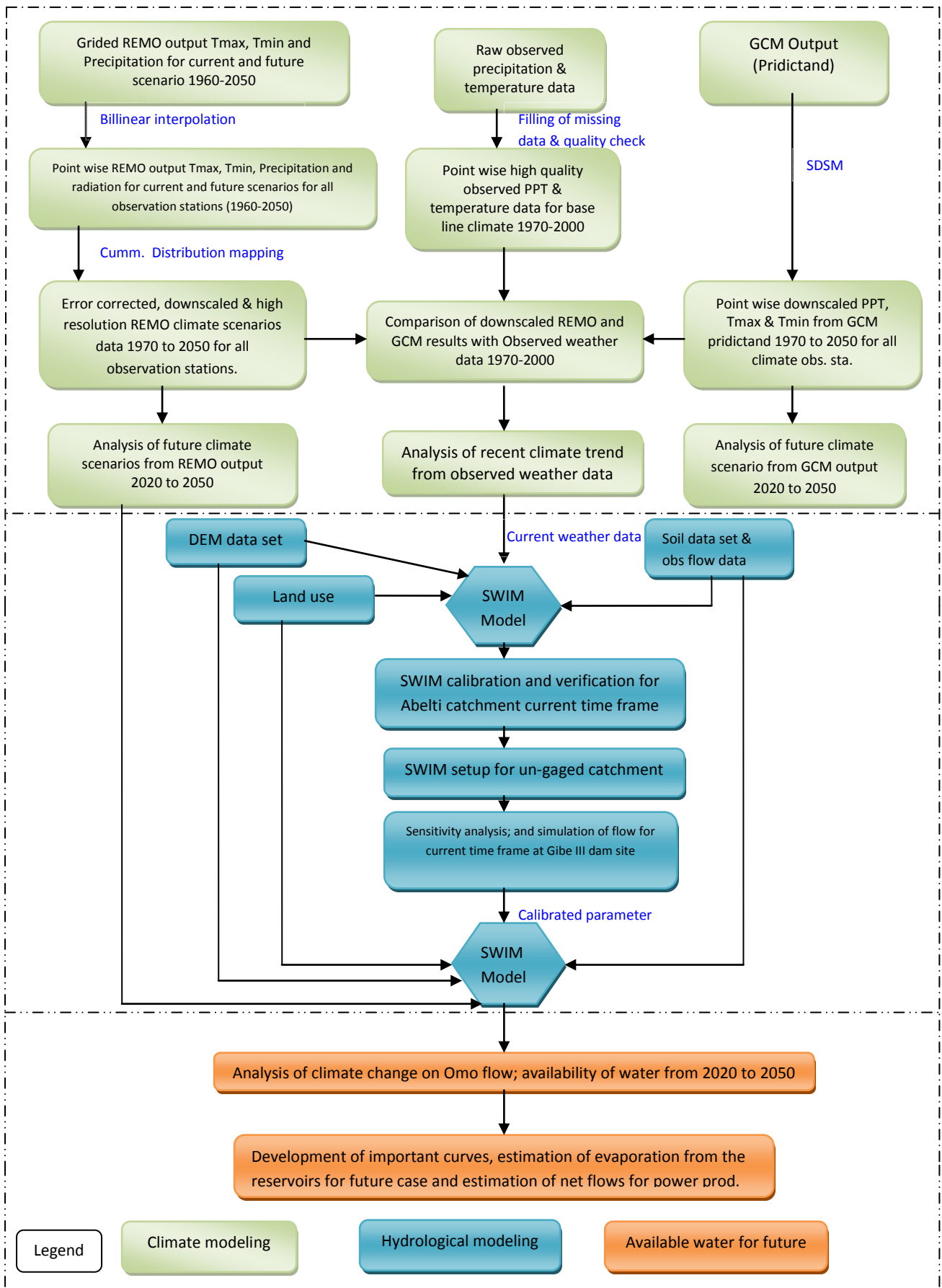


Figure 1.1 Flow chart of the methodology followed throughout of this research

# Chapter 2 Literature Review about Climate Change

## 2.1 Introduction

Scientists look in many places to find clues about climate change. For example; they examine historical records, collect measurements, and observe trends in temperature, weather patterns, sea level, and other features of the environment. Because there are so many clues from all over the world that the climate is changing from time to time, we know that climate change is already happening today and it imposed so many problems.

According to (IPCC, 2007) climate change can be defined as a change in the state of the climate that can be identified (e.g. using statistical tests) by changes in the mean and/or the variability of its properties, and that persists for an extended period, typically decades or longer. It refers to any change in climate over time, whether due to natural variability or as a result of human activity. So one way of detecting such an influence is through long-term changes in mean conditions, preferably guided by climate model studies as to which variables and how they should change. This requires long averages to overcome the effects of natural variability (climate noise), and for quantities such as global temperatures (Santer et al. 2011). Accordingly, a change in climate is most likely to be perceived by encountering new “weather” and breaking records of changes in the extremes. Changes in certain extremes, such as higher temperatures and increases in heavy rains and droughts are expected with climate change (IPCC 2007; Trenberth., 2011a). Extremes are always expected to happen as the climate record gets longer, but certain extremes related to heating are becoming more evident. For example in the United States, extremes of high temperatures have been occurring at a rate of twice those of cold extremes (Meehl et al. 2009), and this has accelerated considerably since June 2010 to a factor of 2.7, and in the summer of 2011 to a factor of over 8 (Skolnik., 2011).

As climate varies or changes because of human and other induced factor, several direct influences alter precipitation amount, intensity, frequency, and type (Trenberth, 2011a). Warming accelerates land-surface drying as heat goes into evaporation of moisture, and this increases the potential incidence and severity of droughts, which has been observed in many places worldwide (Dai., 2011).

Scientists are frequently asked about increasing climate change events especially change in global surface temperature. Different climate researcher are given similar answer to this question for instance (Trenberth K., 2012) gave a short and precise answer to this question on his study “framing the way to relate climate extremes to climate change” as; all-weather events are affected by climate change because the environment in which they occur is warmer and moister than it used to be.

The general change in global climate is very fast from time to time this include the change in global temperature always shows an increasing trend and the rise in sea level due to melting ice for the past time frame. If these change are continue in these patter climate change might have a devastating impact on natural resources and human being. (IPCC 2007) report noted that eleven of the last twelve years (1995-2006) rank among the twelve warmest years in the instrumental record of global surface temperature (since 1850). The linear warming trend over the 50 years from 1956 to 2005  $0.13^{\circ}$  [0.10 to 0.16]  $^{\circ}\text{C}$  per decade is nearly twice that for the 100 years from 1906 to 2005. Recently the temperature increase is widespread over the globe. Increases in sea level are consistent with warming. Global average sea level rose at an average rate of 1.8 [1.3 to 2.3] mm per year over 1961 to 2003 and at an average rate of about 3.1 [2.4 to 3.8] mm per year from 1993 to 2003 (IPCC 2007). There is very high confidence, based on more evidence from a wider range of studies, that recent warming is strongly affecting hydrology, ecosystem and fresh water availability. Observational evidence



from all continents and most oceans shows that many natural systems are being affected by regional climate changes, particularly temperature increases.

The causes for all these climate change can be taken as natural and anthropogenic drivers including the chain from greenhouse gas (GHG) emissions to atmospheric concentrations to radiative forcing to climate responses and effects. Greenhouse gas (GHG) emissions resulting from the provision of energy services have contributed significantly to the historic increase in atmospheric GHG concentrations (IPCC 2012). The IPCC Fourth Assessment Report (AR4) concluded that “Most of the observed increase in global average temperature since the mid-20th century is very likely due to the observed increase in anthropogenic greenhouse gas concentrations. As very well know carbon dioxide (CO<sub>2</sub>) is the most important anthropogenic GHG. Its annual emissions have grown between 1970 and 2004 by about 80%, from 21 to 38 gigatonnes (Gt), and represented 77% of total anthropogenic GHG emissions in 2004. The rate of growth of CO<sub>2</sub>-eq emissions was much higher during the recent 10-year period of 1995-2004 (0.92 GtCO<sub>2</sub>-eq per year) than during the previous period of 1970-1994 (0.43 GtCO<sub>2</sub>-eq per year) (IPCC 2007).

## **2.2 Climate models**

### **2.2.1 (GCM) General circulation model**

Climate models, both global and regional, are the primary tools that aid in our understanding of the many processes that govern the climate system (S. Jeremy et al., 2007). Climate is one of the most challenging geophysical systems to simulate because of the number of interacting components and the wide range of time and spatial scales of relevant processes and their complexity (Laprise R., 2008). Global climate models also known as general circulation models (GCMs) are the most complex of climate models, since they attempt to represent the main components of the climate system in three dimensions. According to many research GCMs are the vital resource used to perform climate change experiments regionally, globally and very fine scale up to point climate pattern from which climate change scenarios are derived; but they have main drawbacks because of their coarse resolution. Most of the time they lack producing of current climate trend including the most important statistical parameters like mean and variance.

GCMs depict the climate using a three dimensional grid over the globe, typically having a horizontal resolution of between 250 and 600 km, 10 to 20 vertical layers in the atmosphere and sometimes as many as 30 layers in the oceans. Their resolution is thus quite coarse relative to the scale of exposure units in most impact assessments. Moreover; many physical processes, such as those related to clouds, also occur at smaller scales and cannot be properly modeled. Instead, their known properties must be averaged over the larger scale in a technique known as parameterization. This is one source of uncertainty in GCM-based simulations of future climate (IPCC-TGICA 2007). A few years ago, GCMs only included a representation of the atmosphere, the land surface, sometimes the ocean circulation, and a very simplified version of the sea ice. Nowadays, GCMs take more and more components into account, and many new models now also include sophisticated models of the sea ice, the carbon cycle, ice sheet dynamics and even atmospheric chemistry (Goosse H. et al., 2013).

### **2.2.2 Regional climate model**

A regional climate model (RCM) is a climate model of higher resolution than a global climate model (GCM). It can be nested within a global model to provide more detailed simulations for a particular location. Local climate change is influenced heavily by local topographical features such as mountains. Due to their coarse resolution, small-scale topographical

features are not picked up by GCMs. RCMs have a higher resolution than a GCM (~ 25 km) even less and are influenced by a smaller scale of topographical features. It is much more computationally intensive to run an RCM so they are usually run over a limited area<sup>4</sup>.

Regional models have been used to conduct climate change experiments for many regions of the world. These methods of obtaining sub-grid scale estimates (commonly down to 50 km resolution or less) are able to account for important local forcing factors such as surface type and elevation, which conventional GCMs are unable to resolve. They have the advantage of being physically based, but are also highly demanding of computer time. For this reason, until recent years there had been very few simulations for a sufficient period of simulated years to allow meaningful climate change statistics to be extracted. Furthermore, the commonest approach, nesting, is still heavily reliant on specialized GCM outputs for its boundary conditions. GCMs do not always provide good simulations of the large scale flow and there can be inconsistencies between the behavior of the physical parameterizations in the driving model and in the finer grid of the regional model (IPCC-TGICA 2007).

Any regional climate modeling approach affords an increase of resolution over a region of the globe of about one order of magnitude compared to CGCMs, with regional grid-point spacing of a few tens of km in the horizontal, for operational use on climate timescales (Laprise R., 2008).

## 2.3 Downscaling techniques

Downscaling, or regionalisation, is the term given to the process of deriving finer resolution data (e.g., for a particular site) from coarser resolution GCM or RCM data set.

Although regional climate models (RCMs) are powerful tools for describing regional and even smaller scale climate conditions, they still feature severe systematic errors (Jakob T. et al., 2011). The projections of the estimates of GCM and RCM climate variables either for present or future period obtained directly from simulation of GCM and RCM outputs are of limited value for any study as the spatial resolution of both results are coarse in nature to resolve many sub-grid scale. This characteristics makes the outputs are always unreliable at individual grid. Spatial downscaling methods have been proposed to solve this problem. The methods used to convert GCM or RCM outputs into local meteorological variables used for hydrological modeling or any other regional climate study are referred to as downscaling techniques (wood et al., 2004; Coulibaly, 2005). Nowadays, there are different types of downscaling methods to provide very fine scale GCM and RCM results at point scale; for instance some of the methods are mentioned in (Jakob T. et al., 2011) as linear and nonlinear empirical-statistical downscaling techniques. Direct point-wise methods like quantile mapping and local intensity scaling as well as indirect spatial methods as nonlinear analogue methods yield systematic improvements in median, variance, frequency, intensity and extremes of daily precipitation. Multiple linear regression methods, even if optimized by predictor selection, transformation and randomization, exhibit significant shortcomings for modelling daily precipitation due to their linear framework. The other downscaling technique which is referred to as dynamical downscaling method mainly applied to derive regional-scale information from GCMs ((Jakob T. et al., 2011). Particularly, small-scale patterns of daily precipitation are highly dependent on model resolution and parameterization and can often not be used directly in climate change impact assessment studies (Fowler et al., 2007).

Recently, the availability of regional RCM-based climate scenarios for different part of the world tremendously increased; it is possible to mention REMO. Recently this regional climate model is available for Ethiopia. However, due to the error characteristics of RCMs it is not possible to use directly for any climate change study in the region when climate information

---

<sup>4</sup> <http://ukclimateprojections.defra.gov.uk/23249> as visited on August 2013



at the point scale is needed. Therefore to overcome this drawback downscaling or bias correction should be employed before using the results of this RCM or GCMs.

## 2.4 Scenarios and their purpose

Future greenhouse gas (GHG) emissions are the product of very complex dynamic systems, determined by driving forces such as demographic development, socio-economic development, and technological change. Scenarios are alternative images of how the future might unfold and are an appropriate tool with which to analyse how driving forces may influence future emission outcomes and to assess the associated uncertainties. They assist in climate change analysis, including climate modeling and the assessment of impacts, adaptation, and mitigation (IPCC 2000).

SRES refers to the scenarios described in the IPCC special report on emissions scenarios (SRES, 2000). The scenarios are grouped into four scenario families (A1, A2, B1 and B2) that explore alternative development pathways, covering a wide range of demographic, economic and technological driving forces and resulting GHG emissions. The scenarios do not include additional climate policies above current ones. The emissions projections are widely used in the assessments of future climate change, and their underlying assumptions with respect to socio-economic, demographic and technological change serve as inputs to many recent climate change vulnerability and impact assessments.

The scenarios are based on different storylines of socioeconomic and demographic developments covering a wide range of plausible and consistent possible future developments. Depending on several assumptions related to economic growth, energy intensity and efficiency as well as the growth of the world population, in IPCC special report 2000 four scenario families have been worked out providing the radiative forcings for a large number of climate model runs (A1, A2, B1, B2).

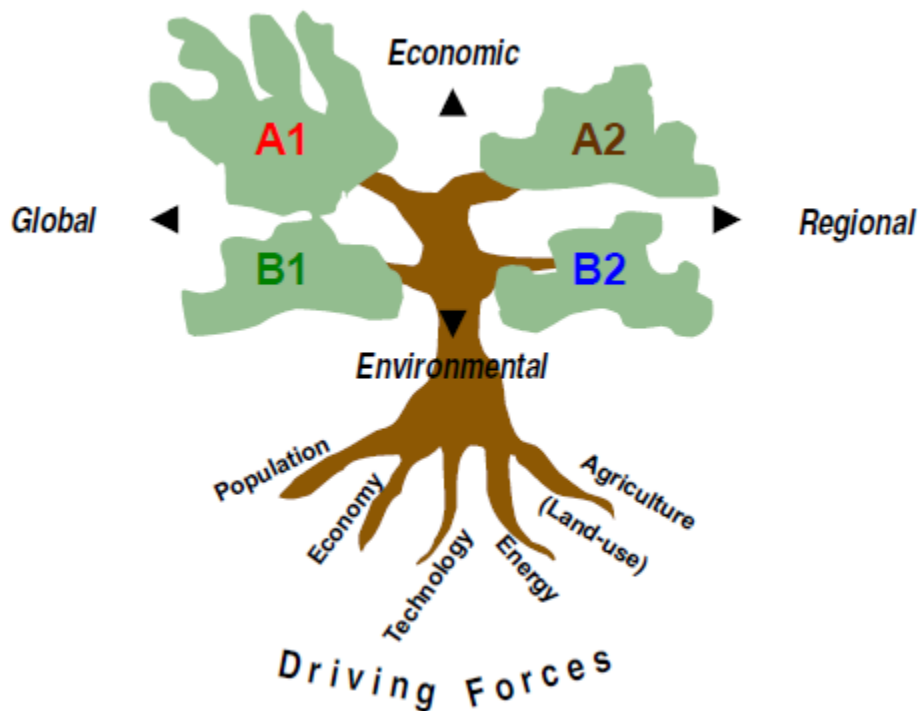


Figure 2.1 The four IPCC SRES scenario storylines (after Nakicenovic et al., 2000).

In simple terms, the four storylines combine two sets of divergent tendencies: one set varying between strong economic values and strong environmental values, the other set between increasing globalization and increasing regionalization (IPCC-TGICA 2007).

The A-families are characterized by a domination of economic drivers, whereas the B families assume environmental concerns to be the driving force. A further differentiation is given by the number associated with the scenario families. While the A1 and B1 scenario families are rather globally orientated, the A2 and B2 scenario families pursue a rather regional policy. The following gives a brief survey of the scenario families and their main characteristics as presented by the (IPCC 2000).

A1: The A1 storyline and the associated scenarios are based on an expanding economic prosperity together with a rapid introduction of new and more efficient technologies. The global population reaches its maximum in the mid-century followed by a later decline in population up to the year 2100. Following its rather global orientation, an increase of cultural and social interactions as well as a substantial reduction in regional differences in per capita income is assumed. The scenario family distinguishes between three directions of technical change in the energy system represented by three different scenario groups. While for the A1T scenario group technological emphasis is put on non-fossil energy sources, the A1FI scenario group assumes an intensive use of fossil energy sources. Not relying on one particular energy source, the A1B scenario group assumes a balanced employment and further development of all available energy sources.

A2: The A2 storyline and scenario pictures a very heterogeneous world characterized by a society willing to preserve local identities. Population is continuously growing due to a retarding convergence of fertility patterns across the regions. Economic development takes place on a regional level with per capita economic growth and changes in technology taking much more time compared to other scenarios.

B1: The B1 scenario and storyline displays a convergent world with similar population growth as in the A1 scenario storyline. Economic structures develop toward a service and information economy going together with an introduction of clean and resource efficient technologies. Solutions to social, economic and environmental sustainability are pursued on a global level, thus not creating additional climate initiatives.

B2: The B2 scenario and storyline pictures a world in which the goals of economic, social and environmental sustainability are pursued on a local and regional level. The world population is continuously growing, however, not as rapidly as in the A2 storyline. Economic development is less distinct and technical change takes more time and is more diverse compared to the storylines of B1 and A1B.

Storyline, scenario and scenario family can be defined as based on (IPCC-TGICA 2007) as follow:

- ✓ Storyline, a narrative description of a scenario (or a family of scenarios), highlighting the main scenario characteristics and dynamics, and the relationships between key driving forces.
- ✓ Scenario, projections of a potential future, based on a clear logic and a quantified storyline.
- ✓ Scenario family, one or more scenarios that have the same demographic, politico-societal, economic and technological storyline.

The basic features of each of the four storylines included quantitative projections of major driving variables such as population and economic development taken from reputable international sources for instance United Nations and World Bank. The storylines were then fully quantified using integrated assessment models, resulting in families of scenarios for

each storyline. In all, 40 scenarios were developed by six modelling teams (Figure 3.3) (IPCC-TGICA 2007).

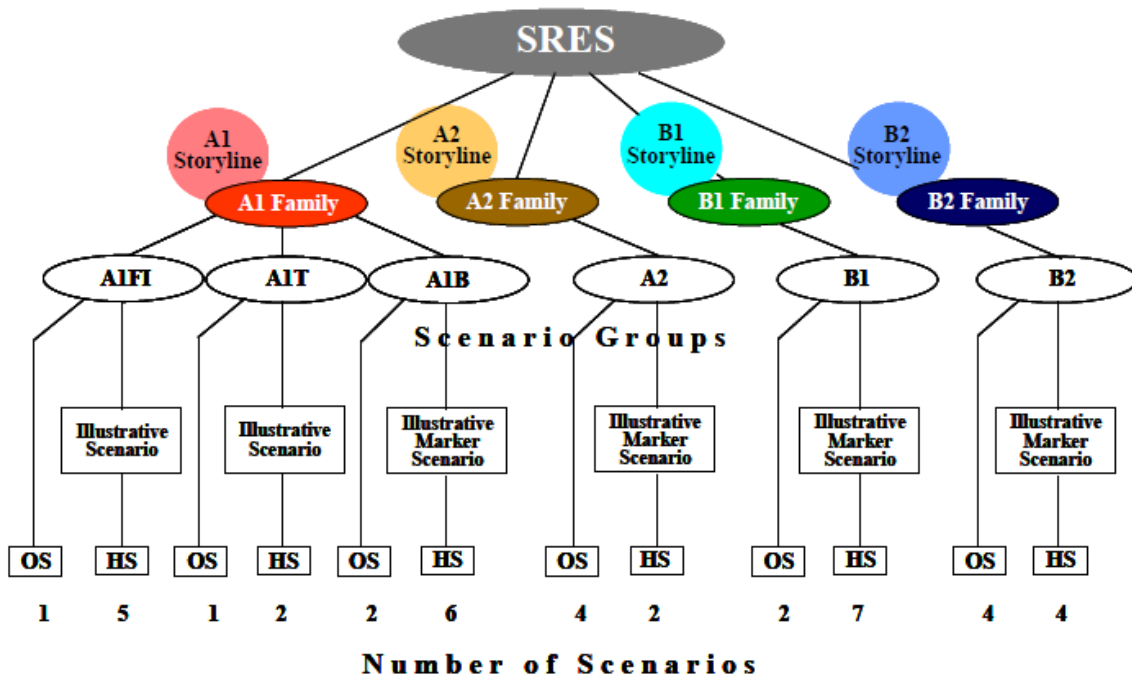


Figure 2.2 Structure of the storylines and scenarios in the IPCC special report on emissions scenarios

From the four sets of scenarios in figure 2.2 called A1, A2, B1 and B2, 40 SRES scenarios have been developed by six modeling teams. All are equally valid with no assigned probabilities of occurrence. The set of scenarios consists of six scenario groups drawn from the four families: one group each in A2, B1, B2 and three groups within the A1 family, characterizing alternative developments of energy technologies: A1FI (fossil fuel intensive), A1B (balanced) and A1T (predominantly non-fossil fuel). Within each family and group of scenarios, some share “harmonized” assumptions on global population, gross world product, and final energy, these are marked as “HS” for harmonized scenarios. “OS” denotes scenarios that explore uncertainties in driving forces beyond those of the harmonized scenarios. The number of scenarios developed within each category is shown. For each of the six scenario groups an illustrative scenario (which is always harmonized) is provided. (IPCC 2000).

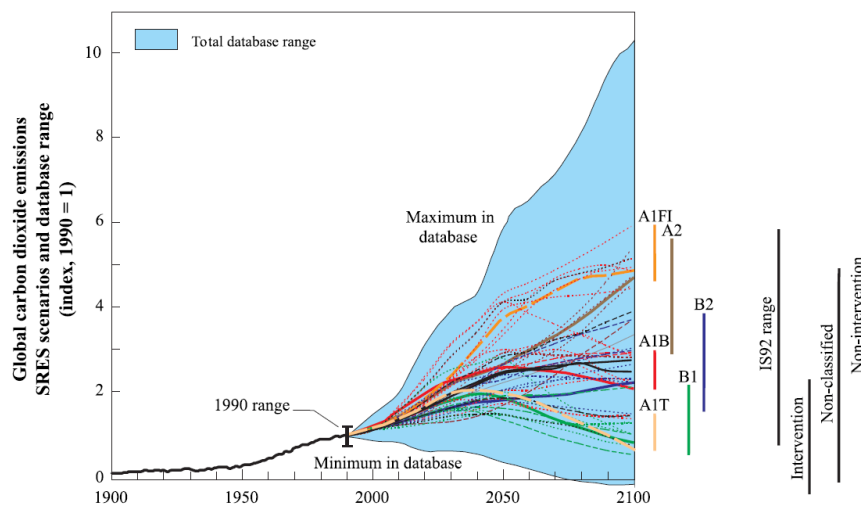


Figure 2.3 global CO<sub>2</sub> emissions related to energy and industry (IPCC 2000)

## **2.5 The expected impacts from climate change**

The increasing awareness that enhanced levels of greenhouse gases of direct/natural or indirect anthropogenic origin in earth's atmosphere might change the climate of different regions of the world, in the long run, has recently instigated a great deal of research into the projection of regional responses to global climate change. Various general circulation model (GCM) experiments and studies indicate that a substantial rise in global temperature would be expected as a consequence of a doubling of carbon dioxide (CO<sub>2</sub>) concentrations. As a result, climatic processes are likely to intensify, including the severity of hydrological events such as; droughts, flood waves, and heat waves (Meenu R., 2013). These projected effects of possible future climate change would significantly affect many hydrologic systems, which in turn affect the water availability and runoff and the flow in rivers. Climate change is already having a profound effect on climate system, hydrology, human being, ecosystem, flooding and drought, snowpack, sea level, and river flows etc.

### **2.5.1 Hydropower impact**

Hydropower is a renewable energy source where power is derived from the energy of water moving from higher to lower elevations. Most hydropower projects are developed by construction a huge hydraulic structure (dam) to create an artificially created manmade lake to store the flowing water for power production. Hydropower sector is one of the systems that might be affected by climate change. Currently due to the advancement of different technology; the rising demand for electricity is observing all over the world especially in Africa. Indeed Ethiopian hydropower takes the lion's share of the energy production the role of climate change may alter the power demand of the country for the coming time period. Although precipitation is anticipated to increase in global level many part of the world are anticipated to see significant drying. Studies indicate that temperature will be increased in most part of the world; regarding to this an increasing trend has been observed in Ethiopia and it will be projected to increasing in the coming time. As the temperature increases the water which will be lost as evaporation from the reservoir will increase in combination of this and declining stream flow as a result of climate change will lead to decline to hydropower production.

### **2.5.2 Water supply and flood impact**

Eventhough, there are no studies conducted regarding to effects of climate change on water supply system to Ethiopian condition, there are a number of researches conducted on this issue around the globe. For instance for mountainous regions of the northeastern U.S. these changes can reduce annual snowpack accumulation, accelerate snowmelt processes and increase water losses due to evapotranspiration (ET) which may lead to more winter flooding and reduced summer flows (Brekke et al. 2009 and Matonse et al. 2011) because of this change it will have change in the river flow in different seasons there by it will affect the demand. The potential impact of climate change on the ability to meet future water supply demands for high quality drinking water and for industrial use might face the same problem, the reason for this justification might be the amount of water which will lost in the form of evaporation might be increase due to high projected future temperature in the region especially in Africa. In general climate change will have a significant effect on hydrological cycle of the watershed.

### **2.5.3 Effects on drought**

While drought has several causes, climate scientists say global warming is a long-term contributor that could be exacerbating current conditions, especially in the already-arid areas. They say it will likely do more damage in the future. Because temperatures cause more

water to evaporate, and unless there's enough rain to offset it, the ground dries up<sup>5</sup>. Even this condition might be worse for areas which are characterized as arid zone.

## **2.6 Climate change studies in Ethiopia**

The nature of Ethiopia's agriculture, primarily rain-fed, means that production is sensitive to fluctuations in rainfall. Ethiopia is one of the countries where climate change studies are rarely taking place because of different problems. One of the problems lacks of awareness between different societies regarding to climate change. To the contrary most African countries including Ethiopia are widely held to be highly vulnerable to future climate change and Ethiopia is often cited as one of the most extreme examples (Conway D. et al., 2011). Despite the prevalent view of Ethiopia's high sensitivity, there have only been a few attempts to quantify the effects of climate change in different sectors like economy, hydropower, water supply availability of water in a basin and ecosystem. In this part of literature review an attempt has been carried out on the available literatures and case studies related to climate change in Ethiopia and the study area (Omo basin).

### **2.6.1 Rainfall variability and trend**

According to Ministry of water and energy of Ethiopia study (UN-WATER/WWAP/2006/7) trend analysis of annual rainfall show that rainfall remained more or less constant when averaged over the whole country while a declining trend has been observed over the northern half of the country and south western Ethiopia. On the other hand an increasing trend in annual rainfall has been observed in central Ethiopia. The following figures show the year to year variation of rainfall over the country expressed in terms of normalized rainfall anomaly averaged for 42 stations. Area averaged rainfall anomalies for northern half of Ethiopia, central Ethiopia and south western Ethiopia are also shown respectively. As it can be seen from the figures the country has experienced both dry and wet years over the last 50 years. Years like 1965 and 1984 were extremely dry while 1961, 1964, 1967, 1977 and 1996 were very wet years.

---

<sup>5</sup> www.ustody.com

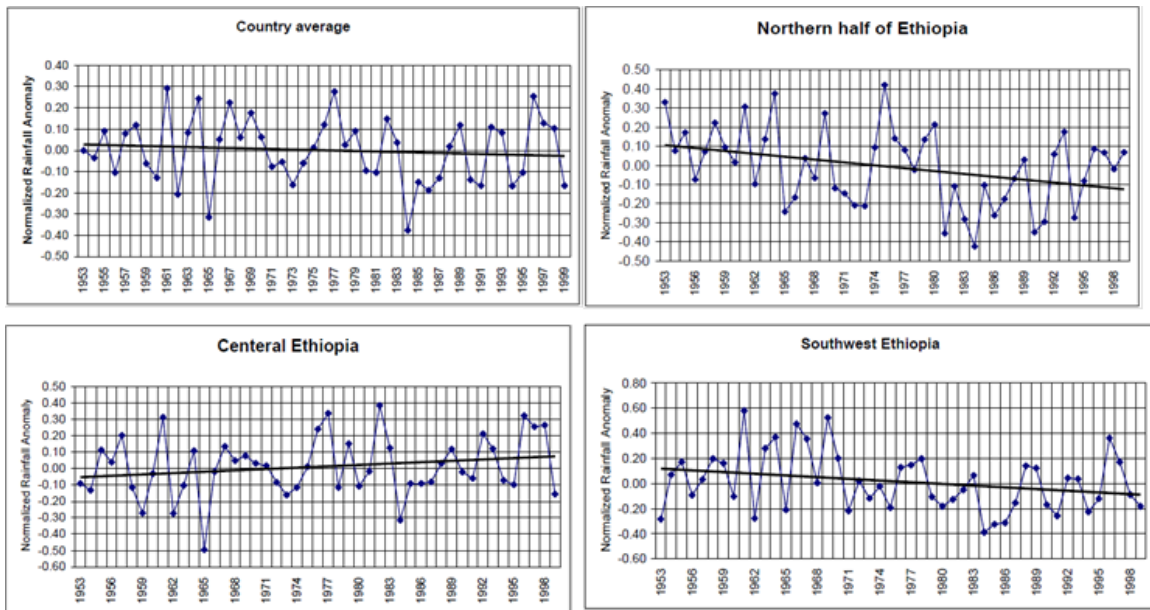


Figure 2.4 Year to year variability of annual rainfall over the whole country, northern half, central and south western Ethiopia expressed in normalised deviation.

## 2.6.2 Temperature variability and trend

Again from the same study document the overall temperature in the whole country show an increasing trend for the entire country. Based on (UN-WATER/WWAP/2006/7 2006/7) revealed that there has been a warming trend in temperature over the past 50 years. The average annual minimum temperature over the country has been increasing by about 0.25 °C every ten years while average annual maximum temperature has been increasing by about 0.1 °C every decade. It is interesting to note that the average annual minimum temperature is increasing faster than the average annual maximum temperature.

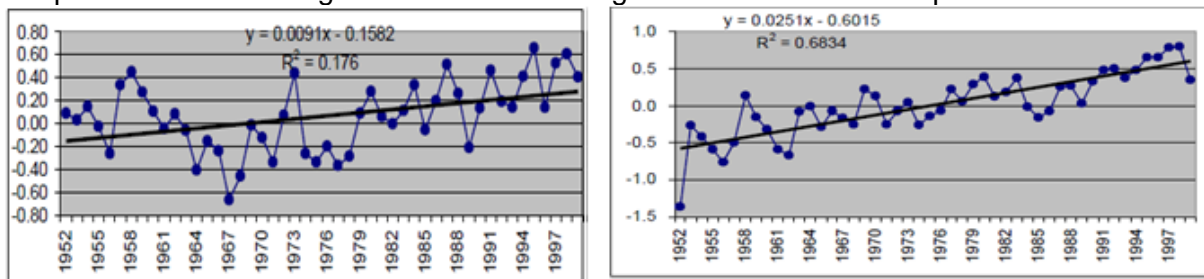


Figure 2.5 Year to year annual mean maximum and minimum temperature variability trend over Ethiopia respectively.

## 2.6.3 Case studies related to climate change in Ethiopia

According to UNDP climate change study (date of visit 2013) which has been conducted in university of Oxford for the entire Ethiopia have pointed out that the recent climate trend showed that mean annual temperature has increased by 1.3°C between 1960 and 2006, an average rate of 0.28°C per decade. The increase in temperature in Ethiopia has been most rapid in July, August and September (JAS) at a rate of 0.32°C per decade. Daily temperature observations show significantly increasing trends in the frequency of hot days<sup>6</sup>, and much large increasing trends in the frequency of hot nights. The frequency of cold<sup>7</sup> days has

<sup>6</sup> 'Hot' day or 'hot' night is defined by the temperature exceeded on 10% of days or nights in current climate of that region and season.

<sup>7</sup> 'Cold' days or 'cold' nights are defined as the temperature below which 10% of days or nights are recorded in current climate of that region or season.



decreased significantly in all seasons except December, January and February (DJF). The frequency of cold nights has decreased more rapidly and significantly in all seasons. Regarding to the precipitation trend for current time there is not a statistically significant trend in observed mean rainfall in any season in Ethiopia between 1960 and 2006. Decreases in JAS rainfall observed in the 1980s have shown recovery in the 1990s and 2000s. In addition to current climate change trend UNDP climate change study investigated the change in climate for future case; this study investigated GCM projections of future climate in Ethiopia according to the result the mean annual temperature is projected to increase by 1.1 to 3.1°C by the 2060s, and 1.5 to 5.1°C by the 2090s. Under a single emissions scenario, the projected changes from different models span a range of up to 2.1°C. Regarding to the change in precipitation regime projections from different models in the ensembles are broadly consistent in indicating increases in annual rainfall in Ethiopia. These increases are largely a result of increasing rainfall in the 'short' rainfall season (OND) in southern Ethiopia. The full study document of this can be accessed from <http://country-profiles.geog.ox.ac.uk>.

According to IPCC mid-range emission scenario, the mean annual temperature will increase in the range of 0.9 -1.1 °C by 2030, in the range of 1.7 - 2.1 °C by 2050 and in the range of 2.7-3.4 °C by 2080 over Ethiopia compared to the 1961-2000 normal. Moreover, a small increase in annual precipitation is expected over the country (NMAE 2007). At a watershed scale in Ethiopia, through regressions of seasonal rainfall averages against time, it was found that a significant decline in June to September rainfall (i.e. winter) for the Baro- Akobo, Rift-Valley and Southern Blue Nile watersheds located in the south- western and central parts of Ethiopia (Wing et al., 2008).

The impact of climate change on the water resources of the Lake Tana sub-basin is significant. If the temperature is increased by 2 °C and there is no change in rainfall, the mean annual flow will be decreased by 11.3%. But if the rainfall is decreased by 10% and 20% the decrease in runoff will be 29.3% and 44.6% respectively. On the other hand, if the rainfall is increased by 10% and 20%, the mean annual runoff will increase by 6.6% and 32.5% respectively. The research findings revealed that the water resources of the Lake Tana area are highly vulnerable to climate change, especially in the distribution of runoff throughout the year. With climate change, the runoff may become much more seasonal and as a result small streams may dry up completely for part of the year (Tarekegn and Tadege, 2006).

Research on Awash River Basin indicated that the basin would be significantly affected by the changed climate; that is, a considerable water deficit is projected for the future by employing various models. All the models suggested that global warming would result in a general increase in dryness, which would decrease water availability. Moreover, a 20% decrease in rainfall in the basin coupled with a 2°C increase in temperature would result in a 41% decrease in the annual runoff. Even a temperature increase of 2°C without precipitation change would result in a 9% decrease in annual runoff. On the other hand, an increase of precipitation by 10% would offset a 2 to 4°C increase in temperature and result in a surplus of runoff ranging from 4 to 12%. In general warming in the Awash River basin simulated by various models would result in a substantial decrease in annual runoff over the basin (Kinfe., 1999).

The other case study considered for this part of literature review was (Conway D. et al., 2011), relatively this study can be considered as a recent study regarding to climate change in Ethiopia. In this study the researchers have examined the changing nature of climate risks using analysis of recent climate variability, future climate scenarios and their secondary impacts. In their study they have assessed the effects of climate variability on agricultural production and national GDP. Based on the findings of this study rainfall behavior in Ethiopia shows no marked emergent changes and future climate projections show continued warming but very mixed patterns of rainfall change. The detail of model projections of future climate is

described as follow. The following figure shows the area average future change for the whole of Ethiopia for three 30-year periods (2020s, 2050s and 2080s) with A2 emissions. Change in rainfall is plotted against change in temperature for each model and the multi-model average. The multi-model average shows warming in all four seasons in all regions.

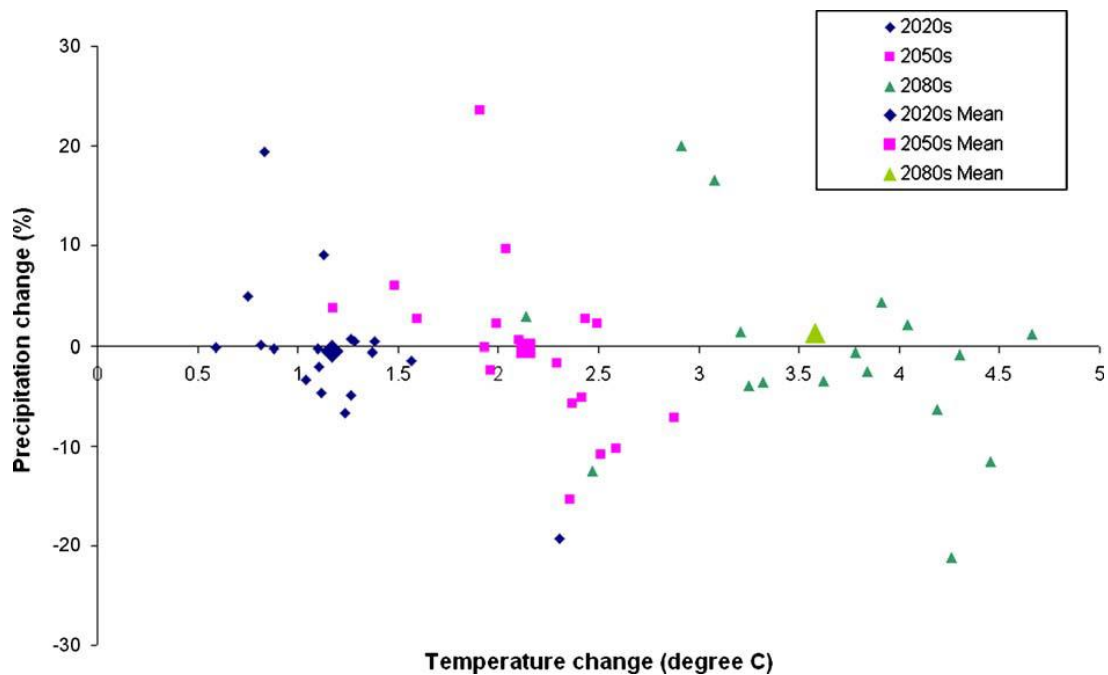


Figure 2.6 Climate model projections of wet season (June–August) temperature and rainfall for the 2020s, 2050s, and 2080s with 18 climate models for all Ethiopia (Conway D. et al., 2011).

With annual warming in Ethiopia by the 2020s of 1.2 °C with a range of 0.7–2.3 °C (2050s 2.2 °C, range 1.4–2.9 °C). The regional differences in warming are relatively modest. Warming will be associated with greater frequency of heat wave events and is likely to lead to higher rates of evaporation. Moreover their study justified that climate models show different projections of annual rainfall over Ethiopia, with some models projecting more rain, others less, but with a tendency for slightly wetter conditions. There are very small changes in multi-model average annual rainfall for the 2020s (+0.4%) and 2050s (+1%).

## 2.7 Conclusion

One of the main challenge regarding to climate change in Ethiopia in general and Omo Gibe in particular, availability of published literature in the region. This shows that very little work has been done to quantify or model in detail the effects of climate variability or extremes at different level especially in Omo Gibe basin. (D. Conway et al., 2011) explained that at present there is no coordinated programme of research on climate and climate change in Ethiopia, supported by the GoE, or any other body, although there has been very rapid growth in activities on the issue. Because of this it was not possible to include specifically any published literature regarding to climate change condition in Omo Gibe basin. However, based on the reviewed literatures about the whole country they indicated that there will be an increasing trend of maximum and minimum temperature in Ethiopia more over they noticed, as there will be small change (increasing sign) in precipitation, but no one of them put any clear justification regarding to precipitation change for future case. As a result this study will have a great input in filling of this missed gap in the area of climate change study in Omo gibe basin.



## Chapter 3 Hydrological Models

### 3.1 Introduction and definition

Models are constructed to serve as proof of an idealized logical structure and they are an important element of methodical theories (Adem, 2005). A model is an expression to show a part of the natural or human created world which can be in the form of a physical, analog or mathematical model (Dingman, 2002). As a simple definition for models, a physical model is defined as a scaled-down form of a real system (Brooks et al., 1991; Salarpour et al., 2011). Mathematical models, on the other hand, include clear chronological set of relation, numerical and logical steps that change numerical inputs into numerical outputs. Today, mathematical models are more preferred due to the rapid development of computer technology.

According to Sharma et al., 2008 hydrological model can be defined as a simplified representation of a real-world system. Similar definition was introduced by Wainwright and Mulligan (2004), who defined model as an abstraction of reality in the simplest way that is adequate for the purpose of the modeling. The best model, according to them, is always that which achieves the greatest realism with the least parameter and model complexity.

An extensive acceleration of new discoveries in rainfall-runoff modeling emerged with a digital revolution in 1960's, when the development of models has gone hand-in-hand with increase of computing power. Thanks to new technologies, modelers' focus was shifted from event-based models (originated in the 1930's) to the first hydrological models for continuous simulation of rainfall-runoff processes emerging in the 1960's with computing power (Sharma et al., 2008). The digital revolution triggered also two other revolutions, namely, numerical simulation and statistical simulation (Frevort and Singh, 2006).

#### 3.1.1 Hydrological modeling in the context of climate change

The concept of modeling in hydrology involves the relationships of water, climate, soil and land use. According to many literatures and researches the climate condition of the world and the land use characteristics are the most actively changing conditions at present; those might have a far or near reaching impact on human being and other natural resources. For instance observational records from different flow stations around the world and climate projections provide abundant evidences that freshwater resources and river flows are vulnerable and have the potential to be strongly impacted by climate change. Global warming is expected to result in an intensification of the hydrological cycle starting from changing amount of flow to shifting major flow seasons but according to different studies that have been made so far the projected changes for different part of the world show large spatial and temporal variability.

Nowadays, hydrological impacts of climate change are the most attractive part of the research since it quantifies and studies effects of the change in flow regimes under different climate scenarios at regional to local scales. Studies on the effects of climate change on hydrology increase our understanding of the sensitivity of the hydrological system to changes in meteorological variables and help determine a range for the projected changes. It is, however, not straightforward to predict how and to what extent a hydrological system will be affected by climate change because this depends on the characteristics of the system, for example which hydrological processes are dominant. Many research showed that average temperature projected to increase in so many part of the world. This increment will have an impact on the evaporation of the watershed components of the hydrological system.

Climate change scenarios carried out with hydrological models help to assess the future development of the hydrological cycle in changing climate conditions in Omo Gibe basin. The assumption which is held in this thesis; SWIM hydrological model is calibrated to recent flow data at the strategic site like Abelti and Gibe III dam site to derive daily flows data for un-gauged part of the basin and to quantify the climate change condition at Gibe III dam site respectively. The climate change scenarios projected from REMO and GCM used as an input to SWIM hydrological model to reproduce the hypothetical hydrological cycle for changing climate conditions within 2020-2050 time frame.

A major challenge for hydrologic research especially in developing regions and country like Ethiopia and Omo Gibe basin in the coming years will be the assessment of climate change impacts on regional water resources, one of the main reasons for their challenge is often severely limited by the lack of stream flow gauges to calibrate watershed models, but we believe that the main challenge of Omo Gibe basin partly will be solved with this research by calibrating SWIM at Gibe III dam site using daily flow data for current time frame.

### **3.1.2 Importance of hydrological modeling**

Hydrological models are important for a wide range of applications, including water resources planning, development and management, flood prediction and design, and coupled systems modeling including, for example, water quality, hydro-ecology and climate. However, due to resource constraints and the limited range of available measurement techniques, there are limitations to the availability of spatial-temporal data; hence a need exists to extrapolate information from the available measurements in space and time; in addition there is a need to assess the likely hydrological impact of future system response, for example to climate and land management change (Pechlivanidis, I.G., 2011).

Hydrological model applications have a variety of objectives, depending on the problem that needs to be investigated. For example in this Ph.D thesis SWIM hydrological modeling is used for two basic objectives. The first one is to extrapolate measured flow at Abelti station to un-gaged part of the basin to derive daily flow data for this catchment, and the second one is to study climate change effects on inflow discharge at Gibe III dam site. Eventhough, SWIM hydrological modeling has been used only for these specific purposes at this thesis, there are several published reviews of hydrological modeling that have been used for different purposes.

Generally, Hydrological models are tools that integrate our knowledge of hydrologic systems to simulate the real world hydrologic processes. These models comprise a set of mathematical descriptions of portions of the hydrologic cycle (Singh and Woolhiser 2002) and they are based on a set of interrelated equations that try to convert the physical laws, which govern extremely complex natural phenomena, to abstract mathematical forms. Moreover different varieties of models can be used, depending upon the considered output, the existing database, input variables and required analysis for the intended purpose.

### **3.2 Classification of hydrological modeling**

There are many hydrological models with different characteristics that are being developed before and still developing for different purposes. So many researchers classified hydrological models based on; the basis of their function and objectives, their structure, and their level of spatial disaggregation. Since there are various ways to classify hydrological models shortly we will try to cover the major classification based on the important future of hydrological modeling.

The unique and common characteristics of many models make classifications of hydrological models an important issue so that the capabilities and limitations of each model can be identified accurately. Proper classification can be helpful for engineers, experts and

researchers to understand the characteristics of models before deciding to employ them for their works. However, the categorizations of hydrological models can be hampered by considerable overlapping characteristics among various classes of models. As a result, even the classification of hydrological models may vary depending on justification (Gosain et al., 2009). Also different types of classifications for hydrological models actually have the same meaning in nature but they are categorized differently due to different views and overlapping characteristics (Milad et. al., 2012). The American Society of Civil Engineers (ASCE, 1982) introduced the basic terms for various types of mathematical model namely; analytical models, deterministic models, dynamic models, empirical models, heuristic models, interactive models, linear and nonlinear models, numerical models, probabilistic (stochastic) models, semi-empirical models, simulation models and theoretical models (Milad et. al., 2012).

**i. Shaw classification**

By considering mathematic structures (Shaw., 1983) divided hydrological models broadly in to two categories, namely deterministic and stochastic. In deterministic category, conceptual models prevail and they are used to describe the catchment processes using mathematical rules, for example by an equation for evaporation. The stochastic models are more prominent in scientific studies because they consider the occurrence of events in space and times (Milad et. al., 2012).

**ii. Chow classification**

Furthermore Chow et al. (1988) stated that hydrological models can be classified into two major categories, namely physical models and abstract (mathematical) models. Furthermore, physical models can be divided into two classes again, namely scale models and analog models. A scale model can be called as a scaled down model of a real system and on the contrary, an analog model applies physical system having the same characteristic with the first sample.

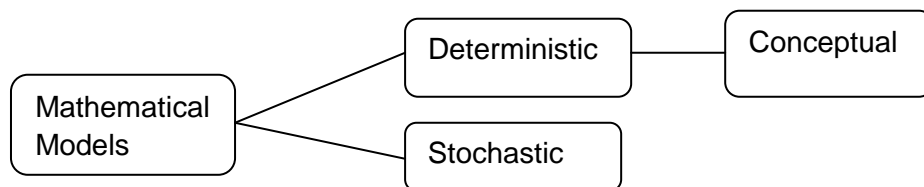


Figure 3.1 Hydrological models classification by Shaw (1983)

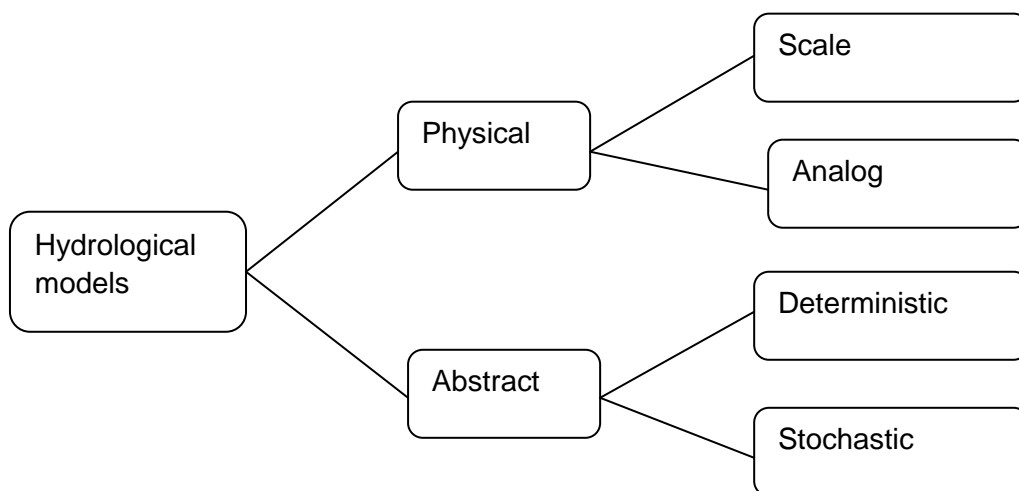


Figure 3.2 Hydrological models classification by Chow et al. (1988)

### iii. Mathematical models

Mathematical model is a symbolic, usually mathematical representation of an idealized situation that has the important structural properties of the real system. A theoretical model includes a set of general laws or theoretical principles and a set of statements of empirical circumstances. An empirical model omits the general laws and is in reality a representation of the data (Woolhiser et.al 1982).

According to Cunderlik., 2003 he has classified deterministic hydrologic models into three major categories without going into much detail as lumped models, semi distributed models and distributed models. Based on his classification parameters of Lumped models do not vary spatially within the basin and thus, basin response is evaluated only at the outlet, without explicitly accounting for the response of individual sub basins. Parameters of lumped models often do not represent physical features of hydrologic processes and usually involve certain degree of empiricism. In semi-distributed models parameters are partially allowed to vary in space by dividing the basin into a number of smaller sub-basins. In fully distributed models parameters are fully allowed to vary in space at a resolution. Distributed modeling approach attempts to incorporate data concerning the spatial distribution of parameter variations together with computational algorithms to evaluate the influence of this distribution on simulated precipitation-runoff behavior. Distributed models generally require large amounts of (often unavailable) data for parameterization in each grid cell. However, the governing physical processes are modeled in detail, and if properly applied, they can provide the highest degree of accuracy. Among the various types of models, semi-distributed models are the most effective for hydrological simulation as it overcomes the difficulties often encountered with fully distributed model and lumped model (Jajarmizadeh et al., 2013).

Based on Gosain et al., 2009 on their assessment to the models classification, they have simply defined as a black-box, conceptual or deterministic model. Additionally they have made sub divisions of these models in to different categories.

#### **Black-box models**

Black-box models explain the relation of the input and output data mathematically (Nor et al., 2007). In this type of model, physical processes are normally not under consideration (Jajarmizadeh et al., 2013). The basic idea of this model is used mathematical and statistical concepts to link a certain input for example rainfall can be used as input to calculate runoff as a result of excess rainfall which can be considered as model output. Commonly used techniques in black box model are regression, transfer functions and etc.

#### **Deterministic models**

If the chance of occurrence of the variables involved in such a process is ignored and the model is considered to follow a definite law of certainty but not any law of probability, the process and its model are described as deterministic. Deterministic models are complex and they require long computational time because of this they are very expensive to develop and hard to work with (Gosain et al., 2009). These models apply non-linear partial differential equations which describe the hydrologic processes. It is important to know that solutions based on analytical operation generally cannot solve the equations. One of the important advantages of the deterministic models is that they present the inside view of a process which enables better understanding of the hydrological system (Jajarmizadeh et al., 2013). They are based on physical knowledge of the watershed and use physically based equations to describe these processes.

#### **Conceptual models**

As a simple definition, conceptual models are a substitution between deterministic and black-box models. Generally these models are formulated with a number of conceptual elements which are simple representations of a reference system. Based on the characterization of conceptual models, there is a classification that divides the models into event and continuous

models. Event models simulate a system in a single event for a period ranging from an hour or less to several days (Salarpour et al., 2011). On the other side, continuous models work over an extended period. One of the advantages of continuous models is that they can be more successful for un-gauged catchment and the study of a system's long term characteristics.

Clearly, proper parameters for conceptual models are very essential and the degree of accuracy for these models also depends heavily on the proper parameters. Based on this, conceptual models can be divided in two major groups, namely lumped and distributed models. Lumped models show the average characteristics of a system and water balance equation is the basis of a lumped conceptual model in hydrological models (Ghandhari and Moghaddam, 2011). On the other hand, spatial variability is considered particularly in distributed conceptual models. One of the advantages of distributed conceptual models is the discretization of a system into a number of zones that have similar hydrological characteristics. For example, REA (representative element area), HRU (hydrological response units) and GRU (grouped response unit) are a few kinds of discretization in distributed conceptual model (Neitsch et al., 2005).

### Semi-distributed conceptual models

To overcome the difficulties of distributed models, researchers developed another semi-distributed model as a compromise between lumped and fully distributed models. The algorithms in semi-distributed conceptual models are simple but physically-based (Arnold et al., 1993). In these models, the average of observable physical characteristics in a catchment is used to represent spatial heterogeneity. Therefore, these models combine the distributed effects of contributing areas during modeling and the model parameters are estimated from measurements accessed in the field.

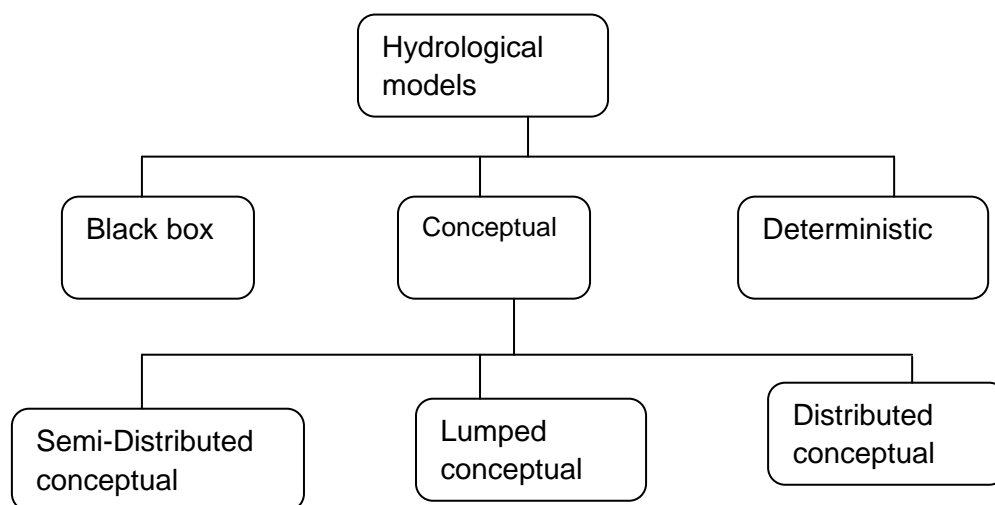


Figure 3.3 Hydrological models classification by Gosain et al. (2009)

### 3.3 Modeling approaches for climate change assessment

Watershed hydrologic models have been developed for many different reasons; and therefore have many different forms based on their internal structure how they are designed. However, they are in general designed to meet one of the two primary objectives. One objective of watershed modeling is to gain a better understanding of the hydrologic processes in a watershed and of how changes in the watershed may affect these phenomena; another objective of watershed modeling is the generation of synthetic sequences of hydrologic data for facility design or for use in forecasting. They are also providing valuable information for studying the potential impacts of changes in land use or climate.

As it was mentioned in the previous section of this study the evaluation of possible climate change impact in Omo Gibe water cycle, water resources and determination of daily flow for un-gauged part of the basin are the major scientific challenges to Omo Gibe hydrology. As a first step it is necessary to get and select based on the general feature of the model which can meet or solve the challenges which have been mentioned above. Hydrological models which simulates the water balance in a basin or which can be calibrated at a point where observational records available are a suitable and primary candidate for Gibe basin, and the candidate model should have a tool to accept input climate variables produced by downscaling procedure or chosen from climate change scenarios to produce corresponding hydrological variables with corresponding future time frame.

### 3.4 Selection criteria for hydrological models

Selection of a particular model is a key issue to get satisfactory answers to a given problem; however selecting an appropriate hydrological model for a particular application is a complicated process, and needs to take into account a variety of considerations for instance to select hydrological model which is needed to study climate change impact; the model should allow possible future hydrological changes caused by climate variation in surface water system and river flow.

Currently, there are numerous hydrological models simulating the hydrological process at different spatial and temporal scales. Although there are no clear rules for making a choice between models, some simple guidelines can be stated. Starting from the studied physical system, the first step is to define the problem and determine what information is needed and what questions need to be answered. This means that it is necessary to evaluate the required output. One of the most important things that should be considered during hydrological model selection is availability of input data to model the watershed. Subsequently the simplest method that can provide the answer to the questions has to be chosen. In particular it's necessary to identify the simplest model that will yield adequate accuracy.

There are numerous criteria which can be used for choosing the right hydrologic model. These criteria are always project-dependent, since every project has its own specific requirements and needs. Further, some criteria are also user depended (and therefore subjective), such as the personal preference for graphical user interface, computer operation system, input-output (I/O) management and structure (Cunderlik., 2003). Because of this different researches have different opinion for guidelines to select appropriate types of hydrologic model. For instance Cunderlik has listed the following four common, fundamental questions that must be always answered during model selection.

- ✓ Does the model predict the variables required by the project such as peak flow, event volume and hydrograph, long-term sequences of flows?
- ✓ Is the model capable of simulating snow accumulation and melt, single-event or continuous processes?
- ✓ Availability of input data (Can all the inputs required by the model be provided within the time and cost constraints of the project?),
- ✓ Price (Does the investment appear to be worthwhile for the objectives of the project?).

According to (Surfleet C. et al., 2012) they have established some criteria to select appropriate model, based on their result they have illustrated how selection of a modeling approach and interpretation of climate change projections required by considering the following three points.



- ✓ Appropriate parameterization of the models for climate and hydrologic processes governing runoff generation in the area under study,
- ✓ Understanding and justifying the assumptions and limitations of the model,
- ✓ Estimates of uncertainty associated with the modeling approach.

Some models are data intensive that often does not exist or are not available in full. The first step in selecting appropriate model for a particular study is to assess data, time, and resource constraints. Therefore to select a model to accomplish the objectives of this research in the Omo Gibe basin as case study, the following selection criteria were formulated against which models could be assessed for suitability.

- ✓ The model must be able to simulate agricultural/rural areas because nearly 65 to 70 percent of Gibe III dam site catchment can be classified as agricultural watershed.
- ✓ It should be able to simulate different components of the stream flow including surface runoff, lateral flow and base flow that are important components of the flow in perennial rivers in tropical catchments such as Omo Gibe basin.
- ✓ It should be able to calibrate at a place where observational flows are available for the sake of determining un-gauged flow from un-gauged part of Gibe basin.
- ✓ It should have a capacity to simulate low and peak flow to acceptable accuracy.
- ✓ The minimum input data requirements by the model must be readily available or can be synthesized with some efforts through application of general formula, for example to convert sunshine hours to solar radiation.
- ✓ Its temporal scale should be long term, continuous and able to simulate on daily bases for water budget analyses at watershed and sub-watershed levels for current and future time frame
- ✓ The model must be readily and freely available, both for research and for future use in Ethiopia to expand the application of the model in different part of Ethiopian basins
- ✓ And the model should be applied in different sizes of the basin starting from small scale to large scale watershed.

Before selection of hydrological model for this specific study a considerable number of existing hydrologic models (nearly 8) were reviewed in the preliminary screening process according to the eight main criteria described above. Among them four of the hydrologic models, which can be potentially used (applied) in Omo Gibe basin are identified and compared major characteristic of the models. The 5 selected models are summarized in the following section. During selection procedure Black-Box and fully distributed hydrological models were not considered; because Black-Box models are unable to give robust predictions of future change i.e. when going outside their range of calibration, whereas fully distributed models due to intensive data requirement. In addition to the above criteria temporal and spatial scale, the type of process in the model, the suitability of the model to transfer modeling methodology to other young hydrological modelers, availability of training and background knowledge were considered.

## Description of five screened hydrological models

Discription	SWIM	SWAT	HEC-HMS	Wasim-ETH
<b>Model type</b>	Semi-distributed, process based	Semi-distributed, process based	Lumped, conceptual	Fully distributed, process based
<b>Model Objective</b>	to provide a comprehensive GIS-based tool for the coupled hydrological/vegetation/water quality sediment on different sizes of river basin	developed to evaluate the effects of alternative management decisions on water resources and diffusion sediment on different sizes of river basin	designed to simulate the rainfall-runoff process of watersheds	Designed to simulate runoff and water balance
<b>Temporal scale</b>	day	day	day	Free to adjust (from minutes up to days)
<b>Watershed represenation</b>	The program defines the basin hydrotope structure by overlaying the sub-basin map with land use and soil layers.	Subdivides the watershed into smaller sub-basins and Hydrological Response Units (HRUs)	Uses sub-basins as primary hydrological units	Cell by cell calculation (Grid based)
<b>Process</b>	Continuous	Continuous	Continuous & event	Continuous
<b>Surface runoff</b>	Runoff volume is estimated by using a modification of the Soil Conservation Service (SCS) curve number technique and the peak runoff uses modified rational formula	Runoff volume using CN and flow peak using rational formula.	Clark's, Snyder's, SCS UHs, ModClark Kinematic wave	The Richards equation calculates infiltration based up on soil moisture conditions and surface runoff occur when the soil infiltration capacity has been exceeded. Macropore flow can be considered, too.
<b>Evapotranspiration</b>	Priestley–Taylor, Penman–Monteith	Hargreaves, Priestley-Taylor & Penman	Monthly average	Penman-Monteith, Wendling, Hamon and Haude
<b>Subsurface flow</b>	Lateral, subsurface flow (or inter flow) is calculated using The kinematic storage model developed by Sloan et al. (1983)	Lateral flow using kinematic storage model and groundwater flow using empirical relations.	Constant monthly, exponential recession or linear reservoir	TOPMODEL approach or Recharads equation is used for describing the water flow within the soil
<b>Flow routing</b>	The Muskingum flow routing method	Variable storage coefficient method or Muskingum method	Kinematic wave, Lag, Muskingum, Muskingum-Cunge	Translation-retention approach using Kinematic wave approach using different flow velocities for different water level in the channel
<b>Managment paractice</b>	Crop management option	Agricultural mang't, Tillage, irrigation, etc	Account human impact on runoff	Irrigation, Water management options
<b>References</b>	(Krysanova. et al, 2008 & 2000), (Huang et. al. 2010)	(Arnold et al 1993) , (Krysanova. et. al 2008 & 2000), (Jajarmizadeh et. al. 2013),	(Meenu, 2013), (Matthew, 2010)	(Schulla J., 2007)

Table 3.1 Description of four screened semi distributed hydrological models



From the preceding discussion and the model criteria included in SWIM, it has been selected for this research. The basic reasons to select SWIM for this study are: for regions under developing like Ethiopia availability of many data are problems and SWIM can be parameterised using regionally available data and from second sources and some efforts from some work that has been already done before, for instance some of the input data extracted from master plan study of the basin especially the soil parameter data. Besides to this the model has not been tried in Ethiopia so far. After checking the performance of the model in Omo Gibe basin it will have potentially important advantages for future use in the region since the model is public domain and freely available.

### **3.5 Description of selected model**

#### **3.5.1 The SWIM model**

SWIM is a continuous-time semi distributed ecohydrological model, integrating hydrological processes, vegetation, nutrients (nitrogen and phosphorus) and sediment transport at the river basin scale. The model developed by (Krysanova et al., 1998a). Its spatial disaggregation scheme has three levels: (1) basin, (2) subbasins and (3) hydrotopes within sub-basins (Krysanova et al., 2005). SWIM subdivides the catchment into relatively homogeneous sub-catchments to consider HRUs or hydrotopes to simulate hydrological and biogeochemical processes in soil, but the lateral flows of water and nutrients are first aggregated at the sub-catchment level and then routed this means that SWIM follows the main characteristics of the semi-distributed model.

#### **3.5.2 Model history**

SWIM is based on two previously developed tools SWAT (Arnold et al., 1993) and MATSALU (Krysanova et al., 1989). SWAT is semi-distributed physically based simulation model and can predict the impact of land use change and management practices on hydrological regimes in watersheds with varying soils, land use and management conditions over long periods and primarily as a strategic planning tool. MATSALU, was developed in Estonia for the agricultural basin of the Matsalu bay for smaller area and the Matsalu bay ecosystem in order to evaluate different management scenarios for the eutrophication control of the bay (Krysanova et al., 2005). Both SWAT and the catchment sub-model of MATSALU were based on the CREAMS model (Knisel, 1980), this includes the GLEAMS model (Leonard et al., 1987) developed to evaluate pesticide and nutrient load to groundwater, the EPIC model (Williams et al., 1984) developed to simulate the impact of erosion on crop productivity; the AGNPS model (Young et al., 1989) developed to evaluate the effect of single precipitation events in complex watersheds; the SWRRB model (Arnold et al., 1990) which is an extension of CREAMS for watersheds with a maximum of 10 sub-basins; and the OPUS model (Smith, 1992) developed as an updated and improved field-scale model for estimating the effects of management practices on nonpoint source pollution (Krysanova et al., 2005).

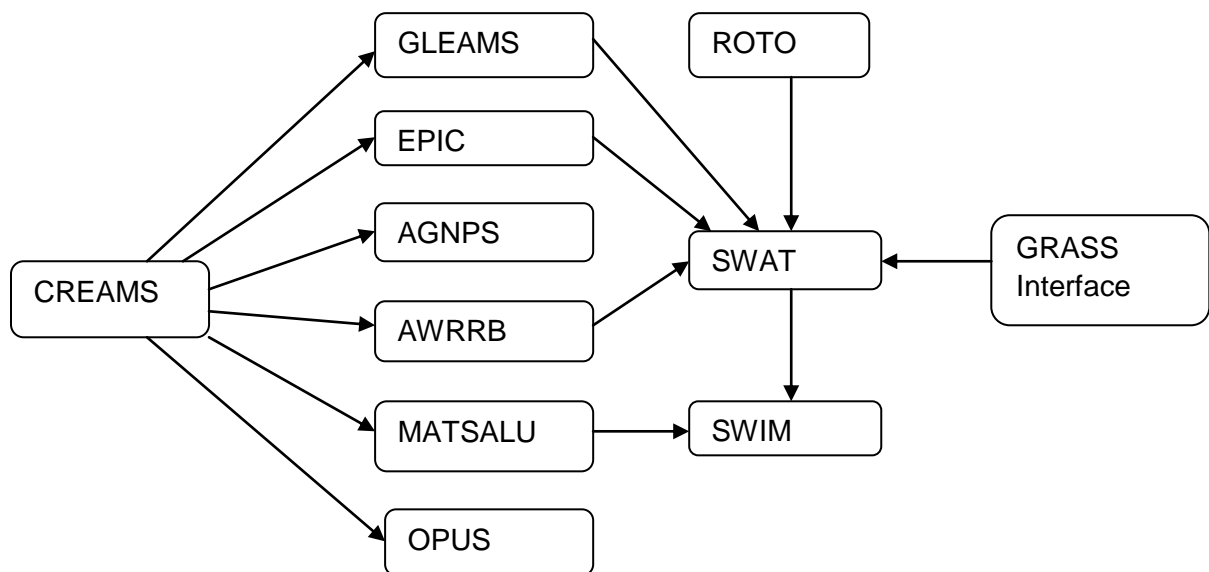


Figure 3.4 SWIM model development based on CREAMS model (Krysanova V. et al., 2005).

### Differences between SWIM and its predecessors SWAT and MATSALU

According to Krysanova et al., 2005 the main difference between SWAT and SWIM has been stated as; SWIM was developed mainly for impact studies in mesoscale and large river basins and at the regional scale, whereas SWAT was predestined mainly for water quality modelling and assessment of land management practices. Development of SWIM began with the introduction of a three level disaggregation scheme. At the beginning, SWAT was designed to have two level disaggregation scheme but now SWAT has a similar three-level disaggregation scheme; however, the hydrotopes are not included explicitly in the code, but as 'virtual sub-basins'.

Climate parameters in SWIM are assumed to be uniform at the sub-basin level. All hydrotopes, disregarding their proportional area in the sub-basin, have to be considered in SWIM, whereas a choice of dominant structures is allowed in SWAT. SWIM does not include several sub-models (e.g. pesticides, lake water quality), which are included in SWAT, as they were not considered necessary at this stage for SWIM. This also helps to avoid over parameterization of the model and improves control over the model behavior. In SWIM several options are included in the estimation of saturated conductivity, one of the most important and sensitive parameters in the modeling procedure.

### Spatial structure of SWIM

A three level scheme of spatial disaggregation, 'basin–sub-basins–hydrotopes' or 'region–climate zones– hydrotopes', plus vertical subdivision of the root zone into a maximum of 10 soil layers is used in SWIM. A hydrotope is a set of elementary units in a sub-basin or climate zone, which have the same land use and soil type (Krysanova et al.,2000).

During simulation

- ✓ Water, nutrients and plant biomass are initially calculated for every soil layer in a hydrotope;
- ✓ The outputs from hydrotopes are then integrated to estimate the sub-basin outputs; and
- ✓ The routing procedure is applied to the sub-basin lateral flows of water, nutrients and sediments, taking into account transmission losses.

Eventhough the model has not been tried in Ethiopia; however it was successfully applied in different part of Europe and some part of Africa. The model has been used to predict streamflow which were compared favorably with measured data for a variety of watershed scales (Huang et al., 2010; Hattermann et al., 2008; Huang et al., 2009). And recently there are ongoing researches to calibrate SWIM at different part of Africa for instance the project which is underway in the upper White Nile under the title of "Adaptation of SWIM for the water balance and vulnerability assessment of Nabajizzi wetland" a case study in Uganda. Currently there are some ongoing projects to setup SWIM in Blue Nile basin too.

### 3.6 Hydrological processes in SWIM

The hydrological module is based on the water balance equation, taking into account precipitation, evapotranspiration, percolation, surface runoff, and subsurface runoff for the soil column subdivided into several layers. The simulated hydrological system consists of four control volumes; the soil surface, the root zone of soil, the shallow aquifer and the deep aquifer. The soil root zone is subdivided into several layers in accordance with the soil database.

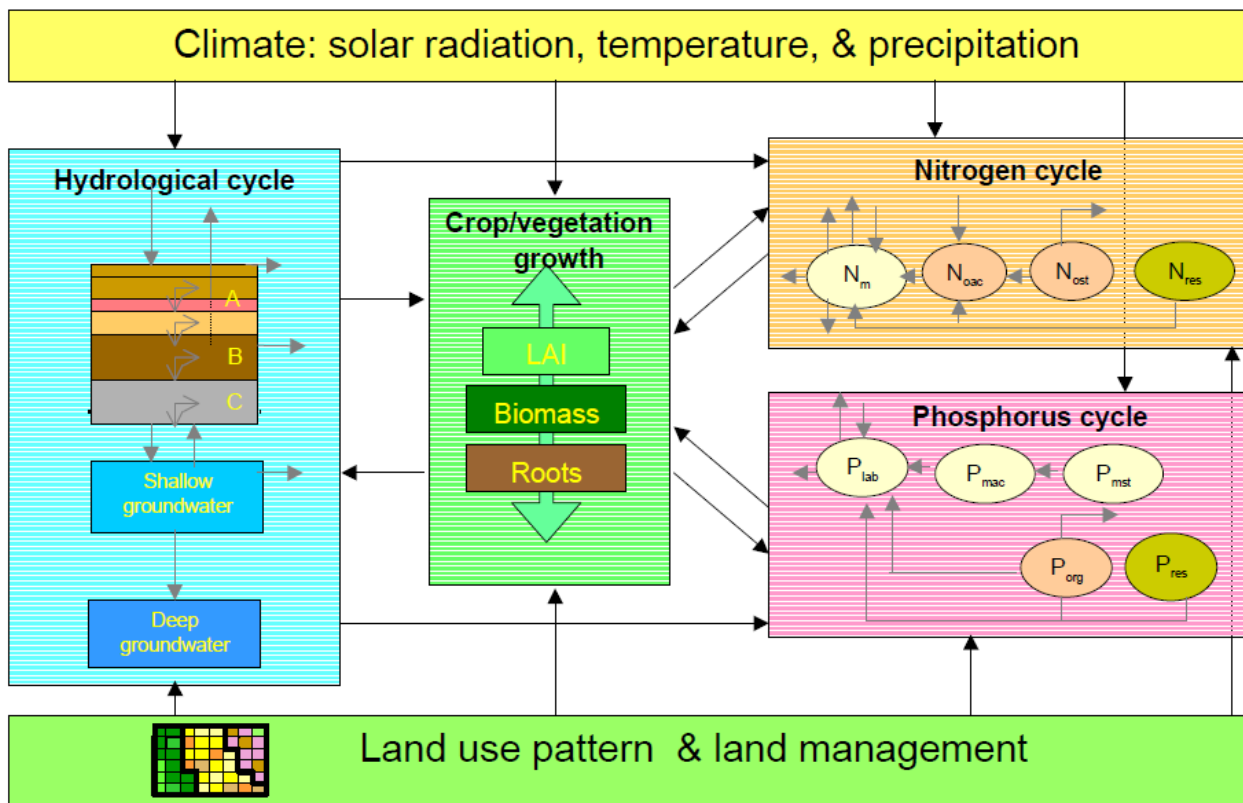


Figure 3.5 Flow chart of the SWIM model, integrating hydrological processes, nitrogen, phosphorus and crop/vegetation growth at the river basin scale (after Krysanova et al., 2005).

There are different components related to hydrological processes in SWIM. Each of these components is described briefly here after. The hydrological sub-model in SWIM is formulated based on the soil water content, total precipitation, on land flow, evapotranspiration, percolation and subsurface flow. The following descriptions are based on SWIM user manual.

Generally the water balance equation is expressed as follow:

$$SW(t + 1) = SW(t) + P - Q - PET - PERC - SSF \quad 3.1$$

Where  $SW(t)$  is the soil water content in the day  $t$ ,  $P$  is precipitation,  $Q$  surface runoff,  $PET$  evapotranspiration,  $PERC$  percolation, and  $SSF$  subsurface flow. All values are in daily amount in mm. Here the precipitation is an input and it may have different value at different sub-basin, but it is uniformly distributed throughout a given sub-basin. The equations described in the above water balance system will be described one by one in the following section.

### 3.6.1 Overland flow generation

Overland flow (surface runoff) is a flow that occurs along a sloping surface and it occurs whenever the rate of water application to the ground surface exceeds the rate of infiltration. It is the major component of the hydrologic cycle. In SWIM runoff volume is estimated using a modification of the SCS curve number method (Arnold et al, 1990). Surface runoff is predicted as a nonlinear function of precipitation and a retention coefficient. The latter depends on soil water content, land use, soil type, and management. The CN method was initially developed for small agricultural watersheds and the CN varies non-linearly with the moisture content of the soil. It drops to zero as the soil approaches the wilting point and increases to near 100 as the soil approaches saturation, with higher CNs associated with higher runoff volume.

$$Q = \frac{(P - 0.2 * SMX)^2}{P + 0.8 * SMX}, \quad P > 0.2 * SMX \quad 3.2$$

$$Q = 0, \quad P \leq 0.2 * SMX \quad 3.3$$

Where  $Q$  is the accumulated daily runoff in mm,  $P$  is the daily precipitation in mm and  $SMX$  is a retention coefficient. The retention coefficient  $SMX$  varies i) spatially, because soils, land use, management, and slope vary, and ii) temporally, because soil water content is changing. The retention coefficient  $SMX$  is related to the curve number  $CN$  by the SCS equation.

$$SMX = 254 \left( \frac{100}{CN} - 1 \right) \quad 3.4$$

### 3.6.2 Peak runoff rate

Generally peak runoff can be defined as the part of runoff which enters the stream quickly after the rainfall or snow melting. The source of peak runoff can also be melting snow, possibly in combination with high rainfall. The peak runoff rate is estimated in SWIM for sub-basins using the modified rational formula (Maidment, 1993; Arnold et al. 1994). A stochastic element is included in the Rational formula to allow a more realistic simulation of peak runoff rates, given only daily rainfall and monthly rainfall intensity. The Rational formula can be written in the form

$$Q_{peak} = \frac{C * RI * A}{360} \quad 3.5$$

Where:

$$Q_{peak} = \text{Peak runoff rate } \left( \frac{m^3}{s} \right).$$

$C$  is runoff coefficient expressing the watershed infiltration characteristics

$RI$  is the rainfall intensity in mm/hr

$A$  is drainage area ( $km^2$ )

### 3.6.3 Computation of evapotranspiration

Evapotranspiration is a collective term that includes all processes by which water at the earth's surface is converted to water vapor. When we search a clear definition of evapotranspiration, it is possible to find various results; as we see this expression combines two words; evaporation and transpiration. In a simple way evaporation can be defined as a type of vaporization of a liquid that occurs from the surface of a liquid surface, open water systems, like natural lakes and man-made pools and reservoirs, rivers, bare soil with water tables at or close to the land surface, and impervious surfaces like roofs and roads into a gaseous phase; whereas evaporation from vegetation surface and stomata like forest, woodland and grass land referred to as transpiration so that the collective sum of evaporation from natural vegetation and above mentioned items are called evapotranspiration.

SWIM offers two models for estimating potential evapotranspiration: the Penman-Monteith model (Monteith, 1965) that requires; solar radiation, air temperature, wind speed and relative air humidity data and Priestley-Taylor model (Priestley and Taylor, 1972) that requires solar radiation and air temperature as input. Once potential evapotranspiration is determined, SWIM calculates the actual evaporation from a given plant canopy using an approach similar to that of (Richtie 1972) concept, separately for soil and plants. Actual soil evaporation is computed in two stages. It is equal to the potential soil evaporation predicted by means of an exponential function of leaf area index (Richardson and Ritchie, 1973) until the accumulated soil evaporation exceeds the upper limit of 6 mm see the following equation.

$$ESO = EO * \exp(-0.4 * LAI) \quad 3.6$$

Where ESO is potential soil evaporation as a function of leaf area index (LAI) under assumption that EO = 6 mm/d.

When the accumulated soil evaporation exceeds the first stage threshold (equal to 6 mm), the second stage begins. Then soil evaporation is estimated with the equation

$$ES = 3.5 * (\sqrt{TST} - \sqrt{TST - 1}) \quad 3.7$$

Where ES is the soil evaporation for day t in mm/d and TST is the number of days since stage two evaporation began.

In the second stage the actual soil evaporation is reduced and estimated as a function of the number of days since stage two began. Plant transpiration is simulated as a linear function of potential evapotranspiration and leaf area index. When soil water is limited, plant transpiration is reduced, taking into account the root depth.

For this particular study (Priestley and Taylor, 1972) is used to estimate potential evapotranspiration, because the data required by this model are solar radiation, air temperature, and elevation easily available at Omo Gibe basin and collected before the commencement of this study.

Priestley-Taylor method estimates potential evapotranspiration with the following equation:

$$PET = 1.28 \left( \frac{RAD}{HV} \right) * \left( \frac{\beta}{\beta + \gamma} \right) \quad 3.8$$

Where:

PET is potential evaporation mm

RAD is the net radiation in MJm<sup>-2</sup>

HV is the latent heat of vaporization in MJ kg<sup>-1</sup>

$\beta$  is the slope of the saturation vapor pressure curve in kPa C<sup>-1</sup>

$\gamma$  is a psychrometer constant in kPa C<sup>-1</sup>

One of the most important modules introduced in SWIM is the module representing crops and natural vegetation which creates an interface between hydrology and nutrients. A simplified EPIC approach (Williams et al., 1984) is included in SWIM for simulating arable crops (like sorghum, onion, pepper, rice, wheat, barley, tomato, lettuce, maize and potatoes) and aggregated vegetation types (like pasture, evergreen forest, mixed forest and forested wetland etc.), using specific parameter values for each crop/vegetation type. A number of plant-related parameters are specified for 71 crop/vegetation types in the database attached to the model. This is a standard file produced by SWIM Grass interface for calculation of different model parameters. Vegetation in the model affects the hydrological cycle by the cover-specific retention coefficient, impacting surface runoff and influencing the amount of transpiration, which is simulated as a function of potential evapotranspiration and leaf area index (LAI).

### 3.6.4 Water movement in soil

#### 3.6.4.1 Percolation

Water movement in a soil can be in any direction, depending on conditions. Mainly water flows in a given soil through the open pores between soil particles. For instance water maintained in the soil profile after infiltration can flow under two conditions either saturated or unsaturated. For the saturation case; flow through soil particle driven by one of the major forces gravity in to downward direction. SWIM directly simulates saturated flow if the water content is above to the field capacity. The model records the water contents of the different soil layers maximum of 10 and assumes that the water is uniformly distributed through the root zone of soil or the upper 1m of soil. The amount of water that moves from one layer to the underlying layer is calculated using storage routing technique (Arnold et al., 1990). The percolation from the bottom soil layer is treated as recharge to the shallow aquifer.

Water that percolates to the next layer is computed as:

$$SW(t + 1) = SW(t) * EXP\left(\frac{-\Delta t}{TT_i}\right) \quad 3.9$$

Where:

SW(t+1) and SW(t) are the soil water contents at the beginning and end of the day in mm,

$\Delta t$  is the time interval (24 h)

And  $TT_i$  is the travel time through each layer i in h

Thus percolation for each soil layer i can be calculated as:

$$PERC_i = SW_i * \left[1 - EXP\left(\frac{-\Delta t}{TT_i}\right)\right] \quad 3.10$$

As the travel time for percolation is unique for each layer and is calculated as:

$$TT_i = \frac{SW_i - FC_i}{HC_i} \quad 3.11$$

Where:

$PERC_i$  is the amount of water percolating to the underlying soil layer on a given day (mm)

$FC_i$  is the water content of the soil layer at field capacity (mm)

$HC_i$  is the saturated hydraulic conductivity for the layer (mm/hr).

### 3.6.4.2 Lateral subsurface flow

Subsurface lateral flow refers to soil water processes in which infiltrating water accumulates and moves laterally downslope along the upper surface of a less permeable layer in the soil. Subsurface lateral flow is known by a range of terms including throughflow, subsurface storm flow, subsurface runoff, and interflow (Hardie et al., 2012). Lateral subsurface flow or interflow is streamflow contribution which originates below the surface but above the zone where rocks are saturated with water. Interflow in the soil profile is calculated simultaneously with redistribution. It can have an important influence on storm hydrographs particularly when vertical percolation is retarded by a shallow, less permeable soil layer (Kassa, 2009).

SWIM incorporates a finite difference form of kinematic storage model developed by (Sloan et al., 1983) to compute subsurface flow as a function of the drainable volume of water, saturated conductivity, hill slope length, drainable porosity of the soil, hillslope steepness and the velocity of water at the outlet.

The equation to compute lateral flow in SWIM is given as:

$$\frac{SUP_2 - SUP_1}{t_2 - t_1} = WIR * SL - \frac{SSF_1 + SSF_2}{2} \quad 3.12$$

Where

SUP the drainable volume of water stored in the saturated zone (water above field capacity)

t is time in hr

SSF the lateral subsurface flow in m<sup>3</sup>/hr

WIR is the rate of water input to saturated zone in m<sup>2</sup>/hr

SL is the hill slope length in m

And subscript 1 and 2 refer to the beginning and end of the time step respectively.

The equation used to calculate lateral flow at the hillslope outlet is given by:

$$SSF = \frac{2 * SUP * VEL * SLW}{PORD * SL} \quad 3.13$$

Where:

VEL is the velocity of flow at the outlet mm/hr

SLW is the hillslope width in m

And PORD drainable porosity of the soil in m/m

Velocity at the outlet is estimated as:

$$VEL = SC * \sin(\gamma) \quad 3.14$$

SC is the saturated conductivity in mm/hr

And  $\gamma$  is the hillslope steepness in m/m

Combination of the above equation 3.11 and 3.12 gives:

$$SSF = 0.024 \frac{2 * SUP * SC * \sin(\gamma)}{PORD * SL} \quad 3.15$$

Where SSF in in mm/day

Lateral flow is significant in areas with soils having high hydraulic conductivities in surface layers and an impermeable or semi permeable layer at a shallow depth. In such a system, rainfall will



percolate vertically until it encounters the impermeable layer. The water then ponds above the impermeable layer forming a saturated zone of water and this saturated zone is then the source of water for lateral subsurface flow.

### 3.6.4.3 Ground water Flow

In hydrologic terms, streamflow which results from precipitation that infiltrates into the soil and eventually moves through the soil in the form of return flow to the stream channel is known as base flow. This is also referred to as ground water flow, dry-weather flow or return flow. Return flow or base flow is the volume of stream flow originating from groundwater. The ground water sub module embedded in SWIM to simulate the ground water flow is designed for general use in regions where extensive field measurements are not available. Thus, the groundwater component has to be parameterized using readily available inputs.

Basically the simulated hydrologic system in SWIM consists of four control volume that includes; the soil surface, the soil profile or root zone, the shallow aquifer and the deep aquifer. Part of the rainfall which percolates from the soil profile is assumed to recharge the shallow aquifer. The stream flow as SWIM simulates, is the contribution of flow from surface runoff, the lateral subsurface flow and the return flow from the shallow aquifer. The contribution of ground water to stream flow is simulated by creating a shallow aquifer storage which is recharged by percolation from the unsaturated zone, and discharges to the reach of the watershed. The water balance for the shallow aquifer is:

$$SAW(t + 1) = SAW(t) + RCH - REVAP - GWQ - SEEP \quad 3.16$$

Where: SAW(t) is the shallow aquifer storage in the day t, RCH is the recharge, REVAP is the water flow from the shallow aquifer back to the soil profile, GWQ is the return flow or groundwater contribution to streamflow, SEEP is the percolation or seepage to the deep aquifer (all in mm/d), and t is the day. To calculate the ground water flow (GWQ) SWIM uses the approach of (Smedema and Rycroft., 1983), who derived the non-steady-state response of groundwater flow to periodic recharge from (Hooghoudt's., 1940)

$$GWQ = 8 * \frac{KD * GWH}{DS^2} \quad 3.17$$

Where KD is the hydraulic conductivity of ground water in mm/d, DS the drain space in m, and GWH is the water table height in m.

## 3.7 Conclusion

Hydrological models play pronounced role in modeling the hydrological processes of a basin. Nowadays, they are involving to greater extent in climate change study sector. Scientists and different societies who are engaged to investigate effects of climate change mainly on water resources potential are using hydrological models to forecast and model a river basin under climate change scenarios. The main purpose of their study is to quantify the availability of water resources (river discharge) for different utilization purposes under the changing climate condition for future time period. Not only this but also; hydrological models are very powerful tools to study the sensitivity of the hydrological components in a basin with different climate change conditions, (like changing of mean surface air temperature and precipitation). The main purpose of this chapter was to introduce the role of hydrological model, their classification and the selection criteria of the model for climate change study. Based on these assessments eight different criteria were identified. Based on these criteria different hydrological models were compared according to their different characteristics, behavior and their design. Selecting of the appropriate type of hydrological model leads to achieve the intended purposes of the study. In consideration of these and other criteria SWIM hydrological model has been selected to model hydrological processes in Omo Gibe basin.



## Chapter 4 Description of the Study Area

### 4.1 Ethiopia

Ethiopia is located between approximately 3<sup>0</sup>-15<sup>0</sup>N latitude and 33<sup>0</sup>-48<sup>0</sup>E longitude. The country covers a land area of about 1.1million km<sup>2</sup>, occupying a significant portion of the Horn of Africa. It shares boundaries to the east and southeast with Djibouti and Somalia, to the north with Eritrea, to the south with Kenya, and to the west with Sudan.

Ethiopia is a country of great geographical diversity with high and rugged mountains, flat topped plateau, deep gorges, river valleys and plains. This diversity in relief makes the country unique in Africa. Ethiopia is the most elevated part of Northeast Africa. The altitude ranges from the highest peak at Ras Dashen (4,620 meters above sea level), in Gonder down to the Danakil depression (120 meters below sea level) with the Afar depression , one of the lowest dry land points on the earth.

The country has more than 80 million inhabitants (2010); Ethiopia is the most populous nation in Eastern Africa and the second-most populous in Africa after Nigeria. The average age of the population is 17 years with an annual population growth of more than 2%. Ethiopia will have more than 120 million people by 2030. Orthodox Christians (>40%) and Muslims (~35%) peacefully live side-by-side in this multi-ethnic country. Altogether there are around 80 different ethnic groups today (FDRE, 2012).

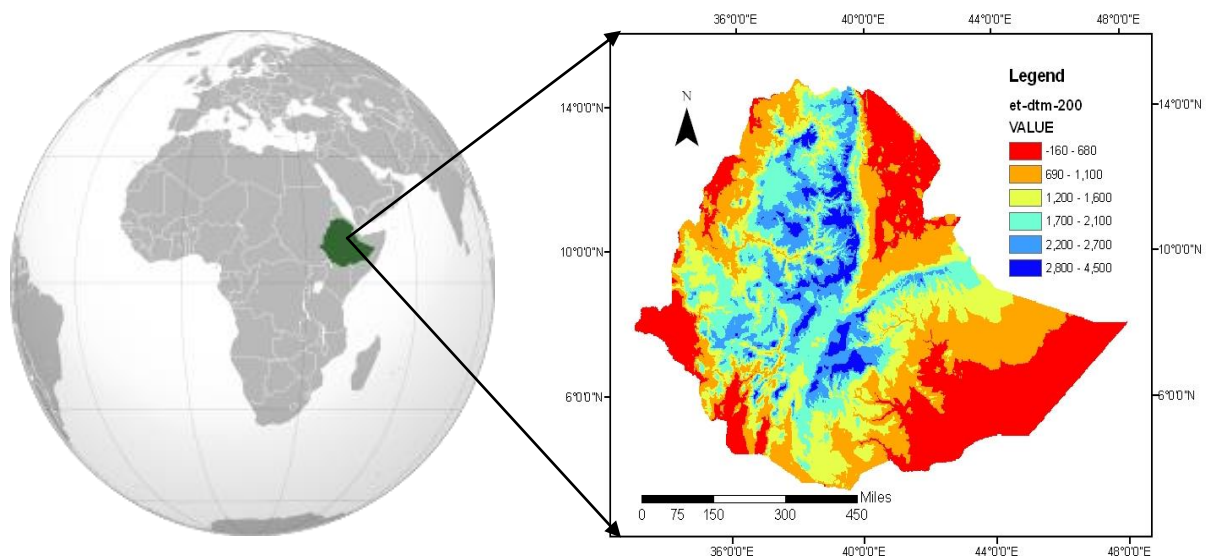


Figure 4.1 Location map of Ethiopia<sup>8</sup>.

The climate of Ethiopia is mainly controlled by the seasonal migration of the Intertropical Convergence Zone and associated atmospheric circulations as well as by the complex topography of the country. It has a diversified climate ranging from semi-arid desert type in the lowlands to humid and warm (temperate) type in the southwest. Mean annual rainfall distribution has maxima (>2000 mm) over the South-western highlands and minima (<300 mm) over the South-eastern and North-eastern lowlands.

<sup>8</sup> Wikipedia.org location of Ethiopia, Source of the left side picture

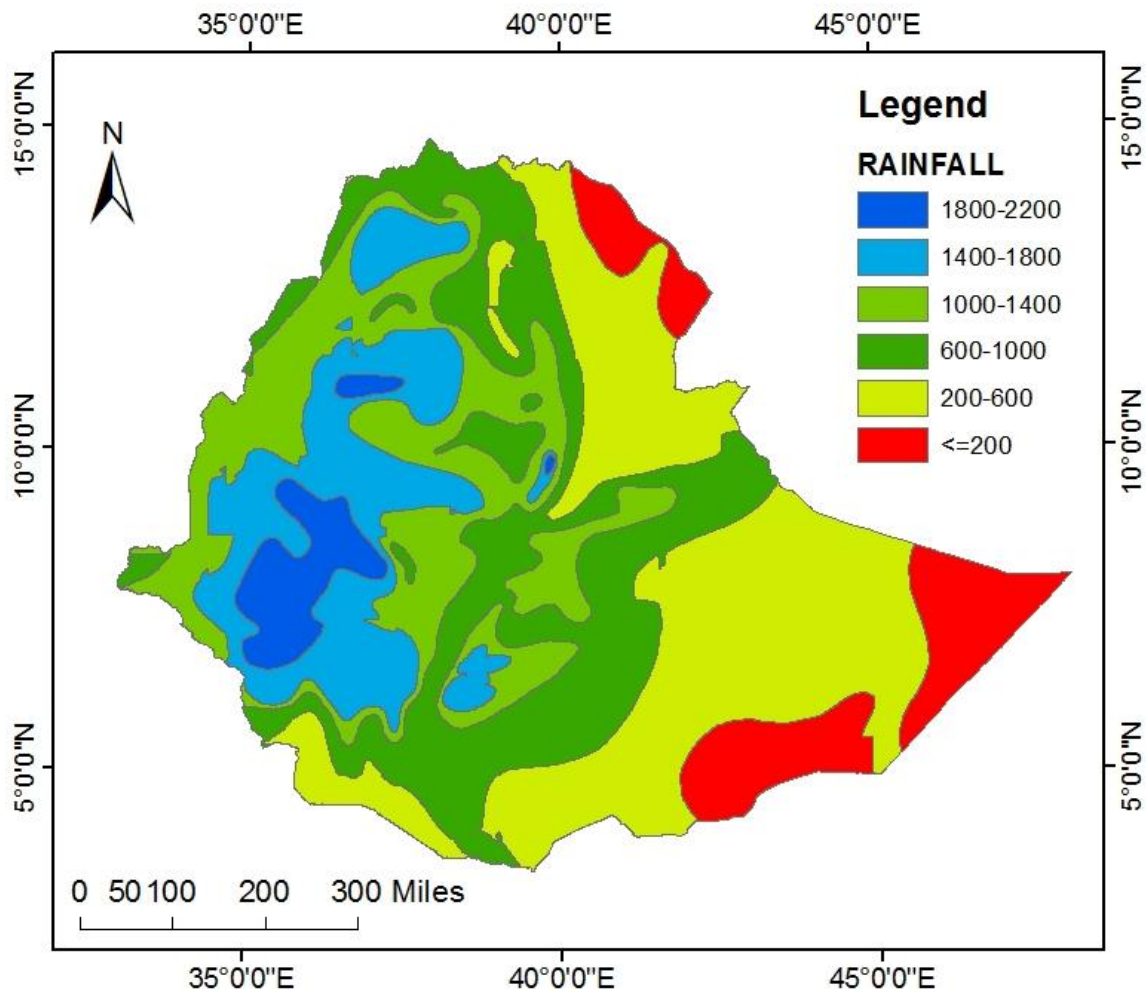


Figure 4.2 Rainfall distributions in Ethiopia<sup>9</sup>

Figure 4-2 shows contours of mean annual rainfall distribution using isohaytal method. Mean annual temperature ranges from < 15°C over the highlands to > 25°C in the lowlands.

## 4.2 Water resources potential of the country

The country has abundant water resources and hydropower potential, second next to the Democratic Republic of Congo in all of Africa, yet only few percentage of this potential has been developed.

The country's annual renewable fresh water resources amount to some 124 BCM/yr in the twelve river basins. However, only 3% remains in the country. The rest, 97% is lost as runoff to the lowlands of neighboring countries. At this stage of water development, where the country withdraws less than 5% of its fresh water resources for consumptive uses (MoWE, 2007). It is estimated that up to 3.7 Million hectares and 155,102Gwh/yr of power respectively can be developed using the available potential and clean water supply to all its people. However, only less than 300,000 hectares of the irrigation and 3 to 5 % of hydropower potentials respectively have been developed (MoWE, 2007).

To gain an insight into the spatial distribution of the fresh water resources one can note that 83% of the surface water potential is generated in the four basins (Tekeze, Abbay, Baro Akobo and Omo-Gibe) located on the western portion of the country representing only 40% of the total

<sup>9</sup> Source of map is MoWEE Ethiopia

land area of the country. This clearly demonstrates the uneven spatial distribution of water resources in the country (UN-WATER/WWAP/2006/7).

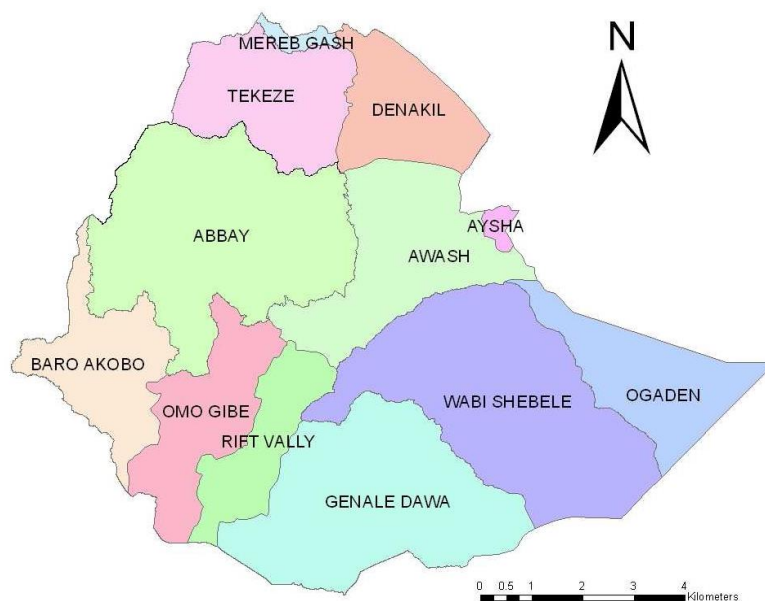


Figure 4.3 Ethiopian river basin map

River basin	Area (km <sup>2</sup> )	Runoff (Bm <sup>3</sup> )	Potential irrigable land (ha)	Gross hydro-electric potential GWH/yr	Estimated ground water potential (Bm <sup>3</sup> )
Tekeze	8235***	8.2	83,368	5,980	0.2
Abbay	199,812	54.8	815,581	78,820	1.8
Baro-Akobo	75,912	23.6	1,019,523	13,765	0.28
Omo-Gibe	79,000	16.6	67,928	36,560	0.42
Rift Valley	52,739	5.6	139,300 *	800	0.1
Mereb	5,900 ***	0.65	67,560		0.05
Afar /Denakil	74,002 ****	0.86	158,776		
Awash	112,696	4.9	134,121	4,470	0.14
Aysa	2,223 ****	-	-	-	-
Ogaden	77,121 ****	-	-	-	-
Wabi-Shebelle*	202,697 **	3.16	237,905	5,440	0.07
Genale-Dawa	171,042 **	5.88	1,074,720	9,270	0.14
<b>Total</b>	<b>1,135,494</b>	<b>124.25</b>	<b>3,798,782</b>	<b>155,102</b>	<b>2.86</b>

Table 4.1 Irrigation and hydropower potential of Ethiopian river basins<sup>10</sup>

Source: (Awulachew, S. B. et al, 2007)

Integrated river basin master plan studies, carried out during 1997-2007

<sup>10</sup> Some values were collected from different tables in <http://www.MoWEE.gov.et> as visited on May 2013.

*	Figures need to be updated from recent studies.
**	Small-scale irrigation is not included in the database
***	Indicates the Ethiopian part of the basin area.
****	Reconnaissance study

### 4.3 Location and description of Omo Gibe basin

The Omo-Gibe basin is one of the major river basins in Ethiopia and is situated in the south western part of the country covering parts of Southern Nations, Nationalities and Peoples Region (SNNPR) and Oromia region. The basin covers an area of 79,000 km<sup>2</sup> with a length of 550 km and an average width of 140 km. The basin lies between 4°00'N & 9°22'N latitude and between 34°44'E & 38°24'E longitude. It is an enclosed river basin that flows in to the Lake Turkana which forms its southern boundary. The total mean annual flow from the river basin is estimated about 16.6 BMC.

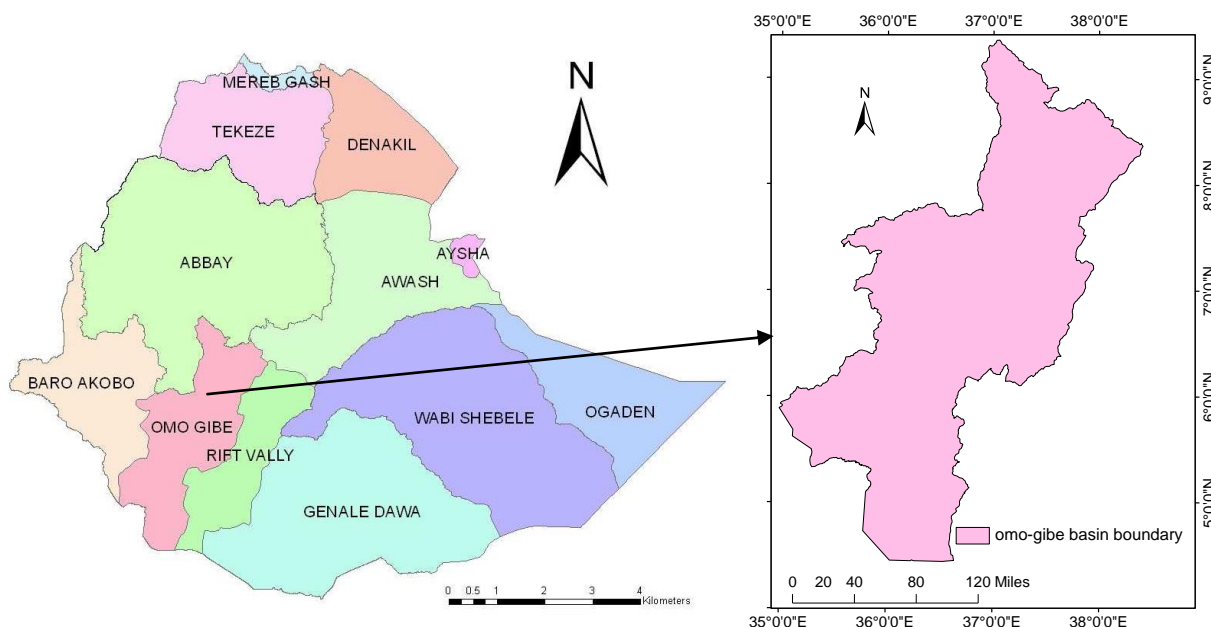


Figure 4.4 Location map of Omo Gibe basin<sup>11</sup>

Omo Gibe watershed is selected as case study for this research because large scale and medium scale irrigation potential are identified in the basin, with an estimated irrigable area of 57,900 and 10,028 hectares respectively, and a total irrigable area of 67,928 hectares. However, this figure could be much higher given the vast land area of lower Omo. In terms of hydropower development potential it is the second largest next to Abbay (Blue Nile), and it is a basin in which most of the current hydropower development is taking place (See table 2.1). In addition, it can be considered as representative watershed where there is high landscape and climatic zone difference within short distances. The population growth and land use systems together with considerable human interventions in the upper part of Omo watershed makes it feasible for climate change impact analysis on hydrological regime.

<sup>11</sup> Omo Ghibe basin boundary is delineated from SRTM data of the basin using ArcMap

### 4.3.1 Climate of the study area

The climate of Omo-Gibe River basin varies from a hot arid climate in the southern part of the floodplain to a tropical humid one in the highlands that include the extreme north and north-western part of the Basin. Intermediate between these extremes and for the greatest part of the basin the climate is tropical sub-humid.

#### 4.3.1.1 Rainfall

Rainfall in Omo-Gibe basin varies from over 1900 mm per annum in the north central areas to less than 300mm per annum in the south. The amount of rainfall decreases throughout the Omo-Gibe catchments with a decrease in elevation. Moreover, the rainfall regime is unimodal for the northern and central parts of the basin and bimodal for south.

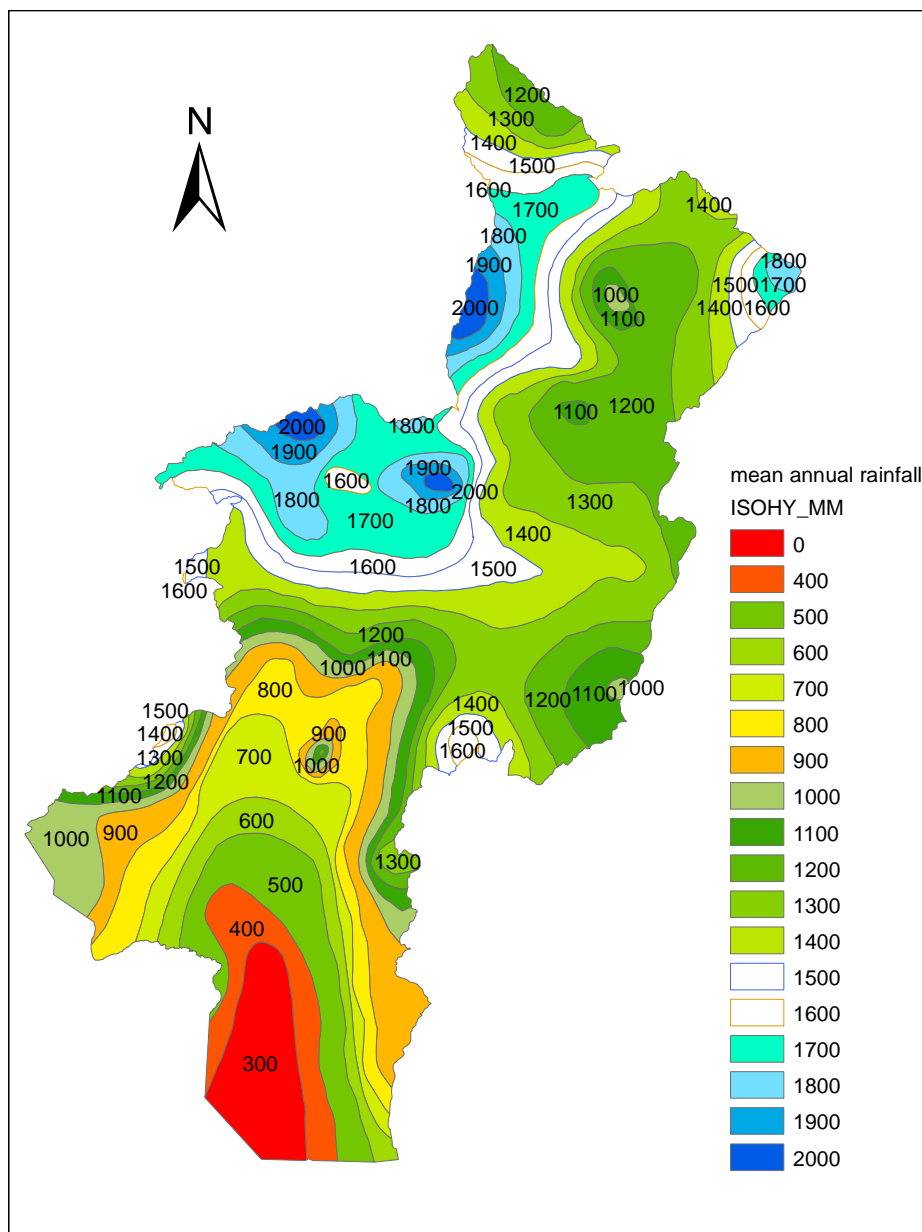


Figure 4.5 Mean annual rainfalls (isohyetal map of the basin)<sup>12</sup>

<sup>12</sup> Isohyetal map of the basin obtained from MoWEE of Ethiopia

### 4.3.1.2 Meteorological stations

In Omo-Gibe River basin there are 86 rainfall stations in and near by the basin. However, most of the stations have established recently. Many of the stations have few years recorded value (less than fifteen years). Since climate change study needs at least thirty years recorded data, stations which have relatively long recorded value have been used for further analysis. In general 21 rainfall and 14 temperature gauging stations have been used for this research. Besides the distribution of the gauged stations are not well organised. Most of the stations are concentrated in the northern part of the basin.

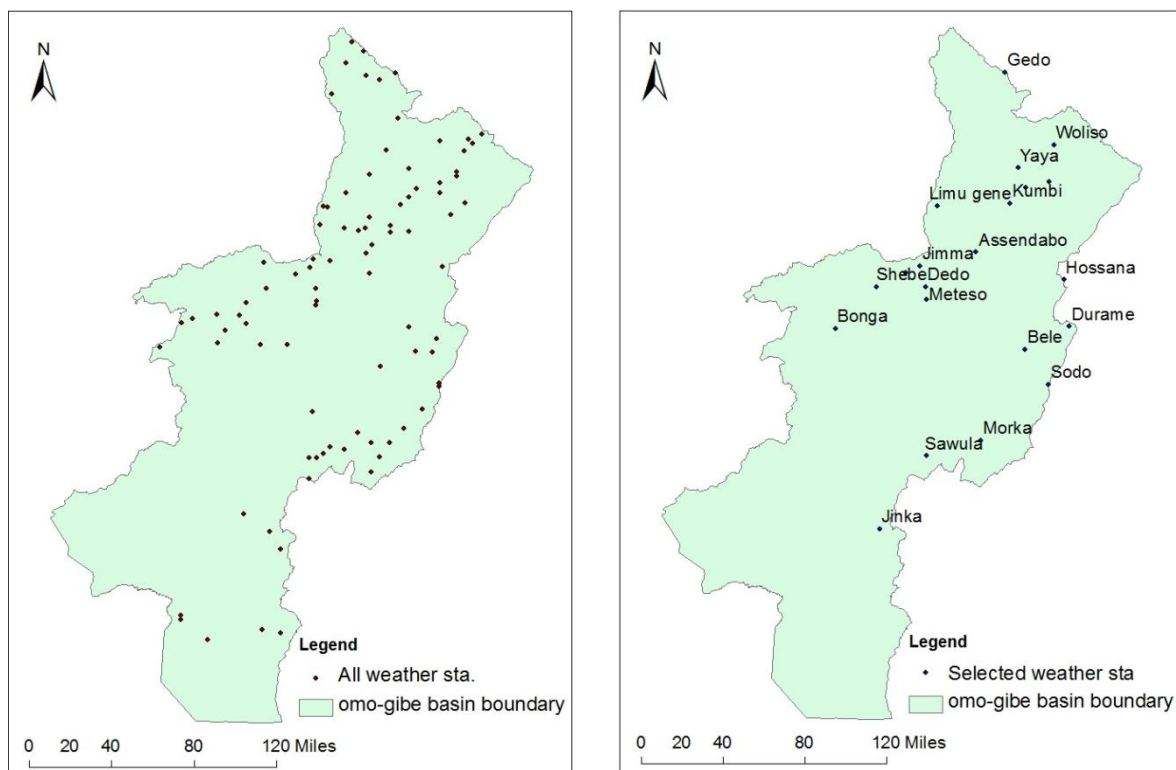


Figure 4.6 All and selected weather stations respectively

To give some insight on the climatological background of Omo-Gibe river basin, a preliminary analysis was carried out by dividing the basin in to three distinct parts. These are upper basin middle basin and lower basin. From 25 to 30 years observed weather data mean monthly depth of precipitation, maximum and minimum temperature roughly computed. For this operation nine observed precipitation stations were used for upper part similarly nine for middle part. Since the lower part of the basin is not well represented regarding to weather observation station it is represented by three gauging stations only.

According to the following results In terms of rainfall, the basin can be split in to two distinct regions, the northern and middle part of the basin having a unimodal rainfall pattern and the southern part which has a bimodal rainfall regime. The northern part of the basin, including Woliso, Welkite, Gedo, and Assendabo has rainfall for about seven months, from March to September with a range of 1100-1800 mm per annum. The small rains are from March to May and the main rainfall season from June to September with a marked increase in July and august.



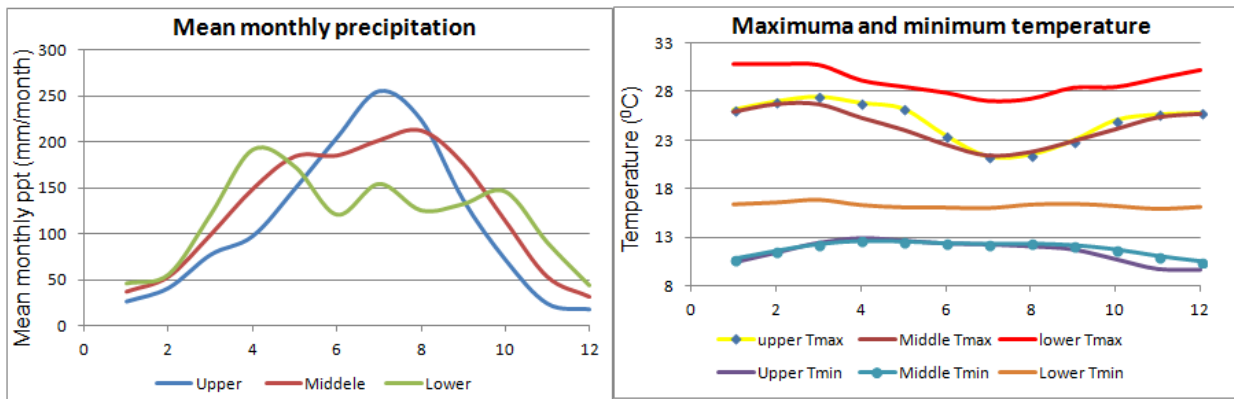


Figure 4.7 Mean monthly rainfall, maximum and minimum temperature for three regions

The middle and north-central area, including Bonga, Jimma, Shebe, Hossana and Sodo, has a more even distribution of rainfall over March to September without any peak in July and August. The region generally receives more than 1200mm, rising to 2000 mm on the western fringes North West of Bonga. This part of the region is the wettest part as compared to the other two regions. For more clarification and location of the stations see the above figure 4.6.

The southern part of the basin includes, Jinka, Sawula and Morka. Even though, the magnitude of the rainfall in this part of the region is small as compared to the other two regions, but it has a prolonged rainy season of bimodal type. According to the above graph (figure 4.7) indicates that the rainfall pattern in southern part of this basin is different from the upper one with a major rains starts in March and end up late April rather than late in the year.

#### 4.3.1.3 Temperature

The mean annual temperature in Omo-Gibe basin varies from 16°C in the highlands of the north to over 30°C in the lowlands of the south. The maximum temperature is higher at the southern part of the basin especially at Morka mean annual maximum temperature reaches up to 30.6 °C. There is a little variation in minimum temperature which varies from 9.2°C in northern part of the basin example in Gedo to 16°C in southern part of the basin at Jinka.

#### 4.3.2 Topography and river systems of the basin

The topography of Omo Gibe basin as a whole is characterized by its physical variation. The northern two-thirds of the basin has mountainous to hilly terrain cut by deeply incised gorges of the Omo, Gojeb, and Gilgel-Gibe Rivers, while the southern one-third of the basin is a flat alluvial plain punctuated by hilly areas. The northern and central half of the basin lies at an altitude greater than 1500 masl with maximum elevation of 3360 masl (located between Gilgel-Gibe and Gojeb tributaries), and the plains of the lower Omo lies between 400-500 m asl (Richard Woodroffe & associates Vol VI, 1996).

The northern part of the catchment has a number of tributaries. Most of the rivers from upper part of the catchment drain largely cultivated land. The head waters of the Great-Gibe River are at an elevation of about 2200 masl. Although there are some important tributaries from different directions, the general direction of flow of the Gibe River is southwards, towards the Omo River and then to Lake Turkana a fault feature, filled with alluvial and lacustrine sediments of recent origin associated with the Great Rift Valley. The Gibe River is known as the Omo River in its lower reaches, south-westwards from the confluence with the Gojeb River. This is the reason behind the name Omo-Gibe River Basin<sup>13</sup>.

<sup>13</sup> Collected from different sources and home page of Ministry of water and energy of Ethiopia

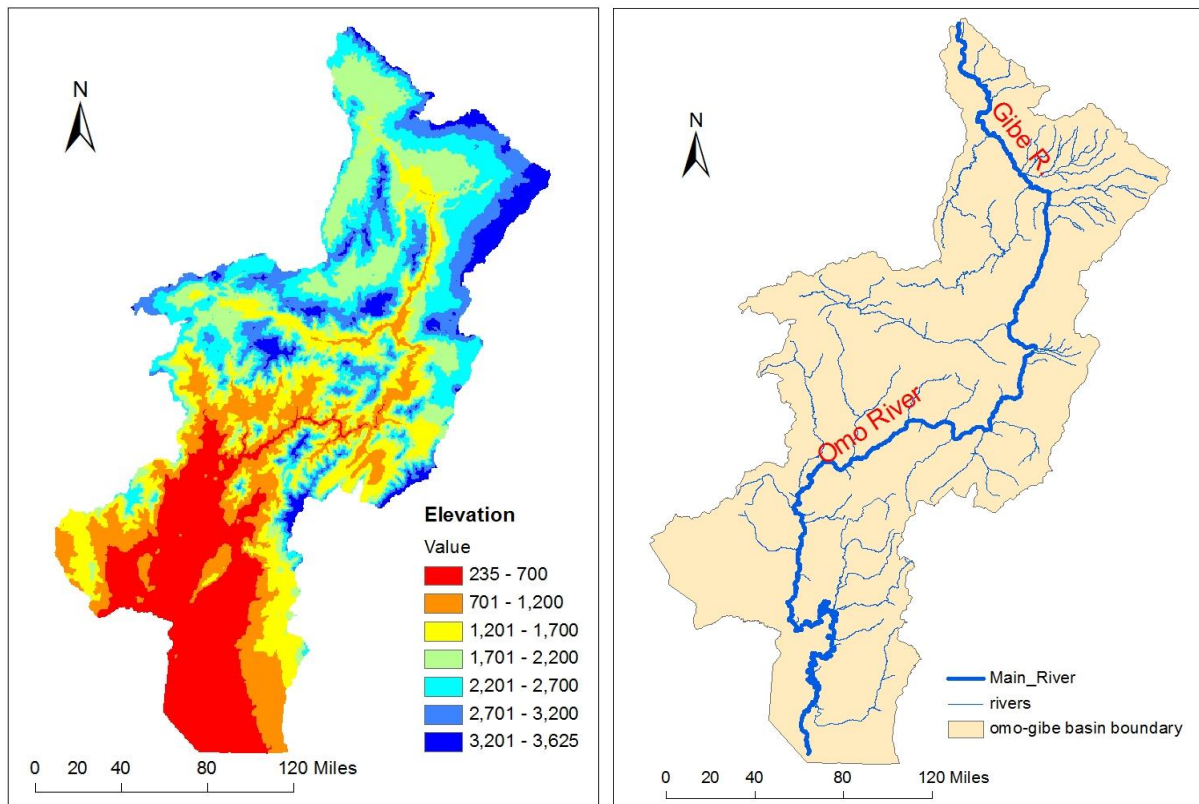


Figure 4.8 Elevation and river system of Omo Gibe as extracted from SRTM data of the basin

### 4.3.3 Geology soil and land use

#### 4.3.3.1 Geology

There is limited information available on the geological formation of the study area. But according to master plan study of the basin the geology can be characterized by tertiary and quaternary age rhyolite and basalt volcanic in the north and middle part of the basin with quaternary alluvial overlying pre-cambrian basement gneisses and granite in the south. Approximately 11% of the Omo-gibe basin is underlain by pre-cambrian metamorphic gneisses and 80% of the Basin is underlain by Tertiary volcanic rocks.

#### 4.3.3.2 Soil

More specific soil studies in the basin have concentrated on the irrigation potential of the lower Omo valley with some work on erosion and conservation measures. During the study of Omo Gibe integrated development master plan detailed soil survey especially on the upper part of the basin were carried out. On this study soil morphology of the basin also included. Soil morphology relates to the appearance of the soil in the field in terms of; depth, color, texture, structure, consistence, drainage and presence or absence of stone and carbonates. These together with soil chemistry, are the criteria used to categorize the soils in to units. The result of this detailed soil survey is used for hydrological analysis as an input to SWIM modeling.

According to Omo-Gibe integrated development master plan study Volume VII land resources survey 1996 the soil depths in the basin categorized as below.

- Very shallow if the depth of the soil is < 30 cm
- Shallow if the depth of the soil is 30-50 cm
- Moderately deep 50-100cm



- Deep 100-150cm
- Very deep > 150cm

According to study of soil survey on the basin 25 soil units were identified in terms of morphology, location in the landscape, land use, fertility (a general indication taking ph, OC%, N% and Ppm into account) current erosion and erosivity (a function of slope, texture, structure, land cover and AWC). All the result of this study is employed for hydrological analysis of the basin using SWIM.

The majority of the soils in the basin are deep to very deep, red and reddish brown clay looms over clays (Soil unit 1 and 5). These soils are well drained. They are wide spread over the whole of the northern basin. Soils developed from volcanic parent materials, often with an ash or pumice layer tend to occur on high ground with in the basin. They are moderately deep to deep, well drained, dark brown to dark reddish brown sandy clay loams to clays. These soils occur on the northern boundary. The other soils in this general category include soils developed on acidic igneous parent materials characterized by brown color (Soil unit 6 to unit 6a). In the south of the basin in the areas of lower rainfall the soils developed are characterized by the presence of a course sand fraction. They are moderately deep to very deep, well drained yellowish brown course grained sandy loams to sandy clays.

Vertisols<sup>14</sup> are poorly drained heavy clays soils with a characteristics dominated clay fraction which causes them to shrink and swell (soil unit 8 and 9). They are characterizes by presence of Gilgai a surface micro relief feature caused by shrinking and swelling and slicken sides in the soil profile. They are generally deep to very deep, black to very dark grey clays. The better drained vertisols (soil unit 8) are dominant to the northern west of Wolkite.

Poorly drained vertisols (soil unit 9) are the dominant feature of the land scope in many areas of the upper basin, and common in the plains of lower Omo where they occur in association with poorly drained sodic clays (soil unit 25).

Alluvial and colluvial soils of lower Omo, these soils are characterized by their highly heterogeneous nature in terms of texture both laterally and vertically (soil unit 19, 21, 22, 23)

Figure 4-9 shows the soil map of Omo-Gibe river basin, which was collected from Ministry of water and energy of Ethiopian. The classifications of the soils were based on the revised FAO-UNESCO-ISRIC legend to the Soil Map of the World 1988.

---

<sup>14</sup>Vertisols are clay-rich soils characterized by vertical cracking during the dry season.

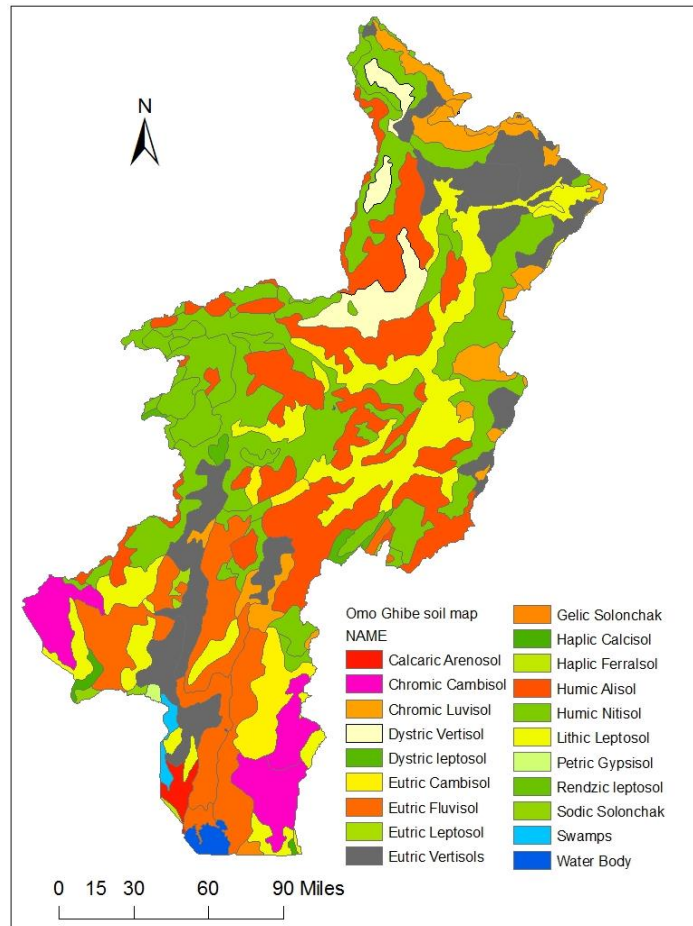


Figure 4.9 Soil map of Omo Gibe basin<sup>15</sup>

#### 4.3.3.3 Land use

Land use pattern of northern catchment is characterized by extensive cultivation with increased land pressure. According to the field visit that has been made in 2011 and mid of 2012 forest areas are now confined to areas too steep and inaccessible to farm.



Figure 4.10 Omo Gibe River and part of the catchment; smoke is seen as people clearing the forest for preparation of charcoal<sup>16</sup>

<sup>15</sup> Source Ministry of water and energy of Ethiopia

<sup>16</sup> Pictures photographed during field visit in April 2012

Generally central western part of the basin boundary area has extensive tracts of high forest. The Gibe, Gojeb and Omo gorges are relatively unpopulated and support a cover of open woodland and bush land through inaccessible area, such as where the Addis Ababa to Jimma road crosses the Gibe Gorge, woodlands are being cleared for charcoal. Eastern catchment boundary has some of the most densely populated and intensively farmed areas in the basin. The south of the basin is more sparsely populated with a greater population of natural vegetation. Figure 4-11 present land use distribution of the Omo river basin. Large proportion of the basin's land use dominated by four land use categories namely Woodland, Agricultural, forest and bush land.

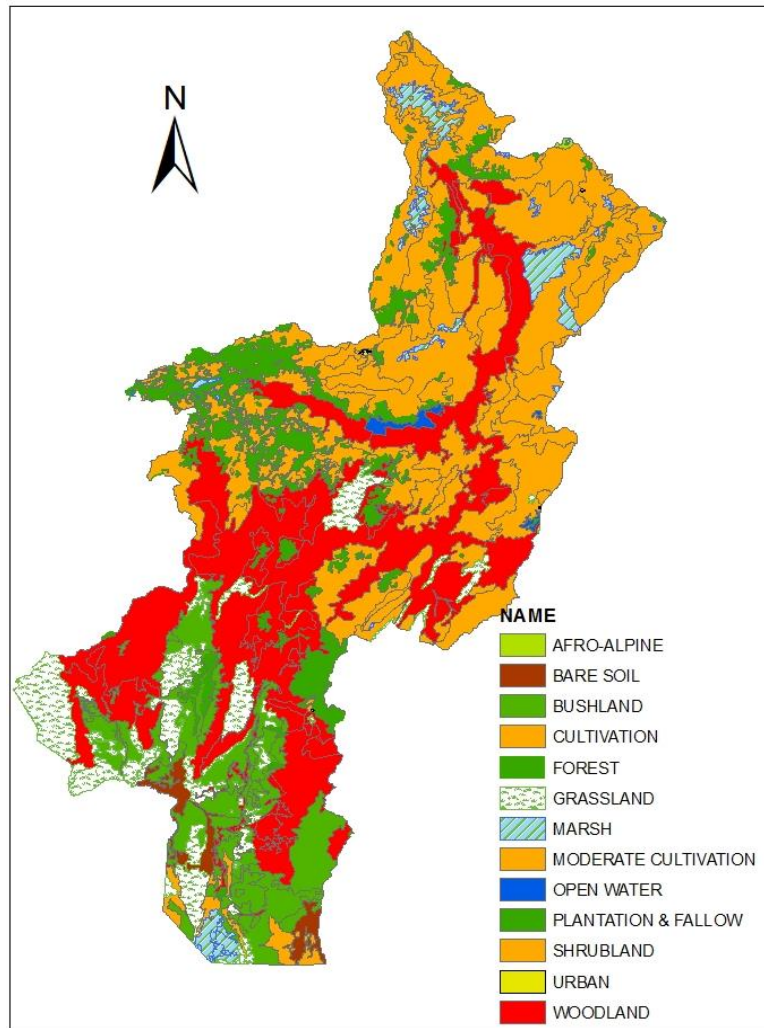


Figure 4.11 Land use map of Omo Gibe basin<sup>17</sup>

<sup>17</sup> Land use map of Omo Gibe basin collected from MoWEE

Table 4-2 shows the relative percentage distribution of these dominant land use categories in the basin, which were computed using ARC-GIS according to the available information on the land use map of the entire Omo Gibe basin.

S no.	Land use type	Area km <sup>2</sup>	Percentage of land use type
1	Woodland	23794	30.02
2	Intensive cultivation	23637	29.82
3	Bushland	7978	10.06
4	Forest	6722	8.48
5	Grassland	5906	7.45
6	Moderate cultivation	5609	7.08
7	Marsh	2103	2.65
8	Shrubland	1111	1.4
9	Bare soil	1037	1.31
10	Plantation and fallow	1001	1.26
11	Open water	321	0.41
12	Afro-Alpine	38	0.05
13	Urban	18	0.02
<b>Total</b>			<b>100</b>

Table 4.2 Percentage of land use type in Gibe basin

#### 4.4 Hydropower development in the basin

Ethiopian water resources and its geographical land scape provide a good opportunity for hydropower production. The Ethiopian government has doing a lot in order to meet the rising demand for electricity and exerts its effort through Ethiopian electric power corporation (EEPCo) for taping its abundant water resources for the production of electric power. The government has a long plan in the construction of several hydroelectric power plants on the main river basins including Omo Gibe basin. Hence the Omo-Gibe basin is a very significant potential hydropower and irrigation resource within Ethiopia, and a logical target for development.

Several other projects are either under preparation to enter into implementation or under various stages of study and tender processes stage. One of those projects is Gibe III hydroelectric projects that shall have an installed capacity of 1,870 MW (Binquet and Asnak, 2013).

The country has a hydropower potential of 45,000 MW, until now it is able to produce 2060 MW. In the GTP-1 (growth and transformation plan-1) which lasts for a period of 2010/11-2014/15 the activities are under going to arrive at 10,000 MW hydropower production capacity. In the GTP-2 is planned to increase the hydropower production up to 15,000 MW from the hydropower potential (Getaneh A., 2013).

The following picture depicts the locations of Gilgel Gibe I, Gibe II and Gibe III cascaded hydropower plants in the basin.

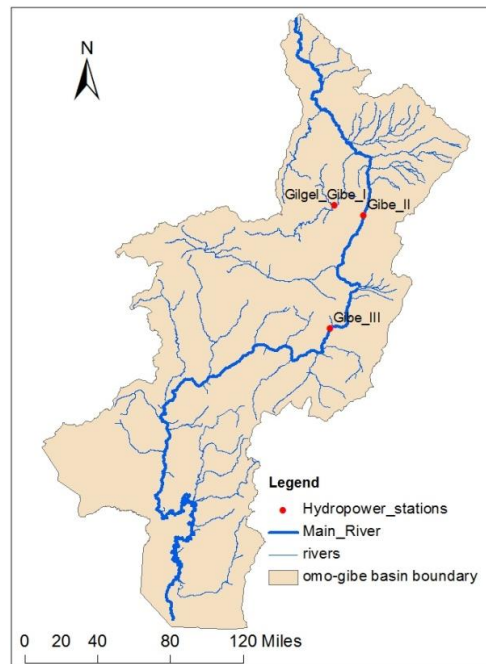


Figure 4.12 Location of main hydropower stations in omo Gibe basin

## 4.5 Description of the three hydropower stations

Construction of a cascade hydropower schemes commenced in the Omo River with Gibe I hydropower scheme commissioned in 2004. The Gibe II hydropower project followed, and was commissioned in 2010, with Gibe III construction having commenced in 2006 (S. Avery, 2012).

### Gilgel Gibe I

The single plant adopted scheme is a purely hydroelectric project, aimed to increase energy and power supply to the National Grid. It is located on the Gilgel Gibe River, some 260 km South-West of Addis Ababa and 70 km North East of Jimma in the Oromiya Region. The general feature of this project is explained in the following table.

<b>Hydrology</b>		<b>Unit</b>
Catchments area	4225	km <sup>2</sup>
Average annual flow	50.4	m <sup>3</sup> /s
Annual runoff	1578	Mm <sup>3</sup>
<b>Reservoir</b>		
Maximum normal water level	1672	m a.s.l.
Normal operating level	1671	m a.s.l.
Minimum operating level	1653	m a.s.l.
Total storage	839	Mm <sup>3</sup>
Live Storage	657	Mm <sup>3</sup>
<b>Dam</b>		
Rockfill with bituminous upstream facing		
Crest elevation	1675	m a.s.l.
Maximum height	40	m
Installed capacity	184	MW

Table 4.3 Basic features of Gilgel Gibe I hydropower plant (EEPCo, 2004).

## Gibe II

The Gilgel Gibe II Power station is the second hydroelectric power station on the Omo River. The power station receives water from a tunnel entrance 7°55'27"N 37°23'16"E on the Gilgel Gibe River. It has an installed capacity of 420 MW and was inaugurated on January 14, 2010. Almost two weeks after inauguration, a portion of the head race tunnel collapsed causing the station to shut down; repairs were complete on December 26, 2010.

The Gilgel Gibe II consists of a power station on the Omo River that is fed with water from a headrace tunnel and sluice gate on the Gilgel Gibe River. The headrace tunnel runs 25.8 km (16 mi) under the Fofa Mountain and converts into a penstock with a 500 m (1,600 ft) drop. When the water reaches the power station, it powers four Pelton turbines that operate four 107 MW generators<sup>18</sup>. The Gibe II plant uses the waters discharged by Gilgel Gibe I and has a gross head of 505 m used by an open air power station of 420 MW installed capacity. This new head is created by a waterway that bypasses about 10 Km of the two rivers (Gilgel Gibe and Omo). The intake is located on the Gilgel Gibe river about 200 m downstream of the Gilgel Gibe I outlet. The waterway crosses the ridge between the Gilgel Gibe valley and the Omo valley by means of 25.8 km of tunnel and 1.2 km of penstocks. The flow discharged by the turbines of Gibe I plant and diverted into the Gibe II intake (EEPCo, 2004). The following table shows the basic features of this hydropower station.

<b>Hydrology</b>		<b>Unit</b>
Catchment area	4304	km <sup>2</sup>
Average flow (receives a regulated flow from Gilgel Gibe I dam)	101.5	m <sup>3</sup> /s
<b>Reservoir</b>		
Max probable flood level(Q= 2325 m <sup>3</sup> /s),corresponding to Max operating level	1437.6	m.a.s.l.
Normal operating level (max retained level)	1431.5	m.a.s.l.
Minimum operating level	1424	m.a.s.l.
Total storage	1.9	Mm <sup>3</sup>
Reservoir area at normal operating level	216	m <sup>3</sup>
<b>WEIR</b>		
Crest Elevation	1439	m.a.s.l.
Max Height (u/s)	49	m
Crest Length	140	m

Table 4.4 Basic features of Gibe II hydropower plant

## Gibe III

The Gibe III hydroelectric is located within the Omo Gibe River basin in the middle reach of the Omo River around 450km by road South of Addis Ababa. The dam for Gibe III is on the Omo River and the reservoir stretches to its tributaries the Gibe and Gojeb Rivers. The scheme, from the end of the reservoir to its tailrace out fall, extends over a corridor 150 km long (EEPCo, 2009).

It is under construction which has 243 m high roller-compacted concrete dam with an associated hydroelectric power plant on the Omo River . Once completed it would be the largest hydroelectric plant in Africa with a power output of about 1870MW. The Gibe III dam would be part of the Gibe cascade, a series of dams including the existing Gibe I dam (184 MW) and Gibe

<sup>18</sup> Source from wikipedia as visited on May 2013  
[http://en.wikipedia.org/wiki/Gilgel\\_Gibe\\_II\\_Power\\_Station#cite\\_note-italy-1](http://en.wikipedia.org/wiki/Gilgel_Gibe_II_Power_Station#cite_note-italy-1)



II power station (420 MW) as well as the planned Gibe IV (1472 MW) and Gibe V (560 MW) dams<sup>19</sup>.

<b>Hydrology</b>		<b>Unit</b>
Catchment area	34,150	km <sup>2</sup>
Average annual runoff	438.2	m <sup>3</sup> /s
Average annual volume	13,820	Mm <sup>3</sup>
<b>Reservoir</b>		
Minimum operating level	800	m.a.s.s
Normal operating level	889	m.a.s.s
Maximum water level in the reservoir	892	m.a.s.s
Live storage volume	11,750	Mm <sup>3</sup>
Surface area at normal operating level	200	km <sup>2</sup>
<b>Dam</b>		
Dam Type	(RCC) dam	
Foundation elevation	665	m.a.s.s
Height above river bed elevation	231	m
Crest elevation	896	m.a.s.s
Crest length	580	m

Table 4.5 Basic features of Gibe III hydropower plant (EEPco, 2009).



Figure 4.13 Gilgel Gibe I and II hydropower plant respectively

<sup>19</sup> [http://en.wikipedia.org/wiki/Gibe\\_III\\_dam](http://en.wikipedia.org/wiki/Gibe_III_dam) as visited on Jun 2013

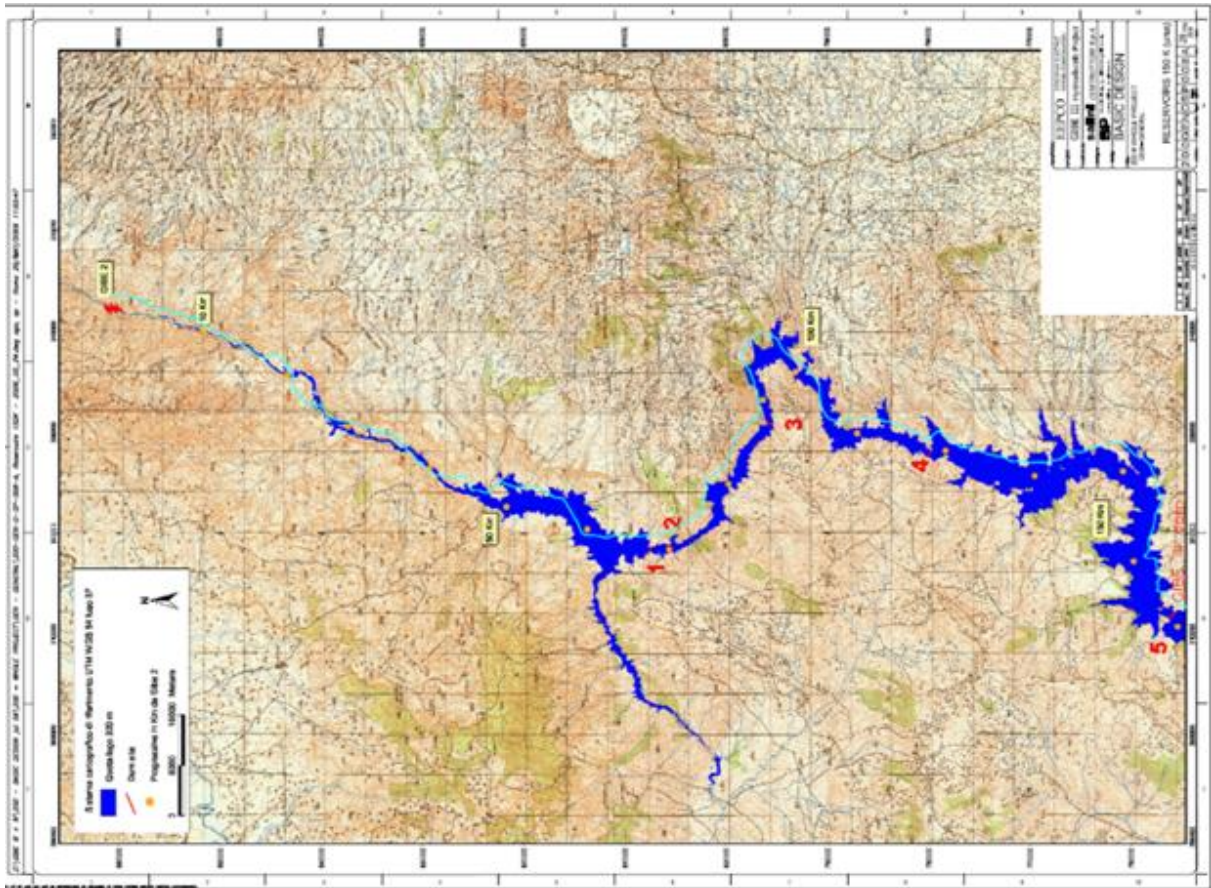


Figure 4.14 Bird eye view of Gibe III reservoir (EEPCo, 2009)



## Chapter 5 Data, Methodology & Downscaling of Climate Model outputs

### 5.1 Climate data

The most important time series data necessary for any climate change research is long time weather data. Baseline climate information is important to characterize the prevailing conditions. It can also be used as a reference with which the results of any climate change studies can be compared. The choice of baseline period has often been governed by availability of the required climate data. According to World Meteorological Organization (WMO), the baseline period also called reference period generally corresponds to the current 30 years normal period. A 30-year period is used by WMO to define the average climate of a site or region, and scenarios of climate change are also generally based on 30-year means. Most impact assessments seek to determine the effect of climate change with respect to 30 years present time frame, Therefore, one crucial step is to set the time reference of analysis in response to the data availability; based on this consideration recent baseline periods for Omo Gibe basin has been set from 1970 to 2000 which accounts the recent 31 years.

#### 5.1.1 Observed climate data

In order to account the climate change study in the basin, precipitation, maximum and minimum temperature data collected from national meteorological agency of Ethiopia for the following weather observation stations. Additionally sunshine hours from six climate stations collected.

S.No	St_Name	latitude	Longitude	Data type collected		
				Prec.	Max T	Min T
1	Assendabo	7.77	37.23	yes	yes	yes
2	Bele	7.08	37.58	yes	no	no
3	Bonga	7.22	36.23	yes	yes	yes
4	Chekorsa	7.62	36.73	yes	no	no
5	Woliso	9	37	yes	yes	yes
6	Dedo	7.52	36.87	yes	yes	yes
7	Durame	7.24	37.89	yes	no	no
8	Gedo	9.05	37.43	yes	yes	yes
9	Gibe Farm	8.23	37.58	yes	no	no
10	Hossana	7.57	38.85	yes	yes	yes
11	Jimma	7.67	36.83	yes	yes	yes
12	Jinka	5.8	36.55	yes	yes	yes
13	Kumbi	8.12	37.47	yes	no	no
14	Limu genet	8.1	36.95	yes	no	no
15	Meteso	7.43	36.88	yes	no	no
16	Morka	6.43	37.27	yes	yes	yes
17	Sawula	6.32	36.88	yes	yes	yes
18	Shebe	7.52	36.52	yes	yes	yes
19	Wolita S.	6.83	37.75	yes	yes	yes
20	Wolkite	8.27	37.75	yes	yes	yes
21	Yaya	8.37	37.53	yes	yes	yes

Table 5.1 List of selected weather stations in Omo Gibe basin

Most of the above listed weather observations have recorded precipitation value starting from 1971 even before; except Morka precipitation station which has a recorded length starting from 1985. Regarding to temperature data long year's data have been collected except Morka, Shebe, Wolkite and Gedo. These four stations have relatively smaller recorded data, accordingly from Gedo 24 years daily data (1977-2000), from Shebe 21 years (1980-2000) and from Wolkite 16 years (1985-2000) have been collected. Many of the above listed stations are found at the upper part of the basin above Gibe III dam site as a result this part of the basin is well represented by 18 weather observation stations. However, Southern part of the basin represented by three weather observation stations these are; Morka, Sawula and Jinka.

### **5.1.2 REMO and GCM data**

The regional climate model data consist of results from RCM named REMO. It is one of the selected climate model outputs for this study. This model has been developed at Max-Planck-Institute of Meteorology. The model domain covers all part of Omo-Gibe basin. The spatial resolution of the analyzed models is approximately 50km (0.5 degree by 0.5 degree) with temporal resolution of 1 day. This climate model output contains basic climatological data like; precipitation, maximum and minimum temperature, solar radiation, wind speed and relative humidity for reference time period (1960 to 2000) and future time period (2000 -2050) as well. The future time period has two scenarios results of A1B and B1 for three conditions each.

REMO is based on the Europa Model (EM), the former numerical weather prediction model of the German Weather Service (DWD) and is described in Jacob D. 2001. The physical parameterization package of the general circulation model ECHAM4 has been implemented. Physical parameterizations are taken from ECHAM4 and adjusted to the scale of REMO (Paeth H. 2005).

Large scale predictors from GCM which cover the entire Omo Gibe basin can be accessed from:<http://www.cics.uvic.ca/scenarios/index.cgi?Scenarios>. And HadCM3 A2 scenario of GCM output has been selected for further processing. HadCM3 is a coupled atmosphere-ocean GCM developed at the Hadley Centre. The atmospheric component of the model has 19 levels with a horizontal resolution of 2.5 degrees of latitude by 3.75 degrees of longitude, which produces a global grid of 96 x 73 grids cells. This is equivalent to a surface resolution of about 417km x 278km ([http://cerawww.dkrz.de/IPCC\\_DDC/IS92a/HadleyCM3/Readme.hadcm3](http://cerawww.dkrz.de/IPCC_DDC/IS92a/HadleyCM3/Readme.hadcm3)). The predictor variables are supplied on a grid box by grid box basis. On entering the location of Omo-Gibe basin the following predictor variables were downloaded;

- NCEP 1961-2001 this directory contains 41 years of daily observed predictor data, derived from the NCEP reanalysis. This used for calibration of SDSM model.
- H3A2 1961-2099 this directory contains 139 years of daily GCM predictor data, derived from the HadCM3 A2 experiment and
- H3B2 1961-2099 this directory contains 139 years of daily GCM predictor data, derived from the HadCM3 B2 experiment. Figure 5.2 illustrates the grid points of REMO and GCM for the whole Gibe basin.

### **5.1.3 Filling of observed precipitation and temperature missed data**

Some of weather observation stations have incomplete records; because of this they should be filled in sequence. To fill the missed precipitation data a well known methodology inverse distance weighing method has been applied this method relies on the data from a number adjacent stations. The locations of these adjacent stations are such that they should be close to and approximately evenly spaced around the site with the missing data. To account this condition stations which have not been selected for climate change study also considered, based on the availability of the data they have.

To check the quality of the data cross correlation between the accumulated totals of the gauge in question are compared with the corresponding totals for a representative group of nearby

gauge. In order to check the consistency of all the rainfall stations the double mass curve was used. According to the result all the selected stations were consistent as a result all the stations have been used for climate change study and simulation purpose.

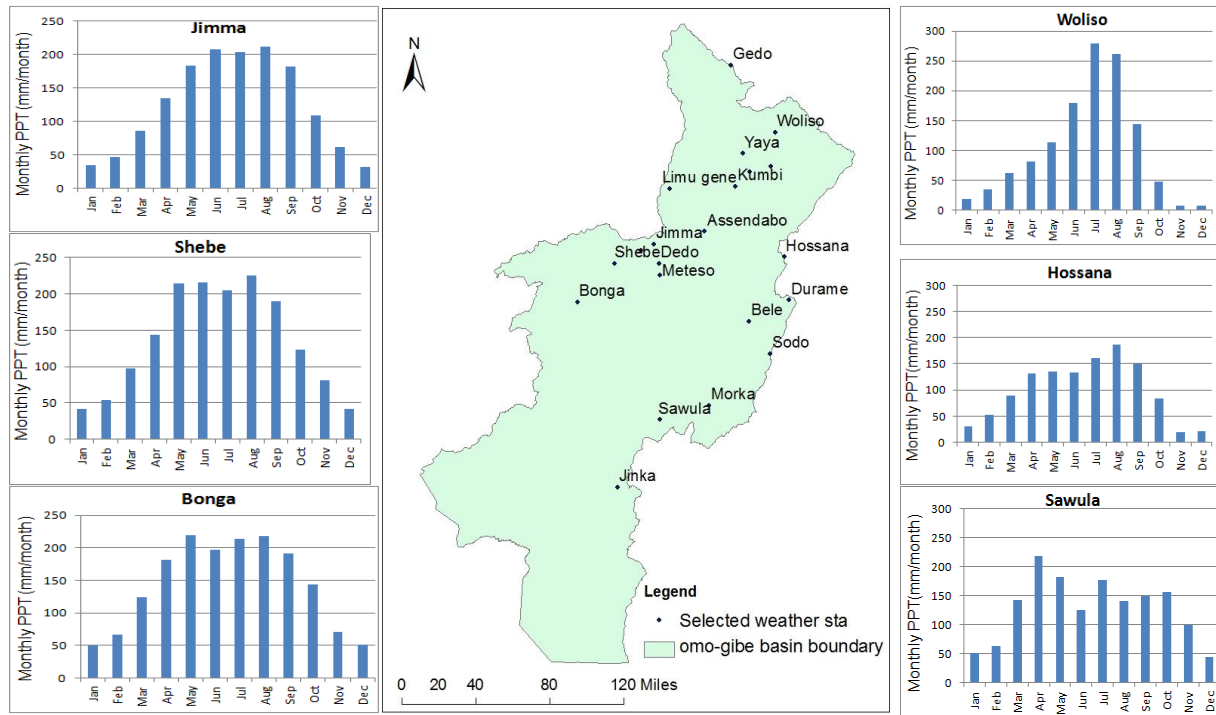


Figure 5.1 locations of representative meteorological stations mean monthly rainfall histogram (1970-2000) from east and western part of the basin.

The missed gaps for maximum and minimum temperature data have been filled using SDSM weather generator methodology. SDSM includes the WGEN (weather generator) section to generate climatic data to fill in gaps in measured records. The weather generator operation produces ensembles of synthetic daily weather series by providing observed large scale predictor (or NCEP re-analysis) atmospheric predictor variables and regression model weights produced by the model during calibration operation for available data sets. During calibration time the observed missed value designates as -999. The weather generator enables the synthesis of artificial time series representative of present climate conditions to reasonable accuracy. Afterwards the missed maximum and minimum temperature filled from this generated value. This procedure is the same as downscaling of current climate condition from NCEP reanalysis data, and detail procedure of this methodology is described on the GCM downscaling section of this thesis.

#### 5.1.4 Hydrological data

River discharge is an important property to know the timing of flow within and between seasons. Moreover, this data is the right hand of this research, because water resource potential of the basin can be determined from this data set for reference time period, additionally the future water condition of the basin due to climate change will be quantified by comparing with the current water potential of the basin. Runoff unfortunately not as many gauging stations as rainfall ones are present in the basin under investigation, but few of them are located at key sites, like Abelti which has particular importance for this research. Daily discharge data of Omo River, for the period of 1970-2000, was acquired from Ministry of water resources and energy of Ethiopia that monitors the Rivers discharges in the country. Table 5.2 and figure 5.2 presents list of flow measuring stations and stream network of Omo River. Most of the flow measuring stations except Shebe, Megecha and Wolkite are found upstream of Abelti flow measuring

stations and they record flow relatively from small catchment areas. Abelti station is the only flow measuring station which measures flow from 15,690km<sup>2</sup> area.

S No.	Station Name	Location		Catchment Area km <sup>2</sup>	Observation	
		Long.	Lat.		available data n. Year	coverage period
1	Gibe@Abelti	37°35'	8°14'	15690	31	1970-2000
2	GG@Assendabo	37°11'	7°45'	2966	31	1970-2000
3	Wabe@Wolkite	37°46'	8°15'	1866	31	1970-2000
4	Gojeb@Shebe	26°23'	7°25'	3577	31	1970-2000
5	G@limugenet	36°56'	8°06'	533	17	1984-2000
6	G@Seka	36°45'	7°36'	280	20	1980-2000
7	Bidru Awana	37°24'	7°55'	41	20	1981-2000
8	Bulbul nr. Serbo	37°02'	7°34'	301	15	1986-2000
9	Megecha@Gubre	37°28'	8°11'	286	31	1970-2000
11	Gecha nr. Bonga	36°13'	7°17'	175	19	1982-2000
12	Shete nr. Bonga	36°14'	7°17'	191	21	1980-2000
13	Gogheber nr Endibir	37°54'	8°6'	190	31	1970-2000

Table 5.2 List of flow measuring stations

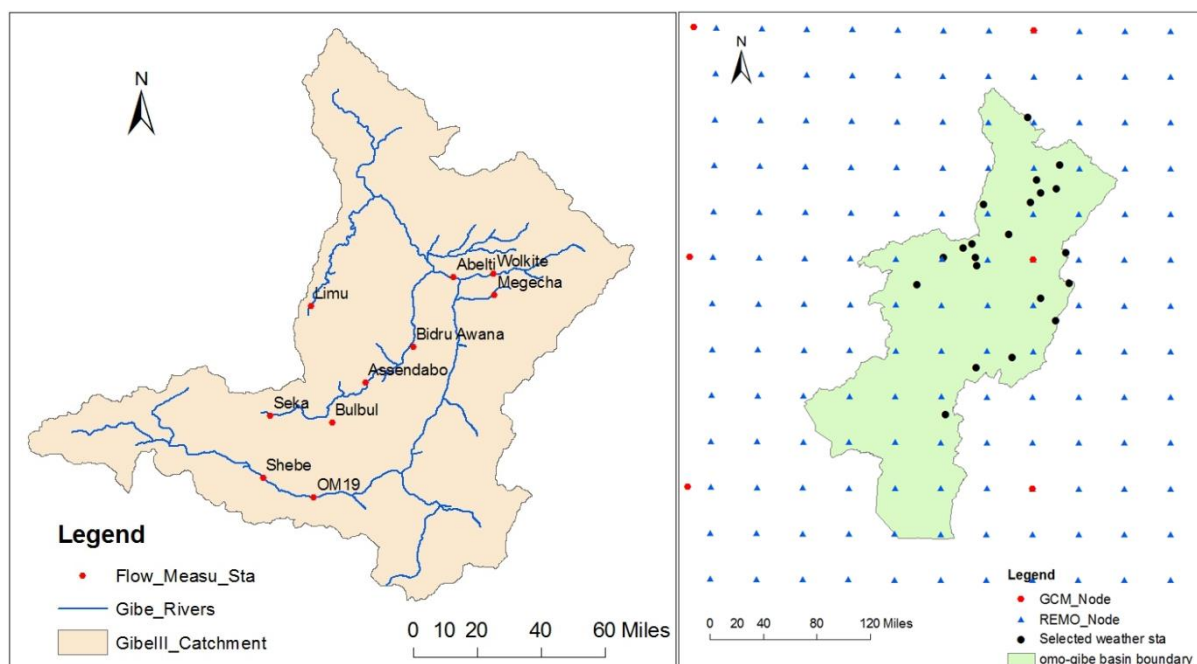


Figure 5.2 Flow measuring stations in the upper part of the basin and observed, REMO and GCM grid node in the entire Omo Gibe basin

In addition to the above mentioned data, spatial data of the basin like soil map and land use map have been collated from MoWEE. The detail preparation of these data for modeling purpose will be discussed in detail during calibration of SWIM at Abelti and Gibe III dam site in chapter six.

## 5.2 Distribution mapping method to downscale Remo output

This part of the study focused on statistical downscaling of daily climate variables from REMO and GCM output for climate change and impact assessment in Omo Gibe basin. Detail methodology and discussions given in the following section.

### 5.2.1 Cumulative distribution mapping method (CDM) for precipitation

One of the main objectives of this part of the research is providing of reasonable and consistent meteorological input data from regional climate model REMO and GCM outputs for modeling of future river runoff at the Omo Gibe basin. The set of 4 model runs were analyzed for future scenario generation; two set of model run from A1B wet and optimum condition and two sets of B1 model run wet and dry conditions. Here; wet, optimum and dry condition are given to the scenarios run outputs based on the amount of precipitation simulated. Accordingly, A1B\_911 wet, A1B\_912 optimum, B1\_921 wet and B1\_923 dry condition will be used throughout this study. At the beginning of downscaling procedure, Instead of choosing the nearest REMO grid data to observation stations, precipitation and temperature scenarios from 1970–2050 with daily temporal resolution have been interpolated with bilinear interpolation from the four nearest REMO grid points, as this method helps in conserving properties of robustness and eliminating unrealistic jumps.

The method is as follow,

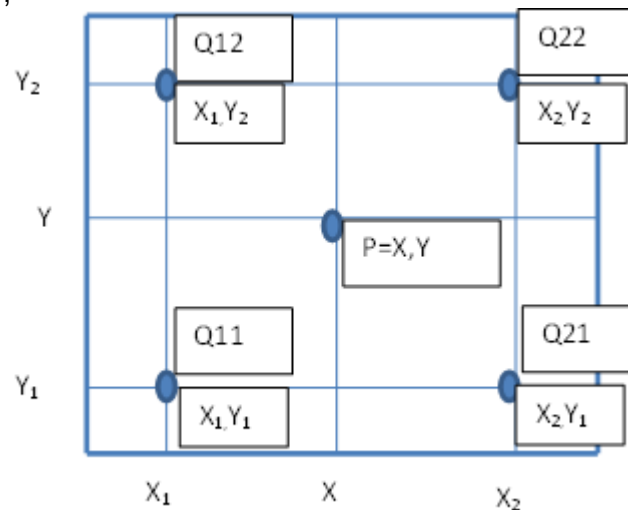


Figure 5.3 Representations of Remo grind nodes and one weather observation station

In the above figure 5.3 let us consider point p is one of observation point, Q11, Q12, Q21 and Q22 are REMO grid data. By considering the x and y distance of these four stations relative to the observation stations daily climate projections from regional climate model (REMO) are first downscaled to specific weather observation sites using bilinear interpolation method. The equation used for interpolation procedure is as follow.

$$p(x, y) = \frac{(x_2 - x)(y_2 - y)}{(x_2 - x_1)(y_2 - y_1)} Q_{11} + \frac{(x - x_1)(y_2 - y)}{(x_2 - x_1)(y_2 - y_1)} Q_{21} + \frac{(x_2 - x)(y - y_1)}{(x_2 - x_1)(y_2 - y_1)} Q_{12} + \frac{(x - x_1)(y - y_1)}{(x_2 - x_1)(y_2 - y_1)} Q_{22} \quad 5.1$$

After interpolation of climate data to observation stations a comparison were carried out for control period, because this comparison would help us how REMO output represents the current climate conditions. The result showed that there is a marked disagreement between observed mean annual values and standard deviation in observed and simulated climate within the control period 1970–2000. These results are depicted in the following table clearly.

S.No	Stations	Observed Precipitation (mm)	Interpolated REMO precipitation (mm) (1970-2000)	Error (Remo prec.-Obs prec) (mm)	%age of error
1	Assendabo	1214.3	1389.6	175.4	14%
2	Bele	1240.9	1234.3	-6.6	-1%
3	Bonga	1726.5	1234.3	-492.1	-29%
4	Chekkorsa	1698.3	1542.2	-156.2	-9%
5	Dedo	1959.3	1514.3	-445.0	-23%
6	Durame	1153.1	1214.9	61.8	5%
7	Gedo	1141.4	1429.7	288.3	25%
8	Gibe	976.5	1291.1	314.6	32%
9	Hossana	1193.6	1235.8	42.2	4%
10	Jimma	1493.3	1515.9	22.6	2%
11	Jinka	1307.9	927.8	-380.1	-29%
12	Kumbi	1283.4	1298.8	15.4	1%
13	Limu	1753.5	1452.9	-300.6	17%
14	Meteso	1925.5	1486.9	-438.6	-23%
15	Morka	1367.0	1236.5	-130.4	-10%
16	Sawula	1547.4	1191.0	-356.4	-23%
17	Shebe	1634.2	1443.5	-190.7	-12%
18	Woliso	1239.0	1310.4	71.4	6%
19	Sodo	1402.1	1232.1	-170.0	-12%
20	Wolkite	1339.5	1283.7	-55.9	-4%
21	yaya	1095.7	1302.9	207.2	19%

Table 5.3 Mean annual precipitation observed and interpolated from REMO simulations for current time period (1970-2000).

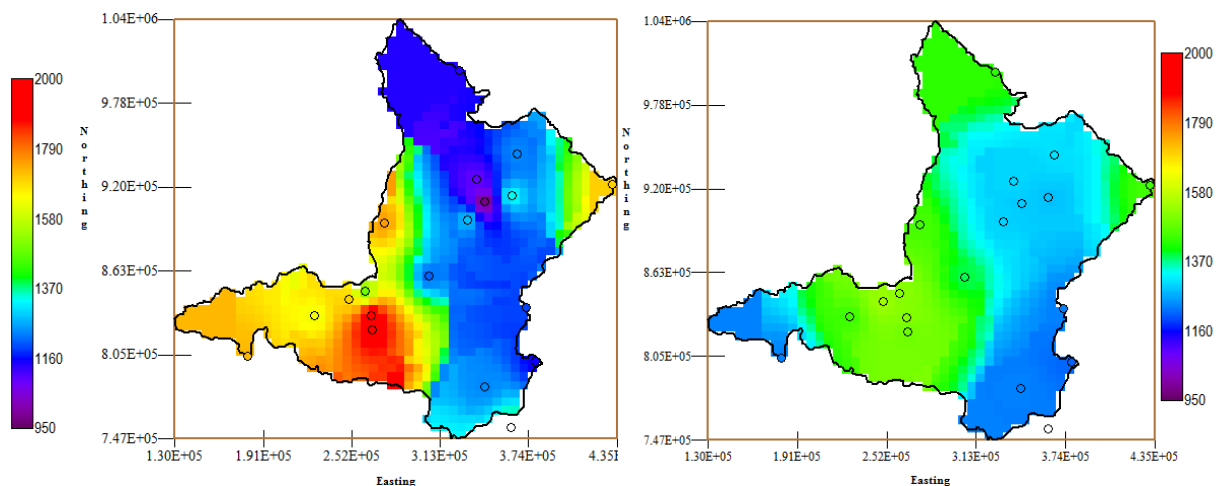


Figure 5.4 Comparisons of mean annual precipitation, spatially interpolated using inverse distance weighing for observed and historical REMO simulations (1970-2000) respectively

As it is possible to see from the above table 5.3 and figure 5.4 there are marked disagreements between observed mean annual values in observed and simulated climate within the control period 1970–2000. Simulated precipitation statistics from REMO are generally affected by a



positive and negative bias in the number of stations. This proved that ,although, REMO simulates the precipitation on a sub-daily time step, its coarse spatial resolution and resulting distortion of day-to-day variability limits the use of its daily output as a direct input data to SWIM hydrological modeling for simulation of future flow in Omo Gibe basin without downscaling and bias correction procedure.

Direct comparison of results from REMO simulation and observations from Omo Gibe stations during the same period showed that temperature and precipitation fields produced by REMO is too coarse to give detailed estimates of point values. The interpolated precipitation from REMO has shown great divergence especially to western part of the catchment. REMO simulation highly underestimated the mean annual rainfall for wettest part and higher altitude of the basin, for instance mean annual rainfall at Bonga, Chakorsa, Dedo, Limu, Meteso and shebe underestimated by 492mm, 156mm, 445mm, 300mm, 438mm and 190mm respectively. Some low-lying sites like Yaya and Gibe and stations which have relatively lower mean annual rainfall, the precipitation value interpolated from the regional climate model REMO is estimated higher value.

According to rough observation made on the output of REMO, precipitation for Omo Gibe basin simulated by this model has a low number of dry days, which is partly compensated by an excessive number of occurrences of drizzle which leads to a bias in the mean and standard deviation (variability), and the inability to reproduce extreme events like the observed high precipitation events. For future flow forecast in Omo Gibe basin a realistic representation of precipitation and temperature fields in future climate projections from climate models is crucial for assessment of flow potential, because of this bias correction method is very important.

To overcome the biases in Interpolated (primarily downscaled) REMO; a methodology applied for correcting climate model output to produce internally consistent fields that have the same statistical intensity distribution as the observations. A frequency distribution mapping methodology is used which corrects the frequency and the intensity distribution of daily REMO rainfall relative to a target stations.

Distribution mapping is a statistical downscaling method developed to correct the bias in a manner that better captures the potential variability of future climate changes. The method is based on a bias correction scheme for downscaling climate model output described by (Wood et al., 2002; Ines and Hansen, 2006; Elshamy et al., 2009).

According to (Ines and Hansen, 2006) If REMO rainfall frequency is greater than observed frequency for a given month, averaged across years, REMO rainfall frequency is corrected by discarding rainfall events below a calibrated threshold. Fortunately there were no such events in many of the stations in Omo gibe basin, however, rainfall values which has very small magnitudes less than 0.3mm ignored from simulations. To correct the intensity distribution, each REMO rainfall amount above the calibrated threshold is mapped from the REMO intensity distribution onto the observed distribution.

Based on this, the methodology involves two stapes bias correction procedures:

- ✓ correction of frequency
- ✓ correction of intensity

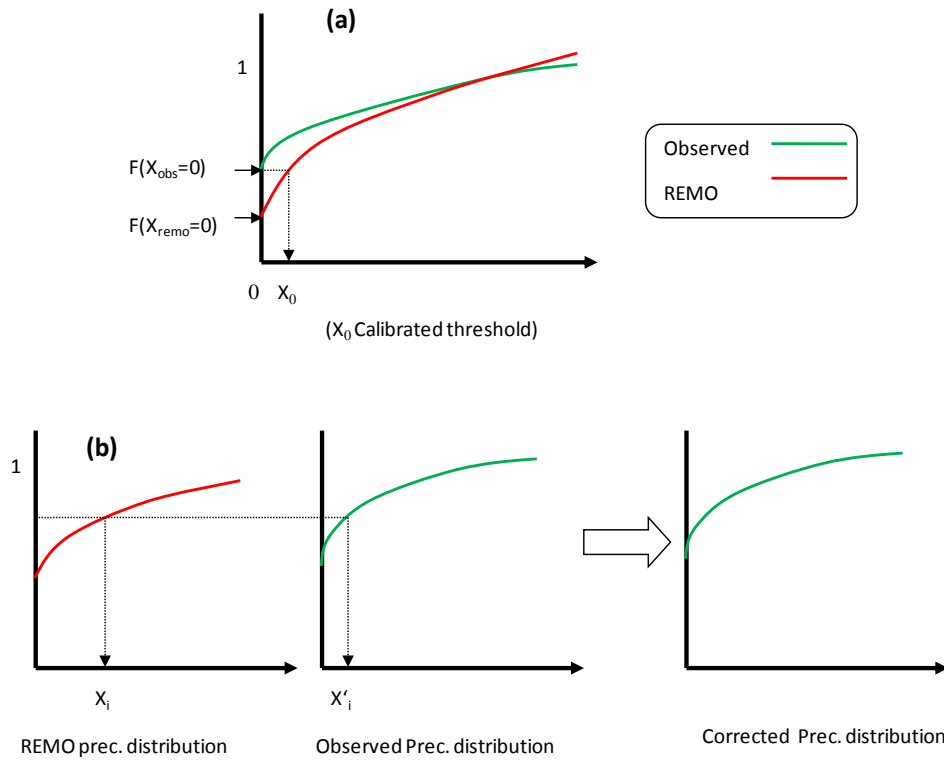


Figure 5.5 Schematic representation bias correction methodology: (a) frequency, (b) intensity (Ines & Hansen 2006). Where  $x_i$  and  $x'_i$  refer to REMO and observed rainfall on day  $i$ , respectively

### 5.2.1.1 Distribution mapping of gamma equation to Omo Gibe precipitation

It is widely recognized that the distribution of daily precipitation can be well approximated by gamma function. Therefore, an assumption has been carried out that observed, historical and scenario simulated intensity distributions are well approximated by the gamma distribution. The effect of this distribution on Gibe basin observed and REMO simulated precipitation can be observed from (Figure 5.6). As a result, all observed and interpolated REMO precipitation scenarios were disaggregated it to monthly basis at each observation station from January to December. Basically three datasets were used in connection with this analysis; observed rainfall from 1970 to 2000, baseline REMO from 1970 to 2000 and projected rainfall from REMO and four scenarios from 2020 to 2050.

Gamma distribution can be expressed by the following probability density function (PDF).

$$PDF = f(x) = \frac{1}{\beta^\alpha \Gamma(\alpha)} X^{\alpha-1} \exp\left(-\frac{X}{\alpha}\right) \quad 5.2$$

The mean rainfall  $x$  (mm/day) in the above equation 5.2 is defined as product of the mean intensity on wet days when precipitation exceeds 0.3mm. Since REMO simulates low number of dry days, which are compensated by too much drizzle, small rainfall magnitudes less than 0.3mm were excluded from simulation.

First, a two-parameter gamma distribution was fitted separately to the observed and REMO rainfall on wet days to model the intensity distributions on monthly basis starting from January to December with the following equation 5.3.



$$F_i(x; \alpha, \beta) = CDF = \frac{1}{\beta^\alpha \Gamma(\alpha)} \int_0^x t^{\alpha-1} e^{-\frac{t}{\beta}} dt \quad 5.3$$

The shape and scale parameters ( $\alpha$  and  $\beta$ ) for each gamma distribution (for each station on monthly basis) were determined using maximum likelihood estimation. For example for one observation station twelve times were fitted out of 31 years available data sets from January to December using equation 5.3. After having the shape and scale parameters, the intensity of the rainfall were corrected for historical REMO simulated output by mapping the distribution of REMO on to observed one for each month and each station using equation 5.4.

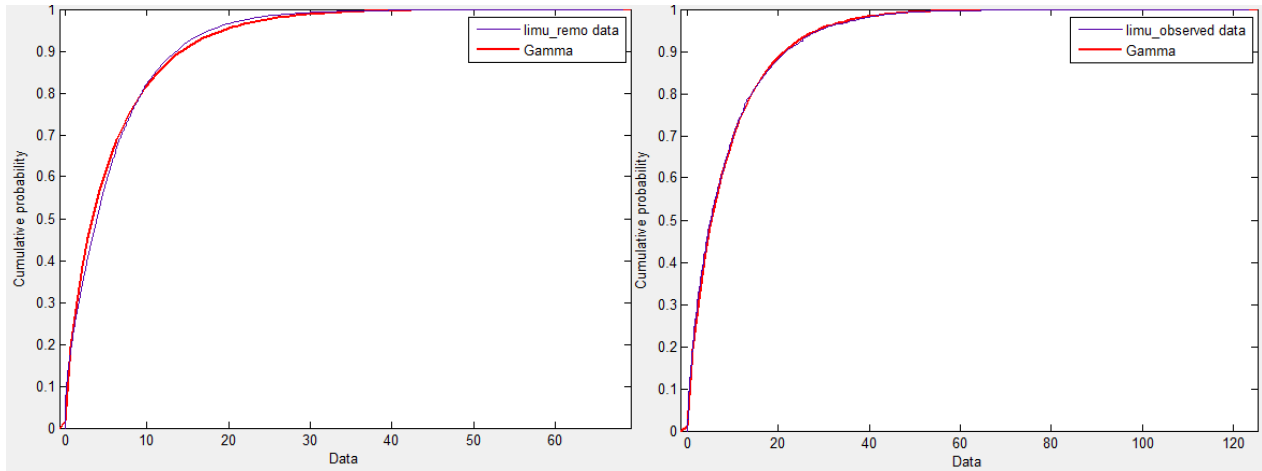


Figure 5.6 The effect of gamma fitting on June precipitation at Limu observation station

Then the cumulative distribution of the daily REMO rainfall  $F_{i,model}(X_i)$  is mapped onto the cumulative distribution of the observations  $F_{i,obs}(X_i)$ . The bias corrected modeled rainfall  $X'_{i,corr}$  on day  $i$  can then be calculated as:

$$X'_{i,corr} = F_{obs}^{-1} \left( F_{i,model}(X_i) \right) \quad 5.4$$

Where  $F_{obs}^{-1}$  is the inverse of observed rainfall distribution function

This whole procedure applied separately for each month of 21 rainfall stations in order to correct errors in monthly and seasonal cycle. As a result, bias free rainfall values from REMO obtained by this procedure from all weather observation stations for current climate condition. The detail results and validation of the methodology will be discussed in the following section.

### 5.2.1.2 Results and discussion on precipitation downscaling

An evaluation procedure is set up to ensure that the accuracy of downscaled daily sequences are consistent with monthly observed values in terms of a number of performance criteria, such as cumulative distributions, differences of the mean, sum and variance between observed and bias corrected data, and also the RMSEs (root mean square errors) of the downscaled values relative to the observed one. The main objective of bias correction method was to reproduce daily and monthly time series of modified precipitation at weather measuring point throughout Omo Gibe basin from REMO. The bias correction method relies on changing of cumulative distribution function (CDF) of modeled data. Additionally the performance of the bias correction methodology is checked by root mean square error (RMSE); because this helps to understand how the magnitude of uncorrected and corrected REMO varying with respect to observed value, since this method compares the pair wise differences of the two data sets that can serve as a measure how far on average the error is from zero. Therefore, the RMSE of the differences is a meaningful measure of the error. The RMSE for each stations were calculate as

$$RMSE_X = \left[ \frac{1}{12} \sum_m (X_m^{obs} - X_m^{cor})^2 \right]^{0.5}$$

5.5

Where  $X_m^{obs}$  mean monthly observed precipitation in control period  
 $X_m^{cor}$  Mean monthly corrected precipitation in control period

Table 5.7 summarizes annual sum of precipitation, inter annual variance and RMSE of observed, REMO simulations and corrected precipitation in control period.

S No	Stations	Annual sum of precipitation (mm)			Variance inter annual			RMSE monthly averaged	
		observed	Uncorr.	corrected	observed	Uncor.	Correct.	Uncorr.	correcte
1	Assendabo	1214.2	1389.6	1206.6	51.6	26.9	54.0	0.76	0.39
2	Bele	1240.9	1234.3	1240.6	55.2	19.8	68.2	0.42	0.08
3	Bonga	1726.5	1513.3	1727.1	60.2	29.7	73.4	0.82	0.04
4	Chekorsa	1698.3	1542.2	1754.5	61.2	31.7	71.6	0.63	0.52
5	Dedo	1959.3	1514.3	1949.6	81.2	35.4	96.5	1.48	0.09
6	Durame	1153.1	1214.9	1154.1	46.8	25.0	57.1	0.54	0.08
7	Gedo	1141.4	1429.7	1142.7	41.7	41.3	48.4	1.32	0.06
8	Gibe	976.5	1291.1	994.0	41.0	23.6	48.3	1.15	0.08
9	Hossana	1193.6	1235.8	1175.4	44.1	30.3	51.3	0.57	0.02
10	Jimma	1493.3	1515.9	1499.6	59.8	64.9	70.1	0.28	0.07
11	Jinka	1307.9	927.8	1270.5	61.2	20.8	69.8	1.16	0.06
12	Kumbi	1283.4	1298.8	1300.2	68.4	23.4	81.4	0.76	0.08
13	Limu	1753.5	1452.9	1751.0	75.7	33.7	85.7	1.16	0.11
14	Meteso	1925.5	1486.9	1924.6	90.4	33.3	104.6	1.50	0.09
15	Morka	1367.1	1236.5	1407.8	45.5	24.6	58.1	0.50	0.09
16	Sawula	1547.4	1191.0	1537.5	74.5	19.5	92.3	1.21	0.12
17	Shebe	1634.2	1443.5	1632.1	56.8	48.4	88.5	1.05	0.09
18	Woliso	1239.0	1310.4	1244.8	47.9	26.0	52.8	0.51	0.04
19	Wolita	1402.1	1232.1	1438.5	72.7	20.7	98.1	0.93	0.14
20	Wolkite	1339.5	1283.7	1352.9	67.9	24.5	76.1	0.70	0.08
21	Yaya	1095.7	1302.9	1108.6	50.7	25.1	59.3	0.84	0.00

Table 5.4 Performance parameters for bias correction methodology between observed, corrected and current time Remo simulation (1970-2000)

As we see from table 5.4 and figure 5.7 RMSE of monthly average parameters were significantly reduced by the bias correction procedure. Except Assendabo and chakorsa the average errors for most of weather observation stations near to zero which indicates that the applied methodology in removing of bias performs very well in producing of current climate data sets. The uncorrected simulation has strong biases which are removed by the correction procedure. In addition to RMSE, sum of mean monthly precipitation and mean monthly variance and cumulative distribution values show great improvement.

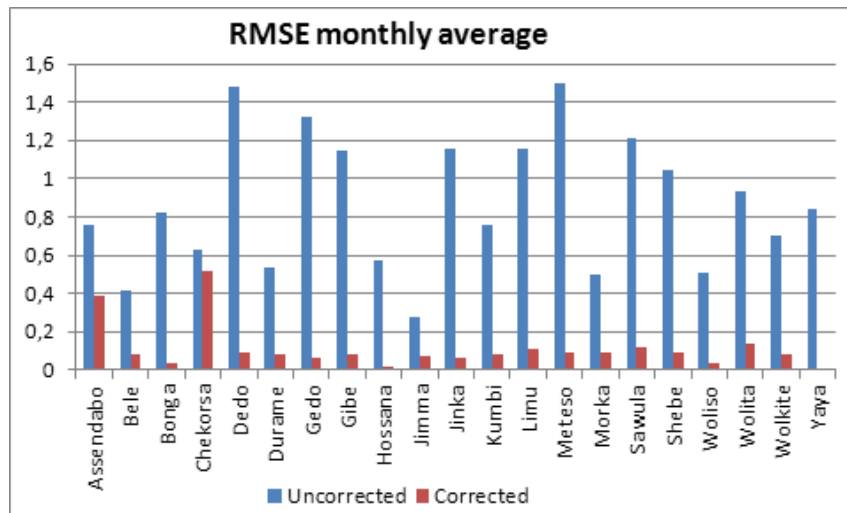


Figure 5.7 RMSE for corrected and uncorrected REMO in historical period 1970-2000

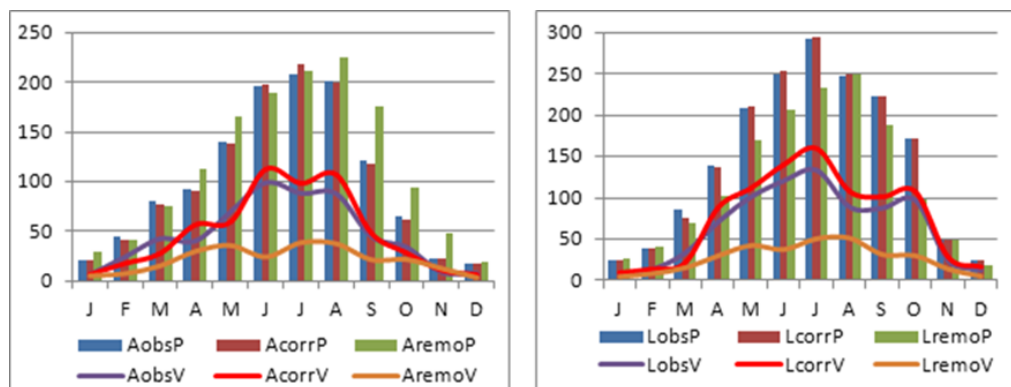


Figure 5.8 Comparison of monthly sum of daily precipitation (mm/month) and variance at Assendabo and Limu from 1970-2000 for observed, corrected and Remo simulation.

Eventhough, this correction procedure has been carried out for all climate stations, at this part of discussion only representative stations considered for elaboration purpose. In figure 5.8 the legends described as follow. The first letter designated the name of the station example (A) Assendabo and (L) Limu, the second three or four letter obs, corr, and remo means observed, corrected and Remo value respectively and the last letter P and V stands for precipitation and variance.

In figure 5.8 uncorrected REMO simulation (yellow green) bar are shown sum of monthly rainfall value overestimated at Assendabo from August to November and the variance under estimated in all months of the year, whereas at Limu the sum of uncorrected REMO rainfall underestimated from March to July. The variance in all observation stations were underestimated to considerable limit. Generally the uncorrected simulation of REMO results has strong monthly negative biases in the overall precipitation and variance especially at Limu precipitation station. Regarding to bias corrected results (dark brown) bar captures the observed (dark blue) bar very well even in monthly basis this means that the corrected model very much closer to observed value. Note that the bias correction was computed using 1970–2000 observations. Hence, the improvements seen in above two figures showed that the corrections method improves the variability, negative and positive biases of the simulated precipitation from REMO significantly. Similar comparisons for the rest of the stations are found at the appendix.

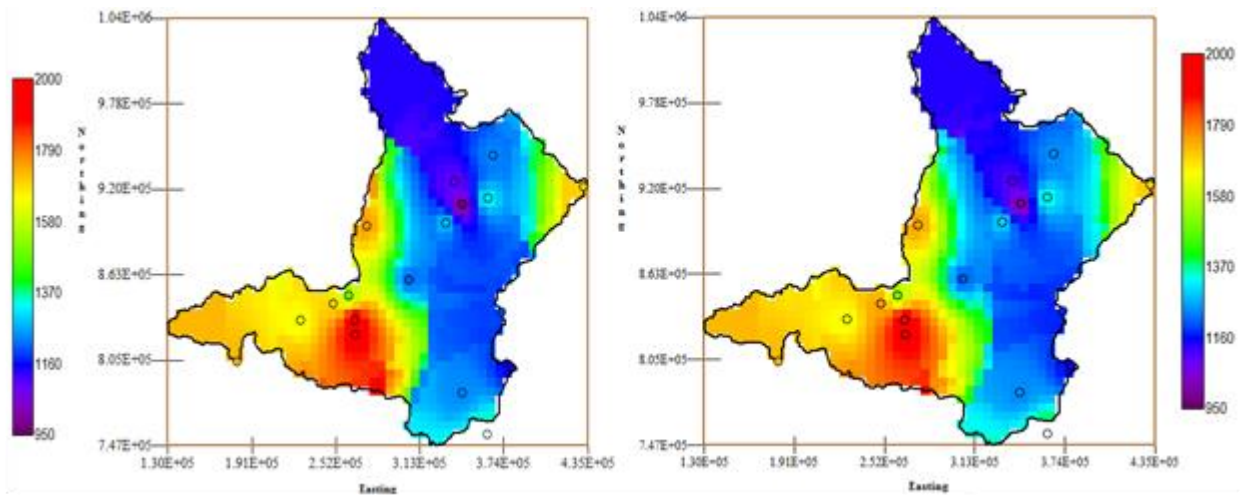


Figure 5.9 Comparison of mean annual rainfall observed and corrected Remo (1970-2000) respectively for upper part of the basin.

Figure 5.9 shows the comparison of spatially interpolated by using inverse distance weighing method for observed and corrected rainfall from Remo simulation. This has been done only for upper part of the basin since most weather observation stations are found in this region. Unfortunately the southern part of Gibe basin below Gibe III dam site is represented only by three weather observation stations because of this interpolation for the entire basin was not carried out. According to the above result the methodology is also robust in simulation mean annual rainfall in all observation stations.

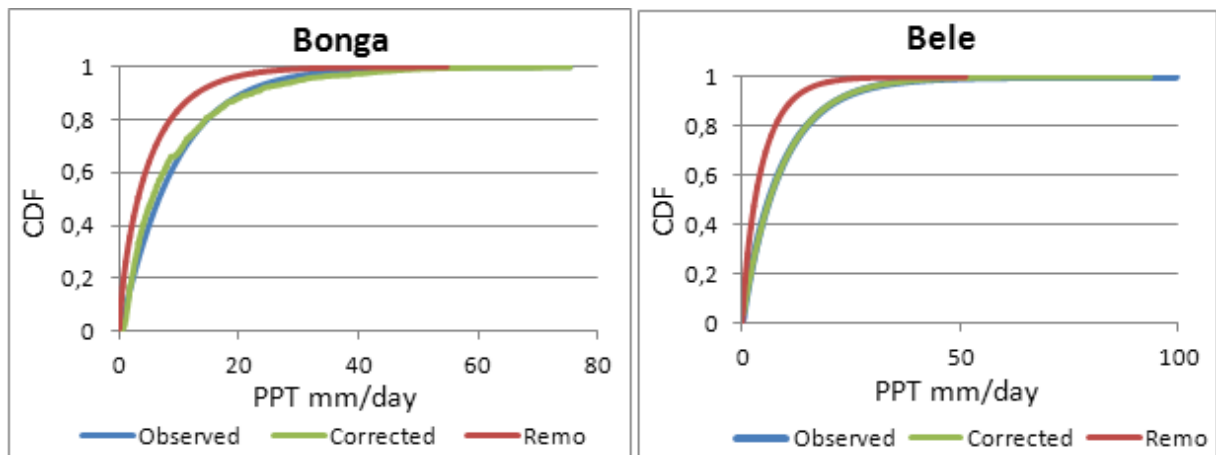


Figure 5.10 Cumulative distributions of observed, corrected and uncorrected Remo precipitation at Bonga and Bele weather stations for reference time period.

The above cumulative distribution graphs show the effects of statistical correction (distribution mapping) methodology in the distribution of corrected Remo simulations. This graph can be used as a check how the bias correction method simulates high precipitation events, in other way this method removes the poorer ability of Remo in simulating higher precipitation spectrum. Because in Remo the simulated daily precipitation has a low number of dry days, which are compensated by too much drizzle, which is the source of a bias in the mean, and the inability to reproduce the extreme events.

Graphs of cumulative distribution functions, comparison of monthly sum of precipitation and seasonal comparison of simulated and observed values for all other stations are found at the end of this thesis in the form of Appendix.

## 5.2.2 Cumulative distribution mapping (CDM) for temperature data

Before any downscaling procedure like that of precipitation, maximum and minimum temperature for historical and scenario period were interpolated to weather observation stations in Omo Gibe basin using bilinear interpolation method as discussed in the above section. As we know the statistical characteristics of temperature values are different from that of precipitation, because of this we proposed a different set of problems for downscaling and correcting biases from maximum and minimum temperature outputs of Remo.

Prior to any bias correction procedure comparison of observed and Remo simulated maximum and minimum temperature carried out. According to the results Remo agrees in general increments of temperature in most of the stations for future time except Yaya. However, it overestimates the mean annual maximum and minimum temperature in most of the weather observation stations for the historical period. The mean annual minimum and maximum temperature shows a strong positive bias in higher altitude for instance in Gedo, because of this downscaling and error correction procedure is unquestionable. Downscaling of maximum and minimum temperature carried out for 14 weather observation stations, these stations are mentioned in the following table 5.5.

Remo simulations of minimum temperature show strong positive bias for most of the stations and maximum temperature shows strong positive bias for the northern tip of the basin. Not only this but also it shows a strong bias on the variance term which is not shown here but it is possible to get these values at the appendix part of this thesis. Like daily precipitation, histograms of mean daily temperature for a given month are not comparably well with observed values. To overcome this problem a new downscaling and error correction method based on the best cumulative distribution fitting equations were selected for each climate observation station on a monthly basis.

S No	Station Name	Mean ann Obs $T_{max}$ °C	Mean ann REMO $T_{max}$ °C	Difference Obs-REMO °C	Mean ann Obs $T_{min}$ °C	Mean ann REMO $T_{min}$ °C	Difference Obs-REMO °C
1	Assandabo	27.0	27.0	0.0	11.9	13.4	-1.5
2	Bonga	26.5	25.0	1.5	11.5	13.7	-2.2
3	Dedo	22.8	27.1	-4.3	10.8	14.9	-4.1
4	Hossana	23.6	25.6	-2.0	11.0	12.7	-1.7
5	Jimma	26.8	26.9	-0.1	11.3	14.8	-3.5
6	Jinka	27.0	29.8	-2.8	15.8	18.1	-2.3
7	Gedo	21.4	27.6	-6.2	9.2	14.0	-4.8
8	Morka	30.6	28.1	2.5	16.0	16.4	-0.4
9	Sawula	29.1	28.9	0.2	17.1	16.8	0.3
10	Wolita	24.4	26.3	-1.9	13.2	14.4	-1.2
11	Wolkite	26.9	25.0	1.9	12.2	11.5	0.7
12	Yaya	29.0	24.7	4.2	12.4	11.3	1.1
13	Shebe	25.6	25.8	-0.2	13.5	13.7	-0.2
14	Woliso	24.9	25.9	-1.0	12.0	13.1	-1.1

Table 5.5 Mean annual maximum and minimum surface temperature of observed and interpolated REMO simulations for current time.

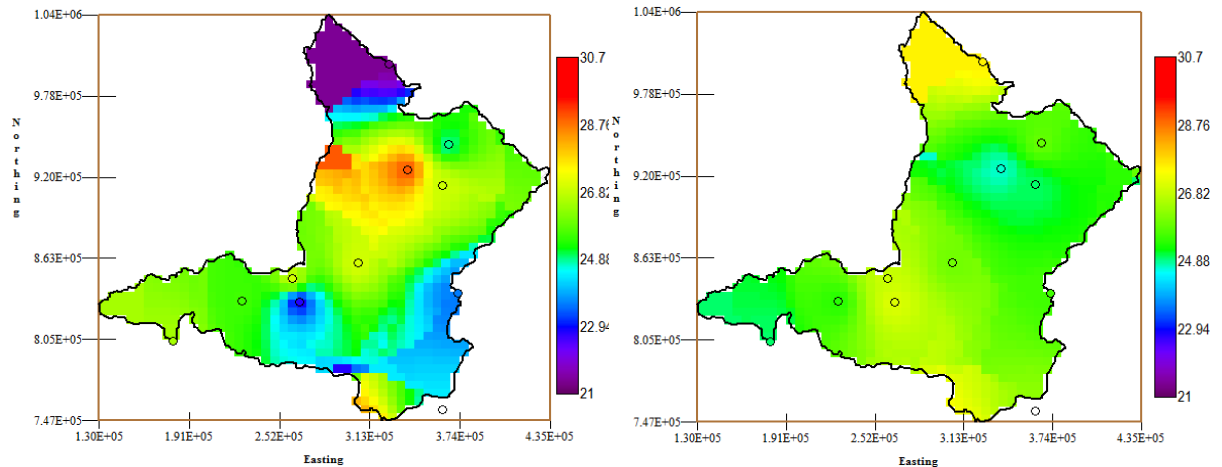


Figure 5.11 Spatially interpolated maximum temperature for upper part of the basin observed and Remo before correction for historical time frame respectively.

The bias correction method has been applied like that of precipitation for historical period, with distinguishing between seasons, and then validation of the methodology was carried out. It is clearly shown in the above section, methods for mapping one distribution onto another are well established in precipitation bias correction for Omo Gibe and it has been used to correct bias of both monthly and daily REMO precipitation. But for precipitation only Gamma distribution was selected to fit the distribution of observed, REMO and future scenario data. For the case of maximum and minimum temperature different distributions were used to fit the data to get the best distribution equation which fits for each months of maximum and minimum temperature.

It is possible to explain that, this method is a data analysis and simulation application allowing fitting probability distributions to observed and REMO data, select the best distribution model, and apply the analysis results to make better decisions. Observed, Remo and scenario data were divided in to monthly basis from January to December for each observation stations and were fitted in to different distribution fitting equation listed in table 5.6. There are so many distributions fitting equations, among these distribution equations the fitting process for Omo Gibe maximum and minimum temperature took place by using the following selected distribution equations based on their relative performance in fitting temperature data in Gibe basin.

Bounded	Unbounded	Non-Negative	Advanced
Kumaraswamy	Gumbel max	Burr	Gen. Extreme value
	Gumbel min	Dagume	Gen. Pareto
	Logistic	Exponential	Log Pearson 3
	Normal	Fatigue life	
		Frechet	
		Gamma	
		Gen. Gamma	
		Log. Gamma	
		Log-Logistic	
		Log normal	
		Weibull	

Table 5.6 Different distribution equations used to fit distributions of maximum and minimum temperature in Omo Gibe basin.

The bounded distribution is simply a standard distribution that has additional upper and lower limits set. Bounded domain distributions naturally come up when random variables should only vary in a finite interval. A distribution that is confined to lie between two determined values is said to be bounded. A distribution that is unbounded theoretically extends from minus infinity to plus infinity. There are a number of well-known methods which can be used to estimate distribution parameters based on available sample data. Among this well known, the estimation of the parameters for Omo Gibe basin was carried out with the method of maximum likelihood estimates (MLM). The fitness of each probability distribution was evaluated by the Kolmogorov-Smirnov, Anderson-Darling and Chi-Squared tests. The selection of best distribution equation has been done based on the performance of the distribution equation in fitting the temperature values.

### 5.2.2.1 Selection of best cumulative distribution equation

Selection of best distribution equation that fitted maximum and minimum observed and uncorrected Remo simulations has been done by using goodness of fit test (GOF) and visual inspection of different graphs. The goodness of fit (GOF) tests measures the compatibility of a random sample with a theoretical probability distribution function. In other words, these tests show how well the distribution which is selected fits to our data. This GOF test helps to decide which model describes the data in the best way.

Three GOF tests have been used mainly KS test:

- ✓ Kolmogorov-Smirnov (KS)
- ✓ Anderson-Darling
- ✓ Chi-Squared

#### a. Kolmogorov-Smirnov

This test is used to decide if a sample comes from a hypothesized continuous distribution. It is based on the empirical cumulative distribution function (ECDF). Assume that we have a random sample  $x_1, \dots, x_n$  from some distribution with CDF  $F(x)$ .

The Kolmogorov-Smirnov (K-S) test is based on the empirical distribution function (ECDF). Given  $N$  ordered data points  $Y_1, Y_2, \dots, Y_N$ , the ECDF is defined as,

$$E_n = \frac{n(i)}{N} \tag{5.6}$$

Where  $n(i)$  the number of points is less than  $Y_i$  and the  $Y_i$  are ordered from smallest to largest value. This is a step function that increases by  $1/N$  at the value of each ordered data point. The Kolmogorov-Smirnov statistic ( $D$ ) is based on the largest vertical difference between the theoretical and the empirical cumulative distribution function

The graph below is a plot of the empirical distribution function with a normal cumulative distribution function.



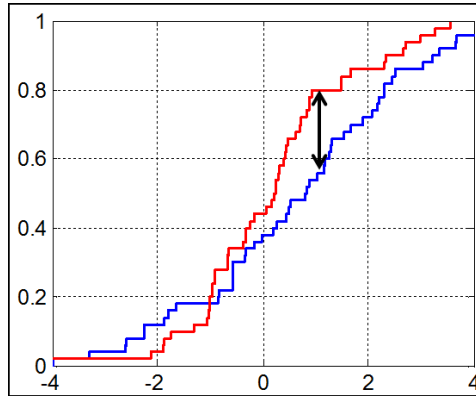


Figure 5.12 Illustration of the two-sample Kolmogorov-Smirnov statistic. Red and blue lines each correspond to an empirical and theoretical distribution function, and the black arrow is the K-S statistic.

#### Definition

The Kolmogorov-Smirnov test is defined by:

- $H_0$ : the data follow the specified distribution
- $H_a$ : the data do not follow the specified distribution

$$D = \max_{1 \leq i \leq n} \left( F(y_i) - \frac{i}{N}, \frac{i}{N} - F(y_i) \right) \quad 5.7$$

The hypothesis regarding the distributional form is rejected at the chosen significance level (alpha) if the test statistic (D) is greater than the critical value obtained from a standard table for the given significance level value. This table is a standard table can be found in any statistics books for different values of significance level.

#### b. Anderson-Darling Test

The Anderson-Darling procedure is a general test to compare the fit of an observed cumulative distribution function to an expected cumulative distribution function. This test gives more weight to the tails than the Kolmogorov-Smirnov test.

#### Definition

The Anderson-Darling statistic ( $A^2$ ) is defined as

$$A^2 = -N - S \quad 5.8$$

$$S = \frac{1}{N} \sum_{i=1}^n (2i - 1) * [inF(Y_i) + \ln(1 - F(X_{n-i+1}))] \quad 5.9$$

The null and the alternative hypotheses are:

- $H_0$ : the data follow the specified distribution;
- $H_a$ : the data do not follow the specified distribution.

The hypothesis regarding the distributional form is rejected at the chosen significance level (alpha) if the test statistic,  $A^2$ , is greater than the critical value obtained from a table.

### c. Chi-Squared test

This test is applied to binned data, so the value of the test statistic depends on how the data is binned. Although there is no optimal choice for the number of bins (k), there are several formulas which can be used to calculate this number based on the sample size (N). For this test the following empirical formula employed:

$$K = 1 + \log_2^N \quad 5.10$$

Definition

The Chi-Squared statistic is defined as

$$X^2 = \sum_{i=1}^k \frac{(O_i - E_i)^2}{E_i} \quad 5.11$$

Where  $O_i$  is the observed frequency for bin  $i$ , and  $E_i$  is the expected frequency for bin  $i$  calculated by

$$E_i = F(X_2) - F(X_1) \quad 5.12$$

Where  $F$  is the CDF of the probability distribution being tested, and  $x_1, x_2$  are the limits for bin  $i$ . Hypothesis testing the null and the alternative hypotheses are:

- $H_0$ : the data follow the specified distribution;
- $H_a$ : the data do not follow the specified distribution.

The hypothesis regarding the distributional form is rejected at the chosen significance level (alpha) if the test statistic is greater than the critical value defined as,

$$X_{1-\alpha, k-1}^2 \quad 5.13$$

Meaning the Chi-Squared inverse CDF with  $k-1$  degrees of freedom and a significance level of alpha, though the number of degrees of freedom can be calculated as  $k-c-1$  (where  $c$  is the number of estimated parameters).

In addition to this goodness of fit test visual inspections of the fitted data were carried out. Visual inspection of the histograms (PDF) cumulative frequency curves and quantile-quantile (Q-Q) plot, helps to judge which of the distribution functions were appropriately fitted the data. Therefore the selection of the best cumulative distribution function for each of the stations on each month were selected based on goodness of fit test with the help of visual inspection method.

According to the following figure 5.13 the empirical PDF (probability density function) for January minimum temperature at Bonga is displayed as a histograms consisting of equal-width vertical bars (bins). The theoretical PDF is displayed as a continuous curve properly scaled depending on the number of intervals. As per the above figure based on the order of best cumulative distribution function the first rank is given to Kumaraswamy the second rank is Burr and etc. Accordingly Kumaraswamy distribution has been selected for January minimum temperature at Bonga for further processing. Moreover, another visual inspection was carried out using the probability-probability (P-P) plot for each selected distribution functions. This is a graph of the empirical CDF values plotted against the theoretical CDF values. It is used to determine how well a specific distribution fits to the observed data. This plot will be approximately linear if the specified theoretical distribution is the correct model.

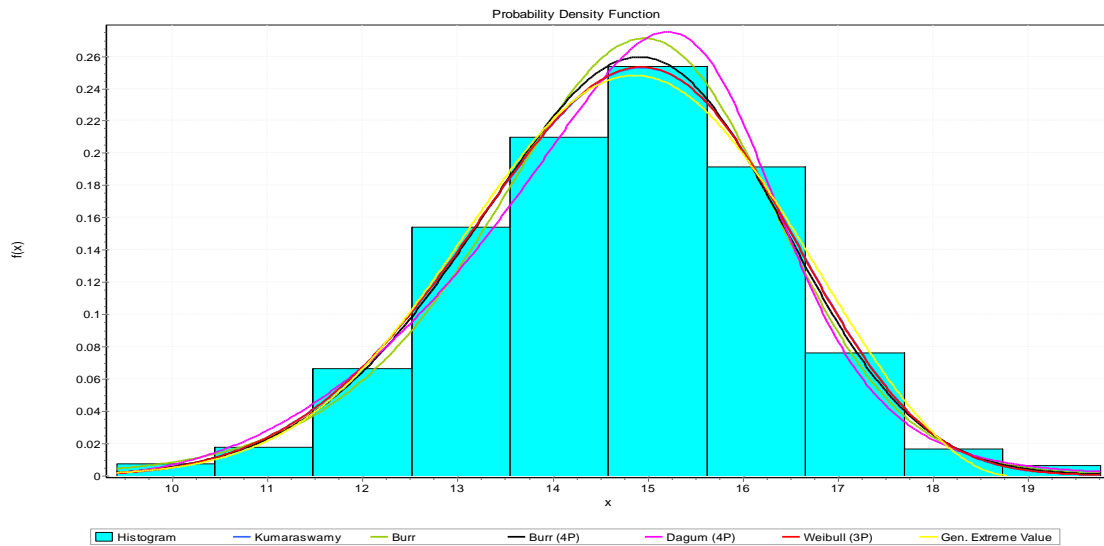


Figure 5.13 PDF of January minimum temperature at Bonga reference time.

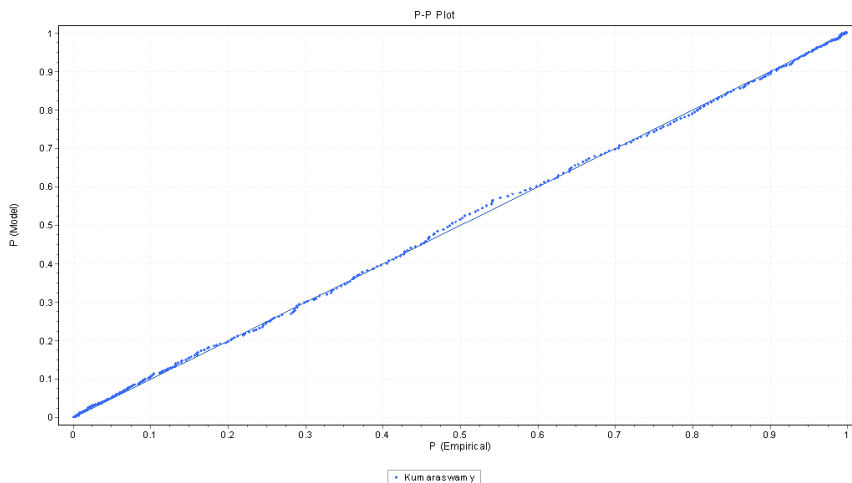


Figure 5.14 Probability-Probability plot of January minimum temperature at Bonga for Kumaraswamy distribution

This graph can also be used to determine where the data do and don't follow the theoretical distribution. Based on all the above goodness of fit test and visual inspection, among the above listed distribution type in Table 5.6 Kumaraswamy, Burr three and four parameters, the generalized extreme value (GEV), and weibull performs very well in fitting Omo Gibe maximum and minimum temperature data for observed, historical and scenario period. Because of this from now on all simulations of maximum and minimum temperature analysis will be done on the above mentioned distribution type. Detail descriptions of the distribution type are given below.

### I. Kumaraswamy distribution

One of the cumulative distribution equation used in this part of the study is Kumaraswamy distribution. In probability and statistics, the Kumaraswamy's double bounded distribution is a family of continuous probability distributions defined on the interval  $[0,1]$  differing in the values of their two non-negative shape parameters,  $a$  and  $b$ . It is similar to the Beta distribution, but much simpler to use especially in simulation studies due to the simple closed form of both its probability density function and cumulative distribution function. This distribution was originally

proposed by Poondi Kumaraswamy for variables that are lower and upper bounded<sup>20</sup>. Ponnambalam Kumaraswamy (often referred to as Poondi Kumaraswamy) was a leading hydrologist from India.

The beta distribution is very flexible to model data restricted to any finite interval since it can take an amazingly great variety of forms depending on the values of the index parameters (Artur J., 2011). In hydrology and related areas, for example, the Kumaraswamy distribution has received considerable interest (Ganji et al., 2006). According to Nadarajah (Nadarajah S., 2008) many papers in the hydrological literature have used this distribution because it is deemed as a 'better alternative' to the beta distribution.

Kumaraswamy's distribution has its genesis in terms of uniform order statistics, and has particularly straightforward distribution and quantile functions which do not depend on special functions (and hence afford very easy random variate generation). The distribution might, therefore, have a particular role when a quantile-based approach to statistical modeling is taken, and its tractability has appeal for pedagogical uses (Jones M.C., 2009).

The probability density function (PDF) and cumulative distribution function (CDF) of the Kumaraswamy distribution are given as:

Probability density function

$$PDF = \frac{a_1 a_2 Z^{a_1 - 1} (1 - Z^{a_1})^{a_2 - 1}}{(b - a)} \quad 5.14$$

$$CDF = 1 - (1 - Z^{a_1})^{a_2} \quad 5.15$$

Where  $Z \equiv \frac{X - a}{b - a}$

$a_1$  Is continuous shape parameter

$a_2$  Is continuous shape parameter

a and b are boundary parameter (a < b)

Domain  $a \leq X \leq b$

According to the goodness of fit test (Kolmogorov-Smirnov, Anderson-Darling and Chi-Squared) the rank of Kumaraswamy distribution in fitting minimum temperature shows very good result for many of the weather observing stations in Omo Gibe basin. Based on its performance this distribution was selected to fit mainly minimum temperature.

## II. Burr distribution

The Burr distribution which yields a wide range of values of skewness and kurtosis can be used to fit almost any given set of unimodal data. Burr (1942) has suggested a number of forms of cumulative distribution functions which might be useful for fitting data (Tadikamalla P. R., 1980). Burr introduced a system of twelve cumulative distribution functions (cdfs) for the primary purpose of fitting data (Todd C. et al. 2010). Burr in 1973 and Tadikamalla in 1980 gave additional attention to the Type III and Type XII distributions because they include a variety of distributions with varying degrees of skew and kurtosis. For example, the Type XII distributions include characteristics of the normal lognormal, gamma, logistic, and exponential distributions as well as other characteristics associated with the Pearson family of distributions (P. R. Tadik., 1980).

---

<sup>20</sup> [http://en.wikipedia.org/wiki/Kumaraswamy\\_distribution](http://en.wikipedia.org/wiki/Kumaraswamy_distribution)

According to the study that has been made by (Todd C. et al. 2010) the Type III or Type XII distributions have been used in a variety of different studies for the purpose of statistical modeling. Some examples include such topics as forestry (Gove et al., 2008), fracture roughness (Nadarajah et al., 2006), operational risk (Chernobai et al., 2007), meteorology (Mielke et al., 1973), modeling crop prices (Tejeda et al., 2008), Flood frequency analysis (Quanxi et.al., 2004) and hydrology (Shao Q., 2005). At this part of the study this distribution has been applied to fit maximum and minimum temperature of Omo Gibe basin.

According to the property of Burr distribution, it is a right-skewed distribution, because of this property, for maximum and minimum observed and Remo simulated temperatures in Omo Gibe basin which has right skewed shape, this cumulative distribution function were approximated very well for some of the months. Based on the above mentioned goodness of fit test and from a modeling perspective the extended three and four parameter Burr distribution is therefore a meaningful candidate distribution in the frequency distribution analysis for some of the weather observing stations and for some months of the year in Omo gibe basin.

Three parameter Burr distribution probability density function (PDF) is give by:

$$PDF = \frac{\alpha K \left(\frac{X-\gamma}{\beta}\right)^{\alpha-1}}{\beta \left[1 + \left(\frac{X-\gamma}{\beta}\right)^{\alpha}\right]^{K+1}} \quad 5.16$$

Where

K is shape parameter (K>0)

α Is shape parameter (α>0)

β Is scale parameter (β>0)

γ Is location parameter (γ ≡ 0) yields the three parameter distribution

Domain  $\gamma \leq X < +\infty$

Cumulative distribution function (CDF)

$$CDF = 1 - \left[1 + \left(\frac{X-\gamma}{\beta}\right)^{\alpha}\right]^{-K} \quad 5.17$$

### III. Generalized extreme value distribution

The generalized extreme value (GEV) distribution is a family of continuous probability distributions developed within extreme value theory to combine the Gumbel, Fréchet and Weibull families also known as type I, II and III extreme value distributions<sup>21</sup>. This distribution performs very well only for few of weather observing stations and for few months of the year. Stations which don't perform well using Kumaraswamy and Burr distributions they showed better results using generalized extreme value and weibull distributions. In consideration of this and using the advantage of GEV and Weibull these two distributions also used for fitting maximum and minimum temperature for some of the months and stations in Omo Gibe basin. Probability density function of this distribution is given by

$$PDF = \begin{cases} \frac{1}{\delta} \text{EXP} \left[ -(1 + KZ)^{\frac{-1}{K}} \right] (1 + KZ)^{-1-\frac{1}{K}}, & K \neq 0 \\ \frac{1}{\delta} \text{EXP}[-Z - \text{EXP}(-Z)] & K = 0 \end{cases} \quad 5.18$$

<sup>21</sup> [https://en.wikipedia.org/wiki/Generalized\\_extreme\\_value\\_distribution](https://en.wikipedia.org/wiki/Generalized_extreme_value_distribution)

$$Z \equiv \frac{X-\mu}{\delta}$$

Where K is Shape parameter

$\delta$  Is scale parameter

$\mu$  Is location parameter

Domain

$$1 + \frac{K(X-\mu)}{\sigma} > 0 \quad \text{for } K \neq 0.0$$

$$-\infty < X < +\infty \quad \text{for } K = 0.$$

Cumulative distribution function

$$\text{CDF} = \begin{cases} \text{EXP}\left[-(1 + KZ)^{\frac{-1}{K}}\right], & K \neq 0 \\ \text{EXP}[-\text{EXP}(-Z)], & K = 0 \end{cases} \quad 5.19$$

#### IV. Weibull distribution

Eventhouh weibull distribution does not perform like that of Kumaraswamy and Burr for many of the stations; it shows good results in some of the stations. For this specific purpose of the study two parameter weibull distribution shows better result than the three parameter distributions.

Probability density functions of two parameter weibull distribution given by:

$$\text{PDF} = \frac{\alpha}{\beta} \left(\frac{X}{\beta}\right)^{\alpha-1} * \text{EXP}\left[-\left(\frac{X}{\beta}\right)^{\alpha}\right] \quad 5.20$$

$$\text{CDF} = 1 - \text{EXP}\left[-\left(\frac{X}{\beta}\right)^{\alpha}\right] \quad 5.21$$

Where  $\alpha$  shape parameter ( $\alpha > 0$ )  
 $\beta$  Is scale parameter ( $\beta > 0$ )

#### 5.2.2.2 Distribution mapping from selected equations to temperature data

The basic idea followed at this part of the research is the same as that of precipitation, but different methodology. The primary objective of fitting maximum and minimum temperature in different cumulative distribution function is to select and construct the best cumulative distribution for observed and Remo simulated temperature. After the selection of the best cumulative distribution function for each stations and each month, distribution mapping procedure performed.

For illustration purpose let's take one of weather observation station in Omo Gibe basin Assendabo. The observed maximum and minimum temperature at Assendabo were disaggregated in to monthly bases from January to December similar procederes followed for historical and scenario runs of Remo data. Now we have three data sets observed, historical and scenario run of Remo data. All these three data sets were fitted independently on monthly basis using the above selected cumulative distribution equations. Based on the performance of distribution, the same distribution type selected for the same months of the year. And then the cumulative distribution of the daily Remo maximum and minimum temperature was mapped onto the cumulative distribution of the observed maximum and minimum temperature on monthly basis.

For the case of clarity the following equation can be referred. The subscript 'c,M,j' to equation 5.22, refers the letter (c) represents error corrected, (M) maximum temperature and (j) months of the year January, February...December. Based on this, bias corrected Remo maximum temperature for the month of January  $T_{c,M,j}$  on a given weather observation station can then be calculated as:

$$T_{c,M,j} = F_{o,M,j}^{-1}[F_{r,M,j}(X_{r,M,j})] \quad 5.22$$

Here  $X_{r,M,j}$  represents a given value of maximum temperature in January to be corrected at the point of interest. This value obtained from interpolated Remo grid points from each weather observation station.

$F_{r,M,j}$  represents the cumulative distribution functions of Remo maximum temperature before correction for the month of January. This distribution function is obtained by fitting interpolated Remo maximum temperature for that specified month in to a number of cumulative distribution fitting equations mentioned above and selecting of the best one using previously discussed selection criteria.

$F_{o,M,j}^{-1}$  represents the inverse of observed distribution function for maximum temperature on January using best cumulative distribution equation.

Accordingly Remo simulated maximum and minimum temperature from each station and on each month were mapped on to observed cumulative distribution function.

### 5.2.2.3 Results and discussion on temperature downscaling

According to the results, the methodology has been showed a realistic representation of maximum and minimum temperature fields in historical period. This bias correction method with daily cumulative distribution functions on monthly basis can remove biases, modifying the control period data obtained by the Remo, therefore, this new technique corrects all ranges of the errors which were inherited in raw Remo simulation. Similarly validation of this methodology has been carried out using daily maximum and minimum temperature data in a number of ways. The performance of the bias correction procedure were analysed by comparing monthly average statistical parameters for observed and corrected maximum and minimum temperature for all stations.

#### Evaluation methods

Evaluating downscaling methods that are designed for assessment of future climate change presents a unique challenge, because comparison to future climate states is clearly not possible, so instead in order to evaluate the methodology efficiency it is possible to compare observed and corrected data sets for current time period, as a result the downscaled daily weather sequences are examined to assess the ability of the downscaling methods to reproduce certain statistical measures of the daily weather patterns.

The evaluation methodologies carried out for this procedure are listed below:

- Comparison between observed and corrected mean monthly and mean annual maximum and minimum temperature
- Comparison of monthly variances of daily temperatures
- Direct comparison of day to day temperatures
- Comparison of spatially interpolated maximum and minimum temperature and
- Root mean square errors (RMSE) between observed and corrected values



The daily weather sequences are examined from observation stations using the statistics derived from the years 1970-2000 for most of the stations. These values are then compared to the downscaled sequence intended to represent the present climate.

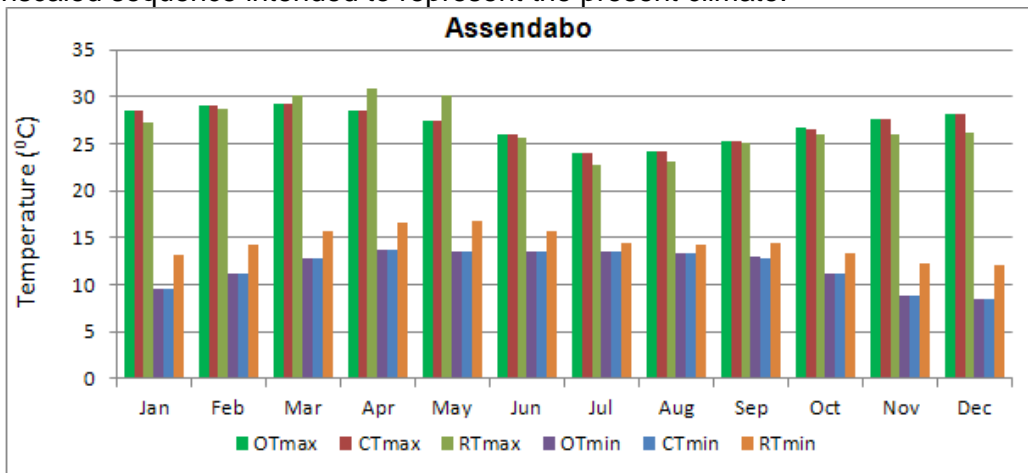


Figure 5.15 Mean monthly observed, corrected and Remo simulated maximum and minimum temperature at Assendabo for historical period.

Figure 5.15 shows examples of results from the downscaling scheme, at Assendabo weather station. The legends in the above figure are described as follow. OTmax represents observed maximum temperature, CTmax corrected maximum temperature, RTmax Remo simulated maximum temperature, OTmin observed minimum temperature, CTmin corrected minimum temperature and RTmin Remo simulated minimum temperature. Comparison of mean monthly values from all part of the data helps in assessing the overall applicability and performance of the proposed methodology at reproducing the 1970-2000 maximum and minimum temperature.

According to the above result the methodology performed very well and reliably estimated the present day mean monthly maximum and minimum temperature in all Omo Gibe weather observation stations. Similar figures for the rest of the station are provided at the appendix in the form of tables and figures. This new bias correction method is a stable and reliable in removing the mismatch between Remo and observed temperature values.

In order to confirm the reliability of the methodology extra validation methodology were employed with other statistical properties between observed and corrected data sets. The root means square error for Remo before and after correction was calculated for all stations in monthly basis and the results are depicted in the following table and figure.

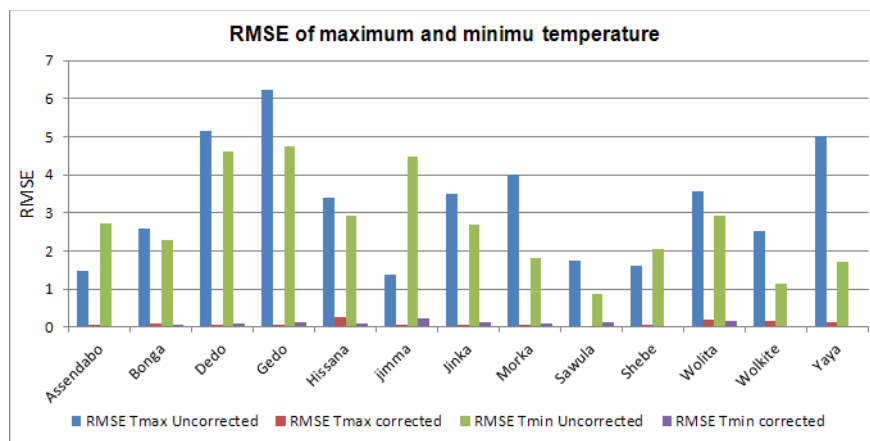


Figure 5.16 Graphical presentation of RMSE for temperature data.

Root mean square error for maximum and minimum temperature					
RMSE maximum temperature				RMSE minimum temperature	
S no	Station	RMSE		RMSE	
		uncorrected	corrected	uncorrected	corrected
1	Assendabo	1.46	0.04	2.72	0.02
2	Bonga	2.57	0.10	2.27	0.04
3	Dedo	5.16	0.04	4.60	0.08
4	Gedo	6.24	0.05	4.75	0.14
5	Hissana	3.40	0.24	2.91	0.08
6	jimma	1.39	0.05	4.49	0.21
7	Jinka	3.50	0.04	2.68	0.13
8	Morka	4.01	0.06	1.82	0.09
9	Sawula	1.73	0.04	0.86	0.12
10	Shebe	1.60	0.07	2.04	0.02
11	Wolita	3.56	0.19	2.92	0.17
12	Wolkite	2.53	0.16	1.13	0.02
13	Yaya	5.02	0.12	1.71	0.01

Table 5.7 Root mean square error for maximum and minimum temperature before and after correction

If a perfect match achieved between observed and corrected temperature it would have an error of zero. Eventhough, it was not possible to achieve error of zero between observed and corrected value, but it was possible to achieve errors which approaches to zero. Based on the above graphical representation of RMSE, the errors which were inherited in Remo data sets were reduced (removed) significantly in all of the stations. This is the indication of the best performance of the method, because the closer the average error is to zero the better the method's performance at reproducing the 1970-2000 data. The first impression upon inspecting Figure 5.16 is that the absolute values of the errors are significantly diminished in the corrected simulation.

Additionally the methodology was validated based on the produced variance value before and after correction. In this experiment the overall applicability of the proposed scheme was assessed based on the variance how it approaches the observed variance for current climate condition of maximum and minimum temperature. Variance analysis involves assessing the difference between observed and corrected figures. This part of validation methodology will help us to measure how far bias corrected Remo value is spread out from observed variance.

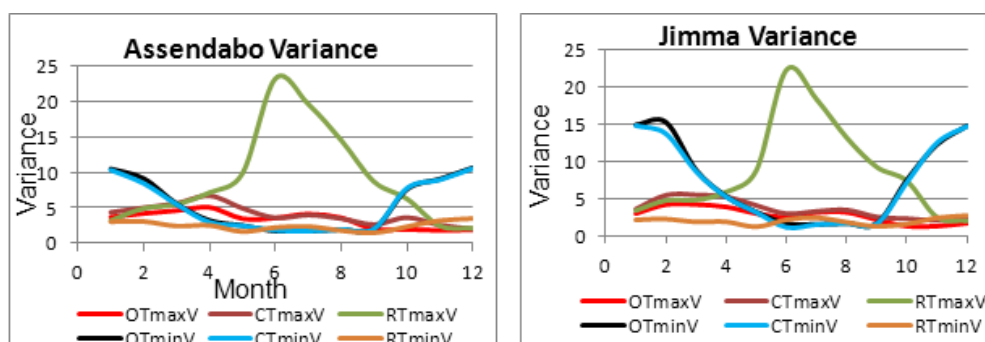


Figure 5.17 Effects of CDM on the variance of maximum and minimum temperature over the entire historical time period 1970-2000.

In figure 5.17 the improvements seen in Assendabo also seen in Jimma and other stations as well. Similar figures for the rest of the stations can be found at the appendix. The analysis based on the variance, raw Remo simulation overestimates the variance for maximum temperature in all of the stations, however by applying the new bias correction method the corrected variance are in fact rather close to the observed variance values. Even in most of the stations a perfect match can be found between observed and corrected variance value especially for minimum temperature. For instance in Assendabo OTminV (black color) and CTminV (blue) color are in a perfect match, this property also observed in Jimma and other stations.

Variations regard to none exceedence probability of observed and corrected maximum and minimum temperatures have been checked. Because probability of non-exceedence graph provides the most detailed outlook information how the bias correction methods performs in producing similar distribution and extreme values for present climate condition.

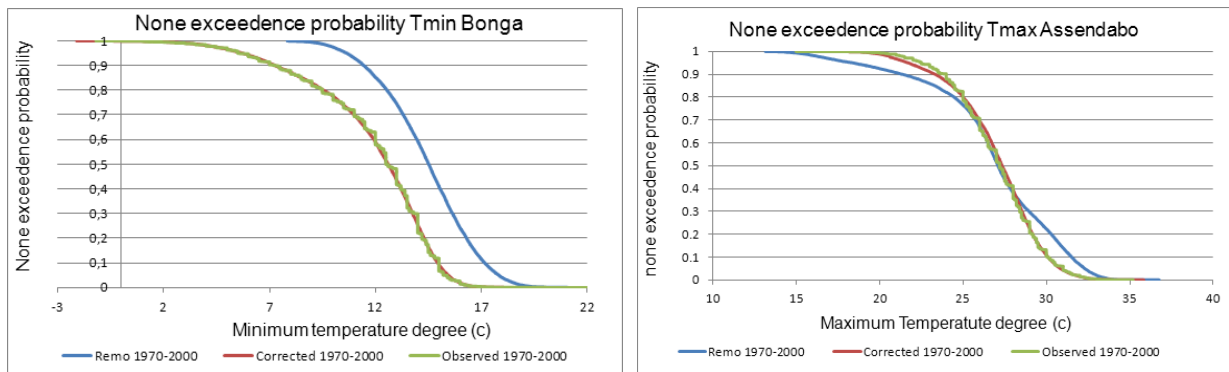


Figure 5.18 None exceedence probability of observed, corrected and Remo simulated minimum and maximum temperature at Bonga and Assendabo.

None exceedence probability curves of maximum and minimum temperature at Bonga and Assendabo revealed that, the corrected curve matches very well with observed value. The uncorrected curve shifts significantly to observed one by far. The chances that any particular average temperature will be exceeded in corrected graph are roughly the same as the chances of 1970-2000 reference periods with observed graph. This new bias correction method is very robust in producing not only the general statistical moments of the corrected data set which are more similar to the observed statistics, but also day to day values of corrected Remo for present climate simulation. As a final validation technique daily maximum and minimum temperature values were compared at one of the station. Results showed that this method is by far better even in producing of daily values.

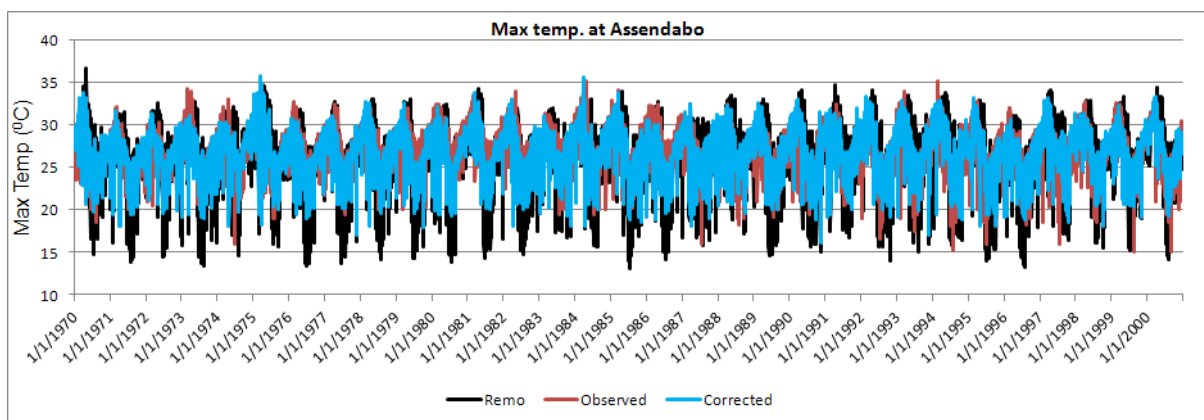


Figure 5.19 Daily maximum observed and Remo temperatures before and after correction at Assendabo.

Figure 5.19 shows the daily maximum temperature at one of downscaling stations. As expected for corrected model (blue line) is closer to the observations (solid brown line) than the non-corrected value (black line). This property is maintained in all stations. The difference between the range of the simulated daily temperature cycle (uncorrected simulations) and the observed one was higher; however it is possible to make the range of this difference very small or negligible by applying the proposed bias correction methodology.

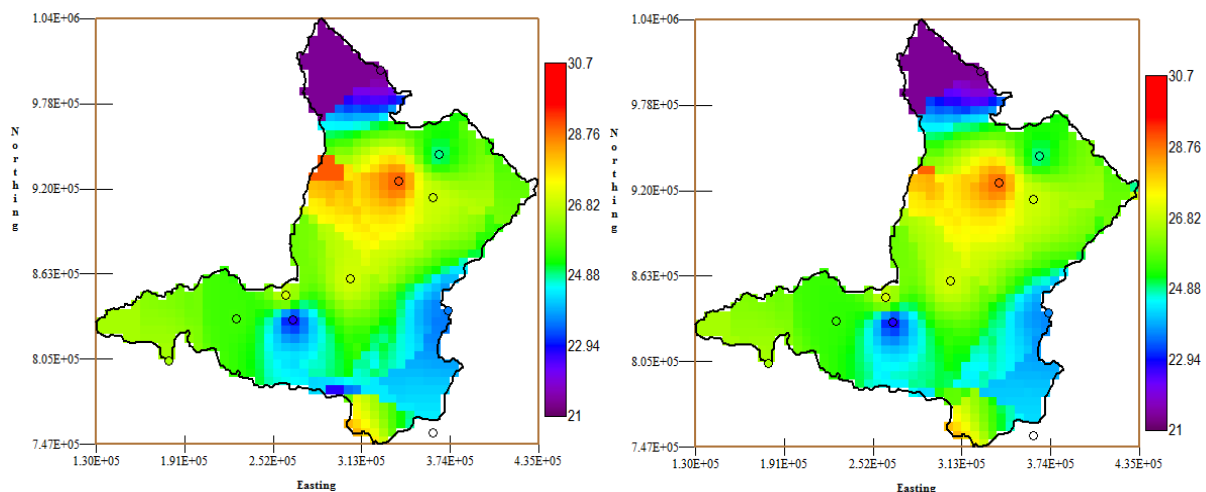


Figure 5.20 Left panel shows spatially interpolated mean annual observed maximum temperature and right panel is spatially interpolated mean annual corrected Remo maximum temperature in the upper part of omo Gibe basin.

Figure 5.20 shows the effects of the methodology on the difference between the corrected and observed mean annual maximum temperature from reference time period for upper part of the catchment (above Omo Gibe III dam site). As per the result the corrected value approaches the observed one excellently.

### 5.3 Downscaling of GCM output using SDSM model

Generally in the previous section, separate downscaling schemes were employed to downscale REMO precipitation and temperature output from two basic scenarios A1B and B1 dry, optimum and wet conditions. To downscale large scale GCM outputs to Omo Gibe weather observation stations SDSM, a decision support tool for the assessment of regional climate change impacts was selected. This downscaling model is a multiple regression based method and is referred to as statistical down-scaling model (SDSM) (Wilby, et al., 2002).

One of the big advantages of SDSM, it enables the downscaling of climate change scenarios for individual sites at daily time scales and directly employs GCM output in the scenario construction processes. According to Mohammad S., 2006 SDSM is the most capable of reproducing various statistical characteristics of observed data in its downscaled results with 95% confidence level, the ANN (artificial neural network) is the least capable in this respect, and the LARS-WG (long ashton research station weather generator) is in between SDSM and ANN. This means that the uncertainty associated with SDSM is small as compared to ANN and LARS-WG, because of this SDSM selected to downscaled large scale GCM output to Omo Gibe basin.

GCM output is important as a raw data set for downscaling procedure using SDSM. SDSM should be supplied with a prepared set of daily predictor variables for selected grid boxes covering Omo Gibe basin. The general characteristics of this downloaded data set described at the beginning of this chapter. According to the information which is obtained from downloaded folder all the predictors, with the exception of wind direction, have been normalized with respect

to the 1961–1990 mean and standard deviation. This means that in each file of large scale predictor the value varies between +5 and -5.

After preparing and obtaining the observed and large scale predictors for downscaling procedure the nearest GCM grid point were selected to each observation station. Prior to downscaling identifying of the empirical relationships between gridded predictors such as temp, mslp, p500 and other large scale variable and single site observed predictands such as observed precipitation, maximum and minimum temperature has been done.

The purpose of establishing empirical relationship between those observed and GCM output helps to choose appropriate downscaling predictor variables for model calibration. In order to elaborate this procedure a relationship has been established between observed maximum and large scale predictor variable and the results depicted by table 5.8. According to table 5.8 the strongest correlation in each month is shown in red, indicating that the relationship between maximum temperature and r500 and rhum are most important. The result in the following table suggests that r500 is a potentially useful predictor for April and from June up to August and rhum from January to March. Blanks represent insignificant relationships at the chosen significance level. Based on this selection criteria identification of strong correlation between observed and GCM output were established for each weather observation stations in Omo Gibe basin. Based on this selection criteria large scale predictors which are listed on table 5.9 have been selected for all climate data set and all weather observation stations from GCM for further processing.

RESULTS: EXPLAINED VARIANCE

Analysis Period: 1/1/1970 - 12/31/2000  
Significance level: 0.05

Total missing values: 0

Predictand: OTmax.dat

Predictors:	JAN	FEB	MAR	APR	MAY	JUN	JUL	AUG	SEP	OCT	NOV	DEC
ncep5_ulag.dat	0.120	0.127	0.071	0.084	0.046	0.076	0.008	0.010	0.014	0.010	0.015	0.033
ncepp5_f.dat	0.098	0.089	0.062	0.071	0.055	0.063	0.021	0.018	0.015	0.012	0.028	0.038
ncepp5_u.dat	0.115	0.117	0.057	0.089	0.051	0.077	0.027	0.026	0.015	0.007	0.020	0.033
ncepp500.dat	0.014		0.010	0.042	0.044	0.119	0.034	0.063	0.050	0.017	0.023	0.026
ncepp5zh.dat	0.054	0.013	0.010	0.008	0.010	0.021	0.014	0.057	0.023	0.034	0.010	0.038
ncepr500.dat	0.097	0.044	0.082	0.134	0.116	0.159	0.109	0.091	0.040	0.033	0.017	
ncepr500lag.dat	0.106	0.039	0.085	0.113	0.110	0.158	0.065	0.043	0.028	0.033	0.019	0.006
nceprhum.dat	0.214	0.178	0.177	0.112	0.109	0.061	0.040	0.050	0.071	0.012	0.039	0.015
nceprhumlag.dat	0.194	0.174	0.172	0.107	0.094	0.069	0.025	0.025	0.074	0.019	0.043	0.018
nceptemp.dat	0.140	0.145	0.168	0.129	0.116	0.139	0.013	0.007	0.017	0.007	0.039	0.040

Table 5.8 Example of correlation results between GCM and observed maximum temperature at Jimma.

In general for Omo Gibe basin some large scale predictor variables such as p\_zh (divergence near surface), p500 (500hPa geopotential height), r850(relative humidity at 850 hPa height), rhum(near surface relative humidity), temp (mean surface temperature) and shum (near surface specific humidity), r500(relative humidity at 500hPa height) showed that strong correlation with many of observed precipitation, maximum and minimum temperature in Omo Gibe basin. Based on the strong correlation between large scale GCM and observed precipitation, maximum and minimum temperature the following listed (table 5.9) large scale GCM predictors were selected for Gibe basin downscaling procedure.

S. No	Variable	Discription
1	Temp	Mean Temperature at 2 meter
2	mslp	Mean sea level pressure
3	P500	Pressure at 500 hPa geopotential height
4	P850	Pressure at 850 hPa geopotential height
5	rhum	Near surface relative humidity
6	R500	Relative humidity at 500 hPa height
7	R850	Relative humidity at 850 hPa height
8	shum	Near surface specific humidity
9	S500	Specific humidity at 500 hPa height
10	S850	Specific humidity at 850 hPa height
11	p_f	Geostrophic air flow velocity
12	p_z	Vorticity
13	p_u	Zonal velocity component near surface
14	p_v	Meridional velocity component near surface
15	p_zh	Divergence near surface
16	p_th	Wind direction
17	p5_u	Zonal velocity component at 500hpa height
18	p8_v	Meridional velocity component at 850 hPa height
19	p8zh	Divergence at 850 hPa height
20	p8_u	zonal velocity component at 850 hPa height

Table 5.9 Large-scale predictor variables selected for downscaling precipitation and temperature in Omo Gibe basin

### 5.3.1 Calibration of SDSM model

The next step is downscaling of those selected large scale GCM output to point scale result. During downscaling using SDSM, a multiple linear regression model is developed between observed large-scale predictor (NCEP) variables and local scale predictands (observed data) such as temperature and precipitation. According to SDSM software the parameters of the regression equation are estimated using the dual simplex algorithm. The selected large-scale relevant predictors for each station are selected using correlation analysis, partial correlation analysis and scatter plots.

Precipitation has been modeled as a conditional process, because for this case there is an intermediate process between regional forcing and local weather, for example observed precipitation amounts depend on wet /dry day occurrence, which in turn depend on regional scale predictors such as humidity and atmospheric pressure. During precipitation downscaling a wet day has been defined as a day with nonzero precipitation amount of greater than or equal to 0.3 mm. As the distribution of daily precipitation is skewed, a fourth root transformation is applied to the original data sets to convert it to normal distribution, and then used it in regression analysis. Maximum and minimum temperatures are modeled as unconditional process to assume that a direct link between large scale predictors and observed pridictands. And no transformation was applied, because the distribution of temperature is not skewed like that of precipitations. Auto-regression option has been selected in order to include an auto-regressive term in the regression equations for downscaling temperatures. To determine the temporal

resolution of the downscaling model from the available options monthly model were selected for both daily precipitation and temperature downscaling, there by different model parameters (regression equations) were derived for each month using different regression parameters.

The model was calibrated and validated separately for daily precipitation, daily maximum and minimum temperatures. Especially for precipitation downscaling for most of the stations twenty one years (1980–2000) predictors and predictand for calibration and ten years (1970–1979) predictors and predictand for validation have been used except Morka and wolkite as these stations have recorded precipitation and temperature data since 1985 respectively . During calibration, mean and variance of downscaled daily precipitation and temperature are adjusted by bias correction and variance inflation factor key interfaced with the model until the model reproduces reasonable results which approaches or resembles the observed data in terms of mean monthly, sum of mean monthly and variance values for all weather observation stations. Bias correction compensates for any tendency to over or underestimates the mean of downscaled variables. Variance inflation changes the variance of downscaled daily weather variables by adding or reducing the amount of noise applied to regression model. Similar procedure were followed for calibration of maximum and minimum temperature for most of the stations except Morka and Wolkite, these two stations have been calibrated by using 10 years data according to the availability of the observed precipitation and temperature data sets. And the rest of the years used for validation.

Once the downscaling model have been calibrated and validated regarding to current climate condition with observed large scale predictors (NCEP) and observed precipitation, maximum and minimum temperature at each station, the next step is to use these calibrated model to downscale the current climate simulated by GCM (HadCM3). In this case, large-scale predictor variables which are simulated by GCM (HadCM3) for A2 scenarios have been taken for current climate conditions (1970 to 2000).

### 5.3.2 Results and discussion on GCM downscaling

The results of downscaled daily precipitation and daily temperature data were compared with observed values to investigate the performance of the model in producing the current climate series. This has been done by direct comparison of simulated mean monthly maximum and minimum temperature, while precipitation is compared as sum of mean monthly value for historical period. For illustration purpose only one station results will be discussed in the following section. Because all of the stations produced similar performance in SDSM downscaling, and later on error evaluation analysis based on important statistics will be carried out by calculating some statistics of precipitation and temperature data sets produced by cumulative distribution mapping (CDM) and SDSM downscaling methodology.

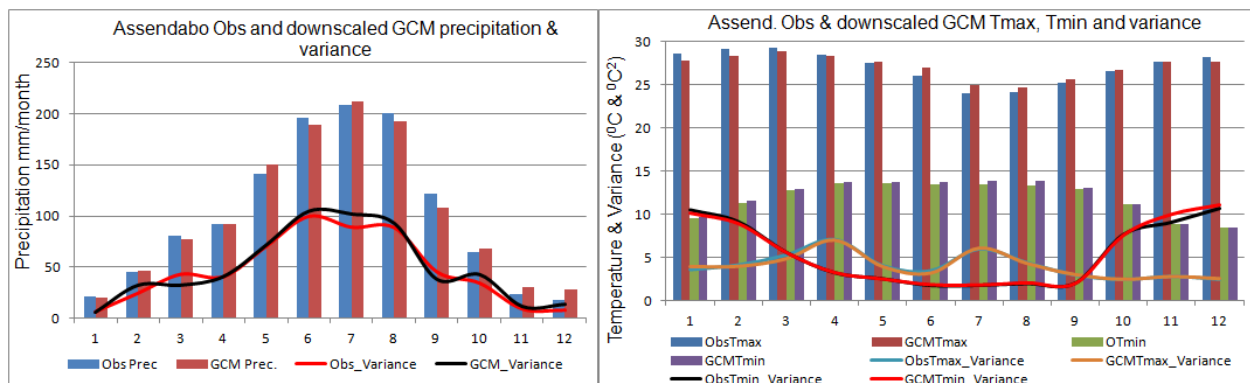


Figure 5.21 Comparison of mean monthly precipitation, maximum and minimum temperature after downscaling from GCM scenario, current time



In order to interpret the downscaling results from SDSM, it is necessary to compare simulated and observed climates for historical period 1970-2000. The plot in the above figure 5.21 shows that there is good agreement between the observed and GCM simulated precipitation, maximum and minimum temperatures throughout the year during control period. The accuracy regarding to producing of minimum and maximum temperature is better than precipitation. This performance also checked by comparing the variances of observed and downscaled maximum and minimum temperature during control period. This result shows that more or less SDSM produced comparable variance with observed value.

Regarding to precipitation, different parameters of each model are adjusted during calibration to get the best statistical agreement between the observed and simulated meteorological variables. During calibration for precipitation downscaling models, in addition to the mean daily precipitation and daily precipitation variance for each month, monthly average dry and wet spell lengths considered. For the cases of Tmax and Tmin, the mean and variances of these variables corresponding to each month were considered as performance criteria.

The results of precipitation downscaling using SDSM are found to be in good agreement with the observed value. However; in some of the months model yielded higher estimates of monthly mean precipitation as compared with the observed values to certain level. For instance in the above example mean monthly precipitation values overestimated in November and December whereas it was underestimated in June and September to certain level. Additionally monthly variance in precipitation can be used as performance criteria and it is well modeled by SDSM. The black line in the above plot represents the variance modeled from GCM and it is well approached the observed variance at Assendabo so that it is possible to say that, the variability in modeled precipitation is well developed. In the case of daily precipitation, Tmax and Tmin downscaling, the graphical comparison of daily variances in each month in figure 5.21 showed that in all months GCM variability is close enough to the observed variability. This comparison tells us SDSM produces the most important statistical parameters from downscaling results fairly.

## 5.4 Error evaluation of downscaling methods

So far two different downscaling models namely; cumulative distribution mapping (CDM) and statistical down-scaling model (SDSM) have been used to downscale fine scale REMO output and large scale GCM results to Omo Gibe weather observation stations respectively. In order to assess the errors associated with these two methods certain basic error assessment have been carried out based on one representative precipitation and temperature station. This part of the study has been carried out using 30 years of Jimma observed and downscaled daily precipitation, daily maximum and minimum temperatures from the two methodologies.

In case of daily temperature data, because of their nearly normal distribution, the error has been assessed with absolute downscaling model errors (absolute values of the observed minus downscaled data) comparison of errors between two downscaling methodology has been carried out for the case of identifying which methodology performs very well in simulating current climate condition. In this comparison, deviations (referred to as model errors) between downscaled and observed monthly means of Tmax and Tmin have been evaluated.

In error evaluation assessment of downscaled daily precipitation data, comparison of means and variances should not be enough because of non-normality of the distribution of daily precipitation amount and also because of mixed distribution of wet and dry days in a daily precipitation series (Mohammad 2006). Therefore, in assessment of errors in downscaled daily precipitation, in addition to comparing means and variances, monthly mean dry-spell and wet-spell statistics have been compared. All error evaluation method has been carried out based on one representative stations i.e Jimma.

### a. Error evaluation in estimates of mean

Since the variability of the model have been compared in the previous section for both SDSM and CDM downscaling methodology this part of error evaluation section focused on the absolute downscaling model errors (absolute values of the observed minus downscaled data) in the estimates of mean monthly maximum and minimum. The absolute mean error which have been produced by both methods for  $T_{max}$  and  $T_{min}$  at the station Jimma have been shown in figure 5.22

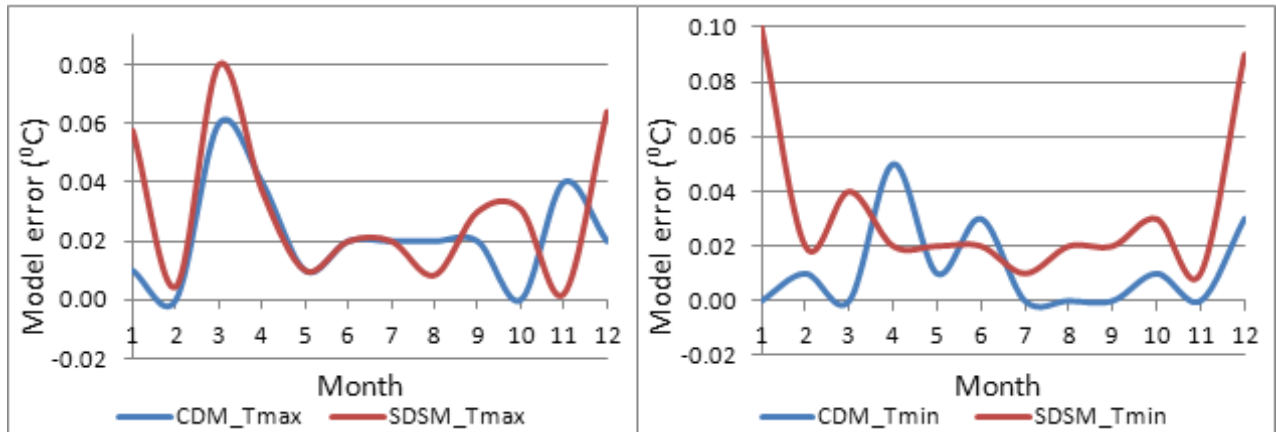


Figure 5.22 Model errors (absolute value) in monthly  $T_{max}$  and  $T_{min}$  downscaling with SDSM and CDM at Jimma station

In  $T_{max}$  and  $T_{min}$  downscaling at the station Jimma, the CDM model errors are the least in most of the months (figure 5.22) except the month of march which produces the largest model error for maximum temperature which is 0.06 °C. But for most of the cases the model error is below 0.02 °C which is nearly zero value. Whereas for minimum temperature the maximum model error observed in April which is 0.045 °C but for most of the months the model error is below 0.02 °C. In the case of model error associated with SDSM it produces a bit higher model error as compared to CDM (cumulative distribution mapping). For instance the heights model error produced for maximum temperature in April which was 0.08 °C. Eventhouhg, it produces a bit higher model error in some of the months as compared to CDM it remains to produce smaller model error in most of the months, for example the model error for minimum temperature from February through November remains below 0.02°C. When we compare the two downscaling methodology cumulative distribution mapping (CDM) model produced the least error in most months. Basically the above result tells us the associated model error in both of the downscaling model is very small, in other word the errors are approached well enough to zero so that all the downscaled maximum and minimum temperature are approached to the observed value. The errors in the estimates of means of the observed and downscaled daily precipitation, has been quantified by estimating the absolute error between the mean of monthly precipitation value for each months of the year. Additionally percentages of wet day which is percentage of days that exceed the threshold value have been evaluated.

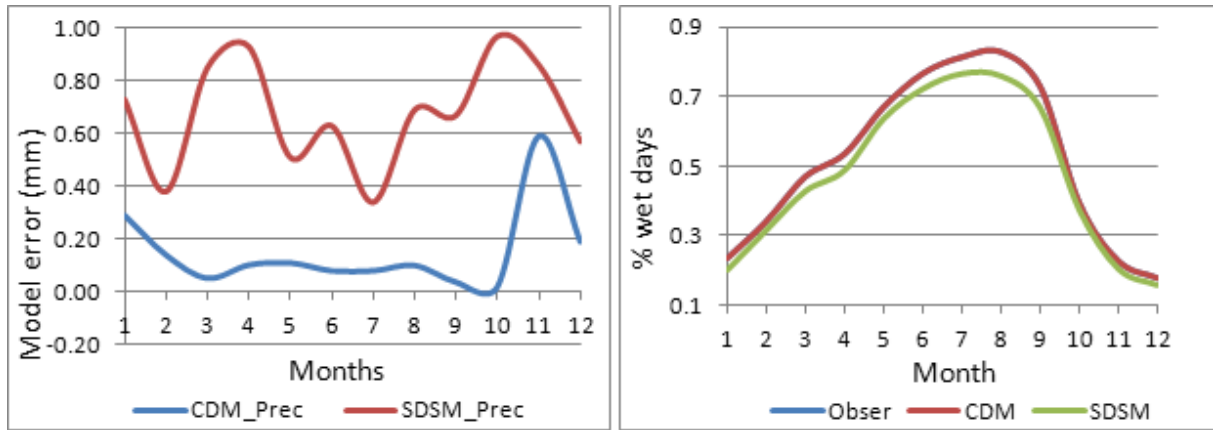


Figure 5.23 Model errors (absolute value) in monthly precipitation and % of wet days respectively at Jimma station

In the case of precipitation downscaling, the graphical comparison of errors in the estimates of means of the observed and downscaled monthly precipitation indicates that at the station Jimma, the CDM model exhibited the least model error below 0.2 mm in all months except November which is 0.6mm. Though SDSM exhibited higher model error in estimating mean monthly precipitation as compared to CDM, but the errors are not significant. In most of the cases the model error is in between 0.4 and 0.8 mm. The percentage of days that exceed the threshold value produced by CDM perfectly matched the observed value and %age of wet days produced by SDSM approaches to observed value to greater extent.

### b. Dry and wet spell length statistics

Mean dry and mean wet spell lengths for a particular month can be defined as average length of spells with amounts less than the wet-day threshold and average length of spells with amounts greater than or equal to the wet-day threshold respectively (Mohammad 2006). For instance, if in a particular month of a given year, maximum seven consecutive days are found dry or days which has a rainfall below threshold value and three consecutive days are found wet, days which have rainfall more than threshold value then we consider that the dry-spell and wet spell lengths for that particular month are 7 and 3, respectively. Dry and wet spell lengths are of particular interest for hydrologic modeling, and are thus considered as additional criteria for assessing the downscaling model performance. Accordingly the dry and wet spell lengths have been calculated for observed and downscaled precipitation data by both methods. And the following results obtained from 30 years daily rainfall data at Jimma station.

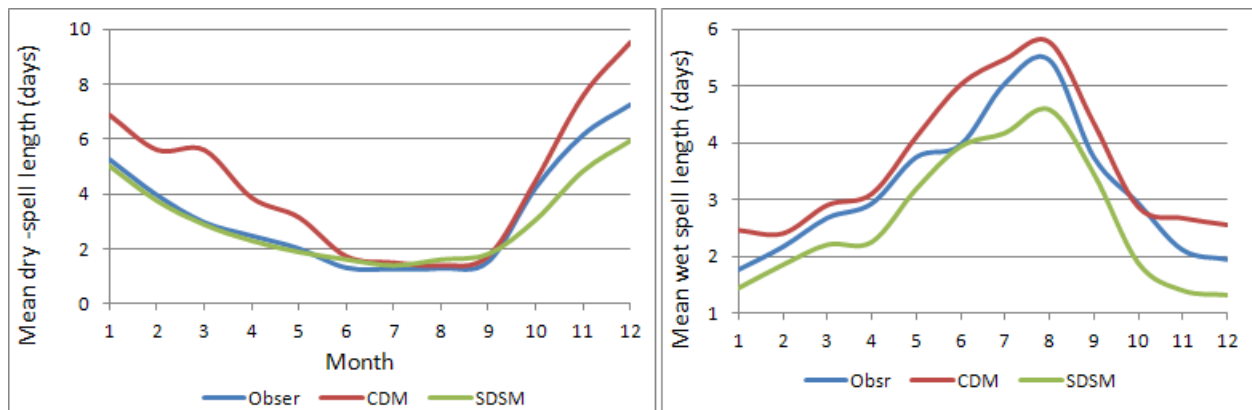


Figure 5.24 Mean dry-spell and mean wet-spell length at Jimma station respectively

The arithmetic average of the 31 years data of dry and wet spells in monthly basis provides mean statistics of dry and wet-spell lengths for each month. Relative plots of that statistics between observed and downscaled daily precipitation are shown in Figure 5.24 for both models CDM and SDSM.

Based on the above comparison plot both downscaling methods approach the observed value. However CDM (cumulative distribution mapping method) found that it overestimates the mean dry spell length for few months like January, February, March and April to certain level and it estimates very well the dry spell length in May, Jun, July, August and November. While SDSM estimated dry-spell length closer to the observed data from January through September it shows a poor performance only in October, November and December. Similar trend is found in wet-spell length comparison, at the station Jimma, for all the months CDM (cumulative distribution mapping method) results are found closer to the observed data, while SDSM model underestimates wet-spell lengths to visible range.

This analysis showed that both downscaling model performs very well in producing historical climate values, but when we compare in producing of important statistical parameters like, variance, mean dry spell and wet spell length and absolute error in their downscaled results CDM (cumulative distribution mapping method) was able to reproduce observed statistical parameter in its downscaled results in almost all months of the year and performs better than SDSM.

## 5.5 Future climate scenarios from Remo and GCM

All the above downscaling and bias correction procedures were carried out to facilitate a conducive environment to produce future climate projections from REMO and GCM outputs, free of any biases. Once the downscaling methodology validated by current climate condition, it is possible to say that, the procedures are reliable to forecast future climate scenarios free from any errors by applying the above methodology and by calculating the climate change factors and using the results for projecting future climate conditions in the studying basin.

### 5.5.1 REMO scenarios

To downscale scenarios data from REMO a correction factor that takes in to account changes in variability between the scenario and base line simulation have been applied. The basic idea of this principle was applied successfully by (Elshamy et al., 2009). For this particular study a correction factor  $f_i$  for each scenario value  $X_{i, scen}$  is found by finding the ratio between the scenario and control values of Remo simulations at the climate station where the cumulative distribution functions for current climate conditions applied. Accordingly the correction factor for each of the day in a given month calculated based on the following formula.

$$f_i(x_{i,scen,J}) = \frac{F_{i,scen,J}^{-1}(F_{i,scen,J}(x_{i,scen,J}))}{F_{i,ctrl,J}^{-1}(F_{i,scen,J}(x_{i,scen,J}))} \quad 5.23$$

Where

$f_i(x_{i,scen,J})$  Is the correction facto in day i in scenario period for the months of January, February etc.

As one of the tiresome process which was noticed in this part of the research is finding out of this correction factor for each days of the months for 21 rainfall stations, 14 maximum temperature and 14 minimum temperature stations and for each scenario data used for this study. After getting out this correction factor it has been used as multiplicative factor for precipitation and additive factor for temperature. For example the final corrected value for the scenario precipitation  $x_{i,scenario,j}^{corrected}$  is then found as follow:

$$x_{i,scenario,J}^{corrected,prec} = F_{i,observed,J}^{-1} \left( F_{i,scen,J}(x_{i,scen,J}) \right) * f_i(x_{i,scen,J}) \quad 5.24$$

To get the scenario period maximum and minimum temperature we used the same formula but the climate change factor added instead of multiplying.

$$x_{i,scenario,J}^{corrected,temp} = F_{i,observed,J}^{-1} \left( F_{i,scen,J}(x_{i,scen,J}) \right) + f_i(x_{i,scen,J}) \quad 5.25$$

### 5.5.2 GCM scenarios

To get more scenarios for comparisons of future climate change in Omo Gibe basin, projections of precipitation, maximum and minimum temperature based on GCM output have been done. The same time horizon followed with Remo simulations. Previously we were calibrated SDSM to downscaled current climate conditions like precipitation maximum and minimum temperature. Once the downscaling model have been calibrated and validated regarding to current climate condition, the next step is to use these calibrated model to downscale the future climate change scenarios simulated by GCM (HadCM3). In this case, instead of using the national center for environmental prediction (NCEP) reanalysis data as the input to each of the downscaling model earlier used for calibration and validation purpose, the large-scale predictor variables which are simulated by GCM, Hadley center for climate prediction and research coupled model (Hadcm3) for A2 scenarios have taken which covers the period of 2020 to 2050.

Finally the change in maximum and minimum daily temperature and the change in precipitation in future period (2020 to 2050) under the two scenarios from REMO A1B and B1 under wet, optimum and dry conditions and A2 scenario from Hadcm3 have been analyzed.

### 5.5.3 Climate trend analysis from downscaled scenarios

The change in temperature in future time period 2020-2050 have been done in two different approaches. At the beginning the change in maximum and minimum temperature has been assessed for each individual station. The increase in maximum and minimum daily temperature in future period under the five scenarios in all-weather observation stations is shown in table 5.10. Generally the downscaled maximum and minimum temperature from all stations show consistently increasing trend in the downscaled values of 2020 to 2050. Table 5.10 summarizes the downscaling results by presenting the simulated increased in annual values of average daily maximum and minimum temperatures between the current and the (2020–2050) time periods from each of the downscaling scenario. All the downscaling scenarios including GCM agreed in increasing of maximum and minimum temperature in all stations except Sawula for GCM simulation which shows no significant trend or change observed between current and future time periods.

Both downscaling models showed a comparable and consistently increasing trend for both Tmax and Tmin. Eventhough the entire scenarios agreed in increasing maximum and minimum temperature in the entire basin they have simulated a bit different change in maximum and minimum temperature. For instance the basin average highest change in maximum temperature is predicted by REMO as 1.37<sup>0</sup>C change at the end of 2050 by A1B\_911 scenario and the minimum simulated maximum temperature obtained as 0.86 <sup>0</sup>C by GCM. Accordingly the output of all the scenarios A1B\_911, A1B\_912, B1\_921, B1\_923 and GCM for A2 scenario revealed that the average maximum temperature in Omo Gibe basin will be increased by 1.37 <sup>0</sup>C, 1.32 <sup>0</sup>C, 1.17 <sup>0</sup>C 1.1 <sup>0</sup>C and 0.86 <sup>0</sup>C respectively. Based on the average results projected by REMO from four scenarios mean annual Omo Gibe maximum temperature is expected to rise by about from 0.9 <sup>0</sup>C to 1.8 <sup>0</sup>C at the end of 2050 for upper part of the basin (figure 5.20).

S no	Stations	A1B_911 °C		A1B_912 °C		B1_921 °C		B1_923 °C		GCM °C	
		Tmax	Tmin	Tmax	Tmin	Tmax	Tmin	Tmax	Tmin	Tmax	Tmin
1	Assendabo	1.4	2.1	1.1	2.3	1.1	1.4	1.15	1.7	0.9	0.6
2	Bonga	1.3	1.8	1.1	2	1.1	1.7	0.9	1.5	0.9	0.4
3	Dedo	1.1	1.8	0.95	1.8	0.95	1	0.7	1.5	0.5	0.5
4	Gedo	1.5	1.2	1.6	1.3	1.3	1.2	1.3	1	0.8	1
5	Hossana	1.8	2.3	2.1	2.4	1.6	1.7	1.5	2	0.5	1
6	Jimma	1.2	2.2	1.2	2.2	1	1.45	0.95	1.6	0.8	0.8
7	Jinka	1.2	1.3	0.9	1.3	0.8	1	0.6	1	0.6	0.5
8	Morka	1.3	1.3	0.9	2.5	0.8	2	0.7	2	0.5	0.6
9	Sawula	1.1	1.3	1	1.7	0.95	1	0.9	1	0	0
10	Shebe	1.1	1.2	1	1.6	0.95	0.9	0.9	1.1	0.6	0.5
11	Woliso	1.1	1.8	1.7	2	1.45	1.05	1.35	1.2	*	*
12	Wolita	1.3	1.8	1.2	2	1.2	1.3	1.2	1.4	1.3	1.3
13	Wolkite	1.8	2	2	2.2	1.6	1.4	1.6	1.6	1.3	0.7
14	Yaya	2	2.3	1.7	2.3	1.6	1.8	1.6	2.3	2.5	1.1
<b>Basin Average °C</b>		<b>1.37</b>	<b>1.7</b>	<b>1.32</b>	<b>1.9</b>	<b>1.2</b>	<b>1.4</b>	<b>1.1</b>	<b>1.5</b>	<b>0.86</b>	<b>0.7</b>

Table 5.10 Change in maximum and minimum temperature in Omo Gibe basin 2020-2050

\* indicates that downscaling at this station was not performed

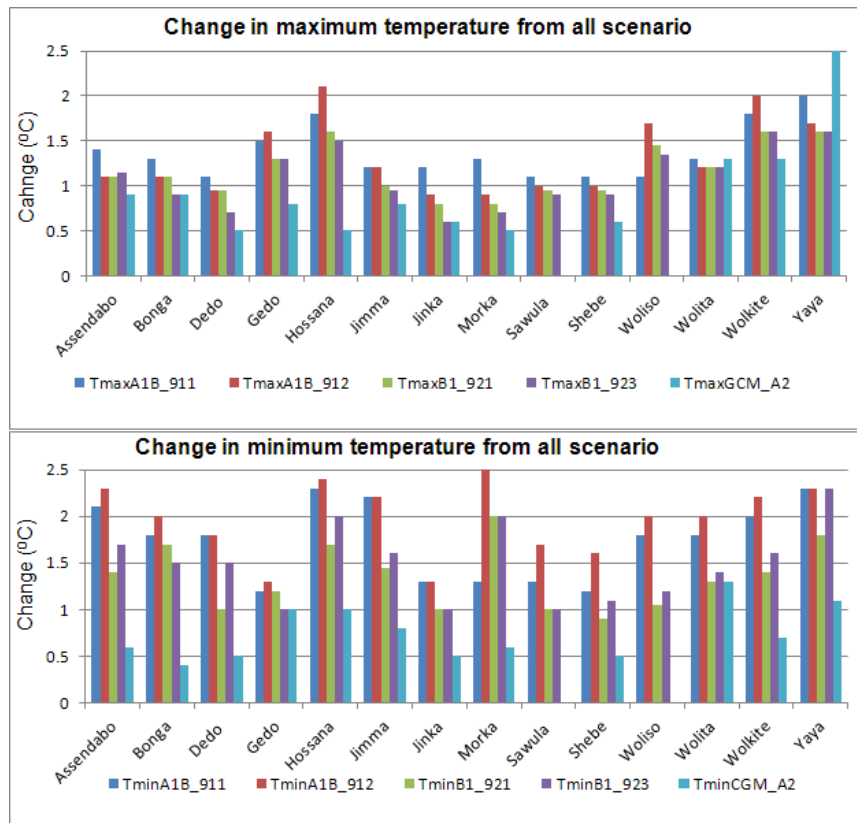


Figure 5.25 Change in mean annual maximum and minimum temperature in 2020 to 2050



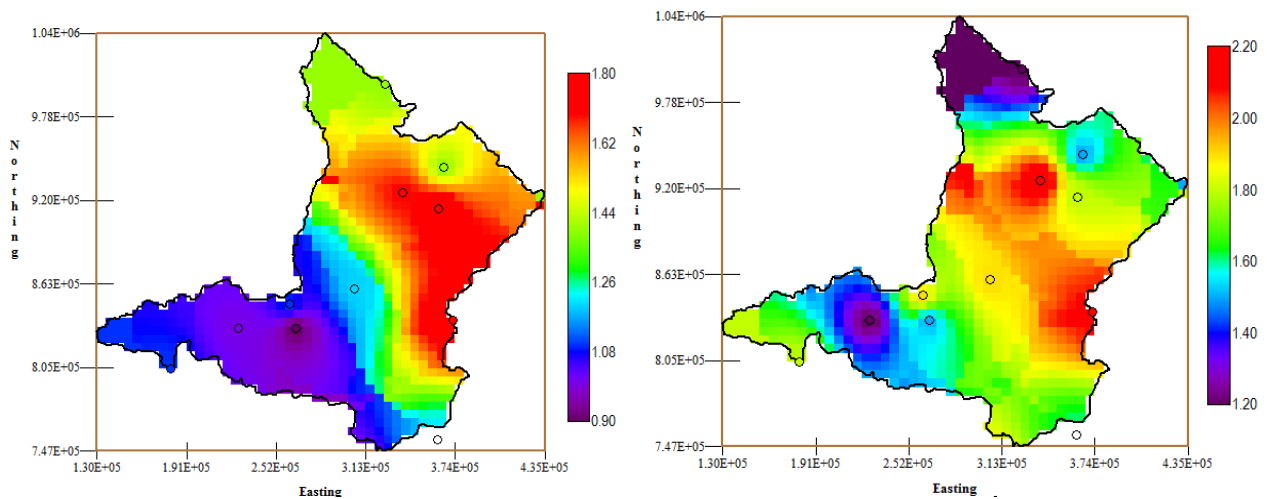


Figure 5.26 Spatial changes in mean annual maximum and minimum temperatures from Remo average result of all scenarios for upper part of the basin

The statistical downscaling results for minimum temperature in Omo Gibe basin showed that minimum temperature will rise in a faster rate than that of maximum temperature. This has been quantified by comparing the change in basin average mean annual maximum and minimum temperature in 2020 to 2050 with reference to present temperature data sets. Based on the results of all scenarios A1B\_911, A1B\_912, B1\_921, B1\_923 and GCM\_A2 minimum temperature is expected to rise by 1.7 °C, 1.9 °C, 1.4 °C, 1.5 °C and 0.7 °C respectively. If we observe the change in mean annual minimum temperature in all cases it is higher than the change in maximum temperature except GCM result. According to the average results projected by REMO from four scenarios mean annual Omo Gibe minimum temperature is expected to rise by about 1.2 °C to 2.2 °C at the end of 2050 (figure 5.26).

Analyzing of downscaled precipitation results has been carried out based on individual and areal values of each station. The areal rainfall change quantified only for upper part of the basin above Gibe III dam site which constitutes 33,901 km<sup>2</sup> watershed area. This part of the catchment represented by 18 precipitation observation stations, the southern part of the basin represented by three precipitation stations Jinka, Sawula and Morka. The change in mean annual precipitation for this part of the basin has been performed by analyzing the changes from these three climate stations.

Table 5.9 shows the change in mean annual precipitation results in all downscaling stations. The change in mean annual value is calculated by subtracting the aggregated mean annual precipitation output from future downscaling results (2020 to 2050) to observed precipitation. This is the delta value between future and control period. The result from all Remo simulation reveals that there is no significant major change in mean annual precipitation in most of the stations. However; three scenarios from Remo downscaling showed that there will be small increment of mean annual precipitation value at the end of 2050, except Sawula for A1B\_911, Hossana and Jinka A1B\_912 which showed a reduced mean annual precipitation by -73.1mm, -114mm and -65.4mm respectively. But one of Remo simulation B1\_923 showed that there will be small reduction in mean annual precipitation in most of the stations.

GCM output simulated a bit different value than Remo. GCM for A2 scenario projected a bit higher increment in mean annual precipitation in some of the stations. For instance stations which are found south of Gibe III dam site, Sawula, Morka and Jinka showed visible increment in mean annual precipitation by 531.5 mm, 409 mm, and 250mm which are equivalent with an increment of 31% at Sawula, 30% at Morka and Jinka. But for the rest of the stations mainly



found at the upper part of the basin doesn't show significant increment as that of Sawula and Morka except Wolita.

Stations	Change in mean annual precipitation ( mm) from 2020 to 2050 all scenarios					
	Obs Ann PPc(mm)	Change GCM A2	Change Remo A1B_911	Change Remo A1B_912	Change Remo B1_921	Change Remo B1_923
Assendabo	1214.2	99.5	49	-11.3	43.9	-34.3
Bele	1240.9	-284.7	42	84.8	29.1	-7.1
Bonga	1726.5	102.8	79.1	89.3	34.8	-45.5
Chekorsa	1698.3	-60.8	39.8	49.8	85.6	-1
Dedo	1959.3	211.5	211.6	-42.7	12.4	-94.8
Durame	1153.1	-102.2	63.8	-32.7	99.6	-107.7
Gedo	1141.4	102.3	109	23	-36.2	-32.3
Gibe	976.5	-21.8	39.9	-29.1	-2	-22.9
Hossana	1193.6	176.1	58.6	-114.4	12.2	-95.2
Jimma	1493.3	135.4	30.4	-5.7	32.7	-38.8
Jinka	1307.9	250.1	21.7	-65.4	-22.1	-29.7
Kumbi	1283.4	-74.5	52.3	-22.4	-35	-68.1
Limu	1753.5	291.9	146.5	-15.2	36.1	11.7
Meteso	1925.5	202.2	-44.7	-43.8	100.7	37.6
Morka	1367.1	409	90	-4.1	-18	-38.6
Sawula	1547.4	531.5	-73.1	21.4	-4.7	11.4
Shebe	1634.2	110.1	61.6	10.1	106.1	40.9
Wolita	1402.1	459.1	123	12.6	9.9	-44.8
Wolkite	1339.5	42.5	190.5	-4	-4.9	-33.3
Yaya	1095.7	-103.5	49.8	61	2.7	-17.1
Woliso	1239	0	0	55.9	12.7	27.1

Table 5.11 Change in mean annual precipitation (2020-2050) in reference to control period

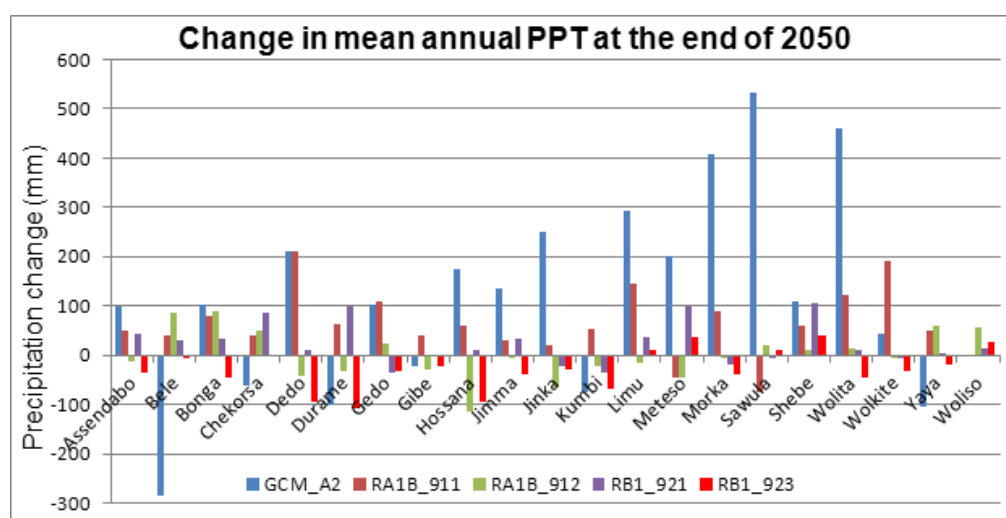


Figure 5.27 Projected change in mean annual precipitation from all scenarios at the end of 2050

In order to investigate the changes in seasonal and mean annual areal rainfall especially for upper part of the basin the following attempt has been done. The areal rainfall for upper part of the basin calculated by developing Thiessen polygon using 18 precipitation stations; accordingly the areal precipitation from observed and all projected precipitation in 2020 to 2050 averaged and compared with observed results. The following table depicts the results obtained from this procedure.

Months	Jan	Feb	Mar	Apr	May	Jun	Jul	Aug	Sep	Oct	Nov	Dec	Winter	Spring	Summr	Autum	Annual
Observed	30	44	85	114	157	192	234	226	154	89	36	24	96	356	652	279	1386
A1B_911 (wet)	32	58	91	126	186	249	250	203	137	91	34	18	105	404	702	262	1477
A1B_912 (optimum)	37	43	89	128	194	201	244	224	136	71	30	26	103	411	668	237	1422
B1_921 (wet)	33	44	85	131	191	202	220	220	155	80	30	22	96	406	643	264	1413
B1_923 (dry)	26	46	92	111	187	212	211	214	140	75	34	19	88	390	637	248	1366
GCM_A2	50	85	117	128	143	151	207	207	124	147	56	32	163	388	565	326	1447

Table 5.12 Comparison of areal precipitation between current and projected scenario 2020 to 2050 for upper part of the basin above Gibe III dam site in mm

Based on rainfall events; seasons in Ethiopian can be defined as:

- ✓ Summer: which has the months of June, July and August this season is characterized by main rainy season
- ✓ Autumn: September, October and November
- ✓ Winter: December, January and February
- ✓ And Spring small rainy season of March April and May.

Small changes have been observed from all scenarios during spring season, all of them projected increased precipitation during this season. This might be a good opportunity for the farmers to have a bit prolonged precipitation during this short rainy time for agriculture. On the other hand A1B\_911 and GCM projected increased summer and winter precipitation respectively, whereas B1\_923 projected decreased summer rainfall. Moreover a small change in mean annual precipitation values has been observed in four of the scenarios. According to the results four of the scenario A1B\_911, A1B\_912, B1\_921 and GCM\_A2 show an increasing trend in areal mean annual precipitation by 6.5%, 2.4%, 1.9% and 4.5% at the end of 2050. One scenario B1\_923 shows a decreasing trend of areal mean annual precipitation by 1.4%. It is possible to say that there is no any significant change in areal precipitation except A1B\_911 in the upper part of the basin above Gibe III dam site under all scenarios. Because the percentage change in precipitation of all scenarios is less than 10%. Generally from these results it is possible to say that the mean annual precipitation in Omo Gibe basin doesn't show significant change under all scenarios except GCM\_for A2 scenario which showed visible change for southern part of the basin in Sawula, Morka and Jinka.

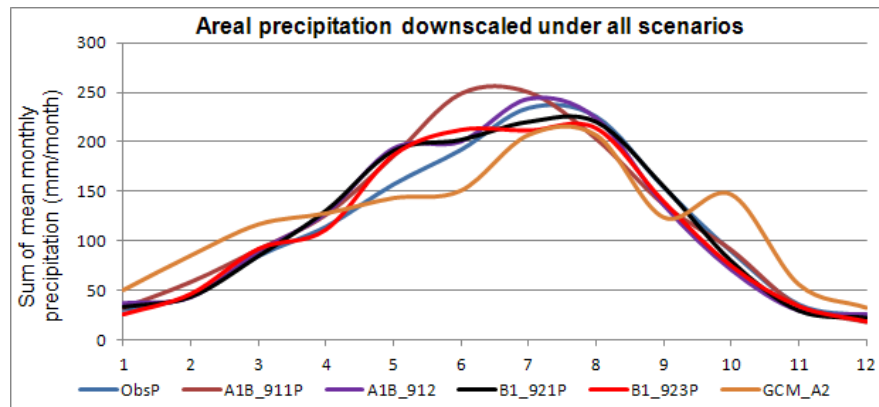


Figure 5.28 Monthly sum of observed (1970-2000) and projected (2020-2050) areal precipitation upper part of the basin.

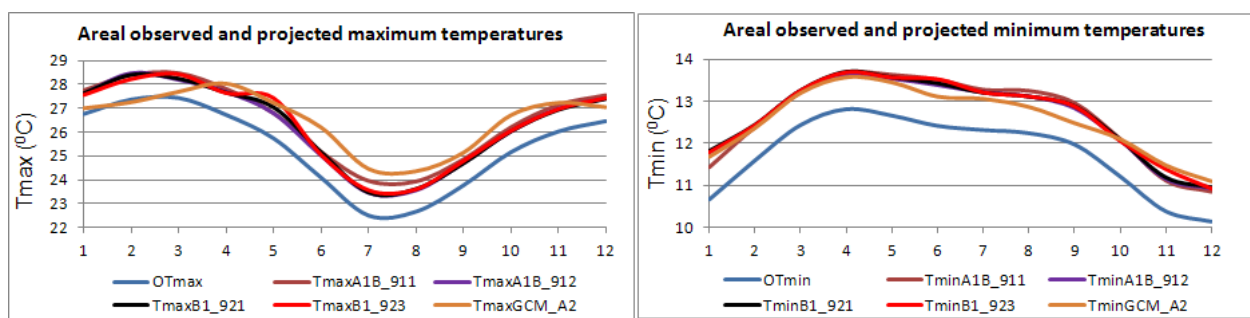


Figure 5.29 Mean monthly observed and projected (2020-2050) areal maximum and minimum temperature for upper part of the basin.

## 5.6 Conclusion

The primary goal of downscaling procedure is to provide error free simulations of future climate and climate change data. Due to the coarse spatial resolution and simulations of Remo and GCM model outputs, their precipitation and temperature cannot be directly used as an input to hydrological model to study effects of climate change. To overcome this problem a robust and practical downscaling and bias correction method applied in relation to Remo outputs. It is possible to mention the methodology as cumulative distribution mapping technique. Precipitations were downscaled by fitting with Gamma distribution. Validation of this procedure carried out using daily precipitation fields in a number of ways. Results show that the method performs surprisingly very well. Not only the monthly mean, monthly sum and other moments of the intensity distribution improved as expected; but also in simulation of heavy precipitation index as well. In general the proposed statistical bias correction methodology with daily cumulative distribution functions removes significantly and consistently positive and negative biases from Remo simulations.

Different approach has been employed to downscale temperature data. Maximum and minimum temperatures are two of important data that should be used as an input to SWIM. Therefore, reliable estimation of future temperature data in Omo Gibe basin is unquestionable. In support of this objective a new temperature bias correction methodology developed based on distribution fitting procedure. Observed and Remo simulated maximum and minimum temperatures were disaggregated in to monthly basis in all-weather observation stations, and then using different cumulative distribution and goodness of fit test the best distribution was selected for each months of the year at all stations. According to the result Kumaraswamy, Generalized extreme value and Burr VI distributions are the best choice for fitting minimum temperature in Omo Gibe basin, additionally Burr III and Burr VI distributions are good choice for fitting maximum temperature.

Instead of applying the methodology directly for simulating future temperature data, it was validated in a number of ways by using control climate data from both observed and corrected Remo data sets, the validation result showed that the bias correction method performs very well in maintaining the statistical moments of corrected value which resembles the observed one. In other way the results show the best match between corrected and observed data sets. Eventhough, the bias correction process is time consuming and exhausting work to apply for many stations, but the methodology was more flexible and it gives an opportunity to create reliable and stable model in downscaling maximum and minimum temperature at point scale.

As we have seen the present methodology (new bias correction method for maximum and minimum temperature) may constitute a step forward and can have a paramount importance in research as a tool to estimate and forecast future point maximum and minimum temperature in different regions.

Moreover, downscaling of climate data sets from GCM has been carried out. The principle behind GCM downscaling is based on multiple linear regression approach between observed weather data and large scale GCM predictors. The performance of this model was checked based on simulated current climate conditions by comparing with observed climate data. During the performance criteria for precipitation data in addition to mean monthly and mean annual values comparisons of average dry spell length and average wet spell length considered, since these components of the climate statistics are very important for hydrological simulation. The results from GCM downscaling showed that it also produces the most statistical parameters that have been involved in observed climate data.

The efficiency of the above downscaling methodologies (CDM and SDSM) was compared. This analysis showed that both downscaling model performs very well in producing historical climate values, but when we compare in producing of important statistical parameters like, variance, mean dry spell and wet spell length and absolute error in their downscaled results CDM (cumulative distribution mapping method) was able to reproduce observed statistical parameter in its downscaled results in almost all months of the year and performs better than SDSM.

After checking the reliability of the downscaling methodology future climate scenarios were projected at the studied basin. All the scenarios projected increased maximum and minimum temperature throughout the basin. However, the statistical downscaling results for minimum temperature in the basin showed that minimum temperature will rise in a faster rate than that of maximum temperature. Accordingly, areal average maximum temperature from REMO is expected to increase in the range of  $0.9^{\circ}\text{C}$  to  $1.8^{\circ}\text{C}$  and minimum temperature is expected to increase in the range of  $1.2^{\circ}\text{C}$  to  $2.2^{\circ}\text{C}$  in the upper part of the basin. On the other hand average mean annual areal precipitation in expected to increase in small amount from four scenarios while one scenario shows mean annual areal precipitation decreased by 1.4%.

# Chapter 6 Application of SWIM for Abelti and Un-Gauged Basins

## 6.1 Introduction

Freshwater is basic, finite and fundamental resource which has close relation to human life. In other way life wouldn't exist without fresh water. But this valuable resource is extremely scarce and the current challenge, effects of climate change may have adverse impact on this precious resource to human being. Estimation of water resources potential for reference period is very important, because this helps to know how much amount of surface water resources generated from any basin in reference to the current time period. Without knowing water resource potential in a basin it is not possible to carry out any development projects like developing of hydropower, water supply and irrigation projects, additionally it will not be possible to carry out any climate change study. In order to carry out effects of climate change on water resources potential of a give basin knowing of reference water resources potential is the main concern as the change is quantified in reference to the current water resources potential.

In order to calculate the water resources potential of any basin measurements of flow (discharge data) especially at the main river courses are very important, because from these measurements it is possible to draw the water resources potential of the basin. However, such flow measuring stations in Gibe basin are very limited, even some of the watershed areas have not been measured directly due to lack of inaccessibility of the area because of rugged mountainous topography and remoteness of the main river course from major city. Nearly more than 30 % of the watershed which contributes flow to Gibe III dam site is not measured, or it doesn't have any historical dignified flow data. This is the main scientific puzzle any one can face during conducting of research in the basin. By considering this great problem, this chapter focused on estimation of water resources potential for un-gauged part of the basin and Gibe III watershed as well. To accomplish this objective this part of the study uses different approaches to quantitatively determine the current status of water resources potential in the basin so as to provide a basis for current utilization and to study effects of climate change in the basin. This part of the study has one primary goal to establish daily and spatially aggregated picture of Omo Gibe current water situation.

## 6.2 Application of SWIM at Abelti

Detail information regarding to SWIM hydrological modeling and mathematical equations describing the physical processes involved in the model can be found in chapter three of this thesis. Here we are dealing with the main application of this model at Gibe basin for two important purposes. Initially this model will be used to generate daily flows data for reference time from un-gauged part of the basin by calibrating the model at Abelti flow station, thereby preparation of first hand input data for the same model for the purpose of climate change study at Gibe III dam site. Secondly the model will be calibrated at Gibe III dam site to study the effect of climate change on the inflow to Gibe III reservoir from 2020 to 2050. Since these two sets of problem have different objectives we will see the application of the model separately.

As watershed models become increasingly sophisticated and useful, there is a need to extend their applicability to locations where they cannot be calibrated or validated, in other way we should use these watershed models to (un-gauged catchments) systematically. At this particular part of the work transferring of hydrologic characteristics of watersheds from available observed data (Abelti) catchment to Un-gauged part of the basin will be used to derive daily flows from un-gauged part of the study area.

Semi distributed, physically-based hydrologic models represent a catchment in great detail; including topography, soil, slope and land uses. One of the main objective of this thesis is to set

up such process based hydrological model at Omo Gibe III dam site for studying climate change on water resources potential of Omo Gibe basin. However, most of process based hydrological model like SWIM requires daily flows data at the site of interest. Unfortunately lack of adequate hydrological information observed in most part of the study area. In order to fulfill this gap this model provides a reliable solution by generating daily flows for the site in question.

The following section will discuss broadly how to calculate daily flows from un-gauged part of the basin by using Gibe III dam site as outlet point of this basin. The following picture revealed main flow measuring stations and un-gauged part of the basin.

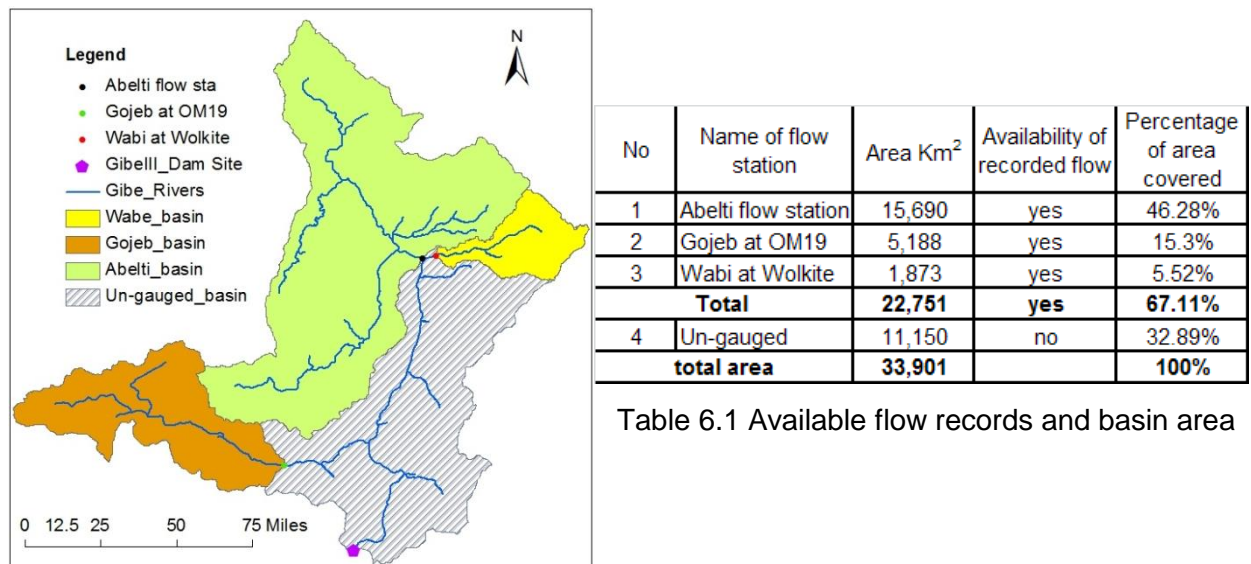


Table 6.1 Available flow records and basin area

Figure 6.1 The three main flow measuring stations and their watershed area

There are a number of stream gauges located above Abelti flow measuring station (Figure 5.2) the source of this stream flows data is Ministry of water and energy of Ethiopia. According to this study the overall catchment size of Gibe III dam site is 33,901km<sup>2</sup>. Based on this calculation Abelti flow measuring station on the Gibe River measures flow from 15,690km<sup>2</sup>. This station is the only station which measures flow from large area and on the major river course as well. Since Abelti measures flow on larger area than the others it has particular importance as it represents alone a considerable percentage of the entire area under investigation (more than 46%). Moreover, Wolkite station on Wabi River located downstream Abelti and it has great importance as it covers an area downstream Abelti, which constitutes 5.5% of the total area. The same consideration can be made for the Shebe gauging station on the Gojeb River (10% of the total area), but to enlarge the area covered by this station the runoff time series at the proposed dam site OM19 location was considered this constitute 15.3% of the total area. The area which is found downstream of Gibe River at Abelti, Wabe River at Wolkite, and Gojeb River at the dam site OM19 is considered as un-gauged catchment this is illustrated by figure 6.1. Unfortunately no hydrometric station is located in this part of the basin. This part of the study area represents almost 32.8% of the total area above Gibe III dam site table 6.1. This part of the watershed is mentioned as un-gauged catchment throughout this study.

According to (IAHS, 2003) an un-gauged basin (catchment) can be defined as one with insufficient records or no record at all (in terms of both data quantity and quality) of hydrological observations to enable computations of hydrological variables of interest (both water quality and quantity) at the appropriate spatial and temporal scales and to acceptable accuracy level for practical applications. In seeking to address the challenges of water resources and water-environmental degradation issues across a basin, a major difficulty is encountered with those basins for which little or no hydrometric data is available. These basins are predominantly in developing country in regions where basin developments are undertaken with limited data. This

frequently led to the depletion of water resources, ecosystem degradation and poor quality of life (IAHS, 2003). Predicting water runoff in the mostly Un-Gauged water catchment areas of the world is vital to practical applications such as the design of drainage infrastructures and flooding defenses, for runoff forecasting and for catchment management tasks such as water allocation and climate impact analysis (Blöschl et. al, 2013). To alleviate some of these problems the following different approaches have been employed to calculate daily and mean annual flow at Omo Gibe basin.

### 6.2.1 Methodology

Several studies have already attempted to address the problem of estimating daily flow data worldwide, but most of the methods are not easily transferable to Omo Gibe basin. However, there are some common approaches used to estimate mean annual flow like area ratio method and rational formula. But these methodologies attempt to calculate only aggregated mean flow, because the approach mostly concentrated on a conceptual background without much reference to the real data or complete hydrological and physiographical background of the basin. Consequently, the problem of daily flow data remains largely unresolved. It is also one of the big challenging issues for those young researchers who want to carry out useful and beneficiary research in Omo Gibe basin. Apart from the fact that this daily flow data has large potential for practical applications, such as climate change study, sustainable water resources planning and management.

In considering all the above problems this part of the study developed a pragmatic approach by which daily flow data from un-gauged part of the catchment can be derived by considering physiographic, evaporation and climatological data of this basin using the art of SWIM modeling technique. The method is designed to be low cost, straightforward and can be used for similar application. The basic idea of this method is based on calibration of SWIM at Abelti catchment which has a watershed area of 15,690 km<sup>2</sup> and daily measured flows. After calibrating the model at Ableti station those calibrated parameters were used as an input to un-gauged catchment to derive daily time series. But before using this procedure a reasonable assumption has been made between Abelti and un-gauged part of the basin.

Assumptions that has been made during the above methodology:

- One of the reason Abelti catchment is selected for prior calibration, the size of the catchment, because this area is ideally comparable with un-gauged part (11,150 km<sup>2</sup>) as compared to OM19 (5,188 km<sup>2</sup>) and Wolkite (1,873 km<sup>2</sup>) figure 6.1.
- The other reason is the meteorological characteristics of the two watersheds. As it is possible to see from table 6.7 the areal depth of precipitation at Abelti is 1,328 mm/year similarly for un-gauged part of the basin is 1,316 mm/year. Although there is a minor disagreement between these two values it is not significant as compared to OM19 catchment which has areal precipitation of 1725.6 mm/year.
- According to the land use data which was collected from Ministry of water and energy of Ethiopia, some attempts have been made to investigate the possible relationships of the land use characteristics of the two basins, because this characteristic has a great influence in evapotranspiration. Based on the analysis made, nearly 77% of the land in Abelti catchment is used for agriculture whereas in Un-gauged part of the basin agricultural land covers nearly 65% this means that in both cases major land use is agriculture and the percentage land cover by agricultural crop is comparable.
- The overall soil data base of the basin above Gibe III dam site has been developed by considering different soil texture classes, chemical and physical properties of the soil, according to this soil data base Abelti and Un gauged part of the basin has similarity in their soil texture class. The percentage of clay content in both catchments is dominant soil texture class. The depth of the soil in both catchments varies from deep to very deep



## 6.2.2 Preparation of Model input data

Modelling is now a common tool in many fields of engineering especially in climate change however, to model the impacts of climate change on hydrology or flow regime would be impossible without spatial data. Spatial data are the raw materials for SWIM hydrological modeling. Application of SWIM to the Omo Gibe Rivers requires the development of important input spatial data describing the basin and the development of a meteorological and hydrological record to drive the rainfall-runoff process. The model runs with daily time scale. Useful spatial data necessary to run the model are:

- ✓ Digital elevation model (DEM),
- ✓ land use map,
- ✓ soil map,
- ✓ map of basin and sub-basins boundaries,
- ✓ map of river network,
- ✓ map of river gage stations,
- ✓ map of climate stations,

The first four maps; DEM, land use, soil and sub-basins are absolutely necessary to run the model. For this particular study all these spatial data were prepared and saved in SCII format for further processing. Detail preparation of the above listed spatial data described below.

### Digital elevation model (DEM)

The digital elevation model (DEM) used as the basis for Gibe basin with 90 and 200 meter resolution have been downloaded and collected from freely available high resolution SRTM (Shuttle Radar Topographic Mission) data from <http://srtm.csi.cgiar.org> in the form of tile up on entering the two extreme coordinates of the basin and the later one collected from ministry of water and energy of Ethiopia. To get the combined raster map of Gibe basin combinations of SRTM tile have been carried out using ArcMap. Delineation of the whole watersheds from digital elevation model (DEM) data has become standardized on the eight-direction pour point model. Each cell is connected to one of its eight neighbouring cells according to the direction of steepest descent, all of these procedures performed using ArcMap to get sink free and processed digital elevation model of the basin. The derived DEM was used to delineate the topographic characterisation of the watershed and determine the hydrological parameters of the watershed such as slope, flow accumulation and direction, stream network and subbasin using Mapwindow. Additionally, sink free and processed digital elevation model map is very important in SWIM to produce routing structure to route flow from each sub-basins along the river channel to outlet points.

### Soil parameter data

Soil data is one of the most important inputs for sound modeling procedure, especially for SWIM hydrological model. The importance of soil properties stems from the important role they play in hydrological modeling (Kassa T. 2009). The use of models for the prediction of runoff and impacts of climate change depends heavily on detailed data on soil physical properties. However, such organised data is unavailable in most part of Ethiopia including Gibe basin, but we have collected the available information at the study area as much as possible and efforts have been carried out to produce reasonable soil data base from available information in the basin.

The soil map of the entire basin collected from Ministry of water and energy of Ethiopia. Additionally the SWIM model requires some details on physical and chemical properties of the soils for watershed being modeled. In order to acquire relevant physical and chemical properties required by the model throughout the watershed additional information has been collected to extract important soil properties from the available study document. Detail investigation on Gibe

basin master plan study document has been carried out, as a result vital information like depths of the soil at different part of the study area, clay, silt, sand content, bulk density, available water capacity, field capacity, organic carbon content, organic N content have been extracted from this document for each type of the soil in the basin. Finally the required soil data base developed for upper part of the basin above Gibe III dam site. This procedure has been carried out only for upper part of the basin above Gibe III dam site because hydrological modeling carried out for this basin only which constitutes an area of (33,901 km<sup>2</sup>). The soil database was established through an intensive data investigation from each of the sample sites that has been carried out during Omo Gibe master plan study.

For consistency purpose, all prepared soil data base were described using the guidelines for soil description based on SWIM data format. And then the soil data base which was already found in SWIM model has been substituted by Omo Gibe soil data base for modeling purpose in Gibe basin. According to the model requirements, the depth of the first soil layer should be 10mm. Based on this requirement 30 soil data base which contains different soil parameters derived from 8 main soil types, and stored in standard soil file of SWIM model. Finally the soil map connected to soil parameters based on the requirement of SWIM using soil number (reclassification) system. The format of soil parameters described in the soil database is Shown in figure 7.2

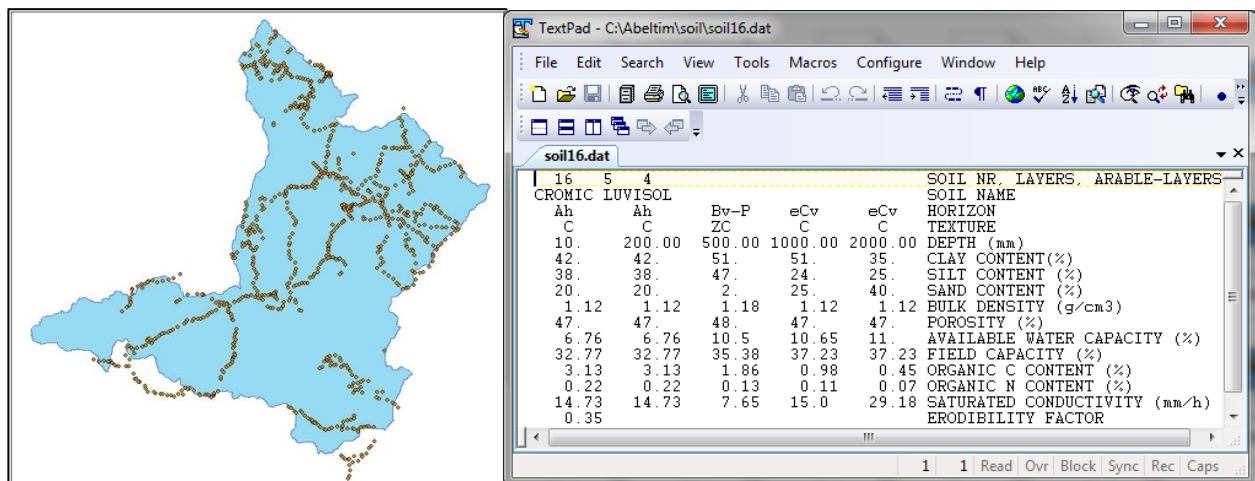


Figure 6.2 Part of soil survey site locations during master plan study and developed soil data base respectively

Since there is no nay information regarding to saturated conductivity and porosity in master plan study document, these soil parameters have been determined separately for each soil layer and type. Saturated conductivity was estimated using Cosby (1984) as a function of clay and sand content.

$$SC = 60.96 * 10^a \quad 6.1$$

$$a = -0.6 + 0.0126 * SN - 0.0064 * CL \quad 6.2$$

SC is saturated conductivity

SN is sand content in %

CL is clay content in %

The porosity of each soil has been determined based on texture classes described on mean physical properties of soils (from Svetlosanov and Knisel, 1982).

## 6.2.3 Preparation of additional input data by SWIM/MapWindow interface

For this study user friendly SWIM/MapWindow interface used to run SWIM at Abelti and Gibe III dam site. MapWindow is open GIS software it can be freely downloaded under the website <http://www.mapwindow.org>. MapWindow is an extensible geographic information system and it allows the users to write plug-ins to add additional functionality (models, special viewers, hot-link handlers, data editors, etc.) and pass them to any number of end users. This characteristic helps the windows users to easily install and use the SWIM/MapWindow interface (Tobias et al., 2009).

The first step during SWIM setup and pre-processing procedure at Abelti station was, delineating of the sub-basins based on the recommended sub-catchment area. Accordingly, by using map of river gage stations at Abelti flow measuring point, basin boundaries of this catchment was defined. The map of sub-basins is important as a mask to extract other information, so this map created in MapWindow based on the DEM map developed before from SRTM data sets, as a result Abelti watershed was divided into 78 sub-basins and saved in ASCII format. Together with sub-basins, the virtual river network calculated which is useful for checking the routing structure.

Before running the main programmer of SWIM it is a mandatory to run the model three times for additional preprocessing purpose, this helps in producing the preliminary input data like climate data with SWIM format, hydrotope structures and routing structures. The main steps that have been carried out during this procedure are listed as follow:

- ✓ Preparation of relational data, mainly climatological data
- ✓ Calculation of hydrotope structure
- ✓ Calculation of routing structures
- ✓ And finally running of SWIM/MapWindow interface, the combined processes of the first three steps are known as pre-processing.

### Preparation of relational data

For the delineated sub-basins in Abelti or Gibe III basin, daily climate data (average, maximum and minimum temperature, precipitation and solar radiation) were interpolated to the centroids of every sub-basin by inverse distance method using data from 21 climate and precipitation stations in and around Abelti and Gibe III catchments. The input climate data for this part of preprocess has been described in chapter five. One of the most important input data for SWIM is the map of climate and precipitation stations, because this map helps during interpolation to select the stations within or close to the target sub-catchment area. Based on this consideration 21 climate stations were prepared according to SWIM format for Abelti and Gibe III basin as well.

ta	mo	jahr	tmax	tmit	tmin	nied	relf	ludr	dadr	sonn	bewo	stra	wind
1	1	1970	27.3	16.3	5.4	0	45	-9999	-9999	-9999	-9999	2417	1
2	1	1970	27.5	15.6	3.66	0	45	-9999	-9999	-9999	-9999	2529	0.9
3	1	1970	27.8	15.9	4.03	0	38	-9999	-9999	-9999	-9999	2523	1.1
4	1	1970	27.5	17	6.45	0	44	-9999	-9999	-9999	-9999	2381	0.8
5	1	1970	27.4	17.8	8.16	0	45	-9999	-9999	-9999	-9999	2274	0.9
6	1	1970	29.2	19.6	10.02	0	49	-9999	-9999	-9999	-9999	2275	0.6
7	1	1970	29.1	17.6	6.14	0	40	-9999	-9999	-9999	-9999	2493	0.7
8	1	1970	28.3	15.8	3.24	0	54	-9999	-9999	-9999	-9999	2609	1.2
9	1	1970	27.7	15.2	2.58	0	50	-9999	-9999	-9999	-9999	2618	1

Figure 6.3 Format of one climate station input data for interpolation purpose

### Preparation of hydrotope and routing structures

To derive hydrotope and the routing structure of the 78 sub-basins, four spatial maps; the preprocessed (sink free) digital elevation model (DEM), soil map, land use map and sub-basins map were stored in a grid format with 200 m resolution. This resolution is recommended for catchment area which has an area of more than 10,000 km<sup>2</sup>. Hydrotope structures were delineated by overlaying the sub-basin, soil and land use map of Abelti and 412 hydrotope structures (figure 6.4 a) that are determined by unique intersections (overlying) of the land use, sub-basin and soils within the watershed developed.

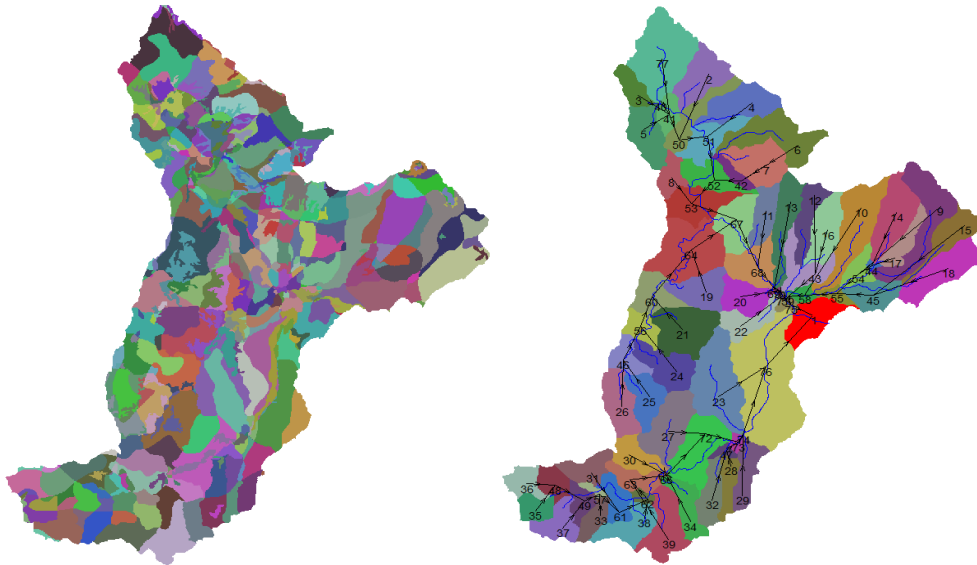


Figure 6.4 (a) Hydrotope structures, (b) routing structures developed during preprocessing of SWIM at Abelti catchment respectively.

The land use map of the whole basin was obtained from ministry of water and energy of Ethiopia based on the available information on this map 8 land cover types agricultural land close grow, agricultural land raw-crops, forest deciduous, forest mixed, heathers, urban, wetland and wetland mixed were considered to setup SWIM at Abelti. The land use map has been reclassified according to SWIM data format. The following figure shows these three maps

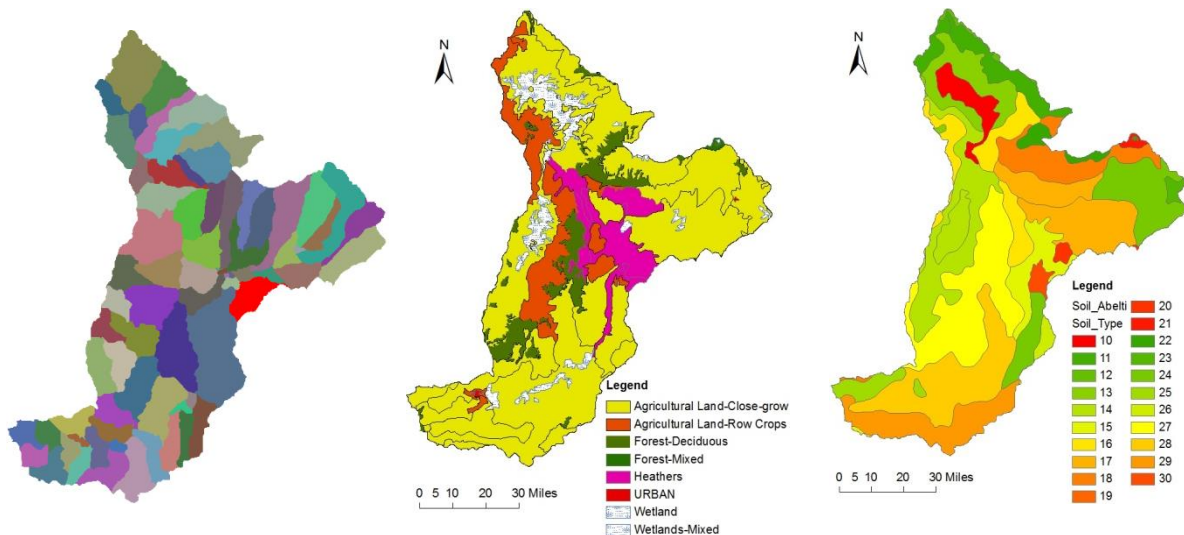


Figure 6.5 Overlaid sub-basins, land use and soil map of Abelti catchment respectively

The numbers in the soil map is used to link the soil map with the soil data base that has been prepared by considering soil texture, chemical and physical properties of the soil figure 6.2.

The main purpose of providing this routing structure is to link all sub-basins to one outlet points which can represent the whole basin; as a result all water generated by each sub-basin will be routed based on this routing structure to get aggregated flow at the outlet point of the whole basin. To check the accuracy of this routing structure a cross check against the real river network which was developed during sub-basins delineation procedure carried out. Now the remaining step is running of the whole model for calibration and validation procedure.

### 6.3 Model calibration and validation procedure at Abelti station

Model calibration needs the modification of model parameters value and comparison of predicted output of interest to measured data until a defined objective function is achieved. The objective function for model calibration generally consists of a statistical test, such as minimization of relative error, minimization of average error, or optimization of the Nash-Sutcliffe Coefficient (Santhi et al., 2001; Grizzetti et al., 2003). After achieving the objective function for calibration, validation of the model follows. Validation procedures are similar to calibration procedures in that predicted and measured values are compared to determine if the objective function is met. However, a dataset of measured watershed response selected for validation preferably must be different than the one used for model calibration, and the model parameters are not adjusted during validation (Kassa T. 2009). Prior to calibration of the model sensitivity analysis has been conducted. The results of sensitivity analysis will discuss during calibration of SWIM at Gibe III dam site for the time being this topic is skipped in order to avoid redundancy.

For model calibration, daily measurements of water discharge at Abelti station used in the period from 1985 to 2000 (16 years). One of the main reason selecting recent time period for model calibration was quality of flow and meteorological data sets. In general the collected hydrological and meteorological data sets from 1980 up to 2000 do not have any significant missed gaps, so this part of the data will be very convenient to use for model calibration procedure. The parameter estimation, routine PEST (Doherty, 2002) was applied to calibrate the simulated discharge. However, some manual tune up carried out to adjust some of the calibrated parameters. During parameter estimation using PEST different files like control, instruction and template files were developed. The full lists of all these files can be found at the appendix. The validation period has been taken from 1970 to 1981 (12 years). One of the big advantages of using long year's more than 10 years data for model calibration and validation procedure is to confirm the model stability in modeling of the physical processes in the basin.

#### 6.3.1 Performance evaluation of the model

The model performance efficiency criteria such as Nash–Sutcliffe model efficiency E (Nash and Sutcliffe, 1970) and the relative deviation in water balance (B) were used to evaluate the quality of simulated daily water discharge. The E value indicates the correlation between the observed and simulated values. If the E value is less than or close to zero, the model simulation is unacceptable or the simulation result doesn't represent or approach the observed values. The best value is 1, or the value of E should approach to 1. E is a measure to describe the squared differences between the observed and simulated values. And it can be related using the following equation.

$$E = \frac{\sum(Q_{obs} - Q_{sim})^2}{\sum(Q_{obs} - \bar{Q}_{obs})^2} \quad 6.3$$

Whereas B shows the long-term differences of the observed values against the simulated ones in percent for the whole modelling period, The percent deviation of stream flows (B) over a specified period with total days calculated from measured and simulated values of the quantity in each model time step is determined using the following equation:



$$B = \frac{\bar{Q}_{sim} - \bar{Q}_{obs}}{\bar{Q}_{obs}} * 100$$

6.4

Where:  $Q_{obs}$  is the observed discharge,  $Q_{sim}$  is the corresponding simulated values, whereas the variables  $\bar{Q}_{obs}$  and  $\bar{Q}_{sim}$  are the mean values of these parameter for the whole simulation period. A value close to 0% is best for B, this means that the overall difference between simulated and observed discharge is zero which is best result. A negative value indicates the model underestimates the result, and a positive value indicates the model produces (estimates more discharge than the observed value) which leads to overestimation.

### 6.3.2 Results and discussion on model calibration and validation

The calibration of SWIM model for Abelti flow station was carried out by comparing the simulated daily stream flows with the observed flow at the outlet of the flow measuring station. As a large number of parameters are involved for calibration purpose, the main calibration parameters were selected based on the sensitivity analysis. However, these sensitivity results have not shown for Abelti station in order to avoid redundancy, because we will discuss in detail regarding to this issue during SWIM setup at Gibe III dam site page 123. The selected parameters and calibrated values are depicted in the following table.

S No	Para	Description of calibration parameter	Calibrated values	Range
1	Thc	Evaporation correction factor	0.4	0 - 1
2	roc2	Routing coefficient to calculate storage time constant for the reach of surface flow	3	1-20
3	Roc4	Routing coefficient to calculate storage time constant for the reach of sub surface flow	13	1-60
4	sccor	Correction factor for saturated conductivity	1	0.1-5
5	bff	Base flow factor	0.6	0.2-1
6	gwq0	Initial ground water contribution to stream flow in mm/day	0.5	0.01-1
7	abf0	Alfa factor for ground water this parameter characterises the rate at which ground water flow is returned to the stream	0.5	0.01-1

Table 6.2 Calibrated parameters and their range for Abelti flow station

The statistics of the observed and SWIM simulated daily flows during calibration and validation results in terms of criteria of fit are presented in table 6.3. In the calibration period (1985 to 2000) 16 years, the Nash–Sutcliffe efficiency varies from 0.66 in the year 1995 to 0.91 in the year 1992, but the overall Nash–Sutcliffe efficiency was 0.83 and the deviation in overall water balance is not more than -1% during calibration period. In the validation (verification) period (1970 to 1981) 12 years, the Nash–Sutcliffe efficiency and the deviation of water balance gives 0.82 and 8% respectively.

Calibration period 1985 to 2000 total 16 years																	
Year	85	86	87	88	89	90	91	92	93	94	95	96	97	98	99	00	Total
E (%)	78	71	84	82	76	87	85	91	73	88	66	90	81	83	90	82	<b>83</b>
<b>Total water difference</b>																	<b>-1%</b>

Verification period 1970 to 1981 total 12 years													
Year	70	71	72	73	74	75	76	77	78	79	80	81	Total
E (%)	90	82	89	66	88	90	56	85	91	77	54	77	<b>82</b>
<b>Total water difference</b>													<b>8%</b>

Table 6.3 Calibration and verification results at Abelti flow station

According to the result depicted above the model efficiency during calibration show very good result throughout calibration period. For the period from January 1985 to December 2000 the best model efficiency obtained. In all years the model efficiency was greater than 0.75 except the year 1995, however the overall efficiency obtained during calibration period is 83% with -1% deviation of water balance which is a very good and satisfactory result for Abelti station. Similar model efficiency also obtained during validation period, however the model overestimates the simulated discharge in validation period a bit higher. The overall model efficiency during validation period was 0.82 and the total water deviation was 8%. The overestimation of the river discharge during validation period might be because of the temperature effect. This means that the model was calibrated for recent time period, a period which has slightly higher mean annual surface temperature than the validation or early period. This effect might lead less evapotranspiration during validation period and results higher runoff value. Generally these results indicate that SWIM can reproduce water discharge in Omo Gibe river basin quite well. The following figures show the comparison between daily and monthly simulated and observed river discharge at Abelti gauge station in the calibration period 1985–2000.

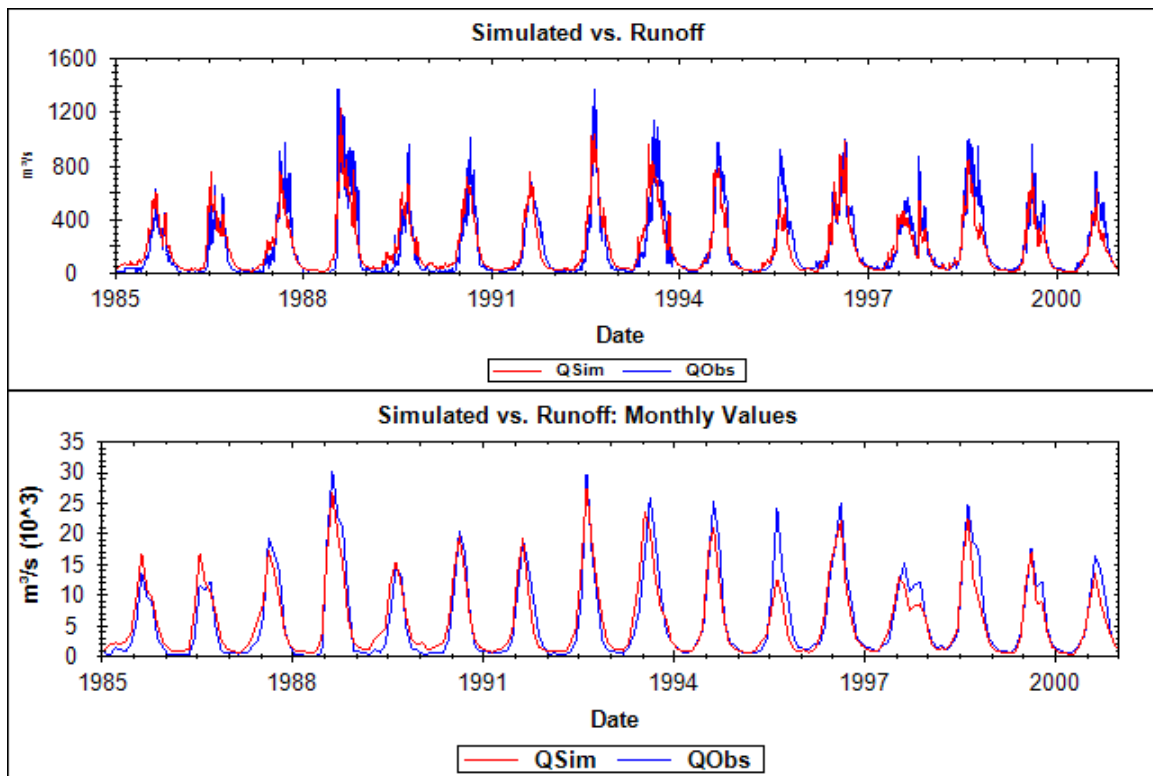


Figure 6.6 Graphical comparison of daily simulated and observed discharge upper panel, and monthly simulated and observed discharge lower panel during calibration period at Abelti



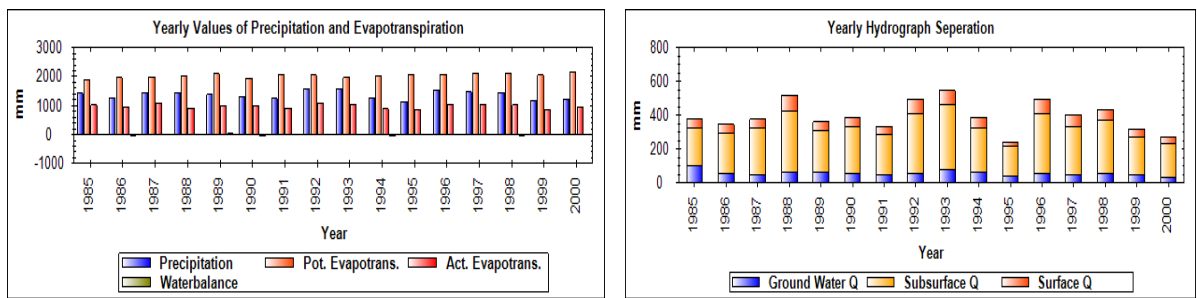


Figure 6.7 Yearly values of precipitation and evapotranspiration left panel and yearly hydrograph separation during calibration period at Abelti station right panel.

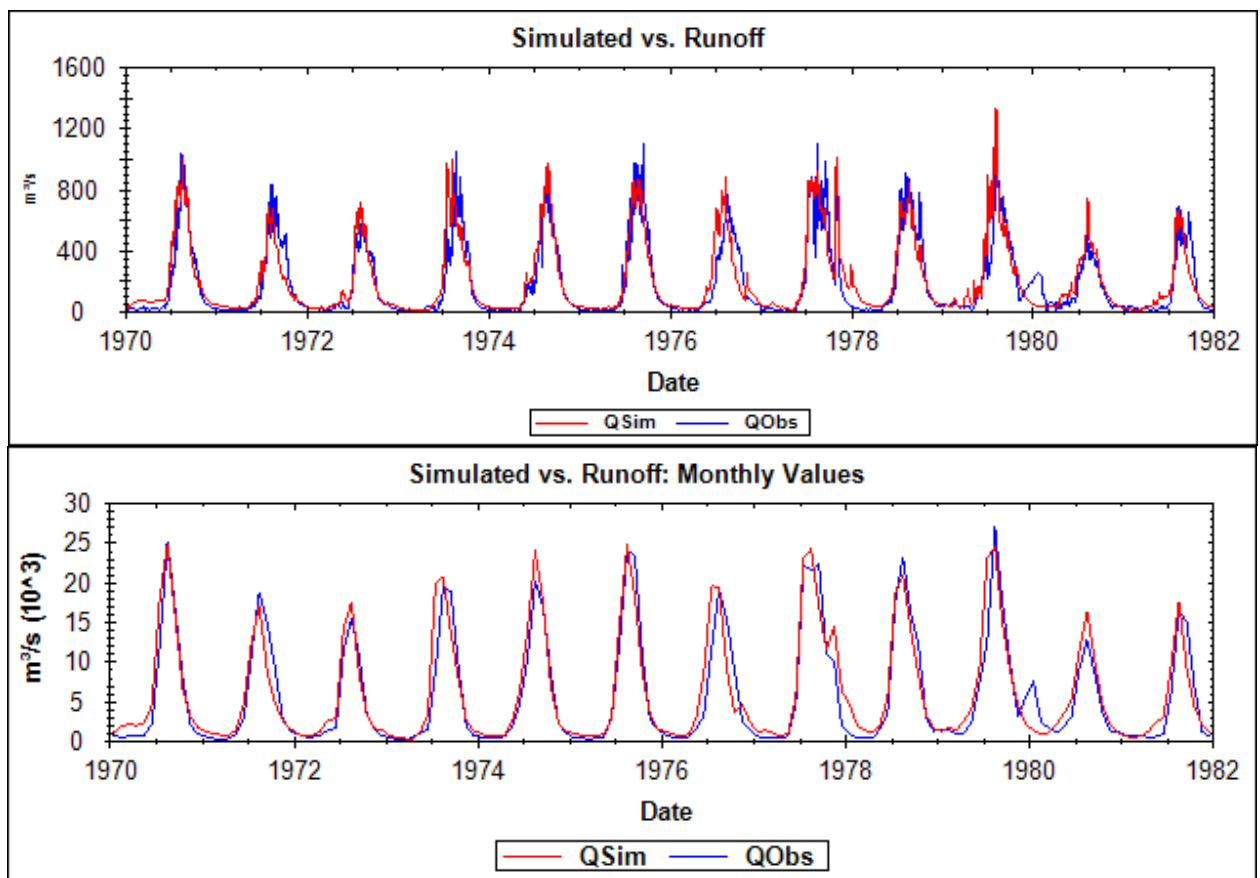


Figure 6.8 Graphical comparison of daily simulated and observed discharge upper panel, and monthly simulated and observed discharge lower panel during validation period at Abelti station.

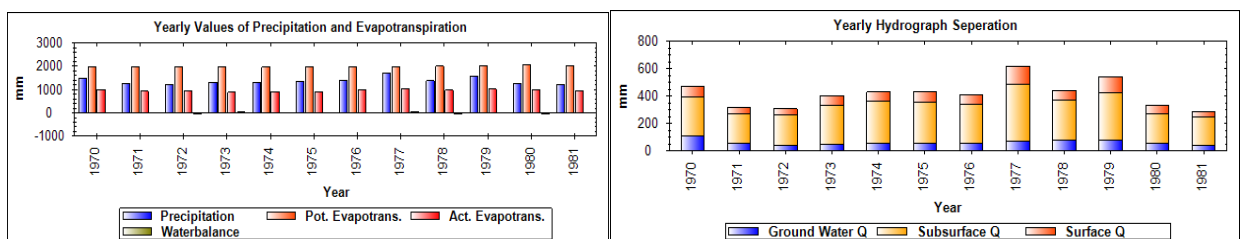


Figure 6.9 Yearly values of precipitation and evapotranspiration left panel and yearly hydrograph separation during validation period at Abelti station.

The plots of observed and simulated daily and monthly flows show that the results are well simulated in most of calibration years, except 1995 which underestimates the overall flow in this year. According to the model underprediction of 1995 year flow was mainly during high flow season; however, the performance of the model in producing the observed flow for most of calibration and validation period was remarkable and awesome. The various performances evaluation measures computed for the daily and monthly stream flows including with graphical comparison of observed and simulated flow in the calibration and validation periods are a means to confirm the behavior of the model to represent the physical processes in Omo Gibe basin. Moreover as one can see, from the above graphical comparisons in both cases the simulated river discharge is in a satisfactory agreement with the observed one, and the seasonal dynamics also well reproduced, high and low flows captured very well by the model which shows that the capability of the model in simulating the extreme events like high flow. This uniformity has already been observed by modeling of flow at Gibe III dam site (next chapter), this addresses the uncertainty involved in the simulations of the model is very low for Gibe basin.

The hydrograph pattern at the gauge Abelti is very typical for most of Ethiopian rivers, as precipitation concentrated in the northern part of the basin starting from June to September as a result there is higher water flow at this season, this dynamics or the seasonal flow pattern simulated by the model very well. This is one of the good conformations about SWIM model performance in Gibe basin.

#### **6.4 Application of SWIM for un-gauged basin**

This part of the study aimed to create a hydrological model for the catchment area of Omo basin at Un-gauged watershed, lying upstream Gibe III dam site, for the purpose of generating daily flow data by transferring the calibrated parameters from Abelti site to un-gauged part of the basin by keeping the assumptions that has been made before. The hydrology of Abelti basin was modelled quite well with satisfactory results and negligible overall water difference (-1%) by SWIM model during calibration. After calibration and validation of SWIM at Abelti flow station, the next step is estimation of daily flow by applying the art of SWIM modeling technique for un-gauged basin. Daily flows are generated at the outlet point of Gibe III dam site for this part of the basin, by transferring the calibrated parameter from Abelti to this basin. In addition to these, climatological data of 29 years, land use map, soil map and digital elevation model of un-gauged basin prepared separately to utilize as an input to the model. The procedure is the same like that of Abelti except the input data are different. Before running the model on un-gauged basin the following input data were prepared.

- ✓ Digital elevation model (DEM) of un-gauged basin which covers an area of 11,150 km<sup>2</sup> from SRTM data
- ✓ Land use and soil map. Soil data for this basin also prepared according to SWIM soil data base requirement.
- ✓ Preparation of climate data on the basin from 1970 to 1998 as an input to SWIM

After preparing the above raw data as an input to the model, using Mapwindow subdivision of un-gauged part of the basin in to reasonable sub-basins to get reasonable result carried out. And preprocess of SWIM carried out to interpolate the relational data (climate data sets) in to all sub-basin area, to calculate hydrotopes and routing structures independently. The outputs of the results displayed in the following figure.

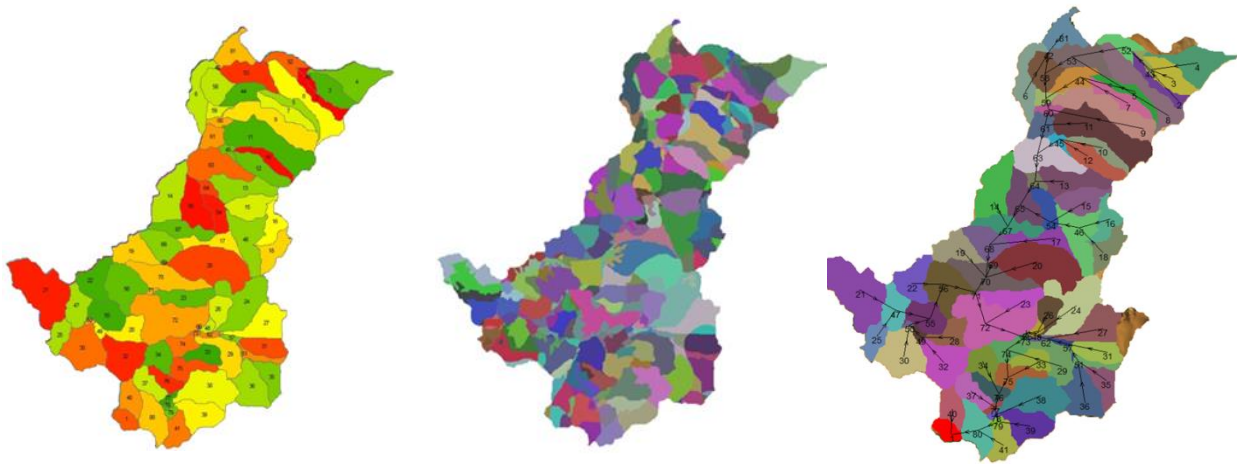


Figure 6.10 Calculated sub-basin, hydrotopes and routing structures of un-gauged basin

After preparing all the necessary input data for SWIM and using calibrated parameter at Abelti as calibrated input parameter for Un-gauged basin, daily flow at Gibe III dam site only for this basin was developed by running SWIM from 1970 to 1998. Consequently, 29 years daily flow data that represents the flow contributed from un-gauged part of the basin to Gibe III dam site estimated. The following figures show the plots of daily flows generated by SWIM for 29 years from this basin.

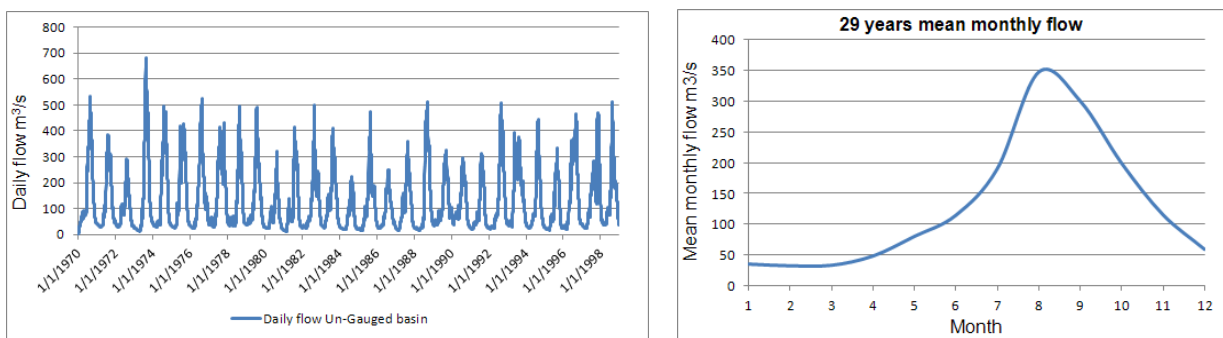


Figure 6.11 Generated daily and mean monthly flows from 1970 to 1998 from un-gauged basin

Month	Jan	Feb	Mar	Apr	May	Jun	Jul	Aug	Sep	Oct	Nov	Dec	Annual
Un-gauged	34.9	32.0	32.8	48.0	79.6	111.4	190.2	347.6	300.4	199.0	114.8	58.9	<b>129.1</b>

Table 6.4 Mean monthly flows contributed to Gibe III dam site from un-gauged part of the basin

The daily flow for this part of the basin has been determined using SWIM hydrological modeling. According to the result the mean annual flow contributed from this part of the catchment to Gibe III dam site is  $129.1\text{m}^3/\text{s}$  and it attains its peak discharge at  $347.6\text{m}^3/\text{s}$  in the month of August. This daily flow data set from this watershed is one of the most important data needed in combination with the other flow data to setup SWIM at Gibe III dam site to study effects of climate change. This flow generated by assuming some basic assumptions between Abelti and un-gauged basin. To strengthen our assumptions, the total mean annual runoff volume from these two catchments were compared to investigate how the flow pattern in both basins react with respect to some moving average results. The following figure depicts this idea.

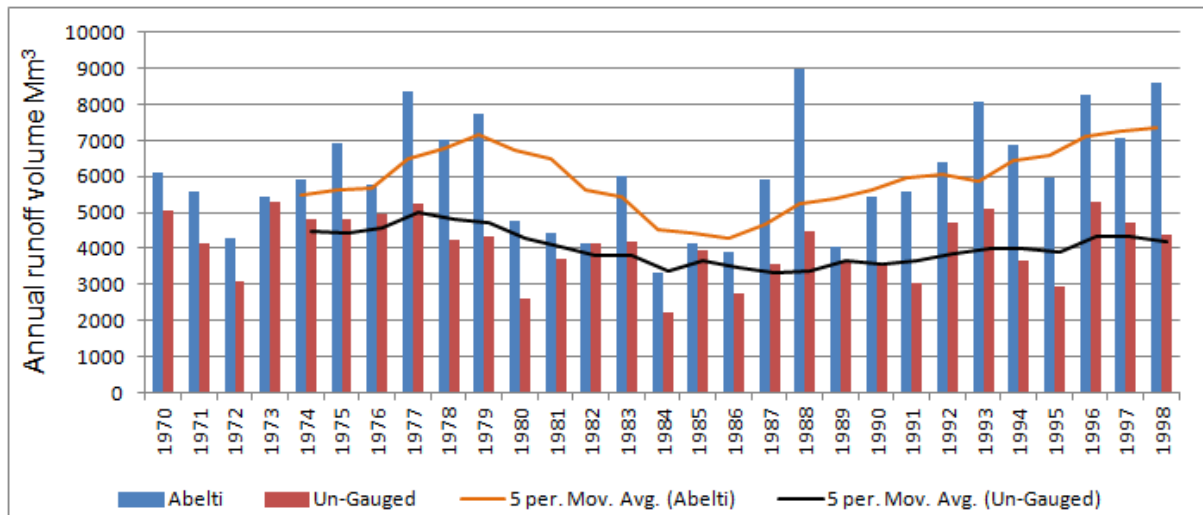


Figure 6.12 Mean annual runoff volume at Abelti and Un-gauged basin

The above figure revealed that these two basins have similarities in the results of five-year moving averages. The trend of five-year moving averages for both basins shows a reduction in flow up to the year 1986 for both cases, followed by an increasing trend starting from 1987 to 1998. This might be one testimony to strengthen the assumptions made before.

After getting the mean annual flows from daily estimated discharge from the un-gauged basin, the total flow at Gibe III dam site has been calculated by considering and summing up Abelti, Wabe, and OM19 mean annual flows at the dam site, and the final result obtained as 431.4 m<sup>3</sup>/s.

## 6.5 Validation of SWIM result for un-gauged basin

The approach employed above, based on a complete rainfall-runoff analysis which considers the hydrological cycle of studying basin at a daily time scale. Generating a time series of daily flows by considering full hydrological behavior of the catchment is expensive and time-consuming. It is clear that the outcome of such a method is continuous daily stream flows for un-gauged catchment, but there should be a means to confirm the outcome of such results' reliability. One of the validation procedures followed in this part of the study is comparison of mean annual discharge obtained in this method with the results obtained by employing other methodologies, which will be discussed in the following section. Therefore, it is logical in this context to investigate the possibilities of deriving daily time series representing daily flow regime of un-gauged part of the study area by considering complete physiographic characteristics of the catchment like slope, vegetation cover, drainage area, and soil.

### 6.5.1 Estimation of mean annual flow in the study area

Mean annual flow or mean annual discharge is defined as the arithmetic mean of all of the individual daily mean flows for a given water year at a specific site on a river. Direct calculation of mean annual flow in Omo Gibe basin, especially at Gibe III dam site, is not possible, because flow values are only recorded at Abelti and other small catchments above Abelti stream gauges, so that there is a need to estimate mean annual average flow on streams without gauges. Mean annual average flow is more difficult to estimate on un-gauged streams without having sufficient input data to local based generated empirical equations like drainage area relationship and rational formula. Regarding to Omo Gibe basin, most part of watershed which contributes flow to Gibe III dam site have gauges (measured flow data) using this gauged flow data an easy and reliable methods to estimate mean annual average flow on un-gauged basin was developed.

The following procedures are similar method that had been used during Gibe III dam design, however, for this particular study data pertaining to (1970-2000) employed. Mainly this mean annual flow computed for comparison and validation purpose with SWIM result.

## **6.5.2 Approaches used for estimation of mean annual flow**

As we know the approach for estimation mean annual flow for a point of interest or project reach along a river is dependent on the availability of streamflow data within the river reach. If a streamflow gage is available, then determination of mean annual flow is relatively easy. For reaches where no streamflow gage exists, the establishment of mean annual flow will be a bit complicated and require some effort to develop relationships with other hydrologic parameters such as drainage area. So far there are different methods to estimate average annual stream flow for sites where no stream flow data were collected, some of the well-known methods include:

- ✓ the drainage-area relationship,
- ✓ regional statistics using regression,
- ✓ and precipitation-runoff modeling.

This section presents methodologies for estimation the mean annual flow to be used in the analysis of surface water hydrology of Omo Gibe for comparison purpose. For this specific study drainage-area relationship and precipitation-runoff methods will be employed. The procedure of each method is described in the following section in detail.

### **6.5.2.1 Derivation of empirical relationship between flow and catchment size**

For the sake of comparison and validation purpose mean flow at Gibe III dam site (figure 6.1) were determined by assessing three basic methods that are capable of estimating mean annual flow at this site. Estimation of mean annual flow by using empirical relationship between flow and catchment size characteristics of un-gauged part of the study area is based on transferring or extrapolating information from gauged (upper part of the basin) to un-gauged sites. This is the most common method and it involves derivation of empirical relationships between flow and catchment characteristics.

Table 6.1 show that nearly 32.89 percent of Gibe III watershed is not gauged, this part of the watershed is mentioned as un-gauged. To determine mean annual flow at this un-gauged site, it will be necessary to collect direct streamflow measurements and establish relationships with other hydrologic parameters. To accomplish this objective streamflow data are collected as mean daily values from 67.11 percent of the catchment area upstream of Gibe III dam site. Eventhough it is possible to get daily flow data from more than 67 percent of the watershed area most of them measured flow from small catchments except Abelti. Moreover there is no any flow measuring stations near to gibe III dam site or nearby, because of this it is not possible to estimate the mean runoff at Gibe III dam site directly. In addition to main flow measuring stations, measured flow from small catchments especially upstream of Abelti were collected. The description of these catchments depicted in table 6.5 and their location can be accessed from figure 5.2.

A reasonable estimate of mean annual flow can be developed by establishing mathematical relationships of these measured flows with other hydrologic parameters such as drainage basin area, most often in different literatures these mathematical relationship using basin characteristics are referred to as “regional curves”. To develop this regional curve for Omo Gibe basin the following flow measuring stations were used.

S No	Station Name	Area km <sup>2</sup>	Q (m <sup>3</sup> /s)	calculated specific q (l/s km <sup>2</sup> )
1	Gibe river nr. Abelti	15690	190.4	11.495
2	Gojeb river at Dam site	5188	84.8	16.549
3	Gojeb river nr Shebe	3577	59.0	16.494
4	Gilgel gibe nr. Asendabo	2966	36.9	12.717
5	Wabi nr. Wolkite	1873	27.1	14.523
6	Gibe river nr. Limu Genet	533	10.8	20.300
7	Rebu river nr. Wolkite	480	3.2	6.645
8	Megecha nr. Gubrie	286	3.5	12.413
9	Gibe river nr. Seka	280	3.7	13.214
10	Gohgeber river nr. Endibir	109	1.6	8.684
11	Bidru awana nr. Sekoru	41	0.5	12.683

Table 6.5 Flow measuring stations used to establish area discharge relationship

The mean annual discharges for above stations have been calculated from 31 years (1970-2000) observed daily flows, except Limu Genet, Seka and Sekoru. As noted in table 6.5, mean annual flow in Omo Gibe basin varies proportionally with drainage area. As such, a regional regression curve for mean annual flow as a function of drainage area is the good option and an easy approach to establish this relationship at the studying area. This can be accomplished by defining a regression equation for measured mean annual flows versus drainage areas from data at streamflow gages in the basin. Two Inputs are necessary to develop the regression equation mean annual streamflow and drainage area. One of the data that should be readily available to develop this regression equation is the area of the watershed where flow measurement is taking place. Therefore, the drainage basin of smaller catchment size less than 5,000km<sup>2</sup> delineated from the SRTM data set of 90m resolution using Arcmap. For larger area 200m resolution SRTM data employed.

As it was mentioned in the previous discussion direct estimation of mean annual flow at Gibe III dam site impossible, but it is possible to determine the mean annual runoff indirectly by creating a relationship between the above listed discharge and their drainage area by defining regression relationship (empirical equation). The regression relationship for hydrologic data was assumed to be logarithmic and the selected gauged sites assumed to be located within the same hydrophysiographic region as the un-gauged site under consideration. Initially an empirical equation has been derived by relating observed mean annual discharge listed in table 6.5 and catchment size, and then this equation being used to estimate mean annual flow generated from un-gauged part of the basin. It should be pointed out that mean annual runoff determined using this method gives to this procedure certain robustness as cautions has been taken during estimation of drainage area and associated input data sets.

The ultimate aim of this section was to develop area discharge relationship in the form of equation 6.5 for estimation of mean annual streamflow generated from un-gauged part of the basin, as a result a unique regression equation developed (equation 6.6) for this region. Additionally the performance of this equation was checked against independent data in the basin.

A relationship between mean annual flows and catchment area size can be expressed as

$$Q = jA^c \quad 6.5$$

Where Q is in this case the mean annual runoff, j and c are constants derived by fitting a regression line to the available data between mean runoff and area. The constant c represents the rate at which discharge (Q) increases downstream when compared to drainage area (A) It is

often assumed that the scaling between discharge and drainage area is linear ( $c \sim 1$ ) (Joschua C., 2009). According to (Chow V.T., 1964, Handbook of Applied Hydrology, McGraw-Hill) the exponent  $c$  falls between 0.5 and 1.1. Accordingly observed discharge and catchment area at the study area were related to derive the values of coefficients in equation 6.5. Based on this procedure the following equation was obtained by assuming linear relationship between discharge and catchment area.

$$Q = 0.0119 * A^1 \tag{6.6}$$

Where  $Q$  is mean annual runoff in  $m^3/s$  and  $A$  is drainage area in  $km^2$

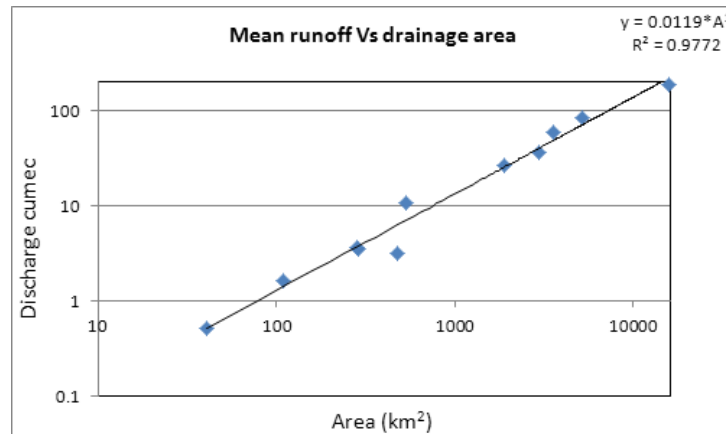


Figure 6.13 Curve of mean annual runoff vs. drainage area for studying basin

The above general law as illustrated with  $R^2$  fits very well and the result is acceptable with the available data. And some experiments (checkup) carried out to check the efficiency of the above empirical equation in estimating of mean annual discharge in the study basin for known value. The experiment carried out as a validation of the above equation for catchment area which was not involved during the derivation of the equation. To examine this procedure calculation of the design discharge at Gilgel gibe I hydropower project using this equation carried out, this catchment is found inside Abelti watershed. There by it showed good agreement with a design discharge of Gilgel Gibe I hydropower project. According to the design document of Gilgel Gibe I hydropower project (ENEL 1998) the design discharge at Deneba (dam site) was  $50.4 m^3/s$ . And according to the above derived empirical equation is as follow. To calculate Gilgel Gibe I design discharge using the above equation the area for Gibe I hydropower site used ( $A=4225km^2$ ) as an input to the equation. There by:

$$Q_{design\ at\ Gibe\ I} = 0.0119 * A_{at\ Deneba}$$

$$Q_{design\ at\ Gibe\ I} = 0.0119 * 4225km^2 = 50.3 \frac{m^3}{s}$$

Which is a reliable result; because this value approaches the design discharge during design of Gibe I hydropower project  $50.4 m^3/s$ . Based on the above  $Q$  and  $A$  relation it is possible to calculate the mean discharge contributed to Gibe III dam site from un-gauged catchment and then this mean discharge value will be added with the rest of the mean discharge contributed form Abelti, Wabe and OM19 to get total discharge at Gibe III dam site from all flow contributing area.

Mean annual flow from un-gauged part of the basin using equation 6.6 calculated as follow. The watershed area for un-gauged catchment is  $11,150 km^2$  and mean discharge contributed from this catchment to Gibe III dam site:



$$Q_{\text{un-gauged}} = 0.0119 * 11150 \text{ km}^2 = 132.6 \text{ m}^3/\text{s}.$$

Now it is possible to add all mean discharge contributed from upper catchment to Gibe III dam site.

S No	Stations name	Area km <sup>2</sup>	Q (m <sup>3</sup> /s) calculated
1	Gibe river at. Abelti	15690	190.4
2	Goj. river at Dam site OM19	5188	84.8
3	Wabi nr. Wolkite	1873	27.1
4	Un-gaged area	11150	132.6
<b>Total mean annual flow at Gibe III</b>		<b>33,901</b>	<b>434.9</b>

Table 6.6 Mean discharge contribution from four catchments to Gibe III dam site

Based on A and Q relationship the total mean annual flow at Gibe III dam site found as **434.9m<sup>3</sup>/s**. And the amount of mean annual discharge contributed from un-gauged part of the basin calculated as 132.6m<sup>3</sup>/s. This mean flow cannot be used as an input to SWIM model, but it can be used as a guide line or a means of validation and comparison for daily flow data which has been estimated using SWIM rainfall runoff methodology.

### 6.5.2.2 Rational method

This method is based on the rational formula. It is a widely used technique in engineering hydrology to determine mean flow. For this specific study the mean flow determined using this method can be used as a comparison purpose which was calculated previously by discharge area relationship and SWIM modeling technique.

In order to employ this method three watershed areas, Gibe River at Abelti, Wabe River at Wolkite and Gojeb River at OM19 (figure 6.1) have been used, because in one way or other these three basins have common characteristics with un-gauged part of the basin, for example they have common boundary or watershed divide. This procedure is based on determination of runoff coefficient for flow measuring stations at Abelti, Wabe and OM19 using the ratio of discharge to areal rainfall amount; and decentralizing these runoff coefficients to un-gauged part of the basin. Runoff coefficients of three of these sub-basins have been determined from hydrologic and climatologic (areal rainfall of each sub-basins) investigations by dividing of the flow generated in a sub-basin to the sub-basin areal rainfall. The runoff coefficient (C) is a dimensionless coefficient relating the amount of runoff to the amount of precipitation received. It is a larger value for areas with low infiltration and high runoff (pavement, steep gradient), and lower for permeable, well vegetated areas like forest and flat land. As a good advantage of the available rainfall gauging stations see figure 6.14 though out the basin above Gibe III dam site it is possible to calculate runoff coefficients at a place where measured flows obtained. Therefore using this method runoff coefficients at Abelti, Wabe and OM19 flow measuring stations have been calculated; and comparisons of these runoff coefficients has been carried out and the least runoff coefficient was selected based on reasonable assumption that was made between un-gauged part of the basin and the selected basin that represents its runoff coefficient to un-gauged basin.

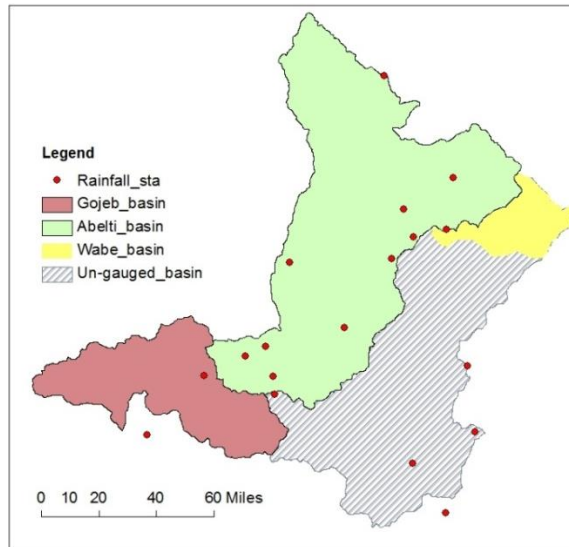


Figure 6.14 Main catchment areas of Gibe III dam site and rainfall gauging stations

Selection of the run-off coefficient 'C' to un-gauged part of the basin relies partly on knowledge of physiographic conditions, engineering judgment and personal experience. It also depends on the rainfall intensity received by the corresponding catchment and the land use pattern. To apply this procedure attention has been given to determine the spatial variability of precipitation (areal depths of rainfall) across each sub-basins using Thiessen polygons method. In order to achieve accurate estimation of the spatial distribution of rainfall the Thiessen polygon method was considered because this method is the most important in engineering praxis especially in engineering hydrology. This method assigns weight at each gauge station in proportion to the catchment area that is closest to that gauge. Station weights are scalar factors used to transform point precipitation observed at this rainfall gauging stations into an associated mean precipitation over an area that the station data are assumed to represent.

Depending on station locations and local climate patterns eighteen rainfall gauging stations with 27 to 31 years measured daily rainfall data used for this approach. Mean monthly and mean yearly spatial rainfall calculated for Abelti, Wabe, un-gaged and OM19 at Gojeb river sub-catchments above Gibe III dam, moreover areal rainfall for all Gibe III catchment also determined. And determination of mean runoff coefficients for each flow measuring stations carried out by taking the ratio of mean annual discharge at the point of interest to spatial rainfall value of corresponding sub-catchment. Finally estimation of mean annual flow for the site in question and the dam site performed.

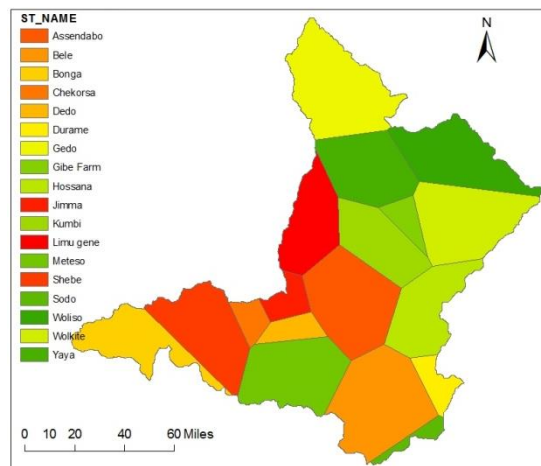


Figure 6.15 Thiessen polygons for Gibe III dam site

S No	Basin Name	Jan	Feb	Mar	Apr	May	Jun	July	Aug	Oct	Nov	Dec	mm/month	mm/year
1	Gibe Abelti	25.4	36.9	72.9	94.9	145.8	197.0	246.2	230.5	81.1	27.0	21.0	110.6	<b>1327.6</b>
2	Wabi Wolkite	21.5	41.3	72.8	94.4	123.9	191.5	289.7	259.0	50.2	14.8	9.4	109.4	<b>1312.5</b>
3	Un-gaug. basin	30.9	46.9	88.6	124.1	149.2	172.0	211.8	207.9	85.6	32.4	21.2	109.6	<b>1315.2</b>
4	Gojeb OM19	46.4	62.1	114.8	158.7	216.7	218.6	227.1	236.4	134.0	73.9	43.7	143.8	<b>1725.6</b>
5	Gibe III dam site	30.4	44.3	84.6	114.4	157.1	192.1	234.3	225.6	89.3	35.7	24.2	115.5	<b>1386.1</b>

Table 6.7 Mean areal rainfall rate in mm/year for catchments of hydrometric stations

Table 6.7 shows the mean annual and mean monthly rainfall, western part of the catchment exhibited higher mean annual areal rainfall which is 1725.6 mm/year Abelti 1327.6, Wabe 1312.5, Un-gauged part 1315.2 and total basin 1386.1 mm/ year. Abelti and Un-gauged part of the basin have comparable mean annual areal rainfall values.

Based on the available information runoff coefficients for three basic hydrometric stations was calculated using rational formula by taking the ratio of discharge to areal rainfall value.

$$C = \frac{Q_{\text{annual mean}}}{P_{\text{areal}}} \quad 6.7$$

Where C is runoff coefficient;  $Q_{\text{annual mean}}$  mean annual runoff rate at the point of interest and  $P_{\text{areal}}$  areal precipitation value obtained at the sub-watershed area.

And the results have shown in the following table.

S No	Basin Name	Runoff			Rainfall			c
		m3/s	Mm3/year	mm/year	m3/s	Mm3/year	mm/year	
1	Gibe Abelti	190.4	6008	383	663	20904	1327.6	0.287
5	Wabi Wolkite	27.1	855	456.6	78	2449	1312.5	0.347
13	Gojeb River OM19	84.8	2676	516	291	9190	1725.6	0.291

Table 6.8 Runoff coefficients for hydrometric stations upstream of gibe III dam site.

In order to determine runoff coefficient for un-gauged part of the basin which is lactated downstream of Abelti, Wabi and Gojeb dam site a simple assumption was carried out based on the available information. The runoff coefficient for Abelti calculated as 0.287, Wabi 0.347 and Gojeb River at OM19 0.291 presented for selection and comparison. By assuming the un-gauged part of the basin has the lowest runoff coefficient from the above calculated value Abelti's runoff coefficient was selected for un-gauged part as 0.287. Moreover this assumption can be supported by similar climatological characteristics of Abelti and un-gauged basin. Which means that the mean areal rainfall in Abelti basin is 1328mm/year where as the mean areal rainfall for un-gauged part of the basin is 1316mm/year these values are more or less the same, which indicates that these basins are homogenous with regard to climate. Additionally, based on the land use map of the basin the vegetation cover of Abelti is more or less homogeneous with Un-gauged part of the basin this characterizes evapotranspiration which influences the runoff coefficient.

The next step is calculating of mean annual runoff generated from this un-gauged basin as a function of the above selected runoff coefficient, spatial rainfall and drainage area corresponding to this basin using rational formula. The following genera equation employed to calculate the value.

$$Q = \left( \frac{1}{31557.6} \right) * ciA \quad 6.8$$

Where  $\frac{1}{31557.6}$  is conversion factor for discharge in to m<sup>3</sup>/s

C is runoff coefficient = 0.287

i is spatial rainfall depth in mm/year for un-gauged part of the basin = 1315.2 mm/year

A is drainage area for un-gauged catchment in km<sup>2</sup> equal to 11,150 km<sup>2</sup>

According to equation 6.8 the following result obtained

S No	Basin Name	c	Rainfall in mm/year	Area km <sup>2</sup>	Runoff m <sup>3</sup> /s
1	Un-gauged catchment	0.287	1315.2	11,150	<b>129.2</b>

The mean annual runoff determined with this method more or less similar with the one determined with the first method for un-gauged part of the basin. Initially it was determined as **132.6** m<sup>3</sup>/s this value obtained by using Q and A relationship. With rainfall runoff (rational) method we have calculated as **129.2**m<sup>3</sup>/s. Even though these values have small discrepancy it is not significant, so that it is possible to ignore the discrepancies between these results. At this stage of the result it is possible to confirm that the mean annual runoff contributed from un-gauged part of the basin to Gibe III dam site is nearly 130m<sup>3</sup>/s.

The overall mean annual discharge at Gibe III dam site will be the summation of discharge from Abelti, Wabi, OM19 and un-gauged basin. Therefore the summation of all discharges will be as follow.

S No	Basin Name	Remark	Runoff m3/s
1	Un-gauged catchment	Calculated using cia formula	129.2
2	Gibe Abelti	Measured discharge at Abelti	190.4
3	Wabi Wolkite	Measured discharge at Wolkite	27.1
4	Gojeb Shebe OM19	Measured discharge at OM19 dam site	84.8
<b>Total discharge at Gibe III dam site= QAbelti+Qwabe+QOM19+Qungauged</b>			<b>431.5</b>

Table 6.9 Calculated mean annual discharge at Gibe III dam site using rational method

Using rational method the calculated mean annual runoff at Gibe III dam site is **431.5** m<sup>3</sup>/s, when we compare this value with the previous total mean annual flow which was calculated using Q/A relation **434.9** m<sup>3</sup>/s more or less they are similar, the above two methods which was employed to calculate mean annual discharge at Gibe III dam site gave comparably the same results, therefore both methods are robust in estimating mean annual flow at the site of interest.

As a means of final check runoff coefficient for entire basin (at Gibe III outlet) calculated based the following general weighted formula:

$$C_{total} = \frac{[(C_{Abelti} * A_{Abelti}) + (C_{OM19} * A_{OM19}) + (C_{Ungu} * A_{Ungu}) + (C_{Wabe} * A_{Wabe})]}{A_{GibeIII(Total)}} \quad 6.9$$

Where  $C_{total}$  is total runoff coefficient for Gibe III catchment and it was found as 0.2909. Now we have to substitute all known variables to rational formula to calculate total mean annual flow at Gibe III dam site.

S No	Basin Name	C
1	Gibe Abelti	0.287
2	Wabi Wolkite	0.347
3	Gojeb Shebe OM19	0.291
4	Un-gauged	0.287
<b><math>C_{Total}</math> At Gibe III dam site</b>		<b>0.2909</b>

Table 6.10 Runoff coefficients for Abelti, Wolkite, Un-gauged and Gibe III dam site

Since spatial depth of precipitation calculated previously for Gibe III catchment, now it is possible to calculate the overall discharge generated from the entire watershed area by using rational equation and the following result obtained.

S No	Basin Name	c	Rain fall in mm/year	Area km <sup>2</sup>	Runoff m <sup>3</sup> /s
1	Total Basin (Gibe III dam site)	0.2909	1386.0	33901	<b>436.2</b>

By considering the total runoff coefficient at Gibe III dam site and spatial rainfall value over total area, mean annual runoff generated from gibe III dam site was **436.2m<sup>3</sup>/s**.

As a means of conformation and validation the mean annual flow from un-gauged basin and Gibe III dam site were compared with the results that have been computed by using A/Q relation, rational formula and SWIM result. Initially mean annual flow from Un-gauged basin estimated by SWIM as 129.1m<sup>3</sup>/s, the corresponding total mean annual flow at Gibe III dam site was 431.4m<sup>3</sup>/s. The previous results, using area discharge relationship the calculated mean annual flow contributed from un-gaged part of the basin was 132.6m<sup>3</sup>/s and the total flow at Gibe III dam site was 434.9m<sup>3</sup>/s. likewise, the rational formula results were 129.2m<sup>3</sup>/s for un-gauged basin and 431.5m<sup>3</sup>/s for Gibe III dam site.

The mean annual flow generated using SWIM hydrological modeling is a convincing result which is more or less similar to the previous results. The following table shows the results summary from all the methods.

	Mean annual flow	
	Un-gauged basin m <sup>3</sup> /s	Total flow at Gibe III dam site m <sup>3</sup> /s
Q/A relation	132.6	434.9
Rational method	129.2	431.5
SWIM modeling	129.1	431.4

Table 6.11 Comparisons of mean annual flows generated from un-gauged and Gibe III dam site computed from three methods

Based on the above table the total mean annual flows at Gibe III dam site has been adapted as 431.4m<sup>3</sup>/s for climate change study before routing. The final SWIM result for un-gauged basin has been taken or considered for further SWIM simulation since this flow is generated from daily flow data and cross checked the reliability of the result with the other methods. The comparison result showed that this flow determined with greater accuracy and negligible discrepancy.

## 6.6 Conclusion

A semi distributed process based hydrological model employed and calibrated at Abelti flow station for the purpose of deriving daily flows data from un-gauged basin by assuming reasonable assumptions between these basins. Then, the hydrology components of SWIM model was calibrated and validated against the observed data at Abelti flow station collected at the watershed outlet. During simulation process quite reasonable result was found throughout calibration period at Abelti. On the other hand, calibration and validation of SWIM has shown that the predicted values have agreed well with the observed data at the outlet of the watershed. This was proved by the performance of the model Nash–Sutcliffe efficiency and total water difference produced by the model. Accordingly, the Nash–Sutcliffe efficiency during calibration period was 0.83 with negligible total water difference of -1%, similar performance was observed during validation period of the model by producing Nash–Sutcliffe efficiency of 0.82 and 8% total water difference. As one can see from these results the efficiency of the model was nearly the same during calibration and validation. This can be taken as the stability of the model for Gibe basin.

As a result, all calibrated parameter obtained from Ableti directly transferred to un-gauged basin. Consequently, for the first time 29 years (1970 to 1998) daily flow data set has been generated from un-gauged part of the basin at the outlet point of gibe III dam site. According to obtained result the mean annual runoff generated from this basin was  $129.1\text{m}^3/\text{s}$ . The generated daily flow was compared with different mean annual flows calculated for un-gauged part of the basin using different methods to cross check the reliability of this generated daily flow data from SWIM modeling technique.

Moreover, different common approaches for estimating mean annual runoff at Un-gauged and Gibe III dam site has been explored. The first approach to estimate mean annual flow from un-gauged basin is based on extrapolation of flow records from gauged sites to un-gauged site the so called area discharge relation. Another approach that has been used for estimating mean annual flow of un-gauged and Gibe III catchments is the use of rainfall-runoff models which is called as rational method whose parameters like runoff coefficient have been decentralized to un-gauged part of the basin. According to the results mean annual flow from un-gauged watershed which have been estimated using two approaches are  $132.6\text{m}^3/\text{s}$  and  $129.2\text{m}^3/\text{s}$  respectively. The main purpose of computing mean discharge by using different approach for un-gauged catchment was to have an idea how much amount of flow generated from this part of the basin and to compare the results of mean flow estimated by SWIM hydrological model.

Due to the different approach used to compute mean discharge at un-gauged catchment it was expected that the results of the computation won't be exactly the same, but results given by all methods are comparably similar. Not only for un-gaged catchment but also mean annual flow at Gibe III dam site has been computed with these approaches by summing up the mean flows contributed from each watersheds to provide the overall picture for current water resources potential of the basin.

Fortunately, all the methods estimated more or less similar results and the SWIM result has been taken to study climate change at Gibe III dam site since this flow determined from daily flow data set.

## Chapter 7 Application of SWIM at Gibe III Basin

### 7.1 Introduction

The other objective of this research is to set up SWIM rainfall runoff modeling at Omo Gibe III dam site for climate change study, after having daily flow input at Gibe III dam which can substitute observed discharge for reference time period. In the preceding two chapters different and reliable procedures have been implemented to calculate mean annual and daily flow in Omo Gibe basin. However, the results were not aggregated to the site of interest. The collected measured flows are found at different outlet point of Wabe, Abelti and OM19 flow measuring stations. Moreover, the estimated daily flows data from un-gauged part of the basin was at the outlet point of Gibe III dam site, because of this all these flows should bring together to represent historical inflow at Gibe III dam site using reach routing technique.

### 7.2 Flow routing in Omo Gibe basin

Flood routing is the process of modeling a flood wave to understand what it will do at various points along a river course. Reach flood routing is a mathematical method for predicting the changing magnitude and celerity of a flood wave as it propagates down rivers. Generally, two basic methods are used to route the flood wave in natural channels, one based on hydrologic routing and the other on hydraulic routing. The hydrologic method is based on the storage continuity equation, while the hydraulic method is based on the Saint-Venant equations consisting of the continuity and momentum equations (Choudhury et al. 2002).

For the purpose of getting daily flows at Gibe III dam site the basin divided in to the following four flow contributing catchments based on the availability of recorded and estimated daily data from un-gauged basin.

- ✓ Abelti catchment with flow contributing area of 15,690 km<sup>2</sup>
- ✓ Wabe catchment with flow contributing area of 1,873km<sup>2</sup>
- ✓ Gojeb catchment (proposed dam site on Gojeb river) with flow contributing area of 5,188km<sup>2</sup>
- ✓ Un-gauged catchment with flow contribution area of 11,150km<sup>2</sup>, this flow has been determined using SWIM,

The watershed areas of the basin have been delineated based on the SRTM data of the basin using ArcMap. Accordingly their areas which contribute flow to Gibe III dam site have been calculated. The flow of Wabe River is measured in Wolkite. The Gilgel Gibe River is the most important tributary, draining mainly cultivated lands from the south west. The flow of this river is measured at Abelti flow measuring station together with other upstream part of the catchment. Going downstream another important tributary is found from the west, the Gojeb River. Daily measured flows from the above mentioned stations collected from MoWEE. Whereas the daily flow from un-gauged catchment has been calculated using rainfall runoff modeling using SWIM.

Since the distances of flow measuring stations of Abelti, OM19 and Wabi are far away from Gibe III dam site it was not possible to add the values of these flows with the output of un-gauged basin. To account the magnitude and celerity of a flood wave as it propagates down rivers reach flow routing technique has been incorporated.



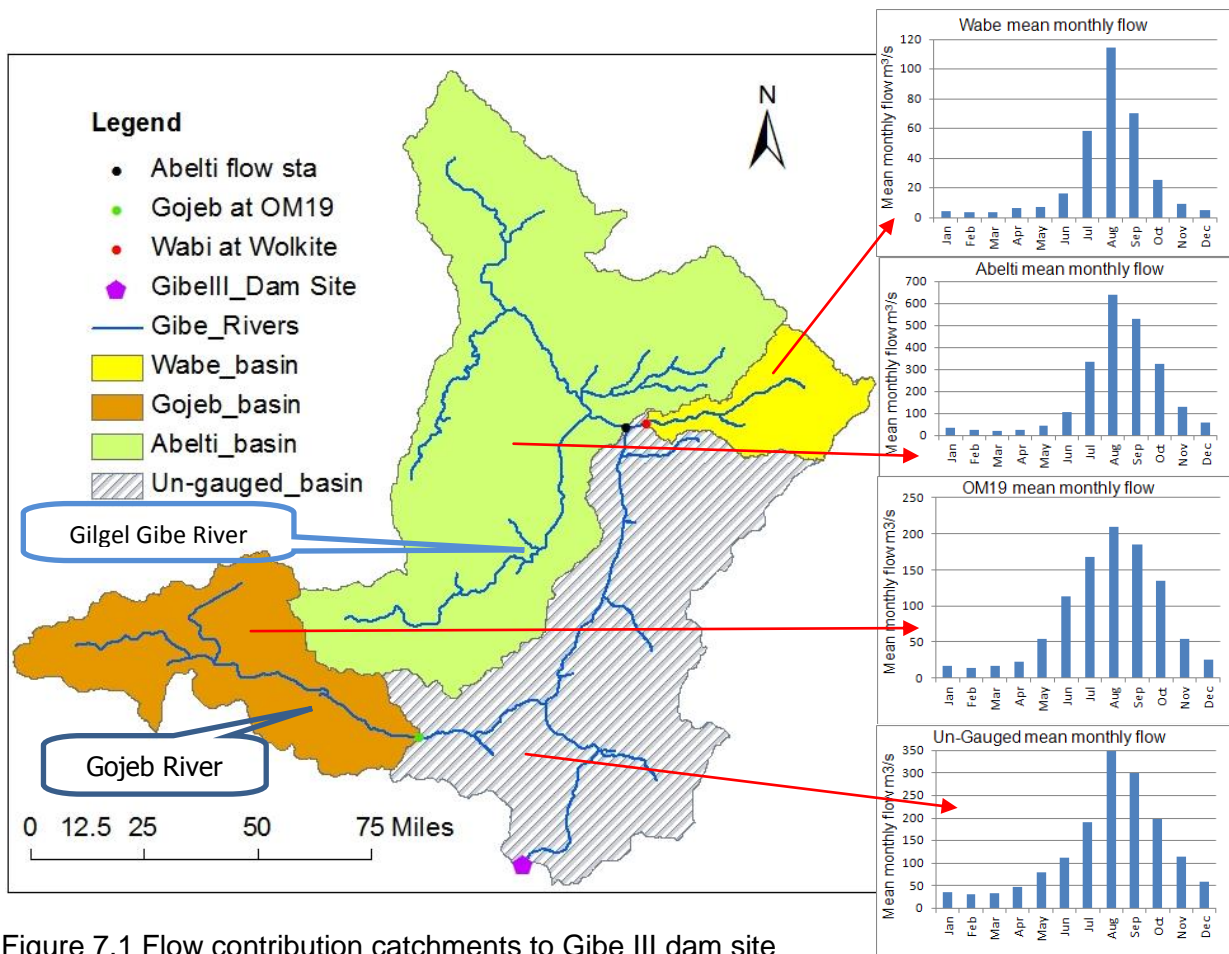


Figure 7.1 Flow contribution catchments to Gibe III dam site

Many different simplified routing models were developed recently and so many years ago. Some of this routing technique was applied successfully for routing of flood in river. The Muskingum method (McCarthy, 1938) is widely accepted and used in flood routing models due to its adequate levels of accuracy. Because of this Muskingum routing method selected to route the flow from Abelti, Wabi and OM19 to Gibe III dam site. As it is well known, the Muskingum model needs different parameter for routing. These parameters are wave travel time  $K$  and weight coefficient of discharge  $X$  so that before routing, these parameters should be determined.

According to Schulze (Schulze, 1995) for a given reach, the continuity equation can be expressed as

$$\frac{d(\text{stor})}{dt} = Q_{in}(t) - Q_{out}(t) \tag{7.1}$$

Where  $\frac{d(\text{stor})}{dt}$  Is the rate of change of storage within the reach ( $m^3/s$ )

$Q_{in}(t)$  Is the inflow rate ( $m^3/s$ )

$Q_{out}(t)$  Is out flow rate ( $m^3/s$ )

The Muskingum method assumes a variable discharge storage equation

$$\text{stor}(t) = K * [X * Q_{in}(t) + (1 - X) * Q_{out}(t)] \tag{7.2}$$

Where  $\text{stor}(t)$  the storage  $m^3$  in a river reach at time  $t$

$K$  is the storage time constant for the reach (s),

and  $X$  is the dimensionless weighting factor in river reach routing.

Here K is the ratio of storage to discharge and has the dimension of time. In physical terms, K is considered to be an average reach travel time for a flood wave, and X indicates the relative importance of the input  $Q_{IN}$  and outflow  $Q_{OUT}$  in determining the storage in a reach.

Thus, from equation 8.2 the change in storage over time  $\Delta t$  is given as

$$\begin{aligned} Stor(t + 1) - Stor(t) &= K[X * Qin(t + 1) + (1 - X) * Qout(t + 1)] \\ &\quad - K[X * Qin(t) + (1 - X) * Qout(t)] \end{aligned} \quad 7.3$$

The general form of Muskingum equation can be give as

$$Qout(t + 1) = C_1 * Qin(t + 1) + C_2 * Qin(t) + C_3 * Qout(t) \quad 7.4$$

Where the parameters  $C_1$ ,  $C_2$  and  $C_3$  are determined as

$$C_1 = \frac{-K * X + 0.5 * \Delta t}{K - K * X + 0.5 * \Delta t} \quad 7.5$$

$$C_2 = \frac{K * X + 0.5 * \Delta t}{K - K * X + 0.5 * \Delta t} \quad 7.6$$

$$C_3 = \frac{K - K * X - 0.5 * \Delta t}{K - K * X + 0.5 * \Delta t} \quad 7.7$$

Here K and  $\Delta t$  must have the same time units and the three coefficients  $C_1$ ,  $C_2$  and  $C_3$  should give a sum of 1. Numerical stability is attained and the computation of negative outflows is Avoided if the following condition is fulfilled

$$2 * K * X < \Delta t < 2 * K * (1 - X)$$

Prior to routing in Omo Gibe basin determination of routing parameter K and X are important which are used as an input to Muskingum routing equation. These parameters can be derived from the relevant morphologic parameters of the watershed. For these purpose River length, slope and area of the watershed determined from digital elevation model of the basin using ArcGis.

Catchment	Area	Mean water course velocity		
		$L_1$	$L_2$	Mean $V^*$
	$Km^2$	Km	km	m/s
Abelti	15,690	1km	208km	0.73
Om19	5,188	54km	89km	0.81
Un-gauged	11,150		208km	0.49
Wabi	1,873	8km	207km	1.16

Note: \* indicates that the data available from the hydrologic reports of basic design of Gibe III dam

Table 7.1 Watershed parameters of Gibe III basin

As it is possible to see from the above table the main water course length is divided in two parts as  $L_1$  and  $L_2$  where  $L_1$  indicates the length of the river on the sub watershed, whereas  $L_2$  indicates the river which travel through the main water course of un-gauged catchment. Division of the river length in this way helps to calculate the value of K independently, which means that

value of K in sub watershed and value of K in the main river course since we have the velocity of the flow in both part of the watershed. Finally value of k will be the sum of ks which is obtained by  $L_1$  and  $L_2$  for each flow that should be routed in to Gibe III dam site.

### Determination of routing parameter K and X for Abelti, Wabi and Gojeb

Generally the value of K can be determined by applying the following equation as a function of reach length and celerity.

$$K = \frac{L}{CLR} \quad 7.8$$

Where L is the reach length and CLR is the wave celerity

$$CLR = \frac{5 * V}{3} \quad 7.9$$

Where V is the average stream velocity in m/s, the average stream velocity to calculate celerity has been taken the value which was determined during preliminary design of Gibe III dam from design manual of the project. Once average stream velocity and the travel distance in each sub catchment and main stream is known it is possible to calculate the value of K by applying equation 7.8 and 7.9. Accordingly we have calculated the value of K independently for each stream length, and finally summed up to get the total k value. The summary of the results depicted in the following table.

	$L_1$	$L_2$	$L_1+L_2$	$K=K_1+K_2$
Om19	54km	89km	143km	1.4463
Abelti	1km	208km	209km	2.9573
Wabi	8km	207km	215km	2.93305

Table 7.2 Values of K for OM19, Abelti and Wabi calculated using equation 7.8 and 7.9

Table 7.2 shows that the calculated value of K. For instance if we take Wabe river it has two k values which have been calculated from river reach 1 and 2. In this case river reach one means the distance of the river which travel from flow measuring point until it meets the main Omo River at some junction points for this river reach it has different average velocity than that of the main river reach, because of this we have calculated  $K_1$  because of the travel distance  $L_1$  and  $K_2$  because of the travel distance  $L_2$  and finally the overall k value is summation of these two. Parameter X, expressing the influence of backwater in the routing process and varying from 0 to 0.5, this value has been taken from Omo Gibe design document as 0.1625. Here the value of K has the unit of time. In Omo Gibe basin it is expressed in day since the observed flows are daily basis.

Once the values of K and X determined for each river reach we can calculate the Muskingum routing coefficients. These values are  $C_1$ ,  $C_2$  and  $C_3$  and they have been calculated by using equation 7.5, 7.6 and 7.7. In order to avoid the computation of negative out flow the following equilibrium equations was checked against all flow contribution catchments and the condition fulfilled  $2 * K * X < \Delta t < 2 * K * (1 - X)$ .

	C <sub>1</sub>	C <sub>2</sub>	C <sub>3</sub>	Sum
Om19	0.1549	0.42951	0.4156	1
Abelti	0.0065	0.3294	0.6641	1
Wabi	0.0079	0.33033	0.6618	1

Table 7.3 Calculated Muskingum routing coefficients for OM19, Abelti and Wabe

Finally the recorded flow from Wabi at Wolkite, Gojeb at OM19 and Gibe at Abelti were routed to Gibe III dam site by using equation 7.4, and the results are shown in the following figure and table.

Month	Mean monthly flow at Gibe III dam site m <sup>3</sup> /s				
	Abelti	Gojeb	Wabi	Un-gauged	Total
Jan	36	17.4	4.4	34.9	93.1
Feb	24.5	14.3	3.5	31.9	75.1
Mar	21.5	16.7	3.9	32.8	76.3
Apr	24.5	22.5	6.5	48	102.2
May	42.1	53.7	7.2	79.6	180
Jun	106.8	112.5	16.2	111.4	347.5
Jul	336.8	167.5	58.6	190.2	751.3
Aug	638.6	209.3	114.3	347.6	1316.8
Sep	528.2	185.1	70.4	300.4	1093.5
Oct	325.9	134	25.6	199	674.8
Nov	128.9	54.2	9.1	114.8	304.3
Dec	56.7	25.5	5.1	58.9	147.5
<b>Annual</b>	<b>189.2</b>	<b>84.4</b>	<b>27.1</b>	<b>129.1</b>	<b>430.2</b>

Table 7.4 Mean monthly and mean annual flow at Gibe III dam site after routing

Table 7.4 reveals the mean monthly and mean annual flows at Gibe III dam site after routing. This flows calculated from 31 years (1970-2000) observed daily data at Abelti, Wabi and Gojeb and simulated daily flow from Un-gauged catchment at Gibe III dam site. The mean annual contributions of flow from Abelti, Wabi, OM19 and un-gauged catchments are 189.2, 27.1, 84.4 and 129.1m<sup>3</sup>/s respectively. The peak discharge of all routed flow occurred in the month of August. The mean annual flow at Abelti, Wabi and OM19 observation stations and routed flow have some discrepancy; the routed flow is a bit smaller than the observed values at the stations this is because the loss of some water through routing processes.

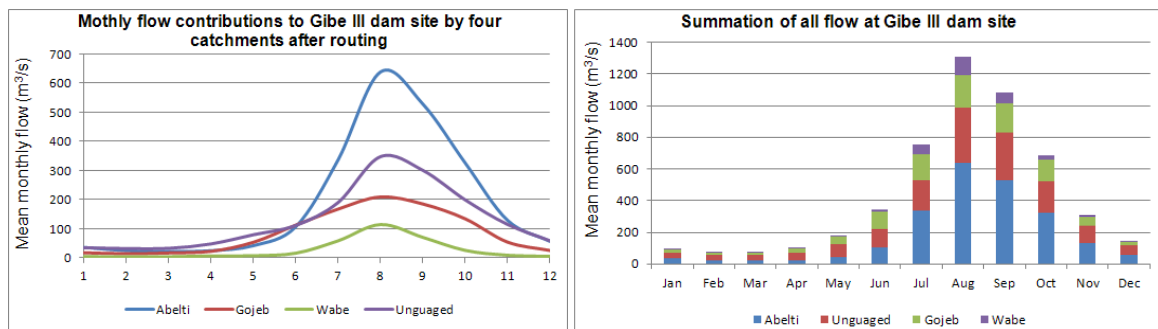


Figure 7.2 Monthly flow contributions from four catchments to Gibe III dam site after routing

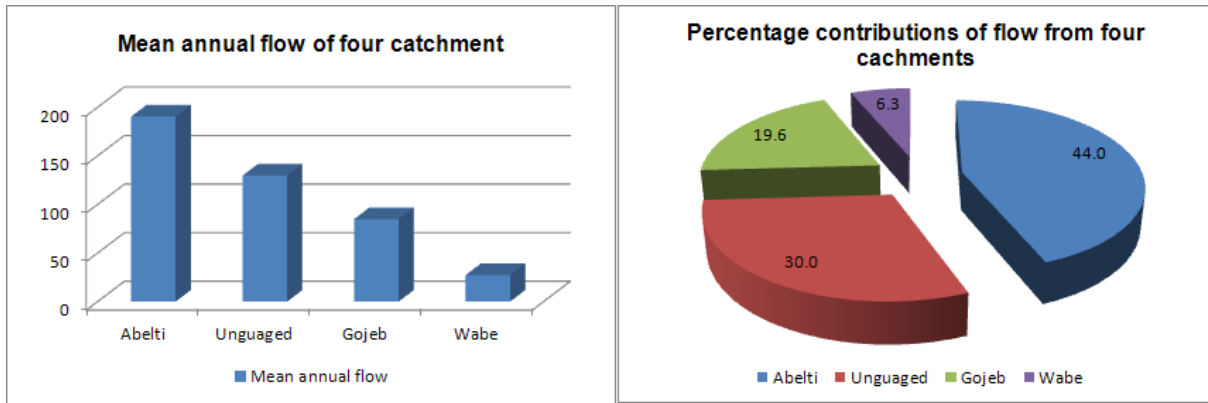


Figure 7.3 Comparisons of mean annual discharge [m³/s] and percentage contributions of flows from all catchments to Gibe III dam site

According to figure 7.3 greater percentage of flow to Gibe III dam site is contributed from Abelti sub-catchment, this constitutes nearly 44% of Gibe III flow. Un-gauged part of the catchment contributes 30% of the flow which is considerable amount next to Abelti. The rest of flow stations Gojeb River at OM19 and Wabi River at Wolkite contribute 19.6% and 6.6% of the total flow at Gibe III dam site. As it was mentioned in the previous section daily flow data at Gibe III dam site is the back bone to set up SWIM at this station, that is why all the above processes and calculations were involved to estimate (calculate) with reasonable accuracy daily flow data at Gibe III dam site. Accordingly, the total mean annual flow at Gibe III dam computed as 430.2m³/s and the average annual volume of water enters to Gibe III reservoir is 13,650 million m³ which was calculated from 29 years daily flow data at Gibe III dam site. The peak flow at this site occurred in the month of August and the value calculated as 1,317 m³/s. From now on this mean and daily discharge at this site will be used as reference period water resource potential of the basin upstream of Gibe III dam site. And effects of climate change will be carried out against this reference time flow. Detail computed water resources potential from all sub-catchments can be found in the appendix.

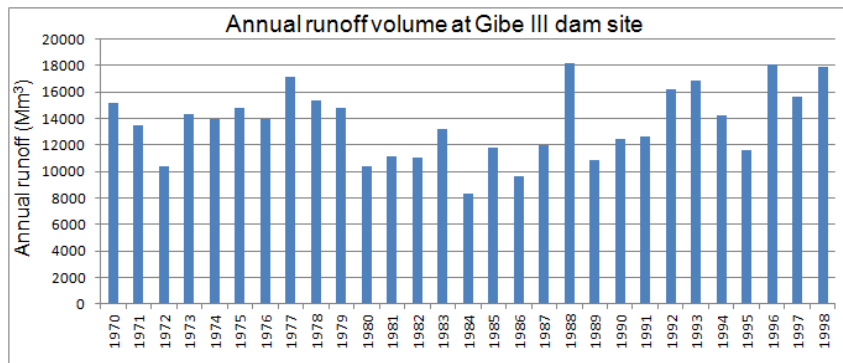


Figure 7.4 Annual runoff volumes at Gibe III dam site

### 7.3 SWIM setup at Gibe III dam site

At this stage it is possible to setup SWIM at Gibe III dam site, because all the necessary data like daily flow, soil map, land use map, DEM and other important data are available. The main objective of calibrating SWIM at Gibe III dam site is to study effects of climate change on Gibe III flow from 2020 to 2050. Prior to calibration sensitivity analysis has been performed.

### 7.3.1 Sensitivity analysis

Sensitivity is measured as the response of an output variable to a change in an input parameter, with the greater the change in output response corresponding to a greater sensitivity. It evaluates how different parameters influence a predicted output. Parameters identified in sensitivity analysis that influence predicted outputs are often used to calibrate a model (Van Griensven et.al. 2006). Sensitivity analysis gives a clear answer in regards to the relative importance of various calibrating parameters. Therefore sensitivity analysis as an instrument for the assessment of the input parameters with respect to their impact on model output is useful not only for model development, but also for model validation and reduction of uncertainty (Kassa T. 2009). Main purpose of sensitivity analysis is to understand the model behavior in response to variations of different calibration parameter, because if someone understand the model very well it will be very easy to calibrate the model without difficulties.

The parameter sensitivity analysis at Gibe III dam site was conducted manually, because this methodology helps to understand the model very well. To identify most sensitive parameters based on numerical and visual inspections of different components of modeled flow like peak, low, seasonal and total flow value were investigated. Moreover, the degree to which model predicted discharge approach measured observations using the given parameter carried out. During this process one parameter was adjusted while others were kept unchanged. For each parameter, changes were made a number of times within its allowable range to test its sensitivity. Accordingly, a total of eight model input parameters (roc2, roc4, thc, abf0, gwq0, bff, sccor and stinco) were selected for sensitivity analysis which may have a potential influence to Gibe III dam flow. Table 8.5 lists the model parameters along with their maximum and minimum estimates with acceptable ranges. The ranges of variation of these parameters are based on a listing provided in the SWIM manual. The sensitivity analysis described here has been done for Gibe III (gauge station area 33901km<sup>2</sup>) from fourteen years simulation period 1985 - 1998. Most parameters used for the sensitivity analysis are from the parameters suggested by SWIM user manual and personal experience with the model. The sensitive parameters were examined by characterizing simulated surface runoff under different parameter ranges using direct model output.

S no.	Designation	Description	Max	min	processes
1	Roc2	Routing coefficient to calculate storage time constant for the reach of surface flow	20	1	Runoff
2	Roc4	Routing coefficient to calculate storage time constant for the reach of sub surface flow	60	1	Runoff
3	Thc	Evaporation correction factor	1	0	Evaporation
4	abf0	Alfa factor for ground water this parameter characterises the rate at which ground water flow is returned to the stream	1	0.01	Groundwater
5	gwq0	Initial ground water contribution to stream flow in mm/day	1	0.01	Groundwater
6	bff	Base flow factor	1	0.2	Runoff
7	sccor	Correction factor for saturated conductivity	0.01	10	Soil
8	chwco	Coefficient to correct the channel width	0.1	1	channel
9	stinco	Initial water content as a fraction of field capacity	0	0.9	

Table 7.5 Parameters and parameter ranges used in sensitivity analysis in SWIM model

### 7.3.2 Results and discussion on sensitivity analysis

**Bff** to investigate the influence of the baseflow factor on water discharge at Gibe flow, different values of bff from (0.2 to 1.2) at 0.2 intervals were used to simulate the corresponding water discharge. According to the result this parameter has a significant effect on hydrograph of the flow, when the value of bff reduced from 1.2 to 0.2 the peaks are lowered the level of low flow are raised and the total discharge lowered by 6%. When the value of bff increased from 0.2 to 1.2 leads to opposite effect. The overall results of this sensitivity analysis illustrated by figure 7.5.

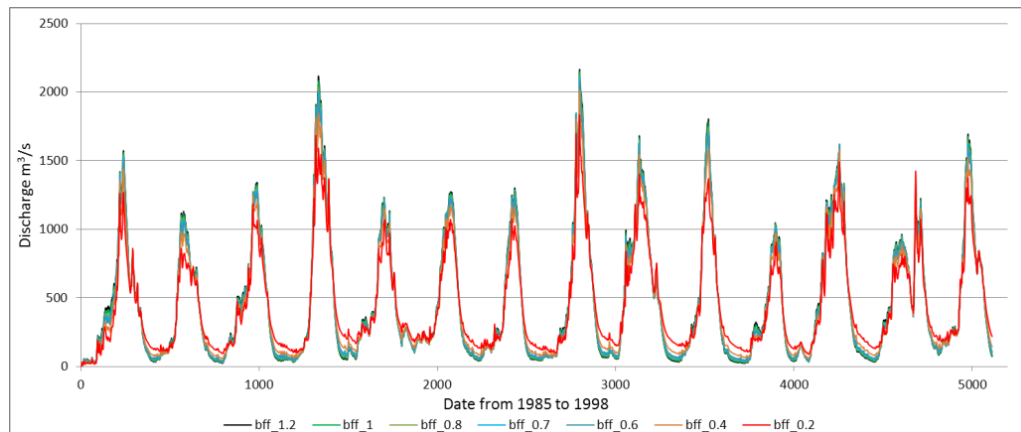


Figure 7.5 Sensitivity of discharge at Gibe III dam site to bff parameter

**Abf0** alpha factor for groundwater, or groundwater recession rate, which characterises the rate at which groundwater flow is returned to the stream, this parameter does not have very significant effect on the hydrograph of the flow especially during dry season. However, it has visible effect on hydrograph during late summer, September, October and November flows. When the alpha factor changed from 0.01 to 0.9 peaks in summer and autumn flow raises, moreover the decrease in abf0 leads to decrease in total flow by 3%. To illustrate the sensitivity analysis of abf0 at Gibe III flow graphical analysis of this results are found at the appendix for the year 1985 and 1988.

**Thc** this parameter is a very sensitive parameter and very important factor for calibration purpose. To see the overall effect of this parameter on Gibe discharge, different flows were simulated for different values of thc (from 0.1 to 1) by taking an interval of 0.2 which can help to identify the effects in detail. Consequently, when we increase the value of thc from 0.2 to 1 peak and low discharge were raised and the overall water discharge changes significantly. Thc has higher impact especially during high flow time and in total flow values. The following figure helps to see the effect of thc on Gibe discharge during high and low flow time.

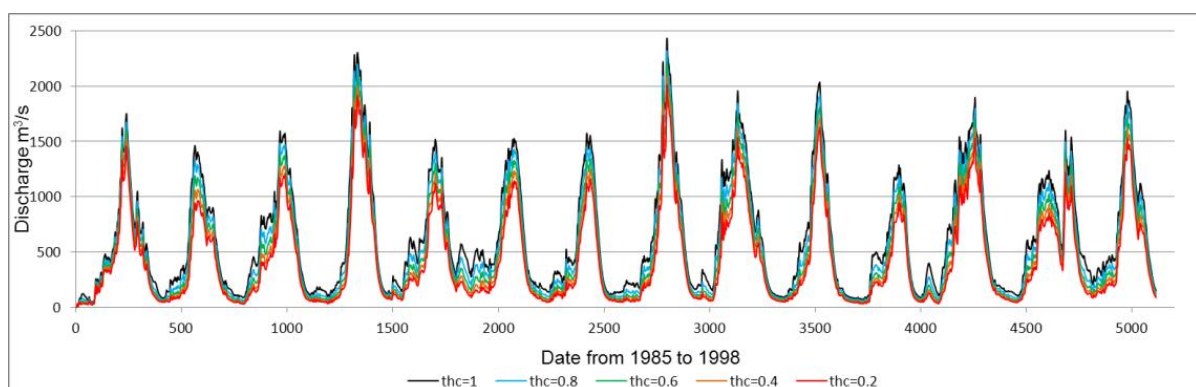


Figure 7.6 Sensitivity of discharge at Gibe III dam site to thc parameter



**Roc4** Initially estimation of the storage time constants for a reach in the model is based on the channel length and celerity, (flow velocity) are estimated based on the DEM. This preliminary estimation can be corrected during the model calibration using parameters roc2 and roc4. Similarly to investigate the effect of this parameter on Gibe discharge different values of Roc4 from (1 to 24) at different interval were used on the discharge of 1985 to 1998. The result show that the increase in this coefficient leads to the lowering of peaks and the smoothing of the dynamics in general. However, the total water discharge does not change significantly or it is possible to say that the total water discharge is stable for different values of Roc4 and as the value of this parameter increases, it attains longer recession on the limbs of the hydrograph. Since the dynamics of the flow changes significantly it is possible to consider this parameter is one of the most important calibration parameter because the correlation coefficient between observed and simulated discharge show significant change as roc4 value changes. For the case of Omo Gibe basin medium value between 8 to 13 leads to better result. The result of this sensitivity analysis can be found in the form of figure at the appendix.

**Roc2** the effect of this parameter on Gibe discharge is the same as roc4. However, the effect is not significant like that of roc4. Lower values of 2 to 5 leads to better result in Omo Gibe basin, while this value gets larger and larger it become insensitive to gibe flow. Similar figure for this sensitivity analysis can be found at the appendix part of this thesis.

**Sccor** this parameter is very important model calibration parameter for Gibe flow. As it was mentioned previously on soil data preparation section, for Gibe basin saturated conductivity was estimated by using Cosby (1984) formula as a function of clay and sand content. However, estimation of this parameter by using different methods leads to different estimates, because of the uncertainties with this estimation SWIM allows to correct the parameter sc in the model globally for all soils and soil layers, using the correction factor sccor. Accordingly an attempt has been carried out to estimate the sensitivity of the model to sccor for different values of (0.01, 0.3, 0.6, 0.9, 2 and 4) to gibe flow. According to the result, as the value of sccor increases the peak flow lowered especially significant decrease in discharge observed in summer flow (June to August) and low flow raised (increased in discharge during autumn and winter) moreover, the total discharge with the change in sccor changes significantly. Graphical results of model sensitivity to the correction of the parameter sccor are shown in the following figure. This parameter was considered as one of the most important calibration parameter at gibe basin.

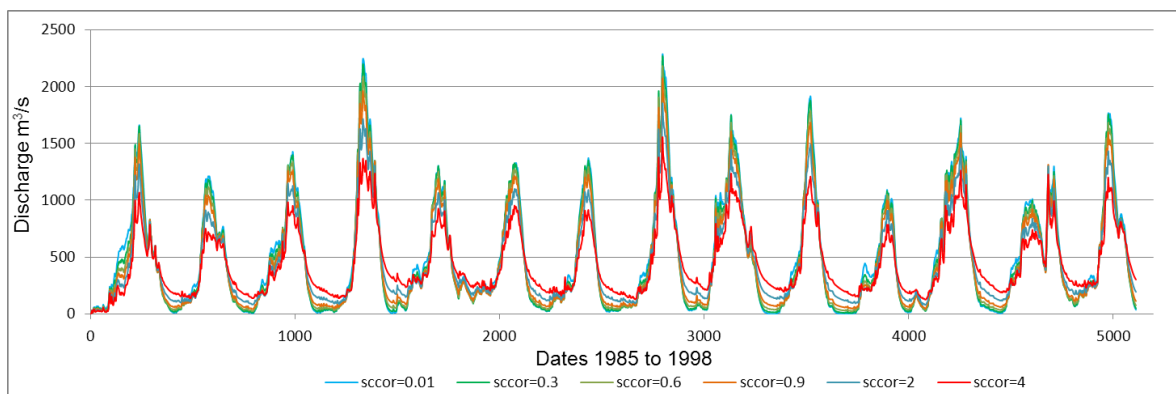


Figure 7.7 Sensitivity of discharge at Gibe III dam site to sccor parameter

**Gwq0** and **Stinc0** are Initial ground water contribution to stream flow in mm/day and Initial water content as a fraction of field capacity. The initial conditions in SWIM may be changed by establishing the initial groundwater contribution to streamflow (parameter gwq0) and the initial water storage (parameter stinco) simultaneously or independently.

Significant influences of these parameters observed on the hydrograph of simulated discharge during the first 3 to 4 months. But for the rest of simulation period the influence of these

parameters were found to be not sensitive at all. Larger gwq0 values resulted in increased surface runoff for the first 3 to 4 months. Moreover, the overall water deviation shows some change from 1 to 4 %.

The following table summarizes the sensitivity characteristics and other important points of the selected parameter, based on rate of change of sum of squares of deviations of measured and simulated model output and visual inspection in different components of modeled flow like peak, low, seasonal flow and total deviation of flow rate.

Para	Reference value	Parameters range taken for analysis	Impact on high flow	Impact on low flow	%age change on total flow	Remark
thc	0.4	0.1-1	very high	high	-6% to +15%	very good calibration parameter
sccor	0.9	0.01-4	very high	very high	+9% to -1.8%	very good calibration parameter
roc4	9.4	1-24	very high	high	+0.6% constant	very good calibration parameter
roc2	2.2	1-15	high	very low	+0.4% constant	good calibration parameter
bff	0.7	0.2-1.2	high	very high	-1.4% to +4.7%	good calibration parameter
abfo	0.95	0.01-1	slightly high after rainy season	low	-1% to +2.2%	good calibration parameter
gwq0	0.04	0.01-1	high during initial simulation period	high during initial simulation period	-1% to +5%	good calibration parameter
stinco	0.9	0.01-1	high during initial simulation period	high during initial simulation period	1.1%	
chwco	0.7	0.1-1	very low	very low	No change	

Table 7.6 Sensitivity characteristics of calibration parameter towards water flow at Gibe III basin

### 7.3.3 Calibration and validation of SWIM at Gibe III basin

The main purpose of calibrating SWIM at Gibe III dam site as mentioned before is to study the potential effects of climate change on hydrology and water resources of Gibe III catchment. Prior to calibration all the necessary data set and preprocessing (mention in Abelti calibration section) have been prepared and performed for Gibe III basin too. Total watershed area corresponding to the outlet at Gibe III dam site is 33901 km<sup>2</sup>. According to the recommendation made by SWIM manual the entire watershed has been divided into 161 sub-watersheds by choosing a threshold area of 3000cells. A total of 866 hydrotopes were generated in these 161 sub-watersheds by overlaying sub-watersheds, land use and soil map of the basin. Routing structures produced during preprocess calculation by taking DEM and sub-watersheds of Gibe III basin.

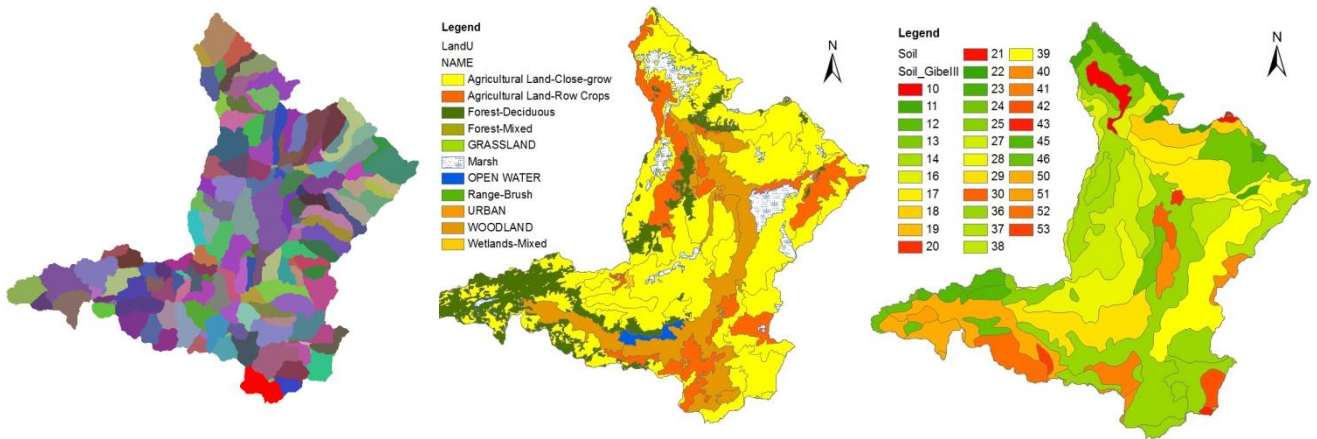


Figure 7.8 Overlaid sub-basins, land use and soil map of Gibe III catchment respectively



Figure 7.9 Hydrotope and routing structure developed during preprocessing of SWIM at Gibe III catchment

The approach to calibrate and validated the SWIM model was based on manual calibration and PEST auto-calibration procedures. However, manual and auto calibration options have not been integrated in SWIM modeling technique. PEST is nonlinear parameter estimation package. The parameter estimation approach is based on the discrepancies between selected model outputs and a complementary set of measurements is reduced to a minimum in the weighted least squares approach. It does this by taking control of the model and running it as many times as is necessary in order to determine this optimal set of parameters. For this purpose three important separate files have been prepared to use PEST auto calibration procedure. These are; template files, one for each model input file on which parameters are identified, instruction files, one for each model output file on which model-generated observations are identified and an input control file, supplying PEST with the names of all template and instruction files, the names of the corresponding model input and output files, the problem size, control variables, initial parameter values, measurement values and weights, etc. The full constructions of these files are depicted in detail at the appendix.

### 7.3.4 Results and discussion on calibration and validation

Daily flow data computed from un-gauged part of the basin using SWIM and routed flow from Abelti, OM19 and Wabi flow observation stations to Gibe III dam site has been used as observed value at Gibe III outlet which can represent current time water resources potential of the basin. SWIM at Gibe III dam site has been calibrated and validated using daily river flow data of 14 years from 1985 to 1998 and 11 years from 1970 to 1980 respectively. Data pertaining to year 1985 to 1998 has been used for calibration and the second part of the data set has been used for validation procedure. The calibration period includes a wide variation of climatic conditions of wet, dry and normal years of flow.

During calibration snow module of the model was ignored because of the climatic characteristics of the study area. Model's input parameters were adjusted automatically using PEST and tuned manually to get better and reasonable results as guided by sensitivity analysis to match the observed and simulated discharge at Gibe III outlet. Consequently, tests were conducted by using separate data other than calibrated data set to validate the calibrated model to make sure that the capability of making sufficiently accurate predictions of the observed discharge at Gibe III outlet. The model is said to be validated if its efficiency in the validation period have been repeated by providing similar performance as calibration period. The performance of the model was measured by equation 6.3 and 6.4. The results of statistical analysis give a Nash Sutcliff efficiency of 0.92 during calibration and 0.93 during verification period. Nash Efficiency criteria gave very high values both for calibration and validation period (Table 7.7). On the other hand, Nash-Sutcliffe coefficient indicates how much the model accurately simulated the natural process.

Calibration period 1985 -1998 (total 14 years data set)															
Year	1985	1986	1987	1988	1989	1990	1991	1992	1993	1994	1995	1996	1997	1998	Total
E (%)	93	83	91	93	89	94	92	94	90	95	82	94	91	91	92
<b>Total water difference</b>															2%

Verification period 1970 -1980 (total 11 years data set)												
Year	1970	1971	1972	1973	1974	1975	1976	1977	1978	1979	1980	Total
E (%)	93	90	94	95	96	97	90	90	92	90	83	93
<b>Total water difference</b>												3%

Table 7.7 Calibration and verification results at Gibe III outlet

The statistics of the observed and SWIM simulated daily flows during calibration and validation results in terms of criteria of fit are presented in the above Table. In the calibration period (1985 to 1998) 14 years, the Nash–Sutcliffe efficiency varies from 0.82 in the year 1995 to 0.95 in the year 1994, but the overall Nash–Sutcliffe efficiency was 0.92 and the deviation in overall water balance is not more than 2% during calibration period. Not only the aggregated results are very satisfactory, but also individual year results are prodigious. In most of the cases Nash–Sutcliffe efficiency was greater than 0.82 during calibration and validation period. In the validation (verification) period (1970 to 1980) 11 years, the Nash–Sutcliffe efficiency and the deviation of water balance gives 0.93 and 3% respectively. As one can see the calibration results of SWIM at Abelti and Gibe III outlet the model produced very high Nash–Sutcliffe efficiency at Gibe III outlet, these results prove that the ability of SWIM in producing monthly and daily streamflow time series in larger river basin is quite well. Generally the overall results obtained from SWIM in Omo Gibe basin were very attractive and satisfactory, so that SWIM has a capability to model hydrological process in Gibe basin quite well. The performance which has been shown by the model in Gibe basin can have similar ability to other part of the basin in Ethiopia, therefore this

model should be tried throughout Ethiopia to model hydrological process at different part of the watershed. Graphical results of SWIM modeling at Gibe III outlet elaborated in the following section.

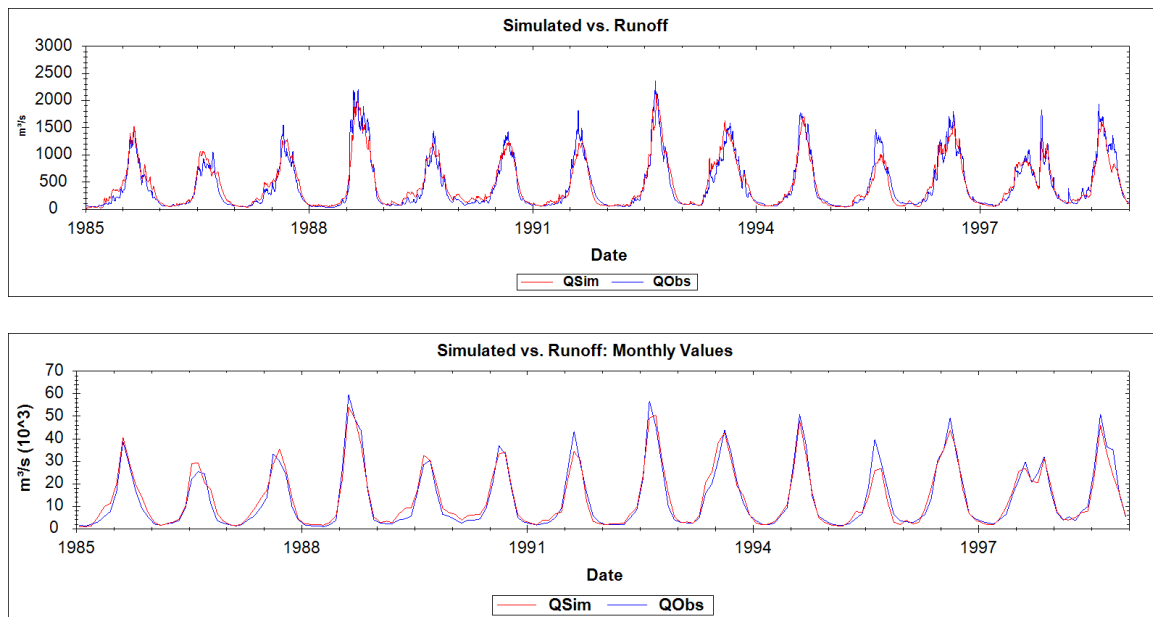


Figure 7.10 Graphical comparisons between observed and simulated daily discharge upper panel and monthly discharge lower panel during calibration period at Gibe III outlet

NOTE: Qobs is summation of simulated daily discharge from un-gauged part of the basin and observed routed flow from Abelti, OM19 and Wabi flow measuring stations for current time at Gibe III outlet point for current time period.

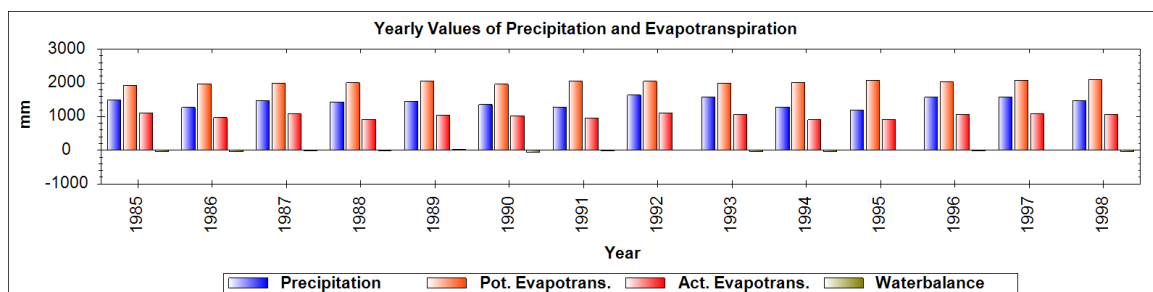


Figure 7.11 Yearly values of precipitation and evapotranspiration during calibration period at Gibe III outlet

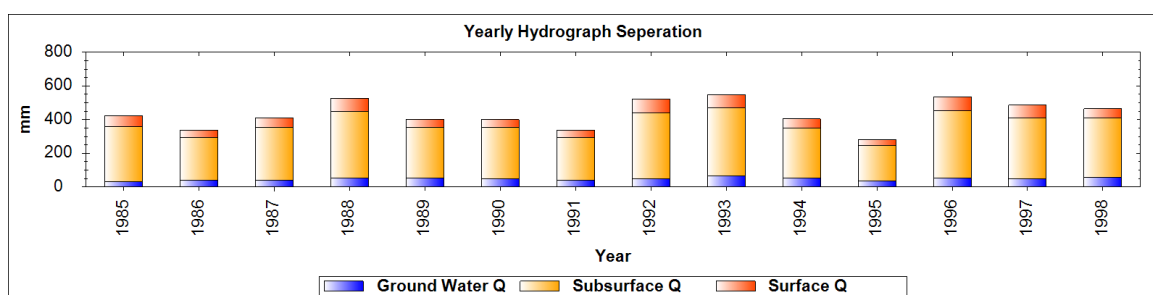


Figure 7.12 Yearly hydrograph separations during calibration period at Gibe III outlet

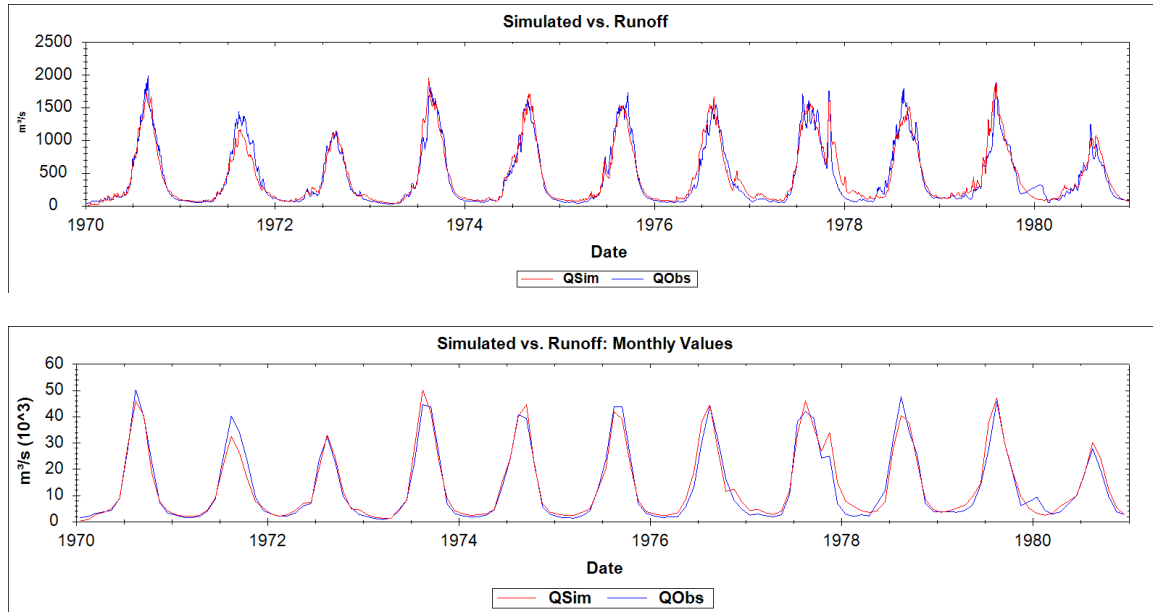


Figure 7.13 Graphical comparisons between observed and simulated daily discharge upper panel and monthly discharge lower panel during validation period at Gibe III outlet

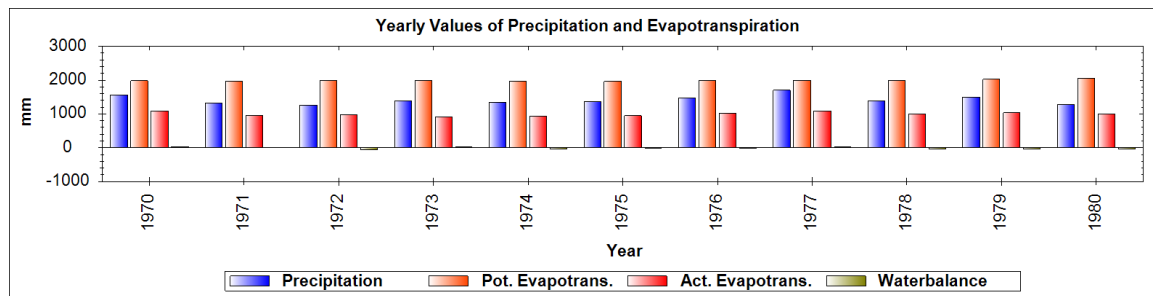


Figure 7.14 Yearly values of precipitation and evapotranspiration during validation period at Gibe III outlet

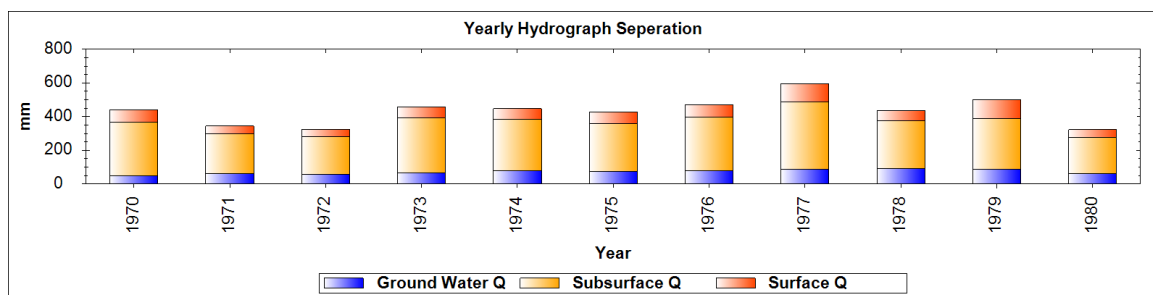


Figure 7.15 Yearly hydrograph separations during validation period at Gibe III outlet

The graphical comparisons between observed and simulated discharge at Gibe III outlet clearly presents the graphical analysis of measured and simulated data that allows for identification of general trends in the data and differences between model simulations and observed data set. As per these results the dynamics of observed discharge at Gibe III dam site simulated very well by the model for both calibration and validation period. The peak and low flows have been captured very well for most of the simulation time. The only year which doesn't capture the peak discharge during calibration period is 1995. At this year the peak discharge is underestimated, additionally during validation period of 1971 the simulated discharge is a bit smaller than the

observed one, but for the rest of the years the result is quite good. As per the yearly hydrograph separation most of the surface runoff generated from subsurface flow component for Gibe basin which is clearly shown in figure 7.12 this graphical interpretation together with the numerical analysis given in Table 7.7 gives a comprehensive measure of the agreement between measured and simulated discharge. Additionally these procedures proved the capability of SWIM in simulating water discharge in Gibe basin to very satisfactory limit.

## 7.4 Conclusion

To investigate the effect of climate change on Gibe III inflow, SWIM hydrological model should be calibrated at this point, for this purpose historical time series of runoff at the dam site was very important, however this flow was not readily available, because of this different technique assessed to estimate the reference period water resources potential at Gibe III dam site starting from empirical relationship up to complete hydrological consideration of the basin. Moreover, daily flow data generated from un-gauged part of the basin by assuming reasonable assumptions between un-gauged and Abelti basin. The results were validated by comparing with different outputs that have been computed by using different methodology to confirm the reliability of the output. Finally daily flow data at Gibe III dam site estimated by routing observed daily flow at Abelti, Wabi, and OM19 and then added with SWIM results from un-gauged basin to obtain total flows enter to Gibe III reservoir. Accordingly the mean annual discharge for current time (1970-1998) at Gibe III reservoir found as 430.2m<sup>3</sup>/s. The average annual volume of water enters to Gibe III reservoir is 13650 million m<sup>3</sup>.

Semi distributed process based hydrological model SWIM employed and calibrated in Gibe basin at Gibe III outlet for the second time, but for different purpose. Before calibrating the model at mentioned location a comprehensive sensitivity analysis was performed on the main input parameters of the model manually in detail by using direct output of the model results. Because the identification of most sensitive parameters help to use the model efficiently, as a result producing of conducive environment to calibrate the model easily. The sensitivity analysis has pointed out seven crucial parameters (thc, roc4, roc2, sccor, bff, gwq0 and abf0) that control the surface, subsurface, evapotranspiration and groundwater hydrological processes of the studied watershed. However, sccor, roc4 and thc were found to be most crucial than other parameters.

On the other hand, SWIM was calibrated and validated at Gibe III dam site for the purpose of studying potential effects of climate change on the inflow of Gibe III reservoir from 2020 to 2050 by producing daily flow data set at this outlet, which can substitute reasonably the observed discharge. The results of calibration and validation at this station show better performance than Abelti with higher Nash–Sutcliffe efficiency of 0.92 and total water difference of 2% during calibration and 0.93 and total water difference of 3% during verification period. Normally no significant differences were found in simulated and observed runoff volumes during the calibration period which is only 2% one of the basic requirement for climate change study. The performance efficiency values in both calibration and validation phases prove that SWIM predicted measured streamflow quite satisfactorily for monthly and daily streamflow time steps and its performance increased as the basin area increased.



# Chapter 8 Modeling of Gibe III Basin under Climate Change Scenarios

## 8.1 Introduction

As we have seen under climate downscaling part mainly surface air temperature for entire Gibe basin showed an increasing pattern from all scenarios. This can have a potential effect on inflow of Gibe III reservoir. As the water cycle in river basin is sensitive to changes in climate characteristics especially to maximum and minimum temperature and precipitation change, it would be worthwhile to study the effect of these changes on the availability of scarce water for different purposes such as irrigation, water supply and hydropower generation. As a result of this, the hydrological impacts of climate changes have received a considerable amount of interest in hydrology.

The water balance components, such as evapotranspiration, runoff and groundwater recharge, that determine river discharge and the availability of water resources, will be inevitably affected, generally, more evapotranspiration can be expected due to the increased temperature (Huang et al., 2010). In order to identify effects of climate change on water resources potential different studies have been carried out around the world. However; similar studies carried out in Ethiopia are very rare especially in Gibe basin. Investigation of potential impacts of climate change on hydrology of river basin can be performed by applying a common approach. This common approach is to use hydrological models driven by projected climate scenario for future time period. Recent studies of these climate change applied by using process based hydrological models (e.g Kassa T. 2009 and Huang et al. 2010). Therefore, in this part of the study the main objective is to study, quantify and evaluate changes in the seasonal, monthly and annual dynamics of inflow to Gibe III reservoir from 2020 to 2050 by applying the downscaled precipitation, radiation, maximum and minimum temperature data set to process based semi distributed hydrological model (SWIM).

## 8.2 Methodology

The last objective of this thesis was estimation of future water availability in the basin under climate change scenarios. However, no changes in land use patterns were assumed between the reference and scenario periods during future water simulation, and land use was considered to be stationary for the whole simulation time. This has been done deliberately, in order to investigate the pure impacts of climate change on the availability of water for power production and other use at Gibe III reservoir from 2020 to 2050 time frame. Therefore, the influence of changing land use pattern has been ignored.

Previously SWIM has been calibrated at Gibe III dam site for reference time period with satisfactory results, very good performance and negligible over all water difference. The entire calibration model parameters during reference period used as model input parameter for future time period, in addition to the following model input data:

- i. Input climate data from each scenarios:
  - ✓ Downscaled precipitation (2020-2050) from 21 stations
  - ✓ Downscaled maximum and minimum temperature data (2020-2050) from 14 stations
  - ✓ Downscaled radiation data (2020-2050)
- ii. Spatial data:
  - ✓ Digital elevation model of the basin
  - ✓ Land use map of the basin (similar with reference time period)
  - ✓ Soil map of the basin (similar with reference time period)
  - ✓ Sub-basins of the basin (produced during reference time simulation)
  - ✓ Hydrotopes of the basin (produced during reference time simulation)

- ✓ Routing structures of the basin (produced during reference time simulation)

By providing all the above input data and calibrated parameter to SWIM hydrological modeling, the model was produced the corresponding future time flow (2020-2050) at Gibe III dam site from each scenario. It is a normal trend that, the impacts of climate change on the basin hydrology are assessed by comparing the present and projected streamflow and the evapotranspiration estimates. As a result the potential effects of climate change on the hydrology and water resources of the Omo Gibe River basin assessed by comparing simulated hydrologic and water resources scenarios derived from downscaled climate simulations in chapter five to observed historical (1970 - 1998) flow data sets at Gibe III basin.

### 8.3 Results and discussion on climate change impacts

This paragraph is an overview of the obtained results after applying the methodology described above on the Gibe III basin. The impacts of climate change on future time flow (2020-2050) at Gibe III dam site (reservoir) has been analyzed based on monthly, seasonal, annual, high and low flows of the simulations. Flow from all scenarios four from REMO and one from GCM summarized in the following table.

Months	Observed	A1B_911	A1B_912	B1_921	B1_923	GCM
January	93.1	80.9	110.6	92.2	62.8	77.5
February	75.1	87.2	90.6	88.7	62.3	76.0
March	76.3	97.3	96.6	106.6	102.5	91.7
April	102.2	216.6	206.9	213.1	168.9	160.8
May	180.0	381.0	329.6	309.2	285.4	265.5
June	347.5	721.3	554.6	563.1	489.1	516.7
July	751.3	1059.7	794.2	766.9	621.6	954.9
August	1316.8	1130.8	1111.0	1045.2	942.9	1266.2
September	1093.5	858.8	931.1	915.6	804.9	960.8
October	674.8	553.9	547.7	574.0	453.8	522.5
November	304.3	305.6	285.2	319.4	273.8	266.3
December	147.5	143.8	149.1	148.0	120.6	123.5
Winter	106.2	104.5	117.6	110.3	82.5	92.8
Spring	119.7	231.8	211.1	209.6	185.7	172.8
Summer	810.2	973.3	822.8	794.3	686.6	916.9
Autumn	690.7	572.6	587.6	602.7	510.2	582.5
Annual	430.2	472.0	435.8	430.2	367.2	442.5

Table 8.1 Observed and projected discharge at Gibe III dam site. Monthly, seasonal and annual values

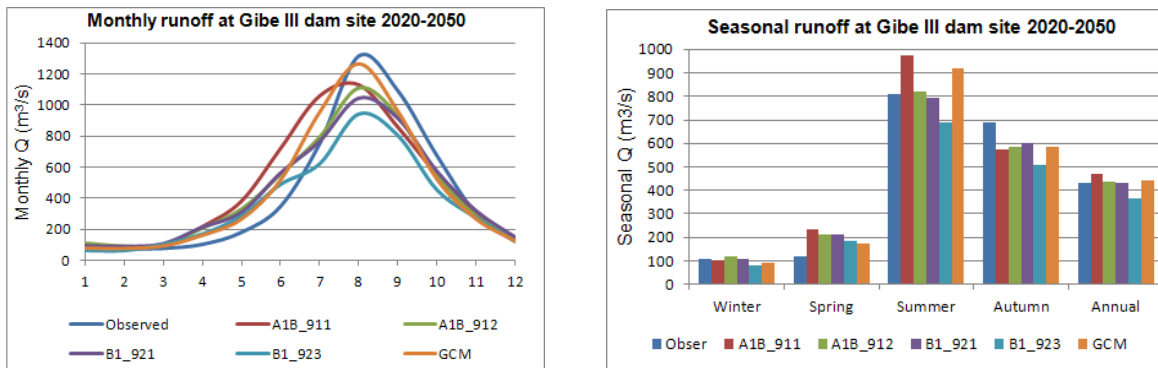


Figure 8.1 Comparisons of observed and projected monthly, seasonal and annual flows at gibe III dam site.

### 8.3.1 Impacts on monthly, low and high flows

Figure 8.1 show the comparisons of observed and simulated discharge for future time period at the outlet point of Gibe III dam site. Based on this results starting from March through July significant increments of flow will be expected from all scenarios, whereas from late July through November certain amount of flow will be decreased to certain level, one of the astonishing results of this analysis is that, similar trend observed from all scenarios for this case too. However, the amount of change is different from scenario to scenario.

The increases/decreases in the monthly low and high flows are clearly presented in table 8.1 and figure 8.1 for every climate scenario. The low flow from observed data set is obtained in the month of February. Long term observed mean flow in this month was  $75.1\text{m}^3/\text{s}$ . This value showed an increasing trend in three of the scenarios by 16%, 20.6% and 18.1% by A1B\_911, A1B\_912 and B1\_921. Whereas it showed a decreasing result by B1\_923 nearly -17% and it doesn't show any change for GCM scenario. Regarding to peak runoff values, all of the projected monthly peak flow attained their peak discharge in the months of August; however, in all cases this value has been showed attenuated discharge as compared to observed value with different outputs. For instance the peak runoff rate in the month of August decrease up to -14.1%, -15.6%, -20.6%, -24.8% and -3.8% from A1B\_911, A1B\_912, B1\_921, B1\_923 and GCM scenarios respectively. The peak discharge in all scenarios showed a considerable reduction except GCM. Generally this analysis tells us that, the low flow regime will increase in average of 9.5% from all scenarios simulation, whereas the percentage of variation of the runoff peaks (difference between the new resulted runoff peaks after applying climate scenarios and the actual observed runoff peaks expected to reduce with an average result of 15.8% throughout August for future time period. According to the overall result of the analysis low flow value increased this might be an opportunity to get more water during low flow (dry) season to use for extended period of time for different purposes.

### 8.3.2 Impacts on seasonal and annual flows

For this specific study seasons were divided in to four groups, accordingly seasonal change in flows at Gibe inflow will be quantified based on this consideration.

	Change in seasonal discharge $\text{m}^3/\text{s}$					Percentage change in seasonal discharge (%)				
	A1B_911	A1B_912	B1_921	B1_923	GCM	A1B_911	A1B_912	B1_921	B1_923	GCM
Winter	-2	11	4	-24	-13	-1.6	10.7	3.9	-22.3	-12.6
Spring	112	91	90	66	53	93.7	76.3	75.1	55.2	44.4
Summer	163	13	-16	-124	107	20.1	1.6	-2.0	-15.3	13.2
Autumn	-118	-103	-88	-180	-108	-17.1	-14.9	-12.7	-26.1	-15.7

Table 8.2 Change in seasonal discharge at Gibe III dam site for future time

Small rainy season in the northern part of Gibe basin is spring; this season is associated with low flow in the basin due to small rainy period, however, the forecasted flow in this season showed considerable increments from all scenarios. The average change in flow from all scenarios indicated that, this season flow is expected to increase by 68.8% due to increased precipitation for this season, however, the autumn season flow showed reduction from all scenarios due to decreased precipitation and increased temperature. Accordingly, -17.1% - 14.9%, -12.7%, -26.1% and -15.7% expected to reduce from A1B-911, A1B-912, B1\_921, B1\_923 and GCM scenarios respectively. The summer season is the major rainy season in the northern part of the basin, this season flow doesn't show similar trend like that of the previous seasons. The results of this season showed increased and decreased flows patterns from different scenarios. Summer flow is expected to increase up to 20% and 13% from A1B\_911 and GCM scenarios whereas this season flow expected to decrease up to -15.3% from B1\_923 scenario.

To assess the impact of climate change on freshwater resources, change in mean annual runoff (MAR) is only a first indicator (Döll et al., 2012). The analysis of climate change impacts on mean annual flow is the most important part, because this flow determines the overall availability of water in the basin under climate change conditions for utilization of the resources for different purposes. Therefore the effects of climate change in Omo Gibe basin can be well addressed by this analysis. To investigate the overall availability of water in the basin the aggregated results of monthly value were considered from all scenarios and the results depicted in the flowing section.

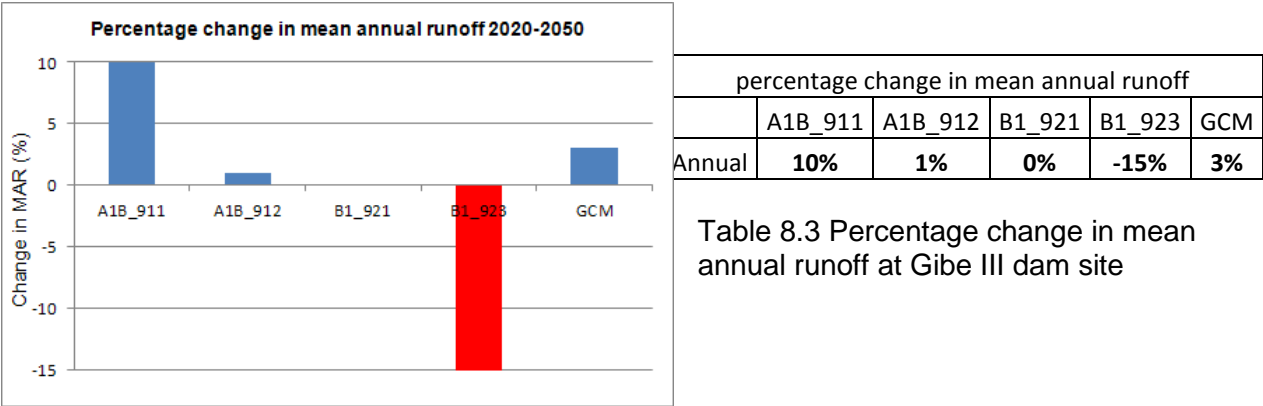


Table 8.3 Percentage change in mean annual runoff at Gibe III dam site

Figure 8.2 Impacts on mean annual runoff 2020-2050

Figure 8.2 show percentage changes in mean annual runoff calculated between observed (1970-1998) and forecasted (2020-2050) runoff averaged over 31 years as compared to reference time period using climate scenarios derived by REMO and GCM. According to the computed results the blue bars show increments of flow, thereby nearly 10% mean annual flow expected to increase from A1B\_911 scenario, the result for this change in mean annual runoff is the increased precipitation for upper part of the basin from this scenario. This result indicated that the increased precipitation from this scenario offsets the loss of water by the increased surface air temperature due to evapotranspiration and yielded additional 10% increment in mean annual flow. Whereas the two scenarios A1B\_912 and B1\_921 do not show visible change, however, both of these scenarios showed areal increased precipitation for upper part of the basin by 2.4% and 1.9%, the increased precipitation values were not sufficient to offset the water loss by increased surface air temperature due to evapotranspiration and to produce extra mean annual flow.

B1\_923 shows moderate change in mean annual flow, the simulated result from this scenario revealed that more than -15% of mean annual flow at Gibe III dam site (reservoir) is expected to decrease for future time flow, however, the decreased areal rainfall from this scenario for upper

part of the basin was 1.9% for this small decrease in precipitation significant percentage of mean annual flow reduced. This might be the evidence that, for small decrease in precipitation the basin is highly sensitive to change in mean annual flow due to increased temperature. The annual mean water flow predictions for the period 2020–2050 from GCM used in this study is close to the present mean annual runoff for A2 scenario, but it shows small raised value of 3% at Gibe dam site.

A separate model run carried out, in order to investigate changing trends in runoff and water balance under warming conditions, to evaluate the extent to which the future change in mean annual runoff by altering the temperature data only, while keeping precipitation unchanged. Accordingly the results from this analysis indicated that for 1.5 °C increased mean surface air temperature, the mean annual flow reduced by 8.6% at gibe III outlet for future time horizon. This result indicated that due to the change in temperature water will be lost in the form of evaporation from the basin. In order to compensate this there should be sufficient amount of rainfall to offset this evaporation loss otherwise considerable amount of flow might be lost in the form of evapotranspiration.

### 8.3.3 Impacts on evaporation loss from the reservoirs

So far attempt has been carried out to project the available water resources potential in Omo Gibe basin for future time from five scenarios without considering evaporation loss from the reservoir surface areas. As we mentioned in the section of description of the case study area, there are three hydropower plants in the basin, these are; Gilgel Gibe I which inundated an area of 60km<sup>2</sup> due to the construction of 40m high rock fill dam and Gibe III power plant will inundate an area of 200km<sup>2</sup> up on completion due to artificially created lake by the dam, therefore the water which will loss in the form of evaporation from this artificial lake helps to determine the net inflow to Gibe III reservoir in 2020-2050. The evaporation loss from Gilgel Gibe II has been ignored since this plant did not inundate significant portion of the land due to the construction of small weir.

The basic idea of this analysis has been carried out by considering the estimation of total reservoir losses for future time by taking representative weather stations from the two power plants. Based on this Hossana and Jimma weather observation stations were selected as a representative stations to Gibe III and Gilgel Gibe I reservoir respectively due to good proximity to the reservoir areas. Evaporation loss from these two stations has been calculated corresponding to future time period. Estimation of evaporation from these two stations is based on projected climate data from downscaling procedure. The data used for this estimation cover the period from January 2020 to December 2050 and include daily data of projected radiation, humidity, maximum and minimum temperature.

Two different methods, modified Penman equation without wind data (Valiantzas 2006) and Priestly Taylor employed to estimate evaporation from the above two stations. For this process the net radiation, net shortwave solar radiation, net outgoing long wave radiation, clear sky radiation, extraterrestrial radiation were calculated. The calculation procedure is based on the method outlined in (Allen et al. 1998).

$$R_n = R_{ns} - R_{nl} \quad 8.1$$

where  $R_n$  is the net radiation (MJ m<sup>-2</sup> day<sup>-1</sup>),  $R_{ns}$  is the net incoming shortwave radiation (MJ m<sup>-2</sup> day<sup>-1</sup>), and  $R_{nl}$  is the net outgoing longwave radiation (MJ m<sup>-2</sup> day<sup>-1</sup>).

Net shortwave solar radiation is estimated from the projected solar radiation  $R_s$  (2020-2050) for both stations and by taking the albedo for the evaporating surface (water) as 0.08.

$$R_{ns} = (1 - \alpha)R_s \quad 8.2$$

where  $R_s$  is the projected incoming solar radiation ( $\text{MJ m}^{-2} \text{ day}^{-1}$ ).

Net outgoing longwave radiation is estimated by:

$$R_{nl} = \sigma(0.34 - 0.14\sqrt{e_a}) \left( \frac{(T_{max} + 273.2)^4 + (T_{min} + 273.2)^4}{2} \right) \left( 1.35 \frac{R_s}{R_{so}} - 0.35 \right) \quad 8.3$$

Where  $R_{nl}$  is the net outgoing longwave radiation ( $\text{MJ m}^{-2} \text{ day}^{-1}$ ),  $R_{so}$  is the clear sky radiation ( $\text{MJ m}^{-2} \text{ day}^{-1}$ ),  $e_a$  is actual daily vapor pressure (kpa) and estimated as  $0.611 \text{EXP} \left[ \frac{17.27T_{min}}{T_{min}+237.3} \right]$ ,  $T_{max}$  and  $T_{min}$  maximum and minimum projected daily air temperature ( $^{\circ}\text{C}$ ), and  $\sigma$  is Stefan-Boltzmann constant ( $\text{MJ K}^{-4} \text{ m}^{-2} \text{ day}^{-1}$ ).

$$R_{so} = (0.75 + 2 * 10^{-5} \text{ELEV}) R_a \quad 8.4$$

Where  $elev$  is the ground elevation of the two stations (m) above sea level,  $R_a$  is the extraterrestrial radiation ( $\text{MJ m}^{-2} \text{ day}^{-1}$ ) and estimated as follow:

$$R_a = \frac{1440}{\pi} G_{sc} d_r^2 [\omega_s \sin(\varphi) \sin(\delta) + \cos(\varphi) \cos(\delta) \sin(\omega_s)] \quad 8.5$$

where  $G_{sc}$  is the solar constant =  $0.0820 \text{ MJ m}^{-2} \text{ min}^{-1}$ ,  $d_r$  is the inverse relative distance Earth-Sun,  $\omega_s$  is the sunset hour angle (rad),  $\varphi$  is latitude of the station (rad) positive for northern hemisphere and  $\delta$  is the solar declination (rad).

The above calculated values used as input to modified Penman (Valiantzas 2006) and Priestly Taylor equation to estimate directly daily evaporation from Hossana and Jimma weather observation stations corresponding to 2020-2050. Accordingly the following results obtained.

	Estimated evaporation from Hossana and Jimma 2020-2050			
	Hossana		Jimma	
	Taylor	Modified Penman	Taylor	Modified Penman
Month	mm/month	mm/month	mm/month	mm/month
January	153	152	152	168
February	155	149	148	160
March	182	169	177	182
April	176	159	166	165
May	167	151	169	164
June	137	122	157	137
July	122	118	134	124
August	127	110	140	131
September	144	128	154	145
October	156	144	167	165
November	145	141	153	163
December	145	145	148	167
Annual (mm/year)	1808	1688	1866	1871

Table 8.4 Estimated evaporation from Hosanna and jimma 2020-2050

According to table 8.4, the results obtained from Taylor and modified Penman are more or less similar for Jimma station, 1866mm and 1871mm of water expected to lose from Jimma station in the form of evaporation annually, similar performance has been observed at Hossana station, however, the results at Hossana from the above two methods are a bit different. These stations evaporation loss from Jimma and Hossana should be converted to lake evaporation by considering a reasonable pan coefficient value. The final result should be deducting from the projected flow data set at Gibe III dam site to get net inflows to Gibe III reservoir from (2020-2050).

#### 8.4 Estimation of net inflows to Gibe III reservoir from 2020 to 2050

It is clearly known that the estimate of lake evaporation for the reservoir is based on historic records of evaporation measured by Piche instruments installed in meteorological stations. These gauges should be converted to Class A Pan evaporation to transform to open water (lake) evaporation using lake to pan coefficients. In most of Omo Gibe weather observation stations this value varies between 0.7 to 0.8 and most text books including FAO suggest multiplying the pan evaporation by 0.75. However, this measurement cannot be obtained for future time; therefore, to be in the safe side a reasonable assumption of this coefficient has been made. For this specific study we have assumed this value as 0.9 and considered the result from modified Penman equation, and then the above calculated evaporation should be multiplied by this value to get the loss of water from both reservoirs by evaporation. The results obtained from this calculation subtracted from projected gross flow to Gibe III reservoir to get net inflow from 2020-2050. The following table 8.5 shows the calculated reservoir loss due to evaporation corresponding to future time horizon.

Estimated evaporation loss from Gibe III and Gilgel Gibe I reservoirs from 2020-2050						
Month	mm/month	Pan coefficient	Reservoir evaporation loss form Gibe III	mm/month	Pan coefficient	Reservoir evaporation loss from Gilgel Gibe I
January	152	0.9	137	168	0.9	152
February	149	0.9	134	160	0.9	144
March	169	0.9	152	182	0.9	164
April	159	0.9	143	165	0.9	149
May	151	0.9	136	164	0.9	147
June	122	0.9	110	137	0.9	123
July	118	0.9	106	124	0.9	112
August	110	0.9	99	131	0.9	118
September	128	0.9	115	145	0.9	130
October	144	0.9	129	165	0.9	149
November	141	0.9	127	163	0.9	147
December	145	0.9	130	167	0.9	150
Annual (mm/year)	1688	0.9	1520	1871	0.9	1684

Table 8.5 Estimated monthly evaporation loss from Gibe III and Gilgel Gibe I reservoirs

The expected mean annual gross evaporation loss from Gibe III and Gilgel Gibe I reservoirs are; 1520mm/year and 1684mm/year, this corresponds the loss of 9.6m<sup>3</sup>/s and 3.2m<sup>3</sup>/s respectively. The total loss from the two reservoirs will be 12.8m<sup>3</sup>/s, this means that 12.8m<sup>3</sup>/s discharge will be lost in the form of evaporation from the two reservoirs annually; therefore, this



value should be deducted from the mean annual inflow to Gibe III reservoir obtained before from five scenarios projection.

Months	Gross projected flow to Gibe III reservoir m <sup>3</sup> /s					projected evaporation	Net inflow to Gibe III reservoir				
	A1B_911	A1B_912	B1_921	B1_923	GCM	Loss m <sup>3</sup> /s	A1B_911	A1B_912	B1_921	B1_923	GCM
January	80.9	110.6	92.2	62.8	77.5	1.2	79.7	109.5	91.0	61.7	76.3
February	87.2	90.6	88.7	62.3	76.0	1.1	86.1	89.5	87.6	61.2	74.9
March	97.3	96.6	106.6	102.5	91.7	1.3	96.1	95.3	105.4	101.2	90.4
April	216.6	206.9	213.1	168.9	160.8	1.2	215.4	205.7	211.9	167.7	159.7
May	381.0	329.6	309.2	285.4	265.5	1.1	379.9	328.5	308.0	284.2	264.4
June	721.3	554.6	563.1	489.1	516.7	0.9	720.4	553.7	562.2	488.1	515.8
July	1059.7	794.2	766.9	621.6	954.9	0.9	1058.8	793.3	766.1	620.7	954.0
August	1130.8	1111.0	1045.2	942.9	1266.2	0.9	1130.0	1110.1	1044.4	942.0	1265.4
September	858.8	931.1	915.6	804.9	960.8	1.0	857.8	930.1	914.6	803.9	959.8
October	553.9	547.7	574.0	453.8	522.5	1.1	552.8	546.6	572.9	452.7	521.4
November	305.6	285.2	319.4	273.8	266.3	1.1	304.5	284.1	318.3	272.7	265.3
December	143.8	149.1	148.0	120.6	123.5	1.1	142.7	148.0	146.9	119.5	122.4
Annual	472.0	435.8	430.2	367.2	442.5	12.8	459.2	423.0	417.4	354.4	429.7

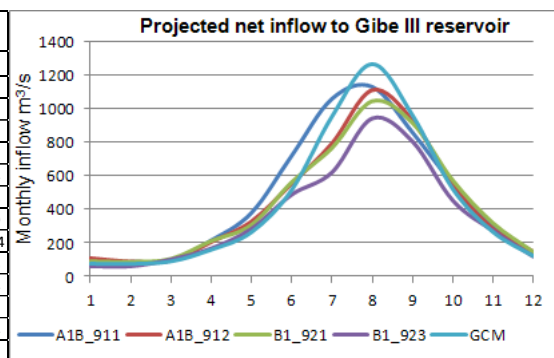


Table 8.6 Projected mean monthly and annual net inflow to gibe III reservoir

The projected net inflow to Gibe III reservoir corresponding to 2020 to 2050 from A1B\_911 scenario is 459.2m<sup>3</sup>/s, this flow projected an excess flow of 29m<sup>3</sup>/s as compared to reference flow, this is equivalent with 6.7% increment, but the rest of the scenarios showed decreased value. For instance B1\_923 scenario projected a decreased flow by -75.8m<sup>3</sup>/s equivalent with -17.2% as compared with current observed flow data set at Gibe III dam site. According to this study the net available mean annual flow at Gibe III reservoir corresponding to future time period 2020-2050 that can be utilized for power generation, irrigation, water supply and other purposes based on five scenarios results are: 459.2m<sup>3</sup>/s, 423m<sup>3</sup>/s, 417.4m<sup>3</sup>/s, 354.4m<sup>3</sup>/s, and 429.7m<sup>3</sup>/s and the average of all the scenarios is found as 416.7m<sup>3</sup>/s (Table 8.6).

## 8.5 Estimation of flow duration curve from net inflow at gibe III dam

### site

One of the most commonly used techniques in hydrology is the flow duration curve (FDC), which provides a graphical representation of the frequency distribution of the complete flow regime. Using the FDC, it is possible to determine the percentage of time that a specified flow is equaled or exceeded. This type of information is commonly used for resource assessments including hydropower design schemes, water supply and water quality assessment and the evaluation of river habitats (Croker et.al, 2009). Flow duration curve analysis identifies intervals, which can be used as a general indicator of hydrologic conditions (i.e., wet versus dry and severity). Flow duration curve intervals can be grouped into several broad categories, or zones. These zones provide additional insight about conditions and patterns associated with the impairment. A common way to look at the duration curve is by dividing it into five zones, representing high flows (0-10%), moist conditions (10-40%), mid-range flows (40-60%), dry conditions (60-90%), and low flows (90-100%) exceedence probability (Narayanan et. al., 2011).

As this flow duration curve has major advantage in characterizing the flow conditions of a river, for this particular study this curve is derived from observed and projected flow data set in order to provide a good insight on future flow conditions of Omo basin at Gibe III dam site. According to the recommendation made by (Narayanan et. al., 2011) and hydrologic condition of Gibe basin, the curve has been divided in to five zones to derive important information's from this curve for future water use. Comparisons between observed and projected FDC has been made by characterizing the derived FDC in two low flows range from (90-100) %, dry flows range from (60-90) %, mid flows range from (40-60) %, moist flows range (10-40) %, and high flows range (0-10) % exceedence probability. This comparison helps to visualize the hydrologic changes between current and future time flow. The results have been drawn in two graphs (figure 8.3) for the purpose of identifying the differences between observed and projected FDC clearly.

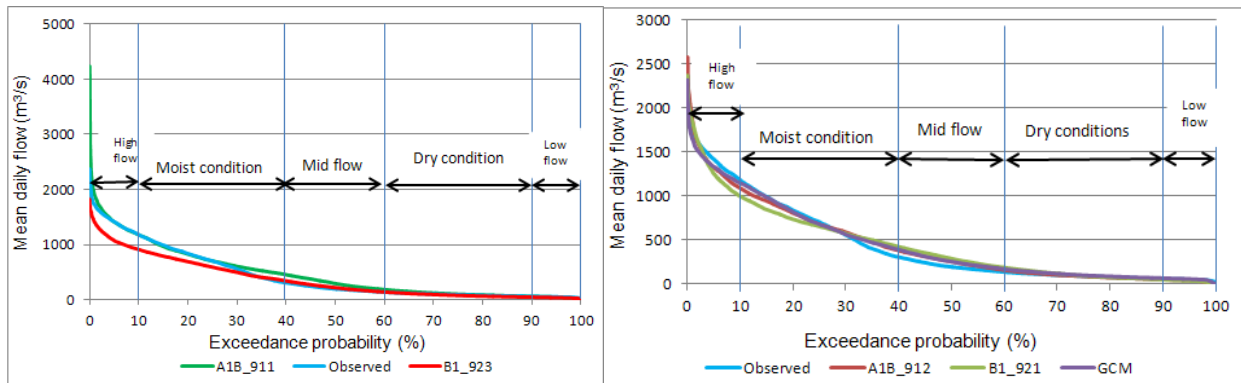


Figure 8.3 Observed and projected flow duration curves

Figure 8.3 shows FDC of observed and all projected scenarios, the left panel deep blue solid curve represents the FDC for observed and red line projected FDC from B1\_923 the comparison of these two curves show significant deficits of flow projected from B1\_923 scenario during high and moist flow ranges conditions, for the rest of the conditions the two curves follow a very similar pattern. Results from A1B\_911 projection shows similar pattern with observed FDC except mid-range flow conditions and a very extreme value when the exceedance probability approaches to zero, at mid-range flow condition this projection showed increased flow. The other scenarios FDC right panel doesn't show visible difference with observed FDC.

## 8.6 Conclusion

In addition to calibrated model parameters at Gibe III dam site future time downscaled temperature, precipitation and radiation sequences were used to produce corresponding time streamflow sequences from five scenarios data sets. The potential effects of climate change on the hydrology and water resources potential of the Omo Gibe River basin at Gibe III dam site were assessed by comparing the projected outputs from five simulated outputs and observed mean annual, seasonal, high and low flows. According to the results climate change has shown strong signal on seasonal flow than mean annual flow. Spring is small rainy season in the northern part of the basin, all projected flow for this season showed increased flow due to increased forecasted areal rainfall; this might be a very good opportunity to get more water during small runoff time that can be used for power generation and other purposes, however, the autumn season flow showed reduction from all scenarios due to decreased precipitation and increased temperature.

The net annual runoff in the projected run from A1B\_911 was about 6.7% higher than observed runoff. However, the projected net annual runoff from B1\_923 moderately decreased by 75.8m<sup>3</sup>/s which is equivalent with 17.2%, this might have a significant influence in degrading the total available water resources potential in the basin. In order to have clear insight on the changes of the projected inflow to Gibe III dam site, flow duration curve have been developed, therefore the overall results of this study and the scenarios output can be used as a primary input for further water resources development and water resources management projects in the basin. According to this study in Gibe basin for a temperature change of 1.5<sup>0</sup>C without changing the rainfall pattern, the mean annual flow will be decreased by 8.6%. And all the scenarios result showed increased temperature throughout Gibe basin. Under such circumstances knowing the amount of flow under climate change consideration will have a vital importance for sustainability of the developmental projects. Therefore, the results of this study can be used as a quick access to water resources potential of the basin in consideration of climate change. I personally believe that the results of this study can be used as a primary input to design the proposed Gibe VI and V hydropower projects and other developmental projects in the basin.

# Chapter 9 Conclusions and recommendations

## 9.1 Conclusions

Nowadays, sustainable water resources management faced challenges from climate change. Surface air temperature has increased all over the world; however its degree of severity differs from region to region. As the temperature increases the energy that is required to evaporate surface water will also increase, thereby reduction of the scarce water resources potential will occur. Under such circumstances knowing the amount of this scarce water resources potential that can be used for power generation, irrigation, water supply and other useful developmental projects under climate change considerations will have a vital importance for sustainability of the developmental projects. One of the big gaps in relation to climate change in developing countries like Ethiopia is lack of studied documents in relation to this vital issue in different parts of the basin. However, most African countries like Ethiopia might face a big challenge from climate change.

Omo Gibe basin is one of the most strategic basins for Ethiopia to develop huge amount of hydropower and irrigation projects, because the basin water resources potential and its geographical land scape provide a good opportunity for hydropower production. Whereas the available vast land in the southern part of the basin makes it favorable for irrigation development. In consideration of these issues this thesis assessed the overall water resources potential for current and future time period by modeling the basin under climate change scenarios using semi distributed hydrological model (SWIM). Before modeling the basin under climate change scenarios reference time water resources potential of the basin has been estimated by using different common approaches and the whole hydrological and physiographic characteristics of the basin above Gibe III dam site. As a result 29 years daily discharge data sets have been determined from un-gauged and the whole basin of Gibe III dam site.

All semi distributed hydrological models need spatial, temporal and time series data to fulfill their objectives. Organized soil data base was one of the most important inputs for sound modeling procedure at the studied watershed. However, such organized data system was not available throughout the basin. In consideration of this 32 soil data bases out of 8 main soil types have been developed for upper part of the basin.

On the other hand semi-distributed physically based model (SWIM) calibrated and validated guided by sensitivity analysis, from current climate and water resources potential of the basin with a very good performance and negligible overall water difference between observed and simulated discharge at the case study area. Finally, based on calibrated parameters from reference time and projected climate data sets for future time, flow at Gibe III dam site corresponding to 2020-2050 have been projected from five scenarios.

From overall study of this thesis the following specific conclusions can be drawn:

- Due to the coarse spatial resolution and simulations of Remo and GCM model outputs, their precipitation and temperature cannot be directly used as an input to hydrological model to study effects of climate change in the basin. Because of this two different types of downscaling mechanism have been used to downscale current and future time climate data in Omo Gibe basin. One of the methods was SDSM and the other one distribution mapping technique. The performance of these methods has been checked by comparing observed climate against current downscaled climate data sets. Moreover, the procedures were validated by applying a number of methodologies. As a result reliable estimation of future climate data 2020-2050 was projected. On the other hand the errors (uncertainty) associated with SDSM and CDM has been evaluated, based on the absolute error in estimates of mean monthly temperatures and precipitation, dry and wet spell lengths of the estimate. According to this evaluation cumulative distribution mapping technique performed better than SDSM.

- The downscaled results from five scenarios projected increased temperature throughout the studied basin. The statistical downscaling results for minimum temperature in Omo Gibe basin showed that minimum temperature will rise in a faster rate than that of maximum temperature. The average results of all scenarios estimated that, current mean annual maximum and minimum temperature is expected to rise by about from 0.9 °C to 1.8 °C and 1.2 °C to 2.2 °C above Gibe III dam site respectively. Rainfall behavior showed no marked emergent. However, it showed mixed patterns of rainfall change. According to the result four of the scenario A1B\_911, A1B\_912, B1\_921 and GCM\_A2 projected increasing trend in mean annual areal precipitation by 6.5%, 2.4%, 1.9% and 4.5% at the end of 2050. While one scenario B1\_923 shows a decreasing trend of areal precipitation by 1.4% above Gibe III dam site.
- SWIM was calibrated at Ableti station for the purpose of deriving daily flow data from un-gauged basin. The result of the model was validated by comparing with different outputs that have been computed by using different common methodology to confirm the reliability of the result. Finally daily flow data at Gibe III dam site was estimated by routing observed daily flow at Abelti, Wabi, and OM19 and then added with SWIM results from un-gauged basin to obtain total flows enters to Gibe III reservoir for reference time period. Accordingly the mean annual discharge for current time (1970-1998) at Gibe III reservoir found as 430.2m<sup>3</sup>/s. Following this; calibration, validation and sensitivity analysis of the model were carried out at Gibe III dam site for the purpose of studying effects of climate change on Gibe III inflow.
- The sensitivity analysis pointed out eight most critical parameters that control the surface, sub-surface and evaporation hydrological processes of the studied area. Three of the model parameters have found as the most sensitive parameters Thc, Roc4 and Sccor. On the other hand, calibration and validation results on Abelti and Gibe III dam site simulated the observed flows quite satisfactory. The capability of SWIM in simulating hydrological processes in larger area would better as compared to smaller areas.
- All the calibrated model parameters together with projected precipitation, radiation, maximum and minimum temperature were used as input to SWIM to project daily flow at Gibe III dam site corresponding to 2020-2050. The projected flow from five scenarios were analysed to quantify climate change impact based on high, low, seasonal, mean annual flows one by one. The analysis showed strong climate change signal in seasonal flow than mean annual flow. Two of the scenarios showed relatively big discrepancies between current and projected time mean annual series. Before evaporation losses from Gilgel Gibe I and Gibe III, A1B\_911 scenario projected 10% excess mean annual flows. However, B1\_923 projected 15% less mean annual flows in 2020-2050.
- Evaporation losses corresponding to future time from the aforementioned reservoirs have been calculated based on modified Penman and Priestly Taylor equations, the combined gross evaporation losses from the two artificial lakes projected as 12.8m<sup>3</sup>/S. On the other hand net projected mean monthly and mean annual inflow to Gibe III reservoir estimated by reducing evaporation losses from the lakes. One of the scenarios A1B\_911 projected 6.7% higher net mean annual flows, whereas B1\_923 projected a significant portion of reduced net mean annual flows by 17.2%.
- The outcomes of these results are based on 2 climate model outputs GCM and RCM. The results from RCM are based on two emission scenarios A1B and B1 each of them has results simulated for three conditions. The range of greenhouse gas (GHG) emission in A1B is greater than B1, however, the projected precipitation from A1B scenario at Gibe basin was higher than observed precipitation by small amount, this indicated that even for higher emission scenario the basin will not face severe drought conditions. However, due to the increased temperature, the evaporation condition of the basin will be high. As a result for 1.5°C raise in mean annual surface air temperature the mean annual flow reduced by 8.6%. This result indicated that due to the change in temperature water will be lost in the form of evaporation from the basin. One of the big challenges regarding to climate change in the basin is increased temperature.

Generally, this study applied the successful application of cumulative distribution mapping technique especially for downscaling of REMO outputs to studied basin. As a result reliable and bias free climate data have been projected. The combined efforts of hydrological simulations and climate projections enabled to project future time net flow at Gibe III reservoir from five scenarios, which can be used as quick access to water resources potential of the basin under climate change condition for decision makers and designers for any developmental projects.

## 9.2 Recommendations

According to this study the following recommendations suggested:

- SWIM has never been used in Ethiopia basins before, however the performance of this model on Gibe basin was quite well and very good in simulating different components of hydrological processes, as the model is public domain and freely available it would be worthwhile to use this model on other basins for similar purpose.
- The projected net flow at Gibe III dam site presented in this study can be used as quick access as primary input, to any developmental projects in the basin, in order to consider climate change with their design. According to this study the worst case scenario can be taken as B1\_923 projection. However, more study by considering other GCMs, RCM and different scenarios and different downscaling methodology should be conducted.
- Availability of hydrological and climatological data are very important while using any hydrological model. The distribution of these gauging stations in studied basin is not well organized. Most of weather observation stations concentrated in the northern part of the basin; therefore, new weather observation stations to south western part of the basin should be established. Moreover, most hydrological stations measured flow from small catchment except Abelti. The application of SWIM in the basin was one of the biggest challenges without having daily flow data at the point of interest. Therefore, the uses of new data gathering technique should be envisage. Additional flow measuring stations should be established on main Omo River at Bele, Omorate and other strategic sites.

## References

- Adem G. (2005). Modeling ground water-surface water interaction by coupling MODFLOW with WetSpa. M.Sc. thesis, Vrije Universiteit Brussel, Belgium.
- Arndt, Channing, Hashim Ahmed, Sherman Robinson, and Derk Willenbockel (2009). Climate Change and Ethiopia. Climate Change: Global Risks, Challenges and Decisions IOP Conference Series:Earth and Environmental Science.
- Allen, R.G., Pereira, L.S., Raes, D., and Smith, M. (1998). Crop evapotranspiration Guidelines for computing crop water requirements FAO Irrigation and Drainage Paper 56, Food and Agriculture Organization of the United Nations
- Artur J. Lemonte (2011): Improved point estimation for the Kumaraswamy distribution, Journal of Statistical Computation and Simulation, [http:// 81:12, 1971-1982](http://dx.doi.org/10.1080/00949655.2010.511621)
- Awulachew, S. B., Yilma, A. D., Loulseged, M., Loiskandl, W., Ayana, M., Alamirew, T. (2007). water resources and irrigation vevopment in Ethiopia. Colombo, Sri Lanka: international water management institute. 78p. (Working Paper 123) ISBN 978-92-9090-680-3
- Arnold, J.G., (1990). ROTO A continuous water and sediment routing model. ASCE Proc. of the Watershed Management Symposium. Durango, Co, 480-488.
- Arnold JG, Williams JR, Nicks AD, Sammons NB. (1990). SWRRB—A Basin Scale Simulation Model for Soil and Water Resources Management. Texas A&M University Press: College Station, TX; 255p.
- Arnold JG., Allen PM., Bernhardt G. (1993). A comprehensive surface—groundwater flow model. Journal of Hydrology 142: 47–69.
- Arnold, J.G., Williams, J.R., Srinivasan, R., King, K.W., Griggs, R.H., (1994). SWAT, Soil and Water Assessment Tool, USDA, Agriculture Research Service, Grassland, Soil & Water Research Laboratory, 808 East Blackland Road, Temple, TX 76502.
- Bates B., Kundzewicz C., Wu W., Palutikof P. (eds) (2008). Climate change and water. Technical Paper of the Intergovernmental Panel on Climate Change. Geneva, Switzerland, IPCC Secretariat, p 210.
- Berger, K. P., & Entekhabi D. (2001). Basin hydrological response relations to distributed physiographic descriptors and climate. J. Hydrol. 247:169–182.
- Binquet P., Asnake J., Ravetta A., Alami E., (2013). The 1870 MW Gibe HPP procurement method and status of the design and construction the view point of EEPCo and its perspective. A paper presented on International Conference and Exhibition on Water Storage and Hydropower Development for Africa, African Union Congress Centre, Addis Ababa, Ethiopia.
- Biggs JS., et al (2012). Interactions between climate change and sugarcane management systems for improving water quality leaving farms in the Mackay Whitsunday region, Australia. Agriculture, Ecosyst Environ. doi:[10.1016/j.agee.2011.11.005](https://doi.org/10.1016/j.agee.2011.11.005)
- Blöschl G., Sivapalan M., Wagener T., Viglione A. and Savenje H (2013). Runoff prediction in un-gauged basins, Cambridge University press, NY 465P.

- Boko M., I. Niang, A. Nyong, C. Vogel, C. A. Cutheko, M. Medany, B. Osman-Elasha, R. Tobo, P. Yonda, "Africa in: Parry in Canziano," In: J. Palutikof, P. Vander Lenden and C. Harison, Eds., *Climate Change (2007). Impacts, Adaptation and Vulnerability. Working Group II Contribution to the Fourth Assessment Report of the Intergovernmental Panel on Climate Change*, Cambridge University Press, Cambridge, pp. 433-467.
- Brekke LD., Maurer EP., Anderson JD., Dettinger MD., Townsley ES., Harrison A., Pruitt T. (2009). Assessing reservoir operations risk under climate change. *Water Resour Res* 45:W04411. doi:[10.1029/2008WR006941](https://doi.org/10.1029/2008WR006941)
- Brooks, K.N., P.F., Ffolliott, H.M., Gregersen and J.L. Thames, (1991). *Hydrology and the Management of Watersheds*. Iowa State University Press, Ames, USA.
- Byerlee, D., Spielman, D.J., Alemu, D., Gautam, M., (2007). Policies to promote Cereal Intensification in Ethiopia. A Review of Evidence and Experience. International Food Policy Research Institute. Development Strategy and Governance Division, Discussion Paper 00707.
- Chow, V.T., (1964). *Handbook of applied hydrology*. McGraw-hill Book company, USA
- C. McSweeney, M. New, and G. Lizcano UNDP Climate Change Country Profiles, Ethiopia available at: <http://country-profiles.geog.ox.ac.uk>.
- Chernobai, A.S., F. J. Fabozzi, and S. T. Rachev (2007). *Operational Risk: A Guide to Basel II Capital Requirements, Models, and Analysis*, John Wiley & Sons, New York.
- Choudhury, P., Shrivastava, R. K., and Narulkar, S. M. (2002). Flood routing in river networks using equivalent Muskingum inflow. *Journal of Hydrologic Engineering*, 7(6), 413-419. [doi:[10.1061/\(ASCE\)1084-0699\(2002\)7:6\(413\)](https://doi.org/10.1061/(ASCE)1084-0699(2002)7:6(413))]
- Chow, V.T., D.R. Maidment and L.W. Mays, (1988). *Applied Hydrology*. McGraw-Hill, USA.
- Cooper MP, Beevers MD, Oppenheimer M (2008) The potential impacts of sea level rise on the coastal region of New Jersey, USA. *Clim Chang* 90:475–492. doi:[10.1007/s10584-008-9422-0](https://doi.org/10.1007/s10584-008-9422-0)
- Craft C, Clough J, Ehman J, Joye S, Park R, Pennings S, Guo H, Machmuller M (2009). Forecasting the effects of accelerated sea-level rise on tidal marsh ecosystem services. *Front Ecol Environ* 7(2):73–78. doi:[10.1890/070219](https://doi.org/10.1890/070219)
- Croker, K. M., Young, A. R., Zaidman, M. D., & Rees, H. G. (2009). Flow duration curve estimation in ephemeral catchments in Portugal. *Hydrological Sciences Journal*, 48(3), 427–439. doi:[10.1623/hysj.48.3.427.45287](https://doi.org/10.1623/hysj.48.3.427.45287)
- Cunderlik, M.J., (2003). *Hydrologic model selection for the CFCAS project: Assessment of water resources risk and vulnerability to changing climatic conditions*, Project Report I. University of Western Ontario, Canada.
- Conway, D., & Schipper, E. L. F. (2011). Adaptation to climate change in Africa: Challenges and opportunities identified from Ethiopia. *Global Environmental Change*, 21(1), 227–237. doi:[10.1016/j.gloenvcha.2010.07.013](https://doi.org/10.1016/j.gloenvcha.2010.07.013)
- Coulibaly P., Dibike Y.B., Anctil, F. (2005). Downscaling precipitation and temperature with temporal neural networks. *Journal of Hydrometeorology*, 6(4): 483-496.
- Dai A. (2011). Drought under global warming WIREs *Clim Change* 2 45–65 DOI: [10.1002/wcc.81](https://doi.org/10.1002/wcc.81)
- Deressa and T.T. (2006) *Measuring the Economic Impact of Climate Change on Ethiopian Agriculture: Ricardian Approach*. CEEPA Discussion Paper No.25. Centre for Environmental Economics and Policy in Africa: University of Pretoria.



Dingman and S.L. (2002). Physical Hydrology. 2nd Edn., Prentice Hall, New Jersey, USA pp. 646.

Sean Avery (2013) Lake Turkana & the lower Omo hydrological impacts of major dam & irrigation developments Volume I, African study centre university of Oxford.

Donner SD, Little CM, Oppenheimer M., Hoegh-Guldberg O. (2005). Global assessment of coral bleaching and required rates of adaptation under climate change. *Glob Chang Biol* 11(12):2251–2265

Döll, P., & Schmied, H. M. (2012). How is the impact of climate change on river flow regimes related to the impact on mean annual runoff. A global-scale analysis. *Environmental Research Letters*, 7(1), 014037. doi:10.1088/1748-9326/7/1/014037

Doherty J. (2002) PEST, model independent parameter estimation, user manual 297p

EEPCo. (2004) Gilgel Gibe II hydroelectric project design (General report) Prepared by Salini contractor, submitted to Ethiopian power and electric corporation Addis Ababa Ethiopia 42p

EEPCoa. (2009) Omo-Gibe River hydropower cascade: prepared by Gibe III technical team Addis Ababa, Ethiopia 1p

EEPCO. (2009) Environmental and social management plan for Gibe III hydroelectric project: prepared by Salini contractor and MDI international consulting engineers 238p

Elshamy ME, Seierstad IA, Sorteberg A. (2009): Impacts of climate change on Blue Nile flows using bias-corrected GCM scenarios: *Hydrol Earth Syst Sci* 13: 551-565.

Enelpower/Elc-Electroconsult (2004), Gilgel Gibe hydroelectric project, final report on the project implementation, submitted to The Federal Democratic Republic of Ethiopia Ethiopian Electric Power Corporation.

ERG. (2009). Diversity and Security for the Ethiopian Power System: A preliminary assessment of risks and opportunities for the power sector. Ethio Resource Group (ERG) for Heinrich Boll Foundation (HBF) and Forum for Environment (FfE) Addis Ababa, Ethiopia. 52p

FDRE, Federal democratic republic of Ethiopia, (2012) Ethiopia's Climate-Resilient Green Economy, Green economy strategy. Ethiopia's action plan to create a green economy. Addis Ababa, Ethiopia 200p

Fowler HJ, Blenkinsop S, Tebaldi C. (2007). Linking climate change modelling to impact studies: recent advances in downscaling techniques for hydrological modelling. *International Journal of Climatology* 27: 1547–1578, DOI: [10.1002/joc.1556](https://doi.org/10.1002/joc.1556)

Fowler HJ, Kilsby CG. (2007). Using regional climate model data to simulate historical and future river flows in northwest England. *Climatic Change* 80: 337–367.

Frevert, D.K., Singh, V.P. (2002). *Mathematical Models of Large Watershed Hydrology*. [s. l.] : WRP, 914 p. ISBN 1-88720-34-3.

Ganji A., K. Ponnambalam, and D. Khalili (2006). Grain yield reliability analysis with crop water demand uncertainty, *Stoch. Environ. Res. Risk Assess.* 20: pp. 259–277.

Ghandhari, A. and Moghaddam S., (2011). Water balance principles, A review of studies on five watersheds in Iran. *Journal od Env. Sci. Tech.* 4:465-478

Getaneh A. (2013). Current capacity building initiatives in Ethiopia for water resources development and management. A paper presented on International Conference and Exhibition

on Water Storage and Hydropower Development for Africa, African Union Congress Centre , Addis Ababa, Ethiopia.

Geographica, A., & Comenianae, U. (2010). Rainfall-Runoff modelling : its development, classification, 54(2), 173–181.

Gove J. H., M. J. Ducey, W. B. Leak, and L. Zhang (2008). Rotated sigmoid structures in managed uneven-aged northern hardwood stands: A look at the Burr Type III distribution, *Forestry*, 81:21-36.

Grizzetti, B., F. Bouraoui, K. Granlund, S. Rekolainen, and G. Bidoglio (2003). Modelling diffuse emission and retention of nutrients in the Vantaanjoki watershed (Finland) using the SWAT model. *Ecological Modelling* 169:25-38.

Gosain, A.K., A. Mani and C. Dwivedi, (2009). Hydrological Modelling-Literature Review. *Climawater*, Report NO.1.

Goosse H., P.Y. Barriat, W. Lefebvre, M.F. Loutre and V. Zunz, (date of view, June 2013). Introduction to climate dynamics and climate modeling. Online textbook available at <http://www.climate.be/textbook>.

Hattermann, F. F., Krysanova, V., & Hesse, C. (2008). Modelling wetland processes in regional applications. *Hydr. Scie. Journal* 53(5), 1001–1012. doi:[10.1623/hysj.53.5.1001](https://doi.org/10.1623/hysj.53.5.1001)

Hardie, M. a., Doyle, R. B., Cotching, W. E., & Lisson, S. (2012). Subsurface Lateral Flow in Texture-Contrast (Duplex) Soils and Catchments with Shallow Bedrock. *Applied and Environmental Soil Science*, 2012, 1–10. doi:[10.1155/2012/861358](https://doi.org/10.1155/2012/861358)

Headrick, T. C., Pant, M. D., & Sheng, Y. (2010). On Simulating Univariate and Multivariate Burr Type III and Type XII Distributions, 4(45), 2207–2240.

Hinkel J, Nicholls RJ, Vafeidis AT, Tol RSJ, Avagianou T (2010) Assessing risk of and adaptation to sea-level rise in the European Union: an application of DIVA. *Mitig Adapt Strateg Glob Chang* 15:703–719. doi:[10.1007/s11027-010-9237-y](https://doi.org/10.1007/s11027-010-9237-y)

Huang, S., Hesse, C., Krysanova, V., & Hattermann, F. (2009). From meso- to macro-scale dynamic water quality modelling for the assessment of land use change scenarios. *Ecological Modelling*, 220(19), 2543–2558. doi:[10.1016/j.ecolmodel.2009.06.043](https://doi.org/10.1016/j.ecolmodel.2009.06.043)

Huang, S., Krysanova, V., Österle, H., & Hattermann, F. F. (2010). Simulation of spatiotemporal dynamics of water fluxes in Germany under climate change. *Hydrological Processes*, 24(23), 3289–3306. doi:[10.1002/hyp.7753](https://doi.org/10.1002/hyp.7753)

Hunt A, Watkiss P (2011) Climate change impacts and adaptation in cities: a review of the literature. *Clim Chang* 104:13–49. doi:[10.1007/s10584-010-9975-6](https://doi.org/10.1007/s10584-010-9975-6)

I. W. Burr. (1973). Parameters for a general system of distributions to match a grid of  $\alpha_3$  and  $\alpha_4$ , *Communications in Statistics*, 2:1-21.

IAHS Decade on Predictions in Ungauged Basins (PUB), (2003). *Hydrological sciences J.* 48 (6). 857-880.

Ines AVM, Hansen JW. (2006). Bias correction of daily GCM rainfall for crop simulation studies. *Agricultural and Forest Meteorology* 138:44–53.

IPCC, (2000). Emissions scenarios special report on IPCC A Special Report of IPCC Working Group III 27p

IPCC, (2001). *Climate Change (2001): The Scientific Basis*. Contribution of Working Group I to the Third Assessment Report of the Intergovernmental Panel on Climate Change [Houghton, J.T., Y. Ding, D.J. Griggs, M. Noguer, P.J. van der Linden, X. Dai, K. Maskell, and C.A. Johnson (eds.)]. Cambridge University Press, Cambridge, United Kingdom and New York, NY, USA, 881pp.

IPCC-TGICA, (2007). *General Guidelines on the Use of Scenario Data for Climate Impact and Adaptation Assessment*. Version 2. Prepared by T.R. Carter on behalf of the Intergovernmental Panel on Climate Change, Task Group on Data and Scenario Support for Impact and Climate Assessment, 66 pp.

IPCC, (2007). *Climate Change 2007: Impacts, Adaptation and Vulnerability*. Contribution of Working Group II to the Fourth Assessment Report of the Intergovernmental Panel on Climate Change, M.L. Parry, O.F. Canziani, J.P. Palutikof, P.J. van der Linden and C.E. Hanson, Eds., Cambridge University Press, Cambridge, UK, 976pp.

IPCC, (2010), statement on the melting of Himalayan glaciers. A statement from the Chair and Vice-Chairs of the IPCC, and the Co-Chairs of the IPCC Working Groups

IPCC, (2012). *Renewable Energy Sources and Climate Change Mitigation*, special report of the Intergovernmental Panel on Climate Change, Technical Support Unit Working Group III Potsdam Institute for Climate Impact Research (PIK) Cambridge university press.

Iglesias A, Rosenzweig C, Pereira D. (2000) Prediction spatial impacts of climate in agriculture in Spain. *Glob Environ Chang* 10:69–80

Jacobs, K., Adams, D. B., and Gleick, P. (2000). Potential Consequences of Climate Variability and Change for the Water Resources of the United States, Chapter 14: US National Assessment of the Potential Consequences of Climate Variability and Change, p.405- 435. Cambridge University Press, United States. Available at: <http://www.usgcrp.gov/usgcrp/Library/nationalassessment/14Water.pdf>

Jacob D. (2001): A note to the simulation of the annual and inter-annual variability of the water budget over the Baltic Sea drainage basin. *Meteorology and Atmospheric Physics* 77: 61-73.

Jajarmizadeh, M., Harun, S., & Salarpour, M. (2013). An Assessment on Base and Peak Flows Using a Physically-Based Model, *Research Journal of Environmental and Earth Sciences* 5(2), 49–57.

Jakob Themeßl, M., Gobiet, A., & Leuprecht, A. (2011). Empirical-statistical downscaling and error correction of daily precipitation from regional climate models. *International Journal of Climatology*, 31(10), 1530–1544. doi:[10.1002/joc.2168](https://doi.org/10.1002/joc.2168)

J. Schulla (2007) model description WaSiM-ETH, water balance simulation model, Zurich. 181p

Jones, M. C. (2009). Kumaraswamy's distribution: A beta-type distribution with some tractability advantages. *Statistical Methodology*, 6(1), 70–81. doi:[10.1016/j.stamet.2008.04.001](https://doi.org/10.1016/j.stamet.2008.04.001)

Jones M.C. (2009). Kumaraswamy's distribution: A beta-type distribution with some tractability advantages, *Statist. Methodol.* 6:70–91.

Joshua C. Galster (2009). Testing the linear relationship between peak annual river discharge and drainage area using long-term USGS river gauging records *Geological Society of America* v. 451, p. 159-171

Kassa T. (2009) *Watershed Hydrological Responses to Changes in Land Use and Land Cover, and Management Practices at Hare Watershed, Ethiopia* PHD thesis. University of Siegen, Germany

- Khan, M. S., Coulibaly, P., & Dibike, Y. (2006). Uncertainty analysis of statistical downscaling methods. *Journal of Hydrology*, 319(1-4), 357–382. doi:[10.1016/j.jhydrol.2005.06.035](https://doi.org/10.1016/j.jhydrol.2005.06.035)
- Kinfe Hailemariam. (1999). Impact of climate change on the water resources of Awash River Basin, Ethiopia. *Journal of Climate Research*. 12: 91–96.
- Knisel WG (ed.). (1980). CREAMS: A field scale model for chemicals, runoff, and erosion from agricultural management systems. USDA Conservation Research Report 26: p643.
- Krysanova V, Müller-Wohlfeil DI, Becker A. (1998a). Development and test of a spatially distributed hydrological/water quality model for mesoscale watersheds. *Ecological Modelling* 106: 261–289.
- Krysanova V, Meiner A, Roosaare J, Vasilyev A. (1989). Simulation modelling of the coastal waters pollution from agricultural watershed. *Ecological Modelling* 49: 7–29.
- Krysanova, V., Hattermann, F., & Wechsung, F. (2005). Development of the ecohydrological model SWIM for regional impact studies and vulnerability assessment. *Hydrological Processes*, 19(3), 763–783. doi:[10.1002/hyp.5619](https://doi.org/10.1002/hyp.5619)
- Krysanova, V., & Arnold, J. G. (2008). Advances in ecohydrological modelling with SWAT—a review. *Hydrological Sciences Journal*, 53(5), 939–947. doi:[10.1623/hysj.53.5.939](https://doi.org/10.1623/hysj.53.5.939)
- Laaha, G. & Blöschl, G. (2007) A national low flow estimation procedure for Austria. *Hydrol. Sci. J.* 52(4), 625-644.
- Laprise, R. (2008). Regional climate modelling. *Journal of Computational Physics*, 227(7), 3641–3666. doi:[10.1016/j.jcp.2006.10.024](https://doi.org/10.1016/j.jcp.2006.10.024)
- Leonard RA, Knisel WG, Still DA. (1987). GLEAMS: Groundwater loading effects on agricultural management systems. *Transactions of the ASAE* 30(5): 1403–1428.
- Matonse AH., Pierson DC., Frei A., Zion MS., Schneiderman EM., Anandhi A., Mukundan R. Pradhanang SM. (2011). Effects of changes in snow pattern and the timing of runoff on NYC water supply system. *Hydrol Process* 25:3278–3288. doi:[10.1002/hyp.8121](https://doi.org/10.1002/hyp.8121)
- Lewarne, M., 2009. Setting up arcswat hydrological model for the verloreenvlei catchment. Master Thesis, Stellenbosch University.
- Maidment, D.R. (ed.) (1993). *Handbook of hydrology*. McGraw-Hill, Inc. New York.
- Matthew J. Fleming (2010). *Hydr. modeling system HEC-HMS, Quick start guide version 3.5*
- McCarthy, J.J., Canziani, O.F., Leary, N.A., Dokken, D.J., & White, K.S. (eds.) *Climate Change (2001): Impacts, Adaptation and Vulnerability .Contribution of Working Group II to the Third Assessment Report of the Intergovernmental Panel on Climate Change*. Cambridge University Press, Cambridge, pp. 195-233.
- McSweeney C., M. New and G. Lizcano (date of visit, May 2013), *UNDP Climate Change Country Profiles, Ethiopia* 27p, available at <http://country-profiles.geog.ox.ac.uk>
- Meehl G. A. Solomon S., Qin D., Manning M., Chen Z., Marquis M., Averyt K. B., Tignor M., Miller H. L. (2007): *Global climate projections Climate change 2007: the physical science basis. Contribution of Working Group I to the Fourth Assessment Report of the Intergovernmental Panel on Climate Change* pp. 433–497 Cambridge, UK Cambridge University Press.

Meenu R., Rehana S. & Mujumdar P. (2013). Assessment of hydrologic impacts of climate change in Tunga-Bhadra river basin, India with HEC-HMS and SDSM. *Hydrological Processes*, 27(11), 1572–1589. doi:[10.1002/hyp.9220](https://doi.org/10.1002/hyp.9220)

Meehl G, Tebaldi C, Walton G, Easterling D, McDaniel L (2009). Relative increase of record high maximum temperatures compared to record low minimum temperatures in the US. *Geophys Res Lett* 36:L23701. doi:[10.1029/2009GL040736](https://doi.org/10.1029/2009GL040736)

Mendelsohn R, Nordhaus WD, Shaw D (1994) The impact of global warming on agriculture: a Ricardian analysis. *Am Econ Rev* 84(4):753–771.

Milad Jajarmizadeh, Sobri Harun and Mohsen Salarpour, (2012). A Review on Theoretical Consideration and Types of Models in Hydrology. *Journal of Environmental Science and Technology*,5:249-261. DOI:[10.3923/jest.2012.249.261](https://doi.org/10.3923/jest.2012.249.261)

Mielke, P.W., Another family of distributions for describing and analyzing precipitation data, *Journal of Applied Meteorology*, 12 (1973), 275-280.

Monteith, J.L., (1965). Evaporation and environment. *Symp. Soc. Exp. Biol.* 19: 205-234.

MoWE, (2001): Initial National Communication of Ethiopia to the United Nations Framework Convention on Climate Change (UNFCCC). Addis Ababa, Ethiopia 127p.

Mohammad S.K., Paulin C. and Yonas D. (2006). Uncertainty analysis of statistical downscaling methods: *Jou. Of Hyd.* 319:357-382

Mujumdar, P. P., & Ghosh, S. (2008). Modeling GCM and scenario uncertainty using a possibilistic approach: Application to the Mahanadi River, India. *Water Resources Research*, 44(6), n/a–n/a. doi:[10.1029/2007WR006137](https://doi.org/10.1029/2007WR006137)

Narayanan K., Jahak J. (2011) An Approach for Estimating Stream Health Using Flow Duration Curves and Indices of Hydrologic Alteration, *Agri Life research and extension Texas A&M system* 65 pages

Nadarajah S. and S. Kotz (2006) q exponential is a Burr distribution, *Physics Letters A*, 359: 577-579.

Nadarajah S. (2008): On the distribution of Kumaraswamy, *J. Hydrol.* 348 (2008), pp. 568–569.

Neitsch, S.L., Arnold G.G., Kiniry J.R. and Williams (2005). Soil and water assessment tool, File documentation version 20 Texas agricultural experiment station.

NMAE, (2007). Climate Change National Adaptation Programme of Ethiopia (NAPA). Addis Ababa, Ethiopia 96p

Nicholls RJ, Tol RSJ (2006) Impacts and responses to sea-level rise: a global analysis of the SRES scenarios over the twenty-first century. *Phil Trans R Soc A* 364:1073–1095. doi:[10.1098/rsta.2006.1754](https://doi.org/10.1098/rsta.2006.1754)

Nicholls RJ, Marinova N, Lowe JA, Brown S, Vellinga P, De Gusmão D, Hinkels J, Tol RSJ (2011) Sea-level rise and its possible impacts given a ‘beyond 4°C world’ in the twenty-first century. *Phil Trans R Soc A* 369:161–181. doi:[10.1098/rsta.2010.0291](https://doi.org/10.1098/rsta.2010.0291)

Nor, N.I.A., S. Harun and A.H.M. Kassim, (2007). Radial basis function modeling of hourly streamflow hydrograph. *J. Hydrol. Eng.*, 12: 113-123.

Oyebande, L. (2001) Water problems in Africa-how can sciences help? *Hydrol. Sci. J.* 46(6), 947-961



- Parry ML, Rosenzweig C, Iglesias A, Livermore M, Fischer G (2004): Effects of climate change on global food production under SRES emissions and socio-economic scenarios. *Glob Environ Chang* 14(1):53–67. doi:[10.1016/j.gloenvcha.2003.10.008](https://doi.org/10.1016/j.gloenvcha.2003.10.008)
- Paeth H. (2005): The climate of tropical and northern Africa – A statisticaldynamical analysis of the key factors in climate variability and the role of human activity in future climate change. Asgard-Verlag: St. Augustin Hippe, Rheinische Friedrich-Wilhelms-Universität Bonn, Germany.
- P. R. Tadikamalla (1980): A look at the Burr and related distributions, *International Statistical Review*, 48:337-344.
- Pechlivanidis, I. G., Jackson, B. M., McIntyre, N. R., & Wheeler, H. S. (2011). Catchment scale hydrological modelling, a review of model types calibration approaches and uncertainty analysis methods in the context of recent developments in technology 13(3), 193-214
- Priestley, C.H.B. & Taylor, R.J., (1972). On the assessment of surface heat flux and evaporation using large scale parameters. *Monthly Weather Review*. 100: 81-92.
- Quanxi S., Heung W., Jun X. and Wai-Cheung Ip2 (2004). Models for extremes using the extended three parameter Burr XII system with application to flood frequency ynylysis: *Hydr. Sci. Jour.* 49(4) p 685-702
- Ritchie, J.T., (1972). A model for predicting evaporation from a row crop with incomplete cover. *Water Resource Res.* 8: 1204-1213.
- Richardson, C.W. & Rictchie, J.T., (1973). Soil water balance for small watersheds. *Trans. ASAE* 16(1): 72-77.
- Richard Woodroofe & associates, (1996), Omo-Gibe River basin Integrated Development Master Plan Study Final Report Vol. VI Water resources Surveys and Inventories, ministry of Water Resources, A.A
- Richard Woodroofe & associates, (1996), Omo-Gibe River basin Integrated Development Master Plan Study Final Report Vol. VII soil and land resource Surveys and Inventories, ministry of Water Resources, A.A
- Santhi, C., J.G. Arnold, J.R. Williams, W.A. Dugas, and L. Hauck. (2001). Validation of the SWAT model on a large river basin with point and nonpoint sources. *J. of the American Water Resources Association* 37(5):1169-1188.
- Salarpour, M., N.A. Rahman and Z. Yusop, (2011). Simulation of flood extent mapping by InfoWorks RS-case study for tropical catchment. *J. Software Eng.*, 5: 127-135.
- Santer BD et al (2011) Separating signal and noise in atmospheric temperature changes: the importance of timescale. *J Geophys Res* 116:D22105. doi:[10.1029/2011JD016263](https://doi.org/10.1029/2011JD016263)
- S. Jemery et al. (2007). Regional climate modelling for the developing world. *American Meteorological Society* DOI:[10.1175/BAMS-88-9-1395](https://doi.org/10.1175/BAMS-88-9-1395)
- Schlenker W, Roberts M (2009) Nonlinear temperature effects indicate severe damages to U.S. crop yields under climate change. *PNAS* 106:15594–15598
- Shaw, E.M., 1983. *Hydrology in practice*. Chapman and hall, London, UK., 569p
- Schulze, R.E. (1995): *Hydrology and Agrohydrology*, University of Natal, Pietermaritzburg, South Africa.

Shao, Q., Wong, H., Xia, J. U. N., & Ip, W. (2005): Models for extremes using the extended three- parameter Burr XII system with application to flood frequency analysis, 49(August 2004). Hydrological Sciences.

Shaw, E.M., (1983). Hydrology in Practice. Chapman and Hall, London, UK., Pages: 569.

SHARMA, K. D., SOROOSHIAN, S., WHEATER, H. (eds.). (2008). Hydrological Modelling in Arid and Semi-Arid Areas. New York : Cambridge University Press, 223 p. ISBN-13 978-0-511-37710-5.

Skolnik S (2011) U.S. summer heat records continue overwhelming cold records by over 8:1. <http://capital.climate.blogspot.com/2011/07/us-summer-heat-records-continue.html>

Singh V.P. and Woolhiser D.A., (2002). Mathematical modeling of watershed hydrology, Journal of Hydrologic Engineering, 7(4), 270-292.

Sloan, P.G., I.D. Morre, G.B. Coltharp, and J.D. Eigel. (1983). Modeling surface and subsurface stormflow on steeply-sloping forested watersheds. Water Resources Inst. Report 142. Univ.Kentucky, Lexington.

Smedema, L.K. & Rycroft, D.W., (1983). Land Drainage - Planning and Design of Agricultural Drainage Systems. Cornell University Press, Ithaca, NY., 376pp.

Surfleet, C. G., Tullos, D., Chang, H., & Jung, I.-W. (2012). Selection of hydrologic modeling approaches for climate change assessment: A comparison of model scale and structures. Journal of Hydrology, 464-465, 233–248. doi:10.1016/j.jhydrol.2012.07.012

Tadikamalla, P. R. (1980) A look at the Burr and related distributions. Int. Stat. Rev. 48, 337–344.

Thornton PK, Jones PG, Alagarswamy G, Andresen J (2009) Spatial variation of crop yield response to climate change in East Africa. Glob Environ Chang 19(1):54–65.

Taylor, P., & Lemonte, A. J. (2011). Journal of Statistical Computation and Improved point estimation for the Kumaraswamy distribution visited at (Jun, 2013), 37–41. (doi.org/10.1080/00949655.2010.511621)

Tejeda, H.A., and B. K. Goodwin (2008). Modeling crop prices through a Burr distribution and analysis of correlation between crop prices and yields using a copula method, Paper presented at the annual meeting of the Agricultural and Applied Economics Association, Orlando, FL, <http://purl.umn.edu/6061>.

Trenberth KE (2011a) Changes in precipitation with climate change. Clim Res 47:123–138. doi:10.3354/cr00953

Trenberth KE, Fasullo JT (2012) Climate extremes and climate change: the Russian heat wave and other climate extremes of 2010. J Climate, submitted.

Trenberth, K. E. (2012). Framing the way to relate climate extremes to climate change. Climatic Change, 115(2), 283–290. doi:10.1007/s10584-012-0441-5

Tsanis IK, Koutroulis AG, Daliakopoulos IN, Jacob D (2011) Severe climate-induced water shortage and extremes in Crete. Clim Chang 106:667–677. doi:10.1007/s10584-011-0048-2

Tobias V., S. Huang, V. Krysanova (2009): MapWindow Interface for SWIM, user manual Potsdam Institute for Climate Impact Research (PIK)



Todd C. Headrich, Mohan D.P., Yanyan S., (2010). On simulating univariate and multivariate Burr type III and type XII distributions: educational psychology and special edition, Southern Illinois University Carbondale. 35p

UN-WATER/WWAP/2006/7 United nation's educational, scientific, and cultural organization world water assessment program: national water development report for Ethiopia, Addis Ababa, Ethiopia 284p

Us army corps of engineers (2010): hydrologic modeling system HEC-HMS user manual version 3.5

Valiantzas, J.D. (2006). Simplified versions for the Penman evaporation equation using routine weather data, *Journal of Hydrology*, 331, 690-702

Varies, O., Kajander, T. and Lemmela, R. (2004). Climate and water: from climate models to water resources management and vice versa. *Climatic Change* 66: 321-344.

Van Griensven A., Meixner T., Grunwald S., Bishop T., Diluzio M. and Srinivasan R. (2006). A global sensitivity analysis tool for the parameters of multi-variable catchment models. *Journal of Hydrology*. 324, 10–23

Vicuna S, Dracup JA (2007): The evolution of climate change impact studies on hydrology and water resources in California. *Clim Chang* 82:327–350. doi:[10.1007/s10584-006-9207-2](https://doi.org/10.1007/s10584-006-9207-2)

Viessman, J.R.W. and G.L. Lewis, (2008): *Introduction to Hydrology*. Prentice Hall, Englewood Cliffs, New Jersey.

Watkiss P. (2009): *Economics of Climate Change: Key Messages*. A paper presented on conference on Climate Change. Kigali, Uganda.

Wagener, T. & Wheeler, H. S. (2006): Parameter estimation and regionalization for continuous rainfall–runoff models including uncertainty. *J. Hydrol.* 320, 152–154.

Wilby, R.L., Dawson, C.W., Barrow, E.M., (2002): SDSM—a decision support tool for the assessment of regional climate change impacts. *Environ. Model. Software* 17, 147–159.

Williams JR, Renard KG, Dyke PT. 1984. EPIC—a new model for assessing erosion's effect on soil productivity. *Journal of Soil and Water Conservation* 38(5): 381–383.

Wing H, Cheung A, Gabriel BS , Singh A (2008): Trends and spatial distribution of annual and seasonal rainfall in Ethiopia. *Int J Climatol* 13: 1723-1734.

Workneh Degefu, (1987). Some aspects of meteorological drought in Ethiopia. pp 23-26 In, *Drought and Hunger in Africa: denying famine a future*, M.H. Glantz (ed.). Cambridge University Press. 457 pp

Wood, A.W., Maurer, E.P., Kumar, A., Lettenmaier, D.P., (2002): Long range experimental hydrologic forecasting for the eastern United States. *J. Geophys. Res.* 107 (D20), 4429, doi:[10.1029/2001JD000659](https://doi.org/10.1029/2001JD000659).

Wood AW et al (2004) Hydrologic implications of dynamical and statistical approaches to downscaling climate outputs. *Clim Change* 62(1–3):189–216

Woolhiser, D.A., D.L. and Brakensiek (1982). *Hydrologic system synthesis. Hydrologic modelling of small watersheds*, American Society of Agricultural Engineers

Xu, C., Widén, E. and Halldin, S. (2005). Modelling hydrological consequences of climate change – progress and challenges. *Advances in Atmospheric Sciences* 22(6): 789-797.

Yimer G, Andreja J, van Griensven A (2009) Hydrological Response of a Catchments to Climate Change in Upper Beles River Basin, Upper Blue Nile, Ethiopia, Nile basin Water Engineering Scientific Magazine 2: 49-59.

Young RA, Onstad CA, Bosch DD, Anderson WP. (1989). AGNPS: A nonpoint source pollution model for evaluating agricultural watersheds. Journal of Soil and Water Conservation 44(2): 168–173.

Yohe, G. (2000): Assessing the role of adaptation in evaluating vulnerability to climate change. Climatic Change 46: 371-390.

Yusuf M. Mohamoud (2008): Prediction of daily flow duration curves and streamflow for ungauged catchments using regional flow duration curves, Hydrological Sciences Journal, 53:4, 706-724 <http://dx.doi.org/10.1623/hysj.53.4.706>

## Appendices

A: Sum of mean monthly and seasonal precipitation comparison between observed corrected and REMO simulated output 1970-2000

Assendabo sum of mean monthly, seasonal and annual precipitation in mm																	
Month	Jan	Feb	Mar	Apr	May	Jun	Jul	Aug	Sep	Oct	Nov	Dec	Winter	Spring	Summer	Autumn	Annual
Observed	22	46	80	92	141	196	209	201	121	65	24	18	83	313	606	210	1214
Corrected	21	41	78	91	138	198	218	199	118	62	23	17	78	307	615	204	1207
REMO	29	41	75	112	166	189	212	226	176	95	49	20	87	354	627	319	1390
Bele sum of mean monthly, seasonal and annual precipitation in mm																	
Month	Jan	Feb	Mar	Apr	May	Jun	Jul	Aug	Sep	Oct	Nov	Dec	Winter	Spring	Summer	Autumn	Annual
Observed	31	40	83	136	146	152	181	179	137	90	43	23	91	366	512	269	1241
Corrected	32	40	82	134	146	149	179	184	140	91	41	24	93	361	512	272	1241
REMO	30	34	78	134	161	146	152	165	151	107	56	20	82	373	464	314	1234
Bonga sum of mean monthly, seasonal and annual precipitation in mm																	
Month	Jan	Feb	Mar	Apr	May	Jun	Jul	Aug	Sep	Oct	Nov	Dec	Winter	Spring	Summer	Autumn	Annual
Observed	50	67	124	181	219	196	214	218	192	143	70	52	164	524	628	405	1726
Corrected	50	67	123	179	222	197	215	216	193	144	70	53	165	523	628	406	1727
REMO	35	45	81	135	183	200	209	219	175	122	83	28	104	399	627	380	1513
Chekorsa sum of mean monthly, seasonal and annual precipitation in mm																	
Month	Jan	Feb	Mar	Apr	May	Jun	Jul	Aug	Sep	Oct	Nov	Dec	Winter	Spring	Summer	Autumn	Annual
Observed	35	63	107	141	202	234	209	235	232	139	69	33	126	450	678	440	1698
Corrected	36	63	107	150	203	235	211	236	232	138	66	33	128	505	681	436	1755
REMO	34	48	83	130	191	210	221	234	188	113	67	24	103	404	664	368	1542
Dedo sum of mean monthly, seasonal and annual precipitation in mm																	
Month	Jan	Feb	Mar	Apr	May	Jun	Jul	Aug	Sep	Oct	Nov	Dec	Winter	Spring	Summer	Autumn	Annual
Observed	43	60	131	176	228	267	293	296	229	142	61	31	131	536	856	433	1959
Corrected	44	61	131	170	229	269	292	291	233	141	59	30	131	530	852	433	1950
REMO	35	49	85	133	191	203	213	224	182	110	64	24	104	410	640	357	1514
Durame sum of mean monthly, seasonal and annual precipitation in mm																	
Month	Jan	Feb	Mar	Apr	May	Jun	Jul	Aug	Sep	Oct	Nov	Dec	Winter	Spring	Summer	Autumn	Annual
Observed	33	55	89	129	150	111	142	163	135	94	31	23	108	367	415	259	1153
Corrected	33	55	89	122	152	113	140	166	137	95	31	22	107	362	419	263	1154
REMO	28	35	76	123	155	146	158	176	155	97	48	18	78	354	480	300	1215

Gedo sum of mean monthly, seasonal and annual precipitation in mm																	
Month	Jan	Feb	Mar	Apr	May	Jun	Jul	Aug	Sep	Oct	Nov	Dec	Winter	Spring	Summer	Autumn	Annual
Observed	26	25	55	64	126	167	227	221	123	54	22	32	80	244	614	199	1141
Corrected	24	24	55	59	126	169	228	223	125	55	22	32	78	240	619	203	1143
REMO	18	26	52	77	150	200	298	288	208	72	29	12	54	279	786	309	1430
Gibe sum of mean monthly, seasonal and annual precipitation in mm																	
Month	Jan	Feb	Mar	Apr	May	Jun	Jul	Aug	Sep	Oct	Nov	Dec	Winter	Spring	Summer	Autumn	Annual
Observed	19	25	52	60	100	154	223	195	90	41	10	8	50	212	572	141	976
Corrected	19	24	51	60	102	157	227	199	93	42	11	8	50	213	583	146	994
REMO	22	30	61	86	141	177	235	243	178	71	32	14	64	288	656	281	1291
Hossana sum of mean monthly, seasonal and annual precipitation in mm																	
Month	Jan	Feb	Mar	Apr	May	Jun	Jul	Aug	Sep	Oct	Nov	Dec	Winter	Spring	Summer	Autumn	Annual
Observed	30	52	90	132	136	133	161	186	150	83	19	22	101	357	480	252	1194
Corrected	30	51	90	129	138	135	139	184	152	86	20	23	100	357	458	258	1175
REMO	27	36	74	106	145	161	188	202	158	82	40	17	77	325	550	281	1236
Jimma sum of mean monthly, seasonal and annual precipitation in mm																	
Month	Jan	Feb	Mar	Apr	May	Jun	Jul	Aug	Sep	Oct	Nov	Dec	Winter	Spring	Summer	Autumn	Annual
Observed	35	46	85	135	184	208	204	212	182	110	61	32	109	404	624	353	1493
Corrected	37	48	85	133	186	209	206	215	181	110	57	33	114	404	630	348	1500
REMO	33	47	82	126	187	207	220	233	186	109	62	23	100	395	660	358	1516
Jinka sum of mean monthly, seasonal and annual precipitation in mm																	
Month	Jan	Feb	Mar	Apr	May	Jun	Jul	Aug	Sep	Oct	Nov	Dec	Winter	Spring	Summer	Autumn	Annual
Observed	48	56	115	176	165	109	125	96	109	147	103	59	158	456	330	359	1308
Corrected	22	56	113	174	159	110	127	98	107	151	100	52	126	447	335	358	1270
REMO	25	27	59	126	125	91	93	95	94	95	72	25	75	310	279	262	928
Kumbi sum of mean monthly, seasonal and annual precipitation in mm																	
Month	Jan	Feb	Mar	Apr	May	Jun	Jul	Aug	Sep	Oct	Nov	Dec	Winter	Spring	Summer	Autumn	Annual
Observed	27	30	72	81	138	214	271	227	128	66	12	16	71	292	712	206	1283
Corrected	28	31	73	82	138	220	276	231	130	65	12	16	72	293	726	207	1300
REMO	23	32	64	90	146	180	226	236	176	76	35	15	68	300	642	288	1299
Limu sum of mean monthly, seasonal and annual precipitation in mm																	
Month	Jan	Feb	Mar	Apr	May	Jun	Jul	Aug	Sep	Oct	Nov	Dec	Winter	Spring	Summer	Autumn	Annual
Observed	24	38	85	138	210	249	292	248	223	172	49	25	84	433	790	444	1754
Corrected	24	38	75	137	211	253	295	250	222	173	48	25	84	422	799	443	1751
REMO	26	41	70	103	169	207	234	251	188	98	48	18	83	342	691	335	1453

Meteso sum of mean monthly, seasonal and annual precipitation in mm																	
Month	Jan	Feb	Mar	Apr	May	Jun	Jul	Aug	Sep	Oct	Nov	Dec	Winter	Spring	Summer	Autumn	Annual
Observed	50	71	137	152	218	265	299	295	202	141	64	33	149	506	858	407	1926
Corrected	48	72	135	145	221	264	300	297	204	145	63	32	147	501	860	411	1925
REMO	34	48	85	135	188	197	207	216	177	110	65	24	103	408	621	352	1487
Morka sum of mean monthly, seasonal and annual precipitation in mm																	
Month	Jan	Feb	Mar	Apr	May	Jun	Jul	Aug	Sep	Oct	Nov	Dec	Winter	Spring	Summer	Autumn	Annual
Observed	42	50	107	181	173	130	161	141	141	135	72	32	121	461	433	349	1367
Corrected	41	50	108	178	176	130	165	144	146	166	71	33	120	462	439	383	1408
REMO	31	34	82	159	169	134	128	141	137	126	72	24	85	410	404	335	1237
Sawula sum of mean monthly, seasonal and annual precipitation in mm																	
Month	Jan	Feb	Mar	Apr	May	Jun	Jul	Aug	Sep	Oct	Nov	Dec	Winter	Spring	Summer	Autumn	Annual
Observed	51	64	143	218	182	124	178	141	149	156	99	43	153	543	443	404	1547
Corrected	50	64	143	217	185	115	178	143	145	160	94	44	153	545	436	399	1537
REMO	31	34	77	149	157	131	130	138	128	116	75	26	88	383	399	319	1191
Shebe sum of mean monthly, seasonal and annual precipitation in mm																	
Month	Jan	Feb	Mar	Apr	May	Jun	Jul	Aug	Sep	Oct	Nov	Dec	Winter	Spring	Summer	Autumn	Annual
Observed	42	54	98	143	214	216	205	225	191	123	81	42	133	455	647	395	1634
Corrected	39	53	97	142	215	218	206	227	192	121	79	42	130	454	651	392	1632
REMO	24	43	87	104	167	218	260	228	157	93	43	20	85	358	705	293	1444
Woliso sum of mean monthly, seasonal and annual precipitation in mm																	
Month	Jan	Feb	Mar	Apr	May	Jun	Jul	Aug	Sep	Oct	Nov	Dec	Winter	Spring	Summer	Autumn	Annual
Observed	19	35	62	81	113	179	279	261	145	48	8	8	60	256	720	201	1239
Corrected	20	36	61	83	114	179	281	263	146	45	9	8	62	258	723	200	1245
REMO	21	28	58	82	132	175	262	267	185	62	26	12	59	272	704	273	1310
Wolkite sum of mean monthly, seasonal and annual precipitation in mm																	
Month	Jan	Feb	Mar	Apr	May	Jun	Jul	Aug	Sep	Oct	Nov	Dec	Winter	Spring	Summer	Autumn	Annual
Observed	22	44	77	99	128	196	294	258	144	51	17	10	73	304	748	212	1340
Corrected	22	44	77	95	130	200	298	262	145	52	17	10	74	302	760	214	1353
REMO	21	30	62	85	133	172	242	250	178	66	29	13	63	280	665	274	1284
Yaya sum of mean monthly, seasonal and annual precipitation in mm																	
Month	Jan	Feb	Mar	Apr	May	Jun	Jul	Aug	Sep	Oct	Nov	Dec	Winter	Spring	Summer	Autumn	Annual
Observed	22	30	59	78	113	170	222	206	112	60	13	12	62	249	598	184	1096
Corrected	22	31	60	83	113	170	225	210	111	59	13	13	63	256	605	183	1109
REMO	21	28	58	83	142	181	243	250	181	70	31	13	61	283	674	283	1303

**B: Mean monthly and seasonal maximum and minimum temperature comparison between Observed corrected and REMO simulated output current period**

Assendabo mean monthly, seasonal and annual maximum temperature in °C																	
Months	Jan	Feb	Mar	Apr	May	Jun	Jul	Aug	Sep	Oct	Nov	Dec	Win.	Spr.	Sum	Aut.	Annual
Observed	28.5	29.1	29.2	28.5	27.5	26.0	24.0	24.2	25.3	26.6	27.6	28.2	28.6	28.4	24.7	26.5	27.0
Correted	28.5	29.1	29.2	28.5	27.4	26.0	24.0	24.1	25.3	26.5	27.6	28.2	28.6	28.4	24.7	26.5	27.0
Remo	27.2	28.8	30.1	30.9	30.2	25.7	22.7	23.2	25.1	26.0	26.1	26.2	27.3	30.4	23.8	25.7	26.8
Bonga mean monthly, seasonal and annual maximum temperature in °C																	
Months	Jan	Feb	Mar	Apr	May	Jun	Jul	Aug	Sep	Oct	Nov	Dec	Winter	Spring	Summer	Autumn	Annual
Observed	27.7	28.0	27.8	27.0	26.2	25.6	24.8	24.7	25.4	26.2	27.0	27.4	27.7	27.0	25.0	26.2	26.5
Correted	27.7	28.0	27.9	26.9	26.2	25.6	24.8	24.7	25.7	26.2	26.9	27.4	27.7	27.0	25.0	26.3	26.5
Remo	24.9	26.3	27.7	28.7	26.2	22.2	20.7	21.8	23.3	24.0	24.2	24.0	25.1	27.5	21.5	23.8	24.5
Dedo mean monthly, seasonal and annual maximum temperature in °C																	
Months	Jan	Feb	Mar	Apr	May	Jun	Jul	Aug	Sep	Oct	Nov	Dec	Winter	Spring	Summer	Autumn	Annual
Observed	23.7	24.2	24.1	23.6	23.0	22.1	20.9	21.2	21.8	22.5	23.1	23.6	23.9	23.6	21.4	22.5	22.8
Correted	23.6	24.2	24.1	23.6	23.0	22.2	20.8	21.1	21.8	22.5	23.1	23.6	23.8	23.5	21.4	22.5	22.8
Remo	28.7	30.1	30.8	31.4	30.2	26.3	23.1	23.4	25.9	27.3	27.5	27.7	28.8	30.8	24.3	26.9	27.7
Gedo mean monthly, seasonal and annual maximum temperature in °C																	
Months	Jan	Feb	Mar	Apr	May	Jun	Jul	Aug	Sep	Oct	Nov	Dec	Winter	Spring	Summer	Autumn	Annual
Observed	22.8	23.6	23.2	23.3	22.1	19.7	18.1	17.9	19.4	21.5	22.2	22.8	23.0	22.9	18.6	21.0	21.4
Correted	22.8	23.6	23.2	23.3	22.1	19.8	18.1	17.9	19.4	21.5	22.3	22.8	23.0	22.9	18.6	21.1	21.4
Remo	27.0	28.7	29.9	30.7	30.8	27.8	24.4	25.1	26.5	25.7	25.6	25.9	27.2	30.5	25.7	26.0	27.3
Hossana mean monthly, seasonal and annual maximum temperature in °C																	
Months	Jan	Feb	Mar	Apr	May	Jun	Jul	Aug	Sep	Oct	Nov	Dec	Winter	Spring	Summer	Autumn	Annual
Observed	25.2	25.5	25.5	24.6	23.9	22.1	20.8	21.1	22.4	23.3	24.2	24.4	25.0	24.7	21.3	23.3	23.6
Correted	25.1	25.4	25.5	24.5	23.8	22.2	20.8	21.1	22.6	23.4	24.8	25.0	25.2	24.6	21.4	23.6	23.7
Remo	26.7	27.9	29.1	29.7	29.5	26.1	23.8	24.5	26.0	25.7	25.7	25.8	26.8	29.4	24.8	25.8	26.7
Jimma mean monthly,seasonal and annual maximum temperature in °C																	
Months	Jan	Feb	Mar	Apr	May	Jun	Jul	Aug	Sep	Oct	Nov	Dec	Winter	Spring	Summer	Autumn	Annual
Observed	28.3	29.2	29.4	28.5	27.3	25.7	24.2	24.5	25.6	26.7	27.3	27.8	28.4	28.4	24.8	26.5	27.0
Correted	28.4	29.2	29.4	28.4	27.2	25.7	24.2	24.5	25.6	26.6	27.3	27.8	28.4	28.3	24.8	26.5	27.0
Remo	28.7	30.1	30.8	31.4	30.2	26.3	23.1	23.4	25.9	27.3	27.5	27.7	28.8	30.8	24.3	26.9	27.7
Jinka mean monthly, seasonal and annual maximum temperature in °C																	
Months	Jan	Feb	Mar	Apr	May	Jun	Jul	Aug	Sep	Oct	Nov	Dec	Winter	Spring	Summer	Autumn	Annual
Observed	29.0	29.5	28.9	26.8	26.1	25.5	25.0	25.6	26.4	26.6	27.0	28.2	28.9	27.3	25.4	26.7	27.0
Correted	29.0	29.5	28.9	26.8	26.1	25.5	25.0	25.5	26.3	26.6	27.0	28.1	28.8	27.2	25.3	26.6	27.0
Remo	30.6	32.1	33.3	34.1	31.3	27.3	25.8	27.3	29.1	29.8	30.2	29.9	30.8	32.9	26.8	29.7	30.1

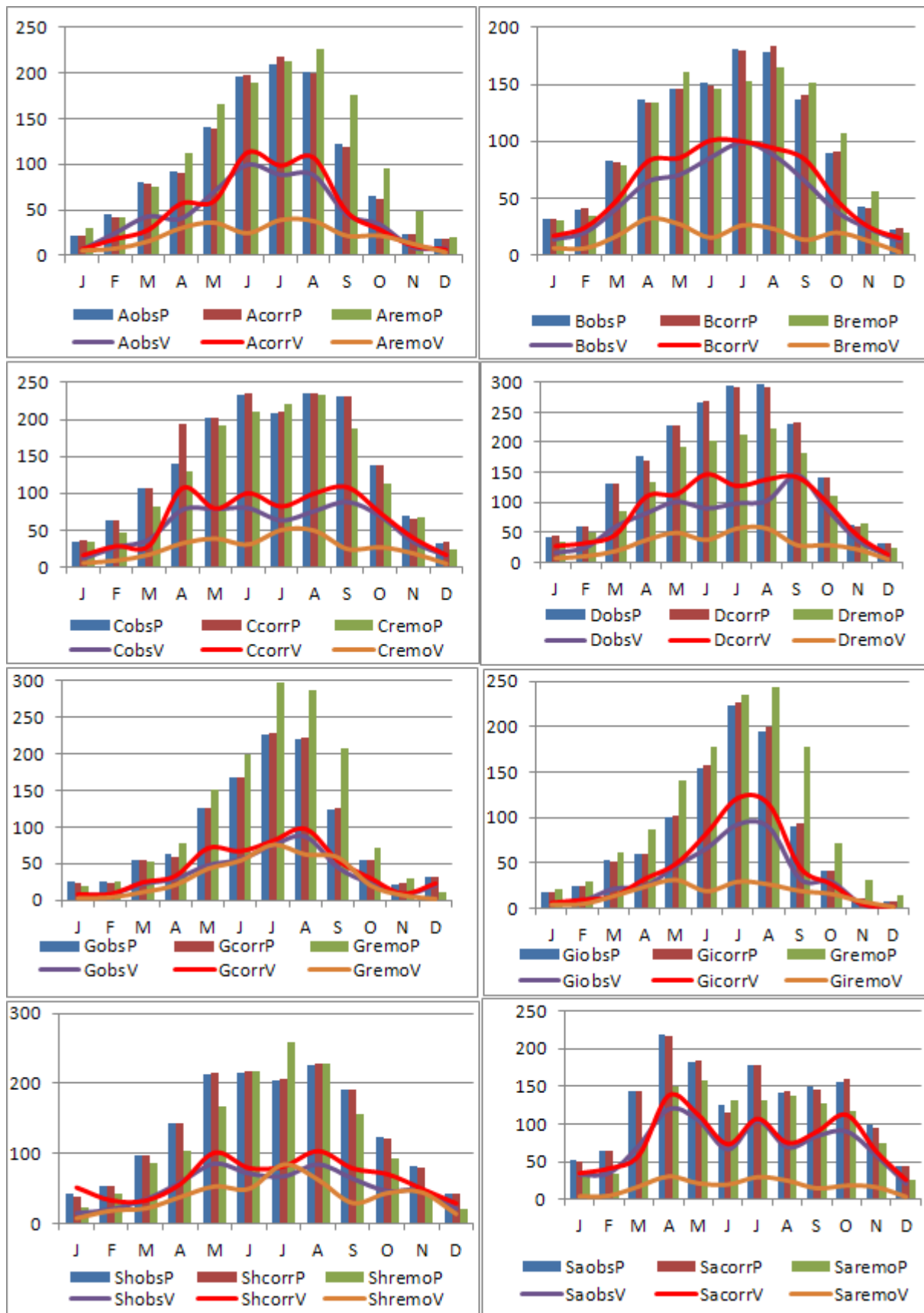
Morka mean monthly, seasonal and annual maximum temperature in °C																	
Months	Jan	Feb	Mar	Apr	May	Jun	Jul	Aug	Sep	Oct	Nov	Dec	Winter	Spring	Summer	Autumn	Annual
Observed	32.5	33.0	33.0	30.9	29.5	29.5	28.8	28.9	29.2	29.4	30.8	32.0	32.5	31.1	29.1	29.8	30.6
Corrected	32.5	33.0	33.0	30.8	29.5	29.5	28.8	28.9	29.1	29.3	30.8	32.0	32.5	31.1	29.1	29.7	30.6
Remo	27.8	29.1	29.9	30.5	28.4	24.3	22.8	24.0	25.9	26.9	27.0	26.9	27.9	29.6	23.7	26.6	27.0
Sawula mean monthly, seasonal and annual maximum temperature in °C																	
Months	Jan	Feb	Mar	Apr	May	Jun	Jul	Aug	Sep	Oct	Nov	Dec	Winter	Spring	Summer	Autumn	Annual
Observed	30.8	30.8	30.7	29.2	28.5	27.9	27.1	27.3	28.4	28.5	29.4	30.2	30.6	29.5	27.4	28.8	29.1
Corrected	30.8	30.8	30.7	29.2	28.5	28.0	27.1	27.3	28.4	28.5	29.4	30.2	30.6	29.5	27.4	28.8	29.1
Remo	30.1	31.6	32.4	32.7	30.6	26.2	24.4	25.8	27.8	28.9	29.0	28.9	30.2	31.9	25.5	28.6	29.0
Shebe mean monthly, seasonal and annual maximum temperature in °C																	
Months	Jan	Feb	Mar	Apr	May	Jun	Jul	Aug	Sep	Oct	Nov	Dec	Winter	Spring	Summer	Autumn	Annual
Observed	27.4	28.0	27.9	26.7	25.3	24.2	22.8	23.1	24.0	25.0	25.9	26.6	27.3	26.6	23.4	25.0	25.6
Corrected	27.4	27.9	27.9	26.5	25.3	24.2	22.8	23.1	24.0	24.9	25.9	26.6	27.3	26.6	23.4	24.9	25.5
Remo	25.6	27.1	28.6	29.7	28.2	23.5	21.1	22.1	24.0	25.0	25.0	24.8	25.8	28.8	22.2	24.7	25.4
Wolita mean monthly, seasonal and annual maximum temperature in °C																	
Months	Jan	Feb	Mar	Apr	May	Jun	Jul	Aug	Sep	Oct	Nov	Dec	Winter	Spring	Summer	Autumn	Annual
Observed	25.9	26.7	26.7	25.3	24.0	22.5	21.4	21.8	22.9	24.1	25.4	25.7	26.1	25.3	21.9	24.1	24.4
Corrected	26.0	26.6	26.7	25.3	24.1	22.5	20.8	21.8	22.8	24.0	25.3	25.7	26.1	25.4	21.7	24.0	24.3
Remo	28.4	29.3	30.2	30.9	30.1	26.2	24.0	24.4	26.2	27.4	27.6	27.6	28.4	30.4	24.9	27.1	27.7
Wolkite mean monthly, seasonal and annual maximum temperature in °C																	
Months	Jan	Feb	Mar	Apr	May	Jun	Jul	Aug	Sep	Oct	Nov	Dec	Winter	Spring	Summer	Autumn	Annual
Observed	28.0	28.4	28.9	28.4	27.3	25.8	24.5	24.5	25.2	26.8	27.6	27.8	28.0	28.2	24.9	26.5	26.9
Corrected	28.0	28.4	29.0	28.5	27.4	25.4	24.5	24.3	25.1	26.7	27.6	27.8	28.1	28.3	24.7	26.5	26.9
Remo	24.2	25.6	26.9	27.7	28.3	26.3	23.6	23.6	24.6	23.6	23.3	23.4	24.4	27.6	24.5	23.8	25.1
Yaya mean monthly, seasonal and annual maximum temperature in °C																	
Months	Jan	Feb	Mar	Apr	May	Jun	Jul	Aug	Sep	Oct	Nov	Dec	Winter	Spring	Summer	Autumn	Annual
Observed	30.5	31.2	31.3	30.6	29.5	27.4	25.2	25.4	26.9	29.0	30.0	30.4	30.7	30.5	26.0	28.6	28.9
Corrected	30.5	31.1	31.4	30.6	29.7	27.2	25.1	25.3	26.7	28.8	30.1	30.4	30.7	30.5	25.9	28.5	28.9
Remo	24.0	25.4	26.7	27.2	27.2	24.4	21.8	22.3	23.6	22.7	22.7	23.0	24.1	27.0	22.8	23.0	24.2

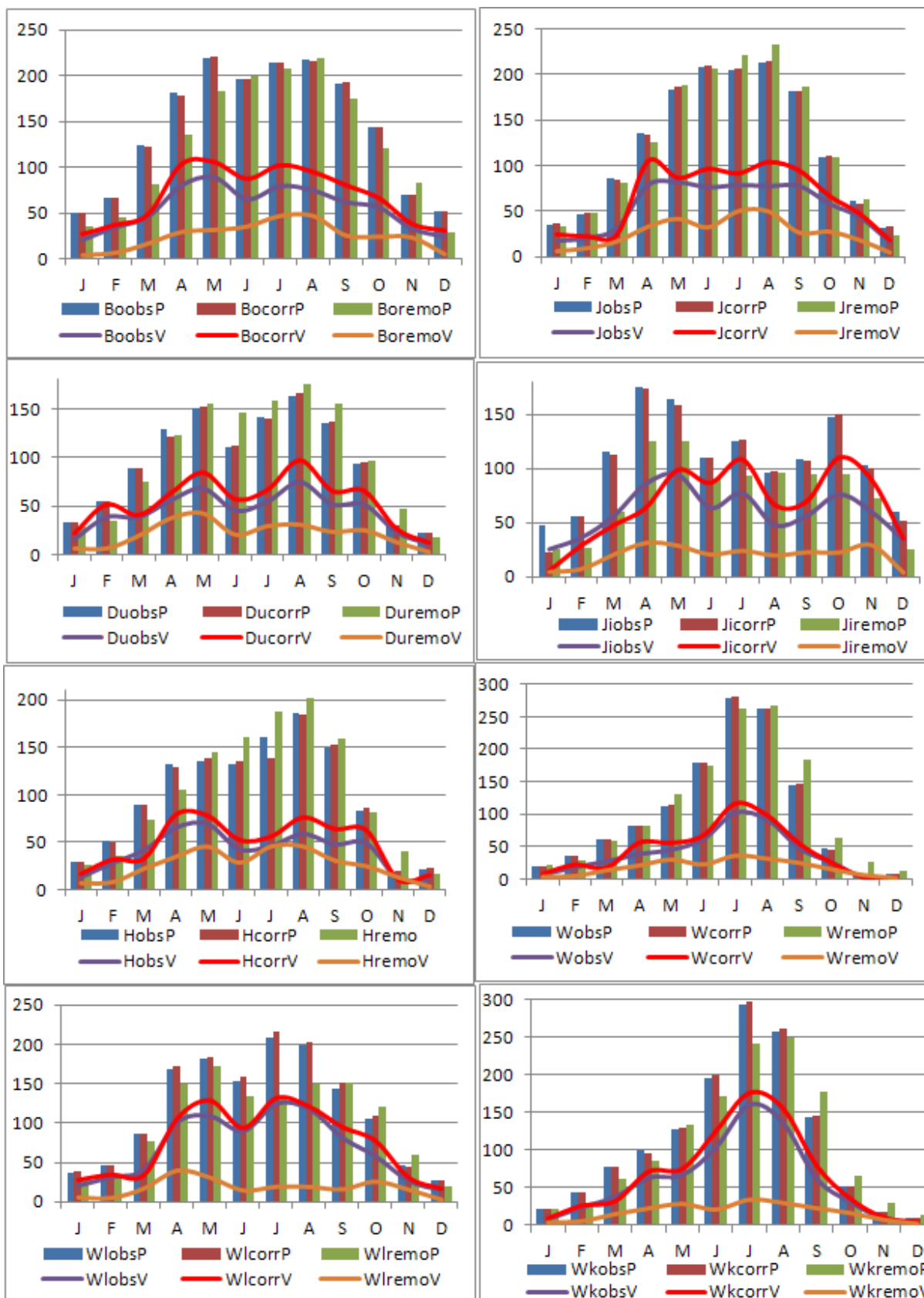


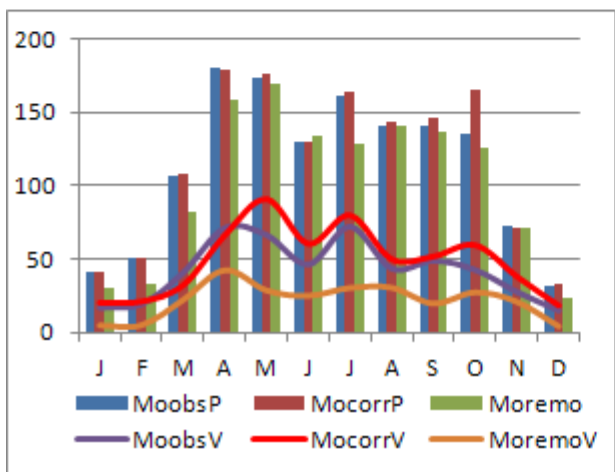
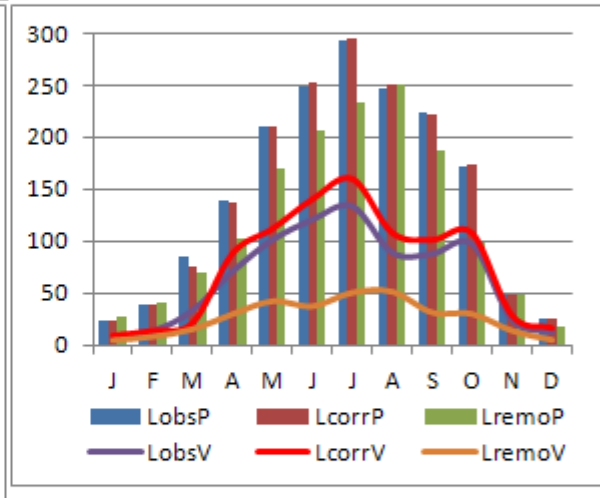
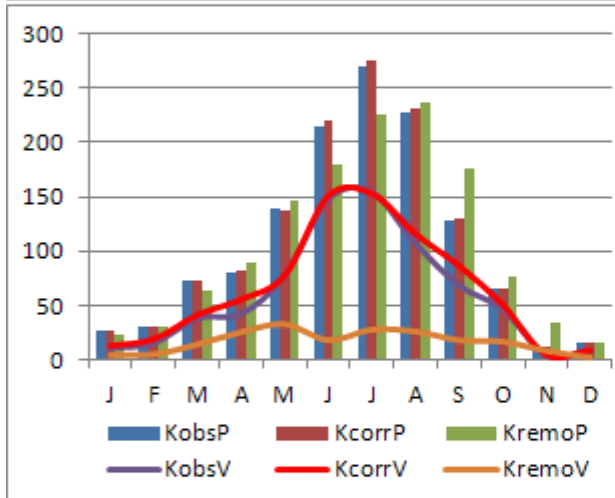
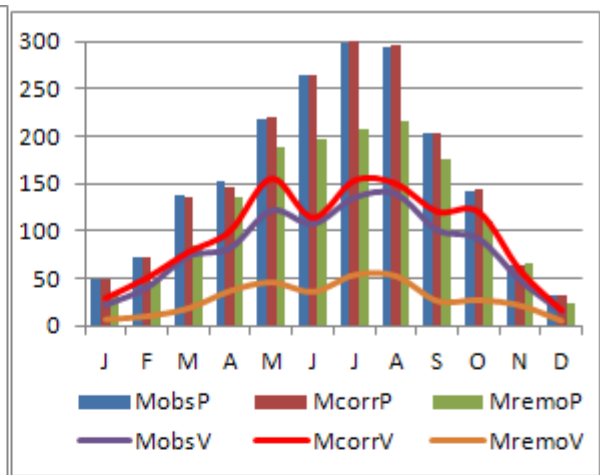
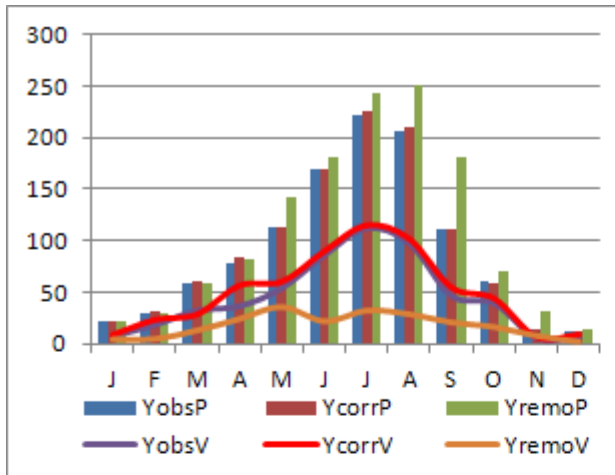
Assandabo mean monthly, seasonal and annual minimum temperature in °C																	
Months	Jan	Feb	Mar	Apr	May	Jun	Jul	Aug	Sep	Oct	Nov	Dec	Winter	Spring	Summer	Autumn	Annual
Observed	9.5	11.2	12.8	13.6	13.6	13.5	13.5	13.3	12.9	11.2	8.8	8.5	9.7	13.4	13.4	11.0	11.9
Correted	9.5	11.3	12.8	13.6	13.6	13.5	13.4	13.3	12.9	11.2	8.8	8.4	9.7	13.3	13.4	10.9	11.9
Remo	13.2	14.2	15.6	16.6	16.8	15.7	14.4	14.3	14.5	13.4	12.2	12.1	13.1	16.3	14.8	13.4	14.4
Bonga mean monthly, seasonal and annual minimum temperature in °C																	
Months	Jan	Feb	Mar	Apr	May	Jun	Jul	Aug	Sep	Oct	Nov	Dec	Winter	Spring	Summer	Autumn	Annual
Observed	9.7	10.8	11.7	12.2	12.3	12.2	12.2	12.2	12.2	11.9	10.9	9.7	10.1	12.1	12.2	11.7	11.5
Correted	9.7	10.9	11.7	12.2	12.3	12.2	12.2	12.2	12.2	11.9	10.7	9.7	10.1	12.1	12.2	11.6	11.5
Remo	12.4	13.2	14.6	15.7	15.6	14.4	13.3	13.4	13.9	13.6	12.1	11.7	12.4	15.3	13.7	13.2	13.6
Dedo mean monthly, seasonal and annual minimum temperature in °C																	
Months	Jan	Feb	Mar	Apr	May	Jun	Jul	Aug	Sep	Oct	Nov	Dec	Winter	Spring	Summer	Autumn	Annual
Observed	10.9	11.1	11.3	11.2	11.2	11.0	10.6	10.6	10.4	10.8	10.5	10.5	10.8	11.2	10.7	10.6	10.8
Correted	11.1	11.2	11.3	11.2	11.2	10.9	10.6	10.5	10.4	10.8	10.5	10.5	10.9	11.2	10.7	10.6	10.8
Remo	14.7	15.5	16.5	17.2	17.1	16.1	14.8	14.7	15.2	14.8	13.8	13.8	14.6	16.9	15.2	14.6	15.4
Gedo mean monthly, seasonal and annual minimum temperature in °C																	
Months	Jan	Feb	Mar	Apr	May	Jun	Jul	Aug	Sep	Oct	Nov	Dec	Winter	Spring	Summer	Autumn	Annual
Observed	9.3	9.6	9.9	10.2	10.0	9.4	8.6	8.6	9.0	8.8	8.9	8.9	9.2	10.0	8.8	8.9	9.2
Correted	9.1	9.6	9.5	10.1	10.0	9.4	8.6	8.6	9.0	8.8	8.9	8.9	9.2	9.9	8.8	8.9	9.2
Remo	12.4	13.4	14.9	15.8	16.3	15.6	14.2	14.0	13.9	12.4	11.3	11.4	12.3	15.7	14.6	12.5	13.8
Hossana mean monthly, seasonal and annual minimum temperature in °C																	
Months	Jan	Feb	Mar	Apr	May	Jun	Jul	Aug	Sep	Oct	Nov	Dec	Winter	Spring	Summer	Autumn	Annual
Observed	9.5	10.6	11.7	12.0	11.6	11.4	11.6	11.6	11.5	10.8	10.1	9.4	9.8	11.7	11.6	10.8	11.0
Correted	9.5	10.6	11.4	12.0	11.6	11.4	11.6	11.6	11.5	10.8	10.1	9.4	9.8	11.6	11.5	10.8	11.0
Remo	12.5	13.2	14.5	15.3	15.8	15.1	14.0	13.9	14.1	13.4	12.2	11.9	12.5	15.2	14.4	13.2	13.8
Jimma mean monthly, seasonal and annual minimum temperature in °C																	
Months	Jan	Feb	Mar	Apr	May	Jun	Jul	Aug	Sep	Oct	Nov	Dec	Winter	Spring	Summer	Autumn	Annual
Observed	8.1	9.5	11.5	12.7	13.2	13.3	13.4	13.4	13.2	11.4	8.6	7.0	8.2	12.5	13.4	11.0	11.3
Correted	8.1	9.5	11.5	12.8	13.2	13.3	13.4	13.4	13.2	11.4	8.6	7.0	8.2	12.5	14.3	11.0	11.4
Remo	14.7	15.5	16.5	17.2	17.1	16.1	14.8	14.7	15.2	14.8	13.8	13.8	14.6	16.9	15.2	14.6	15.4
Jinka mean monthly, seasonal and annual minimum temperature in °C																	
Months	Jan	Feb	Mar	Apr	May	Jun	Jul	Aug	Sep	Oct	Nov	Dec	Winter	Spring	Summer	Autumn	Annual
Observed	15.0	16.1	16.9	16.9	16.7	16.0	15.6	15.6	15.9	16.0	14.6	14.4	15.1	16.8	15.7	15.5	15.8
Correted	15.0	16.1	16.9	16.9	16.3	16.1	15.6	15.6	15.9	16.0	14.6	14.4	15.1	16.7	15.7	15.5	15.8
Remo	17.9	18.7	19.8	20.7	19.8	18.2	17.2	17.5	18.2	18.3	17.6	17.2	17.9	20.1	17.6	18.0	18.4
Morka mean monthly, seasonal and annual minimum temperature in °C																	
Months	Jan	Feb	Mar	Apr	May	Jun	Jul	Aug	Sep	Oct	Nov	Dec	Winter	Spring	Summer	Autumn	Annual
Observed	16.8	15.8	15.7	14.6	14.7	15.4	15.6	16.9	16.7	16.2	16.6	17.2	16.6	15.0	16.0	16.5	16.0
Correted	16.8	15.8	16.0	14.6	14.7	15.4	15.6	16.9	16.8	16.2	16.6	17.1	16.6	15.1	16.0	16.5	16.0

Remo	14.9	15.7	16.6	17.1	17.0	15.9	14.9	15.0	15.5	15.1	14.1	13.9	14.8	16.9	15.3	14.9	15.5
Sawula mean monthly, seasonal and annual minimum temperature in °C																	
Months	Jan	Feb	Mar	Apr	May	Jun	Jul	Aug	Sep	Oct	Nov	Dec	Winter	Spring	Summer	Autumn	Annual
Observed	17.5	17.9	18.1	17.5	16.9	16.8	16.9	16.7	16.8	16.5	16.6	16.9	17.4	17.5	16.8	16.6	17.1
Correted	17.5	18.0	18.1	17.5	17.0	17.2	16.9	16.7	16.8	16.5	16.6	16.9	17.4	17.5	16.9	16.7	17.1
Remo	16.6	17.4	18.4	18.9	18.4	17.1	16.0	16.3	16.8	16.6	15.7	15.6	16.5	18.6	16.4	16.4	17.0
Shebe mean monthly, seasonal and annual minimum temperature in °C																	
Months	Jan	Feb	Mar	Apr	May	Jun	Jul	Aug	Sep	Oct	Nov	Dec	Winter	Spring	Summer	Autumn	Annual
Observed	13.4	13.7	13.6	14.1	13.9	13.6	13.9	13.8	13.3	13.0	13.1	13.3	13.4	13.8	13.7	13.1	13.5
Correted	13.4	13.7	13.6	14.1	13.9	13.6	13.9	13.8	13.3	12.9	13.1	13.3	13.4	13.9	13.7	13.1	13.5
Remo	12.2	13.1	14.8	15.8	16.1	14.9	13.6	13.7	14.2	13.2	11.6	11.3	12.2	15.5	14.1	13.0	13.7
Wolita mean monthly, seasonal and annual minimum temperature in °C																	
Months	Jan	Feb	Mar	Apr	May	Jun	Jul	Aug	Sep	Oct	Nov	Dec	Winter	Spring	Summer	Autumn	Annual
Observed	13.1	13.9	14.2	13.8	13.5	13.1	12.4	12.7	12.7	12.8	13.4	13.2	13.4	13.8	12.7	13.0	13.2
Correted	13.1	14.0	14.8	13.8	13.5	13.0	12.5	12.7	12.8	12.8	13.4	13.2	13.4	14.0	12.7	13.0	13.3
Remo	15.4	16.0	17.0	17.7	17.8	16.8	15.6	15.3	15.5	15.6	15.0	14.7	15.3	17.5	15.9	15.4	16.0
Wolkite mean monthly, seasonal and annual minimum temperature in °C																	
Months	Jan	Feb	Mar	Apr	May	Jun	Jul	Aug	Sep	Oct	Nov	Dec	Winter	Spring	Summer	Autumn	Annual
Observed	11.0	11.6	12.6	13.1	13.3	13.1	13.2	13.2	12.7	11.6	10.6	10.3	11.0	13.0	13.2	11.7	12.2
Correted	11.0	11.7	12.6	13.1	13.3	13.1	13.2	13.2	12.7	11.6	10.6	10.3	11.0	13.0	13.2	11.7	12.2
Remo	9.4	10.2	11.9	13.0	13.7	13.4	12.3	11.9	11.7	10.5	9.0	8.7	9.4	12.9	12.5	10.4	11.3
Yaya mean monthly, seasonal and annual minimum temperature in °C																	
Months	Jan	Feb	Mar	Apr	May	Jun	Jul	Aug	Sep	Oct	Nov	Dec	Winter	Spring	Summer	Autumn	Annual
Observed	10.5	12.0	13.5	14.2	14.2	14.2	14.1	14.0	13.1	10.7	9.0	9.0	10.5	14.0	14.1	11.0	12.4
Correted	10.5	12.0	13.5	14.2	14.2	14.2	14.1	14.0	13.1	10.7	9.0	9.0	10.5	14.0	14.1	10.9	12.4
Remo	9.0	9.9	11.5	12.3	12.7	12.7	12.0	11.7	11.2	9.6	8.2	8.1	9.0	12.2	12.1	9.7	10.7

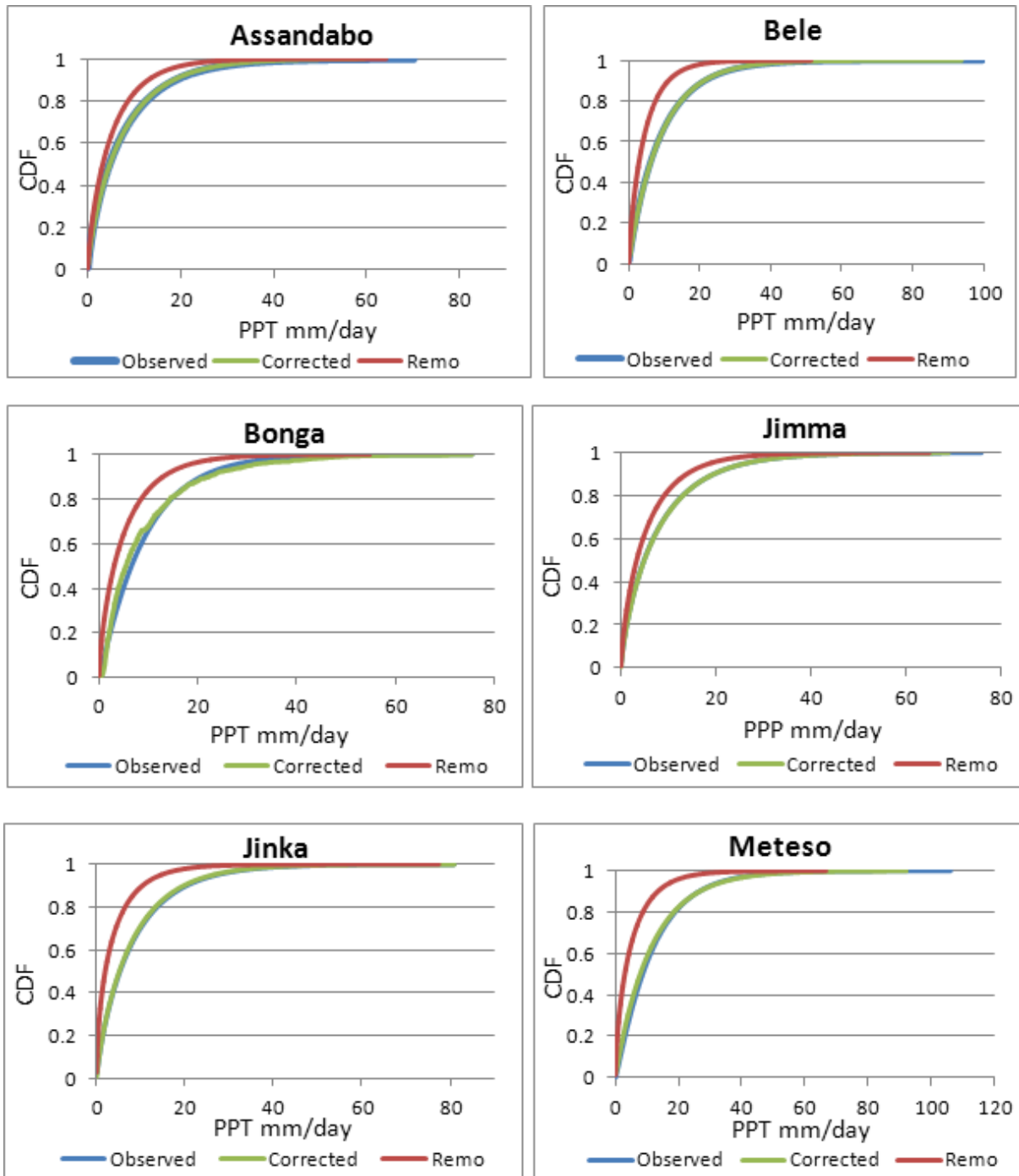
C: Observed and downscaled sum of mean monthly and variance comparison for precipitation data (1970-2000), Observed, corrected and REMO simulation

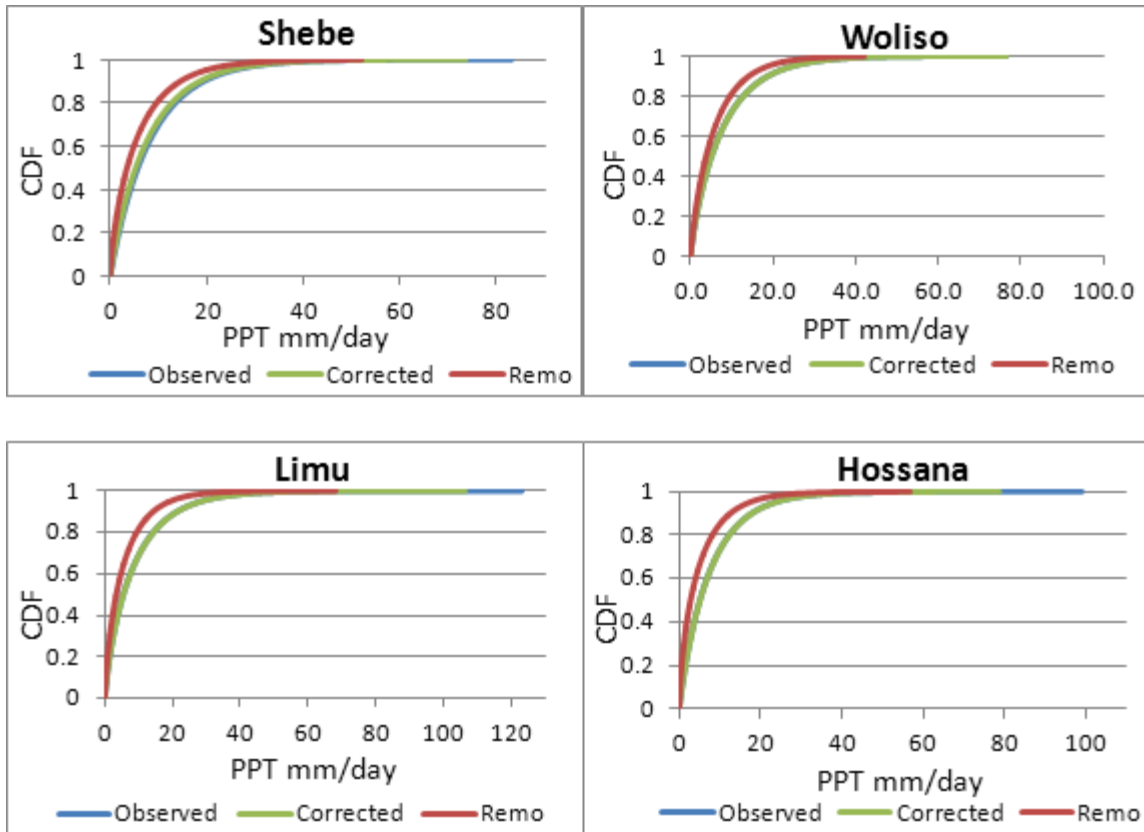




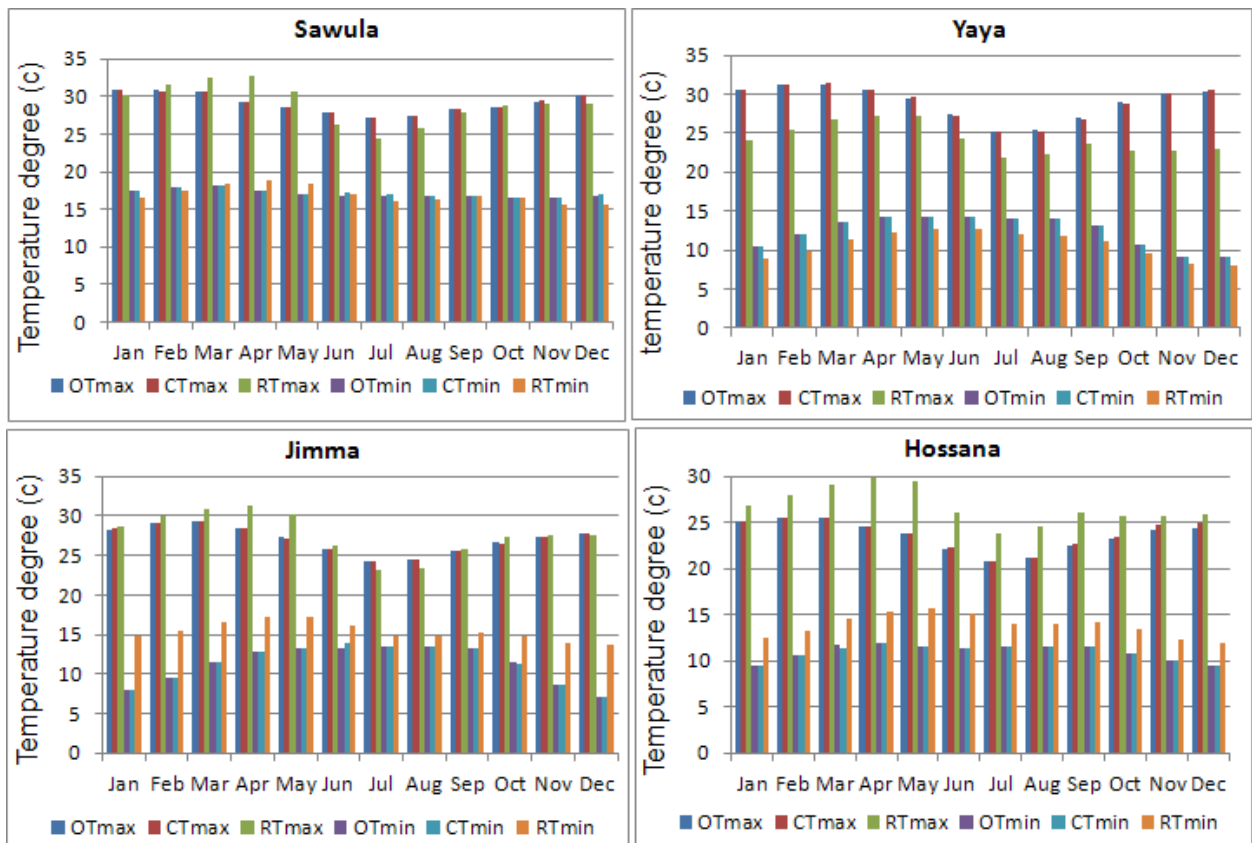


D: Graphical comparison of observed and downscaled (REMO) daily precipitation cumulative distributions curves.

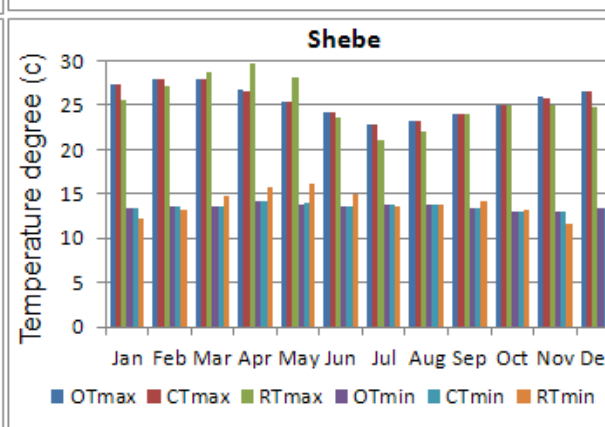
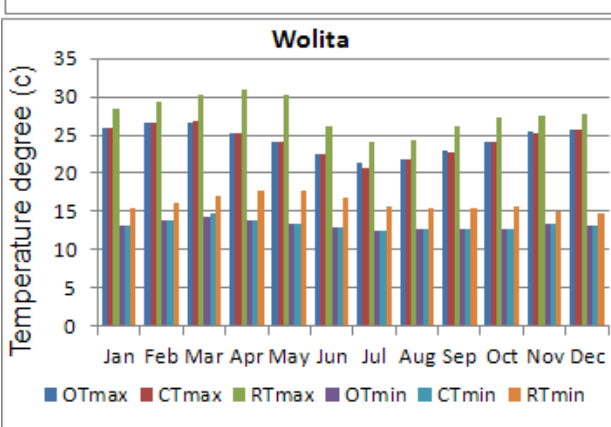
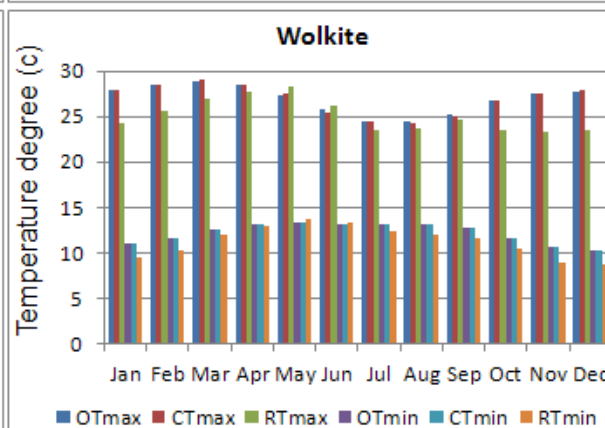
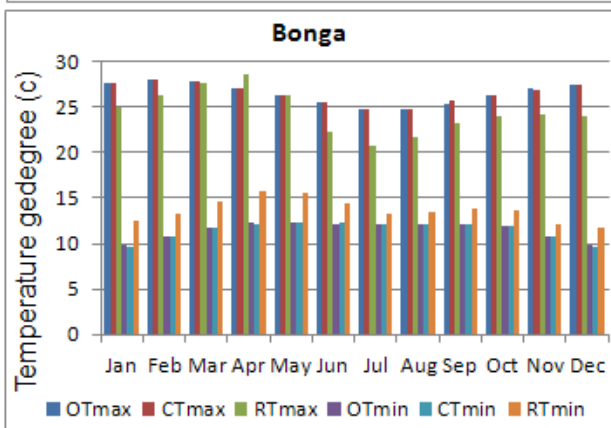
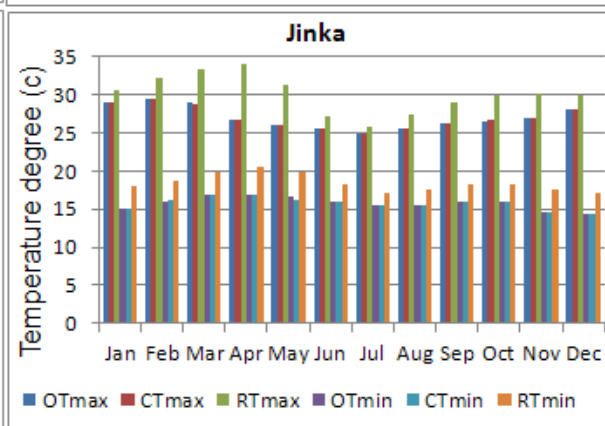
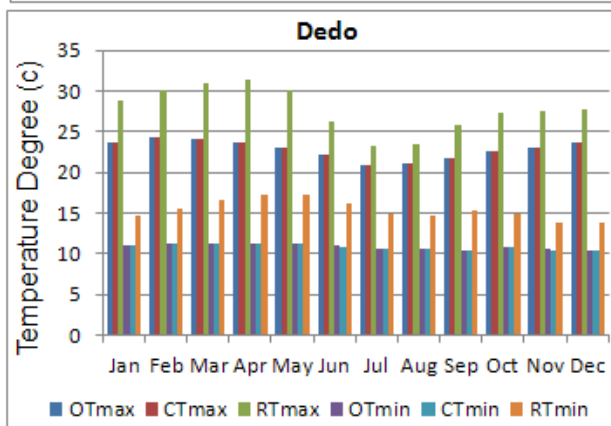
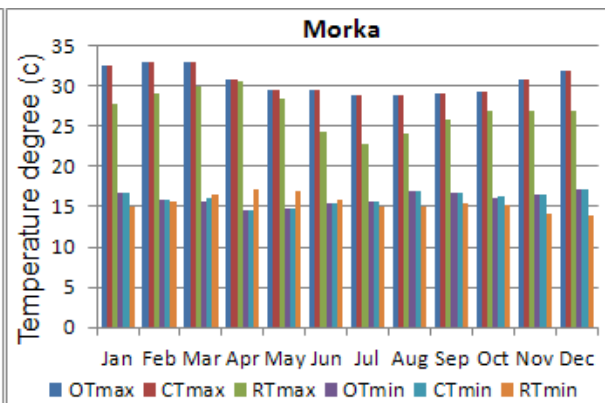
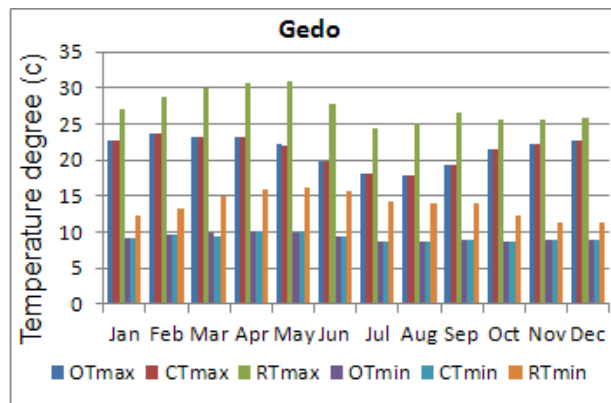




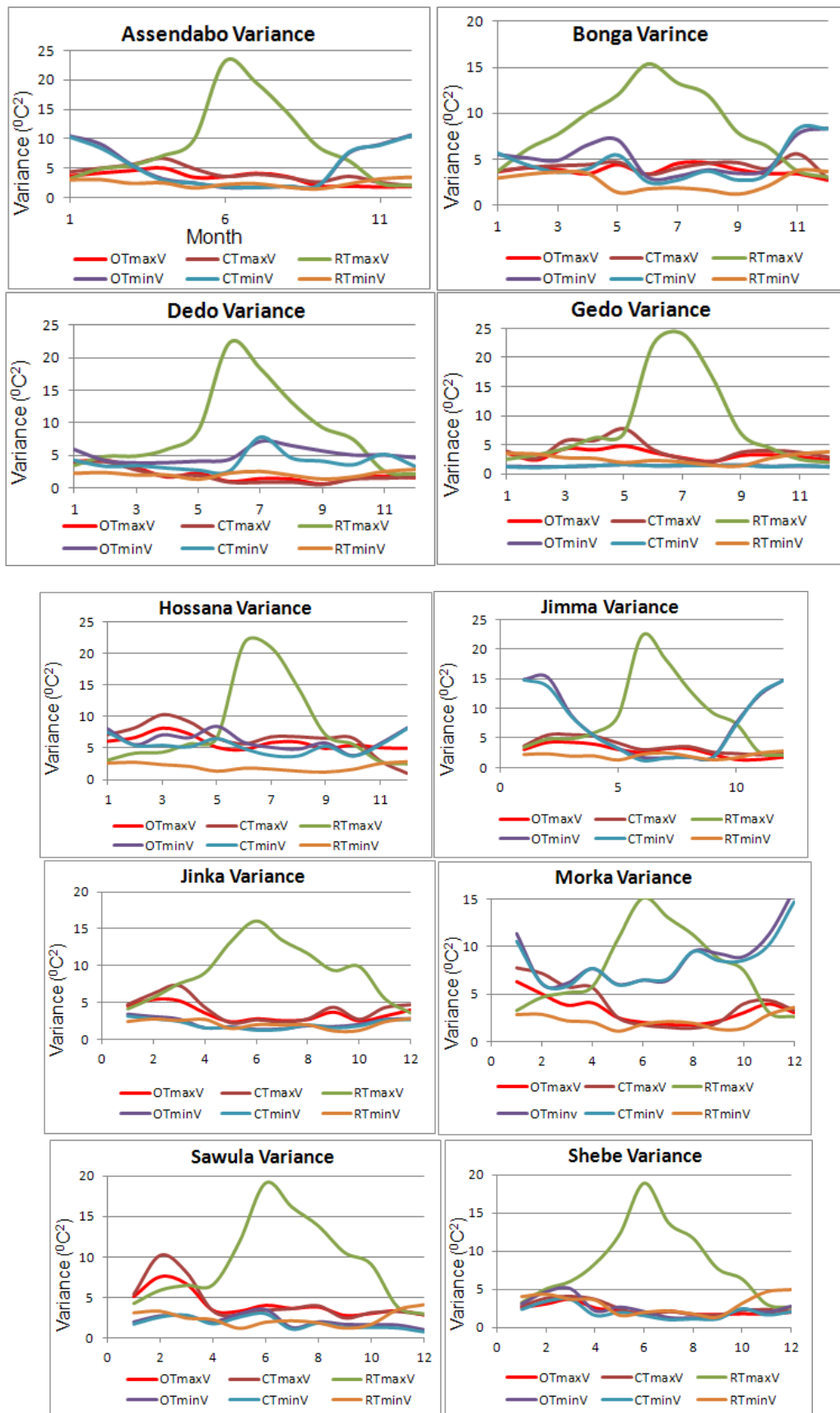
E: Graphical comparison of observed and downscaled (REMO) mean monthly maximum and minimum temperature current time







F: Graphical comparison of observed and downscaled (REMO) monthly maximum and minimum temperature variance



G: Hydrological calculations (1970-2000)

Abelti flow m <sup>3</sup> /s after routing at Gibe III dam site													
Year	Jan	Feb	Mar	Apr	May	Jun	Jul	Aug	Sep	Oct	Nov	Dec	Mean
1970	23	18	25	22	23	62	340	796	601	287	78	33	192.3
1971	21	14	10	13	27	84	310	610	517	340	109	46	175.2
1972	31	21	19	26	45	53	343	503	372	132	55	26	135.5
1973	16	9	4	16	33	47	265	598	656	326	69	24	172.0
1974	17	21	13	22	45	157	298	636	591	318	87	38	186.9
1975	17	15	9	14	17	89	356	747	807	390	103	49	217.7
1976	30	19	18	17	47	97	352	606	531	316	92	53	181.5
1977	22	21	15	15	16	136	664	701	753	365	388	71	264.0
1978	31	19	19	12	44	108	528	746	557	434	108	46	221.0
1979	48	49	35	35	71	227	369	874	592	346	107	173	243.9
1980	240	107	52	38	58	92	282	412	302	136	46	43	150.7
1981	27	30	21	21	18	32	167	521	502	270	47	20	139.7
1982	17	11	40	41	23	59	163	421	345	293	100	55	130.8
1983	20	16	15	18	45	88	178	636	565	491	149	59	190.1
1984	27	17	13	11	16	78	292	479	198	79	21	14	103.7
1985	16	11	40	41	23	59	163	421	345	293	100	55	130.7
1986	10	6	9	9	8	65	370	357	408	177	34	15	122.4
1987	19	16	15	18	45	88	178	594	565	491	149	59	186.4
1988	9	6	5	2	4	17	515	982	768	697	349	32	282.2
1989	26	17	12	31	24	59	197	426	479	169	47	35	126.9
1990	15	14	15	16	20	82	323	629	608	255	53	29	171.7
1991	26	19	18	21	30	77	307	597	510	320	128	49	175.1
1992	14	15	10	8	24	69	272	909	635	319	97	34	200.5
1993	25	23	14	45	116	233	497	836	650	351	167	87	253.6
1994	55	27	17	27	80	121	432	817	649	244	78	59	217.2
1995	28	19	18	20	30	78	307	765	499	311	126	48	187.5
1996	40	40	62	64	143	433	555	815	480	315	109	68	260.3
1997	48	42	26	58	65	211	368	491	368	336	430	228	222.8
1998	99	55	56	34	64	100	451	799	637	571	281	100	270.6
1999	57	32	28	22	40	101	325	569	394	401	165	59	182.9
2000	40	23	16	22	60	108	273	504	487	330	126	48	169.8
<b>n</b>	31	31	31	31	31	31	31	31	31	31	31	31	
<b>Mean</b>	<b>36</b>	<b>24</b>	<b>22</b>	<b>25</b>	<b>42</b>	<b>107</b>	<b>337</b>	<b>639</b>	<b>528</b>	<b>326</b>	<b>129</b>	<b>57</b>	<b>189.2</b>
<b>St Dev</b>	42	19	15	14	30	79	123	165	141	126	100	43	

Abelti flow Mm <sup>3</sup> after routing at Gibe III dam site														
Year	Jan	Feb	Mar	Apr	May	Jun	Jul	Aug	Sep	Oct	Nov	Dec	Total	Mean
1970	62	44	66	58	61	161	910	2132	1557	768	202	88	6110.0	509.2
1971	57	35	27	35	73	217	831	1633	1341	909	282	124	5564.8	463.7
1972	84	53	50	68	121	138	920	1348	965	353	142	69	4308.7	359.1
1973	43	21	12	42	89	122	709	1602	1701	873	178	66	5456.8	454.7
1974	45	51	34	58	122	407	797	1702	1533	851	225	101	5926.9	493.9
1975	45	37	23	36	45	231	954	2000	2093	1043	267	131	6906.2	575.5
1976	79	48	49	45	127	251	943	1623	1376	846	238	143	5768.0	480.7
1977	60	52	42	38	44	354	1777	1878	1951	976	1007	189	8366.5	697.2
1978	83	46	52	31	119	280	1414	1997	1444	1162	279	125	7031.5	586.0
1979	129	119	95	92	190	587	988	2342	1535	927	278	463	7743.8	645.3
1980	643	267	140	99	156	238	755	1104	784	364	119	114	4783.2	398.6
1981	73	73	55	54	48	83	448	1396	1302	723	121	54	4430.1	369.2
1982	45	26	106	106	61	153	438	1129	895	786	259	148	4152.9	346.1
1983	54	38	40	45	121	228	478	1704	1465	1316	385	159	6033.6	502.8
1984	73	44	34	27	44	203	781	1282	513	211	55	37	3303.4	275.3
1985	44	26	106	106	61	153	438	1129	895	786	259	148	4151.4	346.0
1986	27	16	23	22	21	169	990	956	1058	475	89	41	3886.5	323.9
1987	50	38	40	45	121	228	478	1592	1464	1316	385	159	5916.3	493.0
1988	25	16	13	6	12	44	1380	2629	1990	1867	906	85	8972.1	747.7
1989	71	42	31	82	65	152	527	1142	1242	452	122	95	4022.4	335.2
1990	41	35	40	42	55	213	865	1684	1576	682	137	78	5448.9	454.1
1991	70	47	49	54	80	200	822	1598	1321	858	331	130	5560.5	463.4
1992	37	38	27	20	64	179	729	2434	1647	855	251	91	6372.1	531.0
1993	68	57	38	116	310	605	1330	2239	1684	939	434	232	8051.5	671.0
1994	149	66	44	70	215	313	1158	2187	1683	654	202	158	6897.4	574.8
1995	74	46	48	53	80	201	822	2050	1294	834	326	130	5958.6	496.6
1996	107	101	165	165	383	1122	1487	2183	1245	844	282	182	8266.9	688.9
1997	129	103	70	151	174	547	987	1316	954	901	1115	610	7056.6	588.0
1998	264	134	149	89	173	258	1209	2139	1651	1529	729	267	8590.8	715.9
1999	153	79	75	57	106	262	869	1524	1022	1075	428	159	5810.3	484.2
2000	108	58	42	58	162	281	732	1349	1263	883	326	130	5389.6	449.1
<b>n</b>	31	31	31	31	31	31	31	31	31	31	31	31		
<b>Mean</b>	<b>97</b>	<b>60</b>	<b>58</b>	<b>64</b>	<b>113</b>	<b>277</b>	<b>902</b>	<b>1710</b>	<b>1369</b>	<b>873</b>	<b>334</b>	<b>152</b>	<b>6007.7</b>	<b>500.6</b>
<b>St Dev</b>	112	48	39	37	81	205	330	443	365	338	260	116		

Wabi flow m <sup>3</sup> /s after routing at Gibe III dam site													
Year	Jan	Feb	Mar	Apr	May	Jun	Jul	Aug	Sep	Oct	Nov	Dec	Mean
1970	1.9	1.9	4.4	1.2	1.4	2.7	50.1	96.1	67.6	19.7	10.4	2.8	21.7
1971	6.1	2.8	3.6	4.4	2.1	12.3	51.6	123.7	131.1	16.5	6.5	2.7	30.3
1972	3.0	2.1	1.9	2.6	4.6	5.9	44.5	65.0	34.3	7.9	3.2	2.2	14.8
1973	1.8	1.4	1.2	1.0	1.9	3.4	25.5	63.0	60.1	30.5	6.9	4.0	16.7
1974	5.1	4.8	4.8	5.3	4.5	9.2	43.9	90.8	67.5	15.8	4.2	2.6	21.5
1975	1.9	1.8	1.4	2.3	2.4	12.5	76.0	137.3	98.9	17.5	3.2	2.0	29.8
1976	2.2	2.0	2.2	2.7	7.2	6.2	45.3	67.1	42.1	8.2	7.7	3.0	16.3
1977	3.1	4.4	2.7	4.0	5.7	8.1	66.5	81.9	58.9	26.9	42.1	6.6	25.9
1978	3.5	3.0	3.1	2.4	3.5	9.3	61.9	122.3	53.0	34.9	6.9	16.1	26.7
1979	20.8	21.1	14.1	16.5	14.7	12.2	56.4	80.4	54.7	29.7	9.7	18.3	29.0
1980	25.4	12.1	6.8	5.2	7.5	11.0	29.1	41.1	30.9	15.5	6.1	5.7	16.4
1981	3.8	4.2	3.1	3.0	2.7	4.5	18.1	49.4	47.9	27.6	6.1	3.0	14.5
1982	2.6	1.8	5.3	5.5	3.3	7.5	18.1	41.1	34.6	30.0	11.9	7.1	14.1
1983	3.0	2.4	2.3	2.7	5.7	10.5	19.4	58.2	53.0	46.7	16.7	7.6	19.0
1984	1.8	1.1	1.1	1.0	3.8	25.2	77.4	55.3	77.9	5.8	2.2	1.5	21.2
1985	1.1	1.0	0.9	2.0	8.4	15.2	60.9	236.9	84.5	10.6	3.4	9.7	36.2
1986	9.1	10.9	17.9	23.7	27.7	45.6	68.8	78.8	77.4	15.1	4.5	3.1	31.9
1987	2.4	2.2	8.9	44.8	18.8	33.0	39.8	75.5	30.0	7.6	2.3	1.4	22.2
1988	1.5	1.8	1.5	1.2	1.6	12.7	105.2	216.2	116.9	79.0	8.1	3.9	45.8
1989	1.7	1.7	1.4	7.6	2.7	7.8	93.8	105.3	92.6	32.8	10.9	3.4	30.1
1990	2.3	2.2	2.3	2.5	3.0	9.9	32.6	58.0	56.3	26.0	6.8	4.1	17.2
1991	2.8	1.3	2.1	1.0	2.5	5.4	114.2	328.5	96.5	12.9	2.7	1.8	47.6
1992	1.6	4.4	3.9	7.1	12.1	38.4	104.0	349.1	262.2	45.0	12.3	5.5	70.5
1993	4.3	4.0	2.7	7.2	15.1	27.5	51.0	77.0	61.7	36.9	18.9	11.8	26.5
1994	8.3	4.4	3.1	4.7	11.3	16.4	90.8	165.1	80.5	14.5	3.7	2.2	33.8
1995	2.8	1.6	1.3	5.7	2.8	8.7	56.0	92.2	59.7	7.6	2.5	1.7	20.2
1996	2.7	1.3	7.9	16.9	28.5	105.9	102.0	204.4	48.5	18.4	6.1	2.8	45.5
1997	2.3	1.5	1.9	10.4	3.6	3.6	31.5	61.5	19.4	15.8	8.4	2.4	13.5
1998	3.2	2.0	5.1	3.3	8.2	12.4	47.2	87.1	73.0	57.9	31.2	13.4	28.7
1999	2.9	1.3	2.0	1.6	2.4	14.1	66.9	137.7	41.3	55.7	9.5	2.8	28.2
2000	1.5	1.0	0.8	1.5	2.9	4.4	67.8	97.6	69.8	24.9	5.8	3.1	23.4
<b>n</b>	31	31	31	31	31	31	31	31	31	31	31	31	
<b>Mean</b>	<b>4.4</b>	<b>3.5</b>	<b>3.9</b>	<b>6.5</b>	<b>7.2</b>	<b>16.2</b>	<b>58.6</b>	<b>114.3</b>	<b>70.4</b>	<b>25.6</b>	<b>9.1</b>	<b>5.1</b>	<b>27.1</b>
<b>St Dev</b>	5	4	4	9	7	20	27	78	44	17	9	4	

Gojeb OM19 flow m <sup>3</sup> /s after routing at Gibe III dam site													
Year	Jan	Feb	Mar	Apr	May	Jun	Jul	Aug	Sep	Oct	Nov	Dec	Mean
1970	14.4	12.0	14.9	29.7	37.9	127.6	203.6	294.9	250.4	193.6	45.8	19.3	103.7
1971	15.0	9.6	9.5	12.9	40.6	79.3	183.0	204.9	213.9	170.6	103.6	32.6	89.6
1972	19.1	17.8	15.5	32.3	49.0	90.7	212.0	198.5	162.6	57.3	67.6	27.8	79.2
1973	20.1	11.3	7.3	15.0	82.0	152.2	212.5	247.8	211.6	135.2	43.3	16.7	96.3
1974	10.8	9.8	12.9	10.5	55.7	123.3	160.6	193.7	235.8	125.9	21.3	11.7	81.0
1975	8.0	10.9	9.0	11.6	19.5	71.3	101.4	147.4	193.6	173.2	38.1	13.0	66.4
1976	8.5	9.9	12.2	8.6	49.2	162.5	244.6	266.0	162.8	52.5	51.5	16.2	87.0
1977	16.3	19.4	14.1	12.3	8.5	62.2	219.6	196.2	209.1	142.4	109.9	26.0	86.3
1978	13.7	9.3	10.8	18.8	127.2	229.0	236.8	259.2	159.7	112.7	38.3	20.2	103.0
1979	14.0	21.5	20.5	29.0	31.3	89.4	149.5	133.3	91.0	71.5	20.9	18.8	57.6
1980	12.6	9.8	11.0	24.8	70.2	175.4	170.8	193.7	129.0	72.1	30.2	18.9	76.5
1981	14.4	11.6	16.7	8.8	31.3	71.3	98.6	341.2	193.8	114.0	27.6	14.3	78.6
1982	15.9	11.4	9.8	13.6	29.4	88.9	130.6	185.9	156.4	161.6	40.6	32.7	73.1
1983	14.3	12.3	12.9	15.1	26.1	50.7	78.1	190.5	338.8	104.9	45.0	28.0	76.4
1984	18.0	13.2	12.4	21.5	28.7	82.1	149.5	184.8	172.3	42.1	37.0	26.8	65.7
1985	15.0	11.9	12.4	20.2	61.9	98.5	148.7	214.8	225.2	77.6	39.5	21.0	78.9
1986	13.3	14.2	18.4	23.8	32.1	113.3	112.7	143.9	169.1	58.9	24.1	20.0	62.0
1987	12.5	11.2	17.5	20.1	32.1	61.8	120.1	136.9	123.6	84.6	56.5	24.8	58.5
1988	20.6	16.8	13.6	10.3	26.6	65.9	123.3	332.9	293.2	286.1	41.4	21.1	104.3
1989	18.3	17.0	16.1	37.7	34.6	50.9	130.0	146.7	186.6	111.1	38.6	58.5	70.5
1990	27.8	25.0	36.5	34.9	43.3	127.9	127.2	244.4	220.3	134.2	44.3	28.0	91.1
1991	20.5	17.3	17.9	25.5	62.9	157.6	254.9	171.6	111.4	60.3	27.8	21.7	79.1
1992	16.0	18.1	15.5	24.4	64.5	95.3	173.5	177.8	180.2	233.4	63.7	32.3	91.2
1993	25.7	25.0	21.6	46.6	112.0	147.1	200.1	160.0	169.1	113.8	48.3	23.9	91.1
1994	17.4	12.9	13.8	15.6	36.9	92.6	220.0	267.1	207.3	51.2	36.2	26.3	83.1
1995	16.6	13.7	13.6	19.5	44.3	84.1	109.9	161.2	153.4	101.3	35.1	38.3	65.9
1996	29.0	19.9	37.7	53.4	91.4	189.2	173.2	183.0	207.6	134.2	38.5	29.6	98.9
1997	25.0	16.6	19.2	30.2	64.0	190.9	125.7	144.9	115.3	227.5	248.2	90.1	108.1
1998	64.8	32.3	75.4	31.7	93.8	130.5	176.5	353.3	192.5	309.3	61.4	8.6	127.5
1999	1.5	0.4	0.3	4.2	61.6	98.9	217.8	190.8	106.7	209.4	41.9	4.0	78.1
2000	0.4	0.3	0.2	34.3	117.7	127.6	227.0	219.9	195.1	231.5	113.5	19.5	107.2
<b>n</b>	31	31	31	31	31	31	31	31	31	31	31	31	
<b>Mean</b>	<b>17.4</b>	<b>14.3</b>	<b>16.7</b>	<b>22.5</b>	<b>53.7</b>	<b>112.5</b>	<b>167.5</b>	<b>209.3</b>	<b>185.1</b>	<b>134.0</b>	<b>54.2</b>	<b>25.5</b>	<b>84.4</b>
<b>St Dev</b>	11	7	13	12	30	45	49	61	53	71	43	16	

Un-gauged flow m <sup>3</sup> /s at Gibe III dam site derived from daily flow (SWIM hydrological modeling result)													
Year	Jan	Feb	Mar	Apr	May	Jun	Jul	Aug	Sep	Oct	Nov	Dec	Mean
1970	12.5	40.6	60.6	73.6	80.9	110.5	282.3	437.4	413.7	242.6	110.1	52.3	159.8
1971	39.9	34.6	30.5	35.5	59.9	111.0	243.9	359.1	275.6	219.0	97.0	57.0	130.3
1972	42.4	31.7	34.4	51.3	94.5	85.0	159.9	277.9	188.0	116.9	52.7	35.4	97.5
1973	24.9	22.4	16.4	14.1	30.0	76.3	240.9	532.0	528.5	348.1	115.2	56.1	167.1
1974	40.0	33.5	32.6	48.6	41.6	162.4	274.6	399.5	417.4	251.2	79.9	41.2	151.9
1975	32.8	28.4	26.7	48.2	98.1	246.3	234.5	377.3	361.1	238.8	90.7	41.8	152.1
1976	32.5	27.6	26.9	38.8	83.6	177.3	340.7	483.8	296.7	150.6	124.2	83.3	155.5
1977	40.3	61.6	44.1	33.0	55.4	140.4	281.2	375.5	295.5	250.4	292.6	122.1	166.0
1978	47.7	41.4	53.6	41.9	50.3	49.3	173.1	408.1	369.6	242.3	84.9	43.2	133.8
1979	39.0	47.3	47.3	63.2	90.6	146.3	316.5	392.4	249.0	151.3	68.9	35.1	137.2
1980	27.0	23.7	25.7	60.6	85.8	58.0	114.3	253.9	190.2	88.0	41.9	22.1	82.6
1981	16.9	14.4	29.5	101.0	79.9	54.8	172.7	354.7	309.4	188.5	59.9	30.0	117.6
1982	27.3	30.9	27.3	41.4	57.8	71.5	153.0	373.2	297.1	185.8	198.3	106.3	130.8
1983	42.7	30.8	28.4	57.1	98.2	134.1	124.1	325.4	322.5	233.6	132.0	53.0	131.8
1984	30.9	25.4	22.1	19.8	27.9	77.5	93.9	198.4	187.2	103.8	35.0	21.7	70.3
1985	22.8	21.4	16.0	37.6	80.7	84.2	162.0	378.6	288.2	167.8	162.5	81.4	125.3
1986	35.4	25.3	27.2	34.4	52.0	92.6	165.3	237.4	160.3	114.6	61.9	42.0	87.4
1987	25.1	17.9	19.6	51.8	90.6	130.3	109.4	269.1	280.1	198.4	110.7	42.6	112.1
1988	24.9	23.8	22.3	19.4	25.5	32.4	107.2	392.8	443.6	342.1	180.7	72.6	140.6
1989	38.1	46.1	45.9	54.9	80.9	72.3	103.9	243.6	259.3	228.1	117.3	83.1	114.5
1990	85.3	49.9	70.4	75.1	75.9	91.6	156.2	260.5	219.5	162.6	61.3	34.5	111.9
1991	25.3	22.2	35.2	46.8	62.1	63.2	161.9	297.5	243.2	128.3	42.0	27.3	96.2
1992	25.5	25.7	28.6	28.2	63.3	80.1	164.8	397.1	442.3	316.4	156.8	53.7	148.5
1993	37.4	43.5	40.5	70.9	268.1	263.7	228.8	345.9	254.6	169.0	143.6	73.0	161.6
1994	36.2	28.3	26.2	37.5	65.4	76.9	161.5	387.9	302.2	158.8	67.4	33.9	115.2
1995	24.8	21.6	19.0	32.1	71.4	58.6	123.9	264.5	265.1	163.3	48.6	25.9	93.2
1996	30.6	32.2	31.6	80.2	172.7	286.8	307.4	389.0	353.1	197.1	70.3	44.0	166.2
1997	33.8	28.9	24.8	44.5	80.7	107.5	181.6	263.8	187.3	218.0	381.8	237.1	149.1
1998	69.0	45.8	38.2	50.3	85.5	90.5	176.4	403.7	311.4	195.5	139.9	55.8	138.5
<b>n</b>	29	29	29	29	29	29	29	29	29	29	29	29	
<b>Mean</b>	<b>34.9</b>	<b>32.0</b>	<b>32.8</b>	<b>48.0</b>	<b>79.6</b>	<b>111.4</b>	<b>190.2</b>	<b>347.6</b>	<b>300.4</b>	<b>199.0</b>	<b>114.8</b>	<b>58.9</b>	<b>129.1</b>
<b>St Dev</b>	14	11	13	20	46	64	70	79	89	66	76	42	



Un-gauged flow Mm <sup>3</sup> at Gibe III dam site derived from daily flow (SWIM hydrological modeling result)														
Year	Jan	Feb	Mar	Apr	May	Jun	Jul	Aug	Sep	Oct	Nov	Dec	Total	Mean
1970	34	98	162	191	217	287	756	1171	1072	650	285	140	5063	422
1971	107	84	82	92	161	288	653	962	714	587	251	153	4133	344
1972	113	80	92	133	253	220	428	744	487	313	137	95	3096	258
1973	67	54	44	37	80	198	645	1425	1370	932	299	150	5301	442
1974	107	81	87	126	111	421	736	1070	1082	673	207	110	4812	401
1975	88	69	72	125	263	638	628	1011	936	640	235	112	4816	401
1976	87	69	72	100	224	460	912	1296	769	403	322	223	4938	411
1977	108	149	118	86	148	364	753	1006	766	671	758	327	5254	438
1978	128	100	144	109	135	128	464	1093	958	649	220	116	4242	354
1979	104	114	127	164	243	379	848	1051	645	405	179	94	4353	363
1980	72	59	69	157	230	150	306	680	493	236	109	59	2621	218
1981	45	35	79	262	214	142	463	950	802	505	155	80	3732	311
1982	73	75	73	107	155	185	410	999	770	498	514	285	4144	345
1983	114	74	76	148	263	347	332	871	836	626	342	142	4173	348
1984	83	64	59	51	75	201	252	531	485	278	91	58	2228	186
1985	61	52	43	98	216	218	434	1014	747	450	421	218	3971	331
1986	95	61	73	89	139	240	443	636	416	307	160	113	2771	231
1987	67	43	52	134	243	338	293	721	726	531	287	114	3550	296
1988	67	60	60	50	68	84	287	1052	1150	916	468	194	4456	371
1989	102	111	123	142	217	187	278	652	672	611	304	223	3623	302
1990	228	121	188	195	203	238	418	698	569	436	159	92	3544	295
1991	68	54	94	121	166	164	434	797	630	344	109	73	3054	254
1992	68	64	77	73	170	208	441	1064	1146	847	406	144	4709	392
1993	100	105	108	184	718	684	613	926	660	453	372	195	5119	427
1994	97	69	70	97	175	199	433	1039	783	425	175	91	3653	304
1995	66	52	51	83	191	152	332	708	687	437	126	69	2956	246
1996	82	81	85	208	462	743	823	1042	915	528	182	118	5269	439
1997	90	70	66	115	216	279	487	706	485	584	990	635	4724	394
1998	185	111	102	130	229	235	472	1081	807	524	363	149	4388	366
<b>n</b>	29	29	29	29	29	29	29	29	29	29	29	29		
<b>Mean</b>	<b>93</b>	<b>78</b>	<b>88</b>	<b>124</b>	<b>213</b>	<b>289</b>	<b>509</b>	<b>931</b>	<b>779</b>	<b>533</b>	<b>297</b>	<b>158</b>	<b>4093</b>	<b>341</b>
<b>St Dev</b>	39	26	35	51	123	165	188	211	230	176	198	113	865	

Total flow m <sup>3</sup> /s after routing at Gibe III dam site													
Year	Jan	Feb	Mar	Apr	May	Jun	Jul	Aug	Sep	Oct	Nov	Dec	Mean
1970	52	73	105	127	143	303	876	1625	1333	742	244	107	477.4
1971	82	62	54	66	130	286	789	1297	1138	746	316	139	425.4
1972	96	73	70	112	193	235	760	1045	757	314	178	91	327.0
1973	63	44	29	46	147	279	744	1441	1456	840	234	101	452.1
1974	73	69	63	87	147	452	777	1320	1312	711	192	93	441.3
1975	60	57	46	76	137	419	768	1409	1461	819	235	106	466.0
1976	73	59	60	68	187	443	983	1423	1032	527	275	156	440.4
1977	82	107	76	64	86	347	1231	1355	1316	784	833	225	542.2
1978	96	73	87	75	225	396	1000	1535	1139	824	238	126	484.5
1979	122	139	117	144	208	474	891	1481	987	599	207	245	467.8
1980	305	152	96	129	222	336	596	901	652	311	124	89	326.2
1981	62	60	70	134	132	162	457	1266	1054	600	141	67	350.4
1982	63	55	82	102	113	227	465	1022	833	671	351	201	348.7
1983	80	61	59	92	175	283	400	1210	1280	876	342	148	417.3
1984	78	57	48	53	77	263	612	917	635	230	95	64	260.9
1985	55	45	69	101	174	257	535	1252	943	549	305	167	371.1
1986	68	57	72	90	120	317	716	817	815	366	125	80	303.6
1987	59	47	61	134	187	313	448	1076	999	782	318	128	379.2
1988	56	49	42	33	58	128	851	1923	1622	1404	580	130	572.9
1989	85	82	75	132	142	190	525	922	1018	541	214	180	342.1
1990	131	92	124	129	143	312	639	1192	1104	578	165	96	391.9
1991	75	60	74	94	158	304	838	1394	961	522	200	99	398.1
1992	57	63	58	68	164	283	714	1833	1520	914	330	126	510.8
1993	93	96	79	169	511	672	976	1419	1135	670	378	195	532.8
1994	117	73	60	85	194	307	905	1637	1239	469	185	121	449.2
1995	72	56	52	78	148	229	597	1283	977	583	212	114	366.9
1996	102	94	139	214	435	1015	1138	1591	1090	665	224	144	571.0
1997	109	89	72	144	213	513	707	961	690	798	1068	557	493.6
1998	236	135	174	120	252	333	852	1643	1214	1133	514	178	565.2
<b>n</b>	29	29	29	29	29	29	29	29	29	29	29	29	
<b>Mean</b>	<b>93</b>	<b>75</b>	<b>76</b>	<b>102</b>	<b>180</b>	<b>347</b>	<b>751</b>	<b>1317</b>	<b>1094</b>	<b>675</b>	<b>304</b>	<b>147</b>	<b>430.2</b>
<b>St Dev</b>	54	28	31	40	93	170	207	284	258	244	212	91	

Total flow Mm <sup>3</sup> after routing at Gibe III dam site														
Year	Jan	Feb	Mar	Apr	May	Jun	Jul	Aug	Sep	Oct	Nov	Dec	Total	Mean
1970	139	176	281	329	382	785	2346	4351	3454	1989	633	288	15152	1262.6
1971	220	149	144	172	347	743	2112	3475	2950	1997	819	372	13499	1124.9
1972	256	182	189	291	518	608	2035	2798	1962	841	462	244	10387	865.5
1973	168	106	78	120	394	723	1992	3860	3775	2249	607	271	14344	1195.3
1974	195	167	169	225	394	1171	2080	3534	3401	1904	498	249	13988	1165.7
1975	160	137	122	197	366	1087	2058	3773	3786	2194	609	284	14773	1231.0
1976	195	147	160	175	502	1147	2632	3811	2676	1412	713	417	13988	1165.6
1977	220	258	205	166	230	900	3297	3629	3411	2101	2159	603	17178	1431.5
1978	257	175	233	195	603	1025	2678	4112	2954	2207	617	338	15393	1282.7
1979	327	337	314	374	556	1230	2387	3965	2558	1604	536	656	14842	1236.8
1980	817	382	256	334	593	872	1597	2413	1691	834	321	240	10351	862.6
1981	167	146	187	346	353	421	1223	3392	2731	1607	364	180	11119	926.6
1982	168	133	220	263	303	588	1246	2736	2160	1797	909	540	11064	922.0
1983	215	147	157	239	469	734	1071	3241	3317	2348	888	396	13223	1101.9
1984	209	143	129	137	205	682	1640	2456	1647	617	247	171	8284	690.4
1985	148	109	184	261	466	666	1433	3353	2445	1472	792	448	11777	981.4
1986	182	138	193	234	320	821	1919	2188	2113	980	324	215	9627	802.2
1987	157	113	163	348	500	812	1199	2881	2589	2094	825	343	12025	1002.1
1988	151	122	113	86	156	332	2278	5152	4203	3761	1502	347	18202	1516.9
1989	226	199	201	341	381	492	1405	2469	2638	1449	555	483	10838	903.2
1990	350	221	333	333	382	808	1711	3192	2862	1547	428	256	12424	1035.3
1991	200	146	197	244	422	787	2244	3734	2490	1397	519	266	12646	1053.9
1992	153	159	156	175	438	733	1914	4909	3940	2448	854	337	16215	1351.3
1993	249	232	211	439	###	1741	2615	3800	2942	1795	980	523	16897	1408.1
1994	314	176	160	220	519	795	2423	4384	3212	1255	480	325	14263	1188.6
1995	193	135	139	202	397	594	1599	3437	2533	1563	549	306	11647	970.6
1996	273	235	372	555	###	2631	3048	4262	2824	1781	580	386	18115	1509.6
1997	292	216	193	372	571	1330	1894	2575	1789	2136	2769	1493	15632	1302.7
1998	631	328	467	310	675	863	2281	4400	3147	3036	1331	476	17944	1495.3
<b>n</b>	29	29	29	29	29	29	29	29	29	29	29	29		
<b>Mean</b>	<b>249</b>	<b>183</b>	<b>204</b>	<b>265</b>	<b>482</b>	<b>901</b>	<b>2012</b>	<b>3527</b>	<b>2834</b>	<b>1807</b>	<b>789</b>	<b>395</b>	<b>13650</b>	<b>1137</b>
<b>St Dev</b>	145	70	83	103	250	441	555	761	670	653	548	244		

## H: Sensitivity analysis results

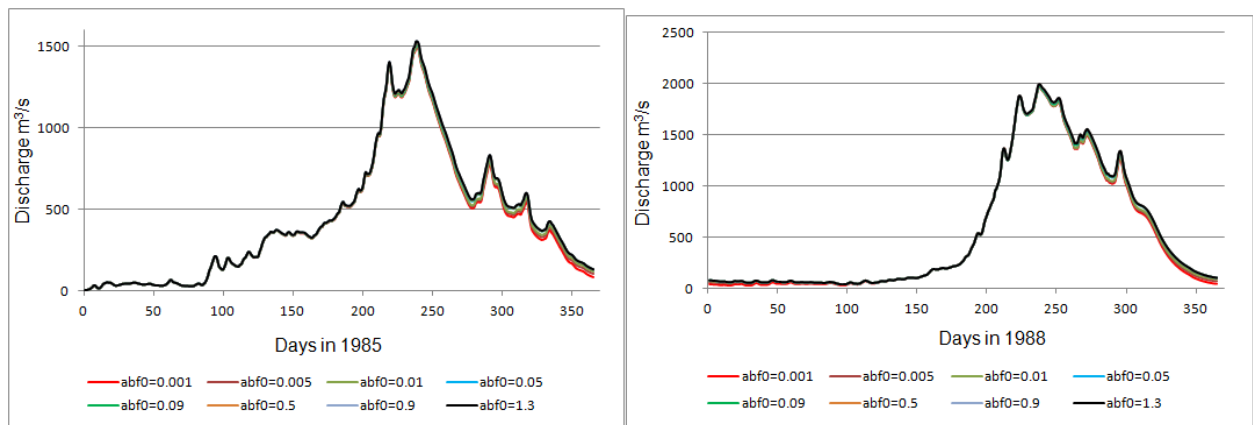


Figure H-1 Effects of abf0 on 1985 and 1988 flows at Gibe III dam site

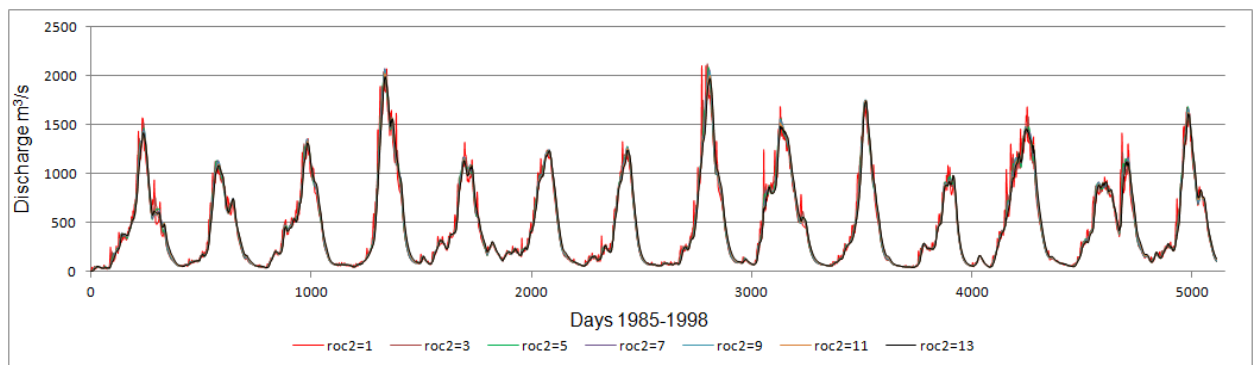


Figure H-2 Effects of roc2 on Gibe III flow

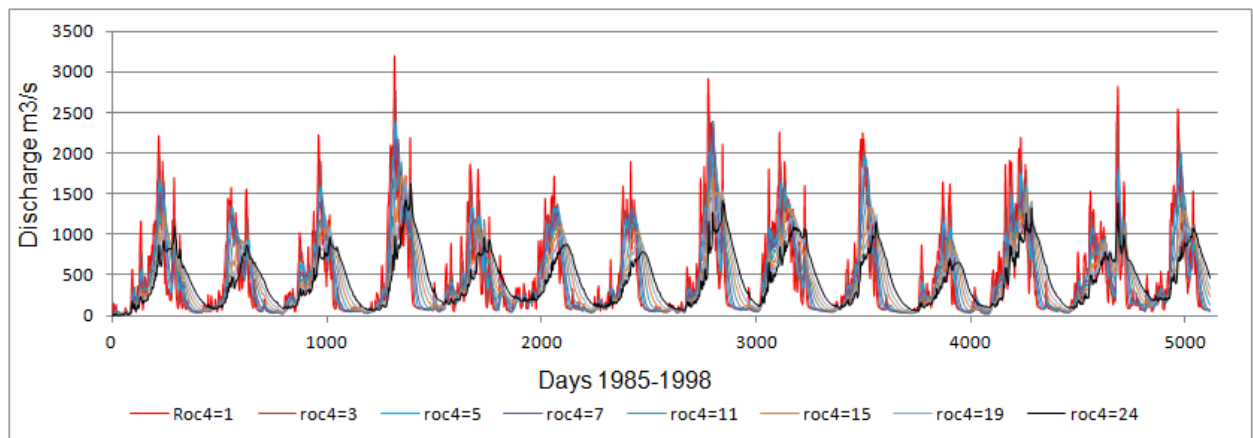


Figure H-3 Effects of roc4 on Gibe III flow

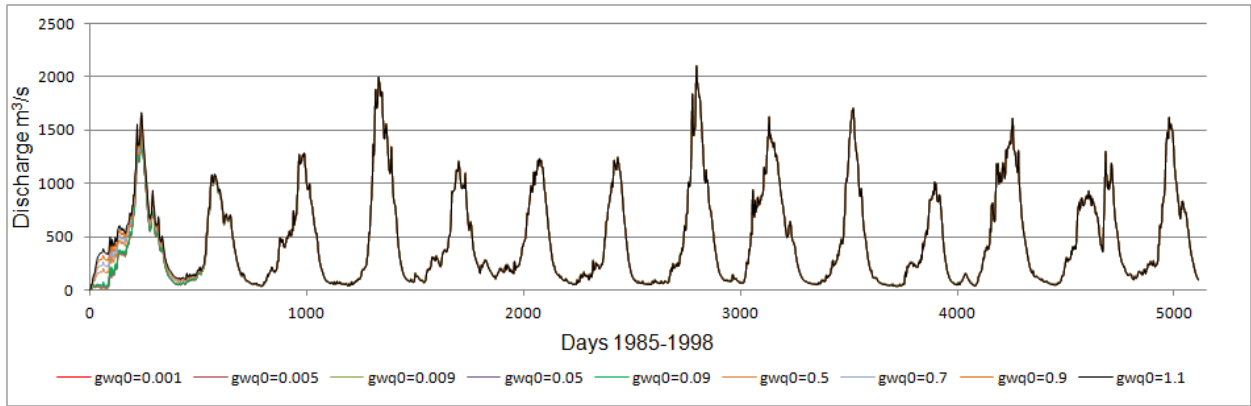


Figure H-4 Effects of gwq0 on Gibe III flow

I: Constructed pest files during automatic calibration at Gibe III and Abelti basin

```

CHE.PST
pef
* control data
restart estimation
9 5113 7 0 1
1 1 double point 1 0 0
5.0 2.0 0.3 0.01 11
1.4 1.4 0.001
0.1
20 0.01 3 3 0.001 3
1 1 1
* parameter groups
* parameter data
thc fixed factor 0.4 0.01 1.5 thc 1.0 0.0 1
bif fixed factor 0.7 0.2 1 bif 1.0 0.0 1
cnum1 fixed factor 40 1.80 cnum 1.0 0.0 1
cnum2 fixed factor 70 51 90 cnum 1.0 0.0 1
gwq0 fixed factor 0.04 0.01 1 gwq 1.0 0.0 1
abf0 fixed factor 0.95 0.01 1 abf 1.0 0.0 1
roc4 fixed factor 2.123307 1.60 roc 1.0 0.0 1
sccor log factor 9.346012 5 90 roc 1.0 0.0 1
* observation groups
group
* observation data
d1 54 4 1 group
d2 55 5 1 group
d3 56 1 1 group

```

```

che.tpl
pif #
SWITCH PARAMETERS
da bff
0 isc =0/1, SC: read/calc
0 icn =0/1, CN: dif for soils/cnum1,cnum3 for all
0 idlef =0/1, day length effect in crop: without/with
0 intercep =0/1, INTERCEPTION: WITHOUT-WITH
# thc # thc =0...1... evap correction on sky emissivity

BASIN, INITIALIZATION & CALIBRATION PARAMETERS
33901.600 # bff # BASIN PARAMETERS
cnum1 cnum2 # cnum3 # Curve number, if icn=1
# cnum1 # 55.000 # cnum2 # Groundwater parameters
gwq0 gwq0 # abf0 #
ekc0 prf spcon spexp Erosion parameters
1.000 1.000 0.0000 1.000
snow1 storcl stinco Initial water storage
0.000 0.500 0.300
chvc0 chxk0 chcc0 Channel parameters
0.700 0.050 0.000
roc1 roc2 # roc3 # roc4 # Routing coefficients
0.000 # roc2 # 0.000 # roc4 #
sccor prcor rdcor # Correction factors
# sccor # 1.000 1.000
retNsur retNsub retNgrv retPsur N & P RETENTION TIME
5.000 365.000 15000.000 20.000
degNsur degNsub degNgrv degPsur N & P DECOMPOSITION RATE
0.020 0.300 0.300 0.020
tsnfall twelt smrate SNOW FALL&MELT PARAMETERS
0.000 0.000 4.000

CO2 EFFECT ON NET PHOTOSYNTHESIS (alpha) & TRANSPIRATION (beta)
(ialpha,ibeta) = (1.0) OR (1.1) ONLY FOR SCENARIO PERIODS!
ialpha ibeta C3C4crop CO2-ref CO2-scen
0/1 0/1 3/4 346 406-436 OPTIONS & RANGES
0 0 4 0 0

```

J: Projected mean monthly discharge at Gibe III dam site (2020-2050)

Projected mean monthly discharge m <sup>3</sup> /s at Gibe III dam site 2020-2050 (A1B_911)													
Year	Jan	Feb	Mar	Apr	May	Jun	Jul	Aug	Sep	Oct	Nov	Dec	Mean
2020	11.5	31.4	35.1	65.6	173.4	925.7	1328.0	1500.9	910.1	293.3	121.5	66.4	455.3
2021	94.9	230.0	197.2	364.3	346.8	1231.3	1392.7	1278.2	843.5	1030.3	785.1	284.0	673.2
2022	104.5	109.4	146.4	229.0	429.5	979.7	1462.0	1199.1	869.8	493.8	226.8	100.2	529.2
2023	72.1	62.7	109.0	146.2	335.8	550.1	509.6	585.7	732.7	684.2	275.8	136.4	350.0
2024	61.7	46.7	64.8	437.8	504.6	584.8	639.0	1028.5	662.3	259.0	484.9	57.7	402.7
2025	45.1	51.2	43.3	121.7	281.0	288.8	417.5	582.8	443.0	232.8	127.5	70.9	225.5
2026	33.6	30.8	31.7	101.4	151.1	417.1	835.2	1007.9	708.7	933.0	499.9	129.6	406.7
2027	65.0	110.9	112.0	490.1	484.0	519.7	418.3	1121.7	1099.3	849.1	382.6	111.6	480.4
2028	66.7	76.2	61.3	108.6	593.2	615.7	1401.9	1395.2	815.0	389.6	200.6	147.7	489.3
2029	73.9	142.2	221.3	1096.9	506.6	558.1	756.1	754.7	519.2	283.6	201.7	105.7	435.0
2030	55.6	68.4	66.0	141.8	399.3	1137.1	1473.7	1797.6	1323.5	731.9	390.0	151.7	644.7
2031	85.3	70.3	131.9	249.6	503.5	808.3	1332.7	1301.9	1092.5	476.5	217.3	127.1	533.1
2032	93.2	74.7	66.9	377.5	434.0	529.2	720.1	757.1	676.5	439.8	248.2	88.8	375.5
2033	53.4	42.8	137.1	102.9	192.3	840.6	943.0	1067.2	809.1	568.7	314.4	129.8	433.4
2034	72.5	57.3	104.8	135.8	328.7	441.1	866.2	1133.1	935.1	333.5	152.8	211.9	397.7
2035	190.7	86.3	105.7	191.9	152.6	304.2	707.5	549.8	815.7	390.4	194.2	85.5	314.6
2036	52.0	54.5	52.9	180.4	658.1	513.1	538.8	629.6	666.0	579.4	456.9	144.0	377.2
2037	59.1	97.8	65.1	118.8	339.3	534.5	983.3	919.2	978.4	676.3	486.5	382.8	470.1
2038	110.1	59.3	72.2	224.7	385.0	1297.9	1581.3	1032.2	625.4	1028.8	422.8	151.4	582.6
2039	77.1	92.2	104.2	151.0	902.2	1555.7	1237.6	817.5	573.8	511.2	306.8	107.2	536.4
2040	72.4	80.3	63.7	49.7	73.3	213.9	809.8	981.9	855.8	593.8	488.5	239.5	376.9
2041	69.2	56.1	64.9	279.7	596.2	695.8	1041.1	2273.5	1398.6	596.9	351.8	150.5	631.2
2042	207.7	160.7	198.2	323.2	887.8	880.4	1267.4	1017.5	760.7	486.2	252.3	138.4	548.4
2043	86.1	80.6	94.5	94.7	361.1	1190.8	1043.1	1130.3	1245.5	612.9	221.5	120.5	523.4
2044	99.5	92.6	85.5	92.4	326.1	347.7	712.0	1079.6	740.8	526.9	410.8	135.9	387.5
2045	6.2	25.4	37.4	87.8	92.0	567.6	1563.6	1558.9	1028.4	513.9	181.8	86.3	479.1
2046	62.0	61.3	103.3	159.9	159.2	190.2	431.3	602.2	496.5	321.5	173.0	62.3	235.2
2047	31.8	49.4	58.3	203.5	322.2	616.7	1382.4	1592.7	1046.8	650.5	598.9	354.1	575.6
2048	113.5	238.8	140.2	169.0	226.5	1135.1	1374.6	1284.7	695.8	354.5	168.5	108.1	500.8
2049	198.1	181.0	138.4	101.8	507.6	1058.3	2308.7	1801.4	1069.8	624.6	234.7	114.2	694.9
2050	83.1	82.7	104.3	115.4	158.9	830.4	1373.4	1272.6	1184.2	704.5	278.7	158.7	528.9
n	31	31	31	31	31	31	31	31	31	31	31	31	
Mean	<b>80.9</b>	<b>87.2</b>	<b>97.3</b>	<b>216.6</b>	<b>381.0</b>	<b>721.3</b>	<b>1059.7</b>	<b>1130.8</b>	<b>858.8</b>	<b>553.9</b>	<b>318.0</b>	<b>143.8</b>	<b>470.8</b>
St. Dv	46.8	53.0	48.8	197.4	206.9	347.5	438.3	402.9	242.6	212.2	154.8	77.4	

	Projected mean monthly discharge m <sup>3</sup> /s at Gibe III dam site 2020-2050 (A1B_912)												
Year	Jan	Feb	Mar	Apr	May	Jun	Jul	Aug	Sep	Oct	Nov	Dec	Mean
2020	3.6	11.5	12.8	309.7	398.3	527.0	831.9	1030.6	484.2	180.9	97.3	49.3	328.1
2021	36.0	30.1	34.5	70.3	94.4	128.7	559.1	1272.5	1016.5	670.8	313.3	105.1	360.9
2022	57.7	61.4	203.1	343.0	243.7	442.5	815.0	1017.5	620.7	318.9	341.5	213.5	389.9
2023	83.0	57.5	249.3	783.7	848.1	940.2	631.4	702.7	481.6	330.0	151.8	73.7	444.4
2024	53.1	42.5	47.8	42.3	55.1	136.4	541.7	1129.6	1113.7	613.2	380.1	92.5	354.0
2025	69.1	68.9	81.4	144.0	297.2	999.2	837.4	1384.8	1173.1	656.1	254.1	122.0	507.3
2026	95.7	145.1	182.8	213.0	272.3	714.0	1086.7	1045.8	502.6	298.4	165.3	85.3	400.6
2027	64.0	95.0	139.9	167.5	584.5	630.9	997.3	1368.9	794.7	385.0	160.2	83.2	455.9
2028	64.6	53.5	173.2	96.7	1047.0	1317.7	798.5	1155.4	1071.4	618.6	421.6	279.0	591.4
2029	285.8	335.0	222.7	1355.7	1417.0	1770.6	2025.1	1722.2	1084.4	596.2	340.8	386.7	961.8
2030	201.9	125.1	100.3	237.4	285.3	266.4	414.4	902.6	1024.5	696.1	338.7	120.3	392.8
2031	75.2	79.1	68.1	52.4	61.6	419.2	822.1	1083.9	898.7	498.5	167.8	105.3	361.0
2032	83.0	50.5	40.9	75.0	110.8	75.1	268.3	701.9	791.9	291.4	93.9	47.5	219.2
2033	38.9	34.3	46.3	117.8	390.1	593.0	873.4	1025.9	825.4	293.9	122.6	71.3	369.4
2034	51.9	52.7	120.2	340.7	545.6	916.7	1248.4	1670.3	1111.0	543.4	268.5	142.2	584.3
2035	205.3	134.3	80.7	71.9	93.2	220.3	430.0	835.1	842.0	1005.7	764.8	277.4	413.4
2036	87.9	66.1	57.7	64.0	58.1	107.0	664.6	1241.1	1285.0	748.3	298.8	112.1	399.2
2037	68.1	55.8	52.0	103.7	334.3	956.0	1171.5	1494.3	1281.9	609.5	219.2	109.3	538.0
2038	82.2	67.6	93.6	99.9	191.3	364.1	409.6	495.3	567.9	350.0	121.6	53.2	241.3
2039	39.5	45.7	92.7	80.5	551.7	504.2	273.4	809.6	740.1	433.9	405.1	282.8	354.9
2040	297.5	139.6	78.2	281.3	281.5	341.6	907.3	1430.3	854.5	335.6	153.8	86.3	432.3
2041	62.6	51.6	45.1	69.9	162.1	782.4	1648.9	1619.0	1027.7	413.0	264.2	160.9	525.6
2042	88.1	117.3	105.6	139.5	107.3	166.7	461.0	670.5	519.0	287.8	132.4	56.8	237.7
2043	136.9	163.0	67.2	84.5	104.3	574.2	753.8	1159.6	974.2	610.1	441.4	291.2	446.7
2044	248.9	130.7	72.7	461.4	356.4	382.4	741.6	1429.2	1303.2	1048.6	533.3	181.3	574.1
2045	7.5	18.4	31.2	61.9	119.5	819.5	892.1	921.1	999.3	581.3	230.3	92.5	397.9
2046	65.7	52.0	44.7	85.1	98.2	329.0	851.4	1147.8	820.3	575.0	275.1	134.2	373.2
2047	65.7	52.0	44.7	85.1	98.2	329.0	851.4	1147.8	820.3	575.0	275.1	134.2	373.2
2048	441.7	166.4	101.6	93.2	103.2	189.1	692.5	1503.8	2238.2	1670.0	912.2	429.3	711.8
2049	170.1	200.4	227.9	158.1	719.6	823.2	823.2	867.1	1012.1	397.8	131.4	97.5	469.0
2050	97.8	108.3	74.6	124.1	187.9	426.3	296.0	454.6	582.9	346.4	185.5	145.8	252.5
n	31	31	31	31	31	31	31	31	31	31	31	31	
Mean	<b>110.6</b>	<b>90.7</b>	<b>96.6</b>	<b>206.9</b>	<b>329.6</b>	<b>554.6</b>	<b>794.2</b>	<b>1111.0</b>	<b>931.1</b>	<b>547.7</b>	<b>289.1</b>	<b>149.1</b>	<b>434.3</b>
St. Dv	97.0	65.9	63.7	262.8	319.1	385.4	377.3	332.3	343.1	290.5	185.4	98.6	



	Projected mean monthly discharge m <sup>3</sup> /s at Gibe III dam site 2020-2050 (B1_921)												
Year	Jan	Feb	Mar	Apr	May	Jun	Jul	Aug	Sep	Oct	Nov	Dec	Mean
2020	3.7	13.7	20.5	26.0	349.3	901.6	716.9	517.0	608.3	372.1	143.1	59.5	311.0
2021	51.8	191.2	78.1	128.3	160.8	481.0	839.2	1741.9	1562.5	556.2	178.6	199.4	514.1
2022	284.3	146.8	89.6	176.0	170.4	409.8	503.5	705.4	725.5	623.6	311.9	129.1	356.3
2023	91.5	62.1	71.3	648.4	392.6	149.9	176.9	663.1	1154.4	1004.1	631.4	419.5	455.4
2024	142.5	144.8	103.1	67.5	214.9	562.6	845.7	1854.3	1537.8	841.7	447.1	201.0	580.3
2025	109.1	80.9	141.7	111.9	326.5	599.1	994.9	964.9	614.1	328.6	231.3	153.0	388.0
2026	264.3	135.8	110.4	285.6	352.7	540.5	642.1	670.7	633.3	364.9	124.1	60.3	348.7
2027	68.7	53.4	87.8	599.1	396.3	470.4	382.2	431.3	459.2	338.3	120.2	49.8	288.1
2028	37.8	39.8	37.6	191.1	108.0	116.6	729.0	1389.7	1751.0	816.5	321.3	125.3	472.0
2029	77.3	69.2	291.1	249.0	418.8	871.1	998.3	983.1	778.0	414.3	161.4	85.8	449.8
2030	130.3	109.7	74.1	349.7	594.1	928.0	1093.8	1012.1	561.2	277.7	230.2	131.6	457.7
2031	68.6	52.9	52.0	284.1	207.6	441.9	681.9	1065.5	772.4	588.2	547.0	243.4	417.1
2032	117.3	66.2	46.6	60.7	61.6	470.4	1154.4	1221.1	664.5	383.9	440.9	157.9	403.8
2033	68.4	72.5	65.7	145.3	271.2	555.2	706.2	874.1	988.1	640.8	203.3	79.5	389.2
2034	55.2	44.2	174.9	242.3	487.5	886.0	605.9	863.8	885.9	850.4	740.2	260.8	508.1
2035	93.9	254.3	237.3	449.7	581.1	310.4	442.5	1110.8	1069.3	489.0	185.2	107.9	444.3
2036	71.4	72.2	181.4	498.7	344.9	1063.0	1363.0	1326.3	1387.9	702.3	212.9	124.5	612.4
2037	107.1	81.4	86.8	248.6	356.8	843.2	951.9	777.4	455.3	350.3	191.7	80.3	377.6
2038	52.5	53.4	400.0	199.1	241.9	470.5	684.0	658.3	623.2	612.2	348.7	192.9	378.1
2039	70.8	43.6	35.4	64.9	256.1	757.4	641.1	750.7	840.3	712.0	448.1	160.5	398.4
2040	74.4	49.1	41.1	132.1	325.8	534.9	657.5	827.4	985.1	1615.1	818.1	215.3	523.0
2041	101.1	72.3	90.6	194.7	188.6	366.0	489.7	1178.1	1065.4	515.0	166.2	80.2	375.7
2042	67.4	51.4	85.7	301.4	473.9	648.9	717.5	900.1	572.9	376.9	335.0	230.7	396.8
2043	85.7	49.0	41.9	50.5	93.3	219.2	934.7	1634.6	1161.3	802.0	567.2	236.1	489.6
2044	99.9	72.9	59.1	168.2	270.2	475.6	584.0	931.5	1011.8	706.0	311.7	111.5	400.2
2045	4.6	15.9	28.0	172.9	173.0	435.5	799.4	804.5	649.8	321.5	160.4	75.1	303.4
2046	36.4	33.5	76.1	62.9	240.0	598.7	607.2	871.1	540.2	202.1	240.2	142.5	304.2
2047	81.9	101.1	35.6	65.3	193.4	166.1	218.8	597.1	726.2	512.6	327.3	93.8	259.9
2048	34.6	34.7	73.2	68.6	73.2	858.1	1534.7	1763.3	1277.1	638.1	507.9	184.4	587.3
2049	239.5	432.5	342.5	295.0	385.4	544.7	840.3	1390.1	1133.9	449.5	215.3	112.5	531.8
2050	65.6	57.4	46.9	67.9	874.0	780.8	1238.1	1923.0	1186.2	388.3	135.2	84.2	570.6
n	31	31	31	31	31	31	31	31	31	31	31	31	
Mean	<b>92.2</b>	<b>89.0</b>	<b>106.6</b>	<b>213.1</b>	<b>309.2</b>	<b>563.1</b>	<b>766.9</b>	<b>1045.2</b>	<b>915.6</b>	<b>574.0</b>	<b>322.7</b>	<b>148.0</b>	<b>428.8</b>
St. Dv	65.2	81.8	93.5	160.4	173.1	245.1	306.1	406.3	344.8	276.8	187.0	78.5	

	Projected mean monthly discharge m <sup>3</sup> /s at Gibe III dam site 2020-2050 (B1_923)												
Year	Jan	Feb	Mar	Apr	May	Jun	Jul	Aug	Sep	Oct	Nov	Dec	Mean
2020	41.1	162.7	93.9	131.0	141.9	224.1	870.5	751.1	445.9	379.7	313.7	165.1	310.1
2021	67.0	43.2	47.0	70.3	243.2	869.2	781.1	1391.3	1151.8	493.8	205.9	90.4	454.5
2022	63.5	54.4	59.9	91.1	150.8	498.1	706.7	789.2	420.4	128.6	95.3	52.5	259.2
2023	35.1	29.8	47.2	158.2	280.7	664.1	383.0	1040.7	865.1	599.0	528.7	180.6	401.0
2024	58.0	77.7	71.3	103.1	132.3	656.9	898.0	887.8	680.3	301.9	358.9	55.2	356.8
2025	53.8	42.5	207.6	202.4	210.3	690.4	674.8	648.9	547.8	336.6	158.3	62.4	319.6
2026	37.0	32.9	45.2	54.3	144.9	179.3	576.7	890.9	569.3	197.5	250.6	140.9	260.0
2027	47.4	49.1	114.4	173.1	205.2	359.2	792.4	1232.4	980.7	398.4	173.7	76.0	383.5
2028	47.5	37.7	104.4	67.6	89.8	505.1	867.7	1108.5	762.2	378.1	191.9	83.0	353.6
2029	47.9	45.1	67.8	84.3	175.7	251.8	633.2	920.9	811.9	622.2	278.4	74.9	334.5
2030	41.9	36.6	37.2	345.0	437.8	473.2	597.8	903.4	853.4	844.3	542.7	174.9	440.7
2031	71.1	57.1	299.1	343.8	707.5	552.1	830.9	1226.4	765.8	392.2	762.8	449.8	538.2
2032	204.9	227.7	503.4	494.5	273.1	463.0	767.6	1011.4	877.5	480.4	477.7	190.6	497.6
2033	79.1	112.3	95.8	72.9	582.8	591.8	324.6	718.3	482.1	343.3	290.1	120.0	317.8
2034	46.8	30.9	52.3	107.8	100.2	59.4	129.8	434.1	583.8	625.8	345.7	189.2	225.5
2035	148.0	64.5	60.7	108.4	170.0	444.1	701.4	934.6	624.8	248.3	184.8	80.2	314.2
2036	44.8	39.9	46.6	227.6	335.7	378.0	627.7	912.6	651.6	305.0	168.4	63.4	316.8
2037	43.1	46.7	68.3	167.8	562.1	560.7	416.5	841.3	756.7	286.9	107.2	52.4	325.8
2038	43.4	117.1	96.8	451.2	450.7	740.2	723.3	792.4	911.7	506.3	169.4	106.0	425.7
2039	57.2	57.0	74.2	165.1	244.7	1015.3	1432.5	1111.5	707.6	434.6	163.3	80.3	462.0
2040	60.8	50.3	75.5	118.7	524.2	462.8	295.0	666.8	848.6	524.4	242.8	132.0	333.5
2041	66.4	48.0	202.4	267.5	156.3	105.3	555.9	1461.2	998.8	387.8	199.9	91.8	378.4
2042	50.7	45.9	96.0	162.7	410.4	946.0	852.7	1195.3	1078.3	418.7	199.3	105.0	463.4
2043	64.4	56.0	50.5	118.9	140.2	223.8	385.8	947.6	967.0	388.4	167.4	63.9	297.8
2044	38.7	29.1	32.4	65.0	533.5	1244.5	997.1	1138.5	1016.5	401.2	157.1	80.4	477.8
2045	8.5	28.4	143.3	239.3	292.4	291.4	148.3	148.3	431.8	601.6	302.3	82.3	226.5
2046	35.4	32.1	40.5	48.7	57.9	486.2	760.1	1184.6	1097.1	790.2	513.2	167.4	434.4
2047	68.1	55.5	99.5	131.6	273.9	397.2	516.7	1209.6	1028.6	322.0	176.6	142.4	368.5
2048	74.6	51.0	87.6	286.7	618.4	581.0	313.7	863.2	698.8	409.0	361.2	155.8	375.1
2049	107.4	97.0	72.7	78.5	87.7	118.8	342.3	1002.7	1414.8	943.5	411.8	124.8	400.2
2050	94.5	68.3	82.9	97.4	111.5	127.8	365.9	863.8	921.8	577.8	231.3	104.8	304.0
n	31	31	31	31	31	31	31	31	31	31	31	31	
Mean	<b>62.8</b>	<b>62.1</b>	<b>102.5</b>	<b>168.9</b>	<b>285.4</b>	<b>489.1</b>	<b>621.6</b>	<b>942.9</b>	<b>804.9</b>	<b>453.8</b>	<b>281.6</b>	<b>120.6</b>	<b>366.3</b>
St. Dv	36.5	42.7	93.7	114.6	182.2	280.7	276.2	268.2	235.9	182.1	152.8	75.0	

	Projected mean monthly discharge m <sup>3</sup> /s at Gibe III dam site 2020-2050 (GCM)												
Year	Jan	Feb	Mar	Apr	May	Jun	Jul	Aug	Sep	Oct	Nov	Dec	Mean
2020	7.6	30.6	33.2	133.6	285.0	674.9	1325.7	1197.0	789.0	375.7	142.1	68.2	421.9
2021	58.7	91.0	94.9	141.1	212.1	527.8	978.1	1411.1	1011.3	546.3	321.7	156.4	462.5
2022	120.8	68.5	126.1	216.6	239.0	625.2	970.0	957.7	596.2	415.4	259.6	108.7	392.0
2023	67.2	60.9	133.1	289.3	434.3	401.5	354.0	721.8	849.2	626.3	367.8	211.9	376.4
2024	66.4	64.3	83.9	168.0	165.1	385.3	701.6	1257.2	1069.6	470.1	416.6	91.5	411.6
2025	71.0	56.8	77.0	98.6	192.1	476.2	824.7	1274.3	1037.2	483.5	205.1	109.4	408.8
2026	117.8	108.5	87.3	153.0	229.8	444.1	896.3	966.2	587.4	312.9	177.9	84.1	347.1
2027	50.1	53.9	84.2	252.8	375.1	478.7	620.8	1091.1	788.1	456.3	229.1	95.7	381.3
2028	53.7	55.5	95.8	106.5	379.7	535.8	1086.9	1476.2	1190.4	480.3	247.7	136.2	487.1
2029	95.3	100.3	126.7	541.7	713.7	1092.2	1540.5	1497.4	1093.6	513.6	228.6	127.0	639.2
2030	91.5	87.0	76.0	155.2	320.6	545.3	1036.0	1323.4	1244.8	821.1	350.9	133.8	515.5
2031	82.1	70.1	97.9	184.6	252.2	493.3	913.7	1231.9	804.9	461.0	327.3	147.4	422.2
2032	89.3	71.1	66.2	151.7	163.9	271.6	797.0	1252.6	951.9	496.9	263.7	100.0	389.7
2033	60.9	59.9	89.3	106.2	246.3	483.5	875.4	1211.8	916.1	454.8	197.2	92.9	399.5
2034	64.4	54.9	93.6	162.2	287.5	596.3	847.4	1019.7	748.6	475.6	278.4	143.9	397.7
2035	129.2	114.1	136.0	130.1	211.8	246.7	551.6	1072.2	1075.4	557.6	224.3	103.4	379.4
2036	70.4	69.5	97.6	153.5	203.3	408.2	1086.6	1367.7	1149.2	631.4	278.4	134.8	470.9
2037	82.2	71.4	78.1	114.7	269.5	544.9	1213.1	1352.6	862.4	420.9	211.1	102.8	443.6
2038	72.6	60.6	113.0	162.1	236.5	539.7	824.2	1051.4	727.4	630.9	332.1	114.5	405.4
2039	61.2	68.8	71.5	95.2	273.2	692.8	735.3	992.9	709.3	453.0	351.0	157.6	388.5
2040	93.6	64.5	79.4	126.8	225.0	345.2	802.5	1132.8	841.5	636.2	334.3	115.2	399.7
2041	60.0	52.3	75.0	152.8	222.6	503.6	1417.4	1841.6	1219.7	460.2	204.8	103.2	526.1
2042	81.7	95.8	115.1	164.1	288.6	470.1	943.2	1064.5	722.2	404.9	210.6	128.6	390.8
2043	72.1	66.9	67.0	97.1	203.7	570.7	1003.7	1553.9	1084.8	636.5	370.6	168.6	491.3
2044	125.9	97.9	94.2	193.3	317.6	471.4	765.4	1239.0	1084.7	667.7	309.5	109.9	456.4
2045	11.4	30.4	55.9	124.1	190.8	621.7	1180.2	1298.7	970.4	478.8	192.5	89.7	437.1
2046	59.7	62.1	59.4	99.4	135.0	405.3	866.0	1312.6	812.0	351.6	237.5	124.6	377.1
2047	67.1	89.5	77.3	130.1	287.1	531.0	1150.1	1506.1	1193.5	585.0	368.4	194.8	515.0
2048	106.4	86.0	114.1	143.5	140.7	521.7	1299.4	1821.9	1402.3	866.8	413.8	165.8	590.2
2049	125.2	221.2	165.3	136.7	327.7	602.3	1183.6	1520.5	1225.9	595.5	227.7	113.9	537.1
2050	85.6	74.9	78.9	101.5	201.5	510.5	812.0	1235.4	1024.3	429.7	200.1	93.9	404.0
n	31	31	31	31	31	31	31	31	31	31	31	31	
Mean	<b>77.5</b>	<b>76.1</b>	<b>91.7</b>	<b>160.8</b>	<b>265.5</b>	<b>516.7</b>	<b>954.9</b>	<b>1266.2</b>	<b>960.8</b>	<b>522.5</b>	<b>273.6</b>	<b>123.5</b>	<b>440.8</b>
St. Dv	29.1	33.5	27.2	83.5	108.7	148.4	257.1	244.2	206.3	125.4	74.2	32.9	

# Curriculum Vitae

## Personal information

First name(s) / Surname: Abdella Kemal, Mohammed

Address: Arbaminch University; Institute of Technology; P.O.Box 21, Arbaminch Ethiopia

Telephone mobile: +251933585793

E-Mail: [Abdellabz@yahoo.com](mailto:Abdellabz@yahoo.com)

## Education and training

May 2010 to December 2013: Ph.D degree from Universität der Bundeswehr München, Institute für Wasserwesen Germany

September 2008 - August 2009: ING-PAED IGIP - International Engineering Educator a certificate on Engineering Pedagogy ING-PAED IGIP, Vienna

Since September 2005 - July 2007: Master of science Degree in hydraulic and hydropower engineering with CGP 3.96 (out of 4.00 calculations) Arbaminch water technology institute, Department of Hydraulic engineering, Arbaminch university Arbaminch, Ethiopia.

Since September 1999 - July 2005: B.Sc. degree in Hydraulic Engineering, Arbaminch water technology institute, Department of Hydraulic engineering, Arbaminch university Arbaminch, Ethiopia.

## Work experience

From August 2007 to April 2010: Head of Hydraulic and water resources engineering department from November 2007 to April 2010. And team leader of Baso integrated water resources development project from August 2009 to April 2010 in Arbaminch University, Ethiopia

Main activities and responsibilities: Lecturer and researcher: and offering courses to undergraduate students, doing applied research, curriculum development and review, consulting and participating in academic administration positions as department head. Among the courses I offered: open Channel hydraulics, hydraulic structures I & II, Water supply and sanitary Engineering, hydraulics I & II, soil and water conservation engineering, engineering economics, Computer application in hydraulic engineering.